Nanomaterials in Bacterial Estimation and Development of Antimicrobial Agents

A Thesis

Submitted in Partial Fulfillment of the Requirements for the Degree of

DOCTOR OF PHILOSOPHY

by

MANAB DEB ADHIKARI

Department of Biotechnology
Indian Institute of Technology Guwahati
Assam, India

August 2013

Dedicated to My Parents

And

Family Members

INDIAN INSTITUTE OF TECHNOLOGY GUWAHATI

DEPARTMENT OF BIOTECHNOLOGY

STATEMENT

I do hereby declare that the research findings of this thesis is the result of research work carried out by me in the Department of Biotechnology, Indian Institute of Technology Guwahati, Guwahati, India, under the supervision of Dr. Aiyagari Ramesh.

As per the general norms of reporting research findings, due acknowledgements have been made, wherever the research findings of other researchers have been cited in this thesis.

Date: 28th August, 2013 **Manab Deb Adhikari**

INDIAN INSTITUTE OF TECHNOLOGY GUWAHATI

DEPARTMENT OF BIOTECHNOLOGY

CERTIFICATE

It is certified that the work described in this thesis entitled "***Nanomaterials in Bacterial Estimation and Development of Antimicrobial Agents***" by Mr. Manab Deb Adhikari for the award of degree of Doctor of Philosophy is an authentic record of the results obtained from the research work carried out under my supervision in the Department of Biotechnology, Indian Institute of Technology Guwahati, India, and this work has not been submitted elsewhere for the award of any other degree.

Manab Deb Adhikari
(Candidate)
Roll No: 08610606

CERTIFIED

Aiyagari Ramesh, Ph.D.
(Thesis Supervisor)
Date: 28th August, 2013

ACKNOWLEDGEMENT

I would like to take this opportunity to offer my heartfelt thanks to a number of people without whose help and support this thesis would never have been possible.

The first person I want to acknowledge is my supervisor, Aiyagari Ramesh, Associate Professor, Department of Biotechnology, IIT Guwahati who made this achievement possible. His guidance and support for the past five years have been invaluable, and much credit goes to him for my growth as a researcher and as an individual. I highly appreciate his never-ending kindness and encouragement, and I am fortunate to have worked with him.

I thank my doctoral committee members, Professor Siddhartha Sankar Ghosh, Professor Pranab Goswami and Dr. Biplab Mondal. Their constructive suggestions and supportiveness has improved the quality and richness of my research experience.

I would also like to extend my sincere gratitude to Professor Gopal Das and Professor Arun Chattopadhyay, Department of Chemistry for giving me the opportunity to work with them and for their valuable suggestions and motivation during the course of my Ph.D. work.

I owe my gratitude to former-Heads of the Department of Biotechnology of IIT Guwahati, Professor Pranab Goswami, Professor Arun Goyal and current Head, Dr. Venkata Dasu Veeranki, for providing me with the necessary facilities. I thank all the faculty and staff members of my department for their warmth and support.

I owe my deepest gratitude to Indian Institute of Technology (IIT) Guwahati for providing research fellowship during Ph.D. programme, which helped me to sustain and pursue research at IIT Guwahati.

I would also like to thank Central Instrumentation Facility (CIF) for providing ambient atmosphere of research and freedom to execute experiments. My sincere thanks go to Mr. Indrajit Talukdar and Mr. Madhurjya Borah for their help in TEM analysis.

It is my pleasure to thank my seniors Dr. Atul Kumar Singh, Dr. Biswa Ranjan Panda and Dr. Bimlesh Ojha for their helpful guidance at the initial stages of my research work.

I also wish to thank my friends, Amit (Babu), Sahil, Zia, Tushar, Rishi, Abhoy, Shashank and Shubamoy, for their unconditional support and all the help they extended from time to time whenever required. I am very much thankful to all of you for making my stay at IIT Guwahati memorable. I would also like to thank my other friends in

department and IITG campus for the wonderful time I had with them. I would also like to extend my gratitude to my old friends Amit, Arun, Manas, Soleman, Pradipta, Jasha, Koushik, Bhaskar, Ujjal, Joy.

It is my pleasure to thank my labmates Sudeep, Sandipan, Thiyagarajan, Pallavi, Umakanth, Vidushi for their support and unconditional gesture of assistance in times of need.

Thanks to my friends Kamal, Pankaj, Sandeep, Arvind Bhaiya, Bipransh. Rudra from University of North Bengal, Darjeeling, West Bengal for their constant support, their encouragement and all the help they extended from time to time whenever required.

Sincere thanks goes to Dr. Asim,P0jul, Ashok, Koushik, Ritika, Mahesh and all other COE labmates for their co-operation during my work and sharing light moments with them. A special thanks to Chockalingam, Jiban, Chirantan, Nilanjan and Argha for their help and support during my Ph.D. tenure.

I also thank Mahitosh, Santosh, Sukhomoy, Bappa, Nazbul, and Prasanta for all the fun we have spent together in IITG.

Hearty thanks to Swagata and her parents for providing their constant support and encouragements during this period.

Lastly, and also most importantly, I would like to thank my parents and my family members (Didi, Dhruba da, Dada, Boudi, Moon, Gajen, Biva, Guddu, and Nandu) for their endless love and affection.

Manab Deb Adhikari

CONTENTS

Contents

Contents

ABBREVIATIONS

AA	Ascorbic acid
ADDLs	Amyloid β-derived diffusible ligands
AgNP	Silver nanoparticle
AMPs	Antimicrobial peptides
ANOVA	Analysis of variance
ATP	Adenosine triphosphate
AU	Arbitrary unit
Au	Gold
AuNP-P	Gold nanoparticle-pediocin
AuNP-PTh	Gold nanoparticle polythiophene
AuNPs	Gold nanoparticles
BHI	Brain-heart infusion broth
CA	Citric acid
CCCP	Carbonyl cyanide m-chlorophenylhydrazone
CD	Circular dichroism
CF	Culture filtrate
cFDA-SE	5(and 6)-carboxyfluorescein diacetate succinimidyl ester
CFS	Cerebrospinal fluid
CFU	Colony forming unit
CTAB	Cetyltrimethylammonium bromide
CTAC	Cetyltrimethylammonium chloride
$DiSC_35$	3,3′-dipropylthiadicarbocyanine iodide
DLS	Dynamic light scattering
DMEM	Dulbecco's modified eagles medium
DMSO	Dimethyl sulfoxide
EIS	Impedance spectroscopy
FBS	Fetal bovine serum
FCS	Fetal calf serum
$Fe(NO_3)_3$	Ferric nitrate
FESEM	Field emission scanning electron microscope
$FeSO_4$, $6H_2O$	Ferrous sulphate
FIC	Fractional inhibitory concentration

Abbreviations

FITC	Fluorescein isothio cyanate
GA	Gallic acid
IONP-P	Iron oxide nanoparticle-pediocin
IONPs	Iron oxide nanoparticles
IPA	Isopropyl alcohol
IU	International unit
K_d	Dissociation constant
LA	Lactic acid
LAB	Lactic acid bacterium
LPS	Lipopolysaccharide
MALDI-TOF	Matrix-assisted laser desorption ionization-time of flight mass spectrometry
MBC	Minimum bactericidal concentration
MIC	Minimum inhibitory concentration
MR	Magnetic resonance
MRS	de Man, Rogosa and Sharpe broth
MRSA	Methicillin resistant *Staphylococcus aureus*
N-AuNP	Nisin-gold nanoparticle
NB	Nutrient broth
Nisin-CA	Nisin-citric acid
N-OAC	Nisin-organic acid complex
NPN	1-N-phenylnaphthylamine
NP-P	Nanoparticle-pediocin
NPs	Nanoparticles
PBS	Phosphate buffered saline
PCR	Polymerase chain reaction
PEG-SH	Thiolated polyethelene glycol
PI	Propidium iodide
PLL	Poly-L- lysine
PSA	Prostate specific antigen
QDs	Quantum dots
ROS	Reactive oxygen species
RSV	Respiratory syncytial virus
SDS	Sodium dodecyl sulphate
SERS	Surface-enhanced Raman scattering

Abbreviations

SGF	Simulated gastric fluid
SNP-P	Silica nanoparticle-pediocin
SNPs	Silica nanoparticles
SPR	Surface plasmon resonance
SRL	Sisco research laboratories
TEM	Transmission electron microscope
TEOS	Tetraethylorthosilicate
TFA	Trifluoacetic acid
VNC	Viable but non-culturable cells

LIST OF TABLES

LIST OF FIGURES

List of Figures

List of Figures

List of Figures

CHAPTER 6

Chapter 1

Introduction and Literature Review

Chapter 1

Introduction and Literature Review

Introduction

Nanoscience and technology has come of age and inspired a remarkable progress in the field of biology and medicine. As an emerging and all encompassing branch of science, it has demonstrated the potential to provide a gamut of materials with unique structural features between those of the atom and the macroscopic material and at least one dimension in nano range. Extensive research in nanoscience in recent years has led to a fundamental understanding with regard to the unique attributes of nanoscale materials and the properties in nanomaterials which are quite different from those observed in the bulk (micron-size) material have been attributed to various factors such as small size, large surface area, enhanced surface reactivity, quantum confinement effects, enhanced electrical conductivity and enhanced magnetic properties. The wide range of existing core materials coupled with unique and tunable surface properties make nanomaterials an excellent tool for a plethora of biotechnological, diagnostic and potential therapeutic applications. The unique size-dependent properties of nanomaterials, their biocompatible chemistry and facile functionalization have facilitated powerful biological applications. The development of sensors, antimicrobial agents, enzyme-nanoparticle complex, cancer therapeutics, bioimaging devices, drug delivery and controlled release of drugs are exemplary cases in point that vindicate the promise of nanomaterials in biology.

Amongst various nanomaterials, gold nanoparticles (AuNPs) have been particularly interesting in terms of a wide array of biological applications. AuNPs have been widely exploited as sensors owing to their characteristic optical properties such as surface plasmon resonance (SPR), which can be tuned depending on their size, shape, degree of aggregation, and local environment. This property has been exploited as a bio-responsive probe and nanoparticle-based detection systems have been devised to probe macromolecules such as proteins and nucleic acids, or set off interactions with bacterial

cells to develop diagnostic tools in the regime of pathogen detection. Recent literature report also suggests that a major endeavor for researchers working at the nanoparticle-biomolecule interface is to develop methods of conjugation of biomolecules to nanomaterials. These methods include the use of biomolecules to drive the synthesis and co-functionalization of nanoparticles as well as direct covalent linkage and non-covalent interactions between the nanoparticle and biomolecules. The ability to conjugate bioactive molecules onto nanoparticles has paved the way for the development of invasive and robust drug delivery and control release systems.

One of the burgeoning issues in modern medicine and healthcare regime is to develop tools for rapid estimation of bacterial cells. This is relevant in the context of clinical diagnosis, food safety, development of therapeutic strategies, and for ameliorating potential infections. It assumes even greater significance in case of pathogens as the presence of even a single viable cell may imply grave health concerns. Conventional microbiological methods for estimating bacterial cells are time-consuming and lack sensitivity. Molecular methods such as immunoassays and polymerase chain reaction (PCR) can achieve high sensitivity and specificity, but these techniques are mostly invasive and cumbersome in nature. There is ample challenge in developing routine and facile methods of estimating bacteria and detecting pathogens. The emergence of nanoscience and technology in recent years offers great promise in developing non-invasive tools for sensitive, cost effective and high-throughput estimation of bacterial cells.

Emergence of antibiotic-resistant pathogenic bacteria has assumed alarming proportions and is of grave concern. These pathogens have evolved mechanisms to evade the action of most commercially available therapeutic antibiotics. This problem is further compounded by the rather disconcerting progress in the discovery of new antibacterial agents. Therefore, there is a huge demand to discover judicious strategies and identify new antimicrobial drugs in order to combat the menace of drug-resistant pathogens. The use of nanoscale materials as bactericidal agents represents a radical paradigm in antibacterial therapeutics. The high surface area to volume ratio of nanomaterials can achieve enhanced interactions with the target pathogen and can thus be explored to generate potent bactericidal agents. Currently, metallic nanoparticles and various nanocomposites are being extensively investigated as potential antibacterials. It is conceived that membrane-

acting nanomaterials would be particularly appealing and counterproductive to development of resistance as extensive membrane damage would demand large scale restoration of membrane components, which would be physiologically exigent upon target cells.

Recognizing the enormous scope for nanomaterials as smart sensing tools and novel therapeutics, the current Ph.D. research work strives to demonstrate the use of nanomaterials, in particular gold nanoparticle, to develop systems for estimation of bacterial cell numbers and potent bactericidal agents. The following section provides a detailed literature review pertinent to the research area of the present work.

Literature review

1.1. Nanomaterials in biology and medicine

The use of nanomaterials in biotechnology represents a cutting-edge interdisciplinary field of research which essentially encompasses chemistry, material science and biology. Nanoparticles represent a particularly innovative regime, displaying unique properties with potentially wide-ranging applications. Intensive research in recent times has led to a fundamental understanding of the properties of nanomaterials and has offered a vista of opportunities to explore these nanomaterials for various biological applications. In particular, the ability to interface nanomaterials with biological systems has resulted in a revolutionary progress in biology and biomedicine. An overview of various biological applications of nanomaterials is presented in Figure 1.1. It is quite evident from the figure that nanomaterials are indeed versatile and render powerful applications in virtually every field of biology and medicine. It is also critical to recognize that certain salient attributes of nanomaterials largely influence their applications in biological context. For instance, it can be envisaged that size-dependent tunable properties of nanomaterials, the development of surface conjugation chemistry which would enable the ability to functionalize nanomaterials with specific ligands and the toxic implications of the developed nanomaterials would largely influence their application potential. These features are also indicated in Figure 1.1.

Development of sensors is one of the fundamental needs in the field of biomedicine. Nanomaterials have several desirable physical and chemical characteristics

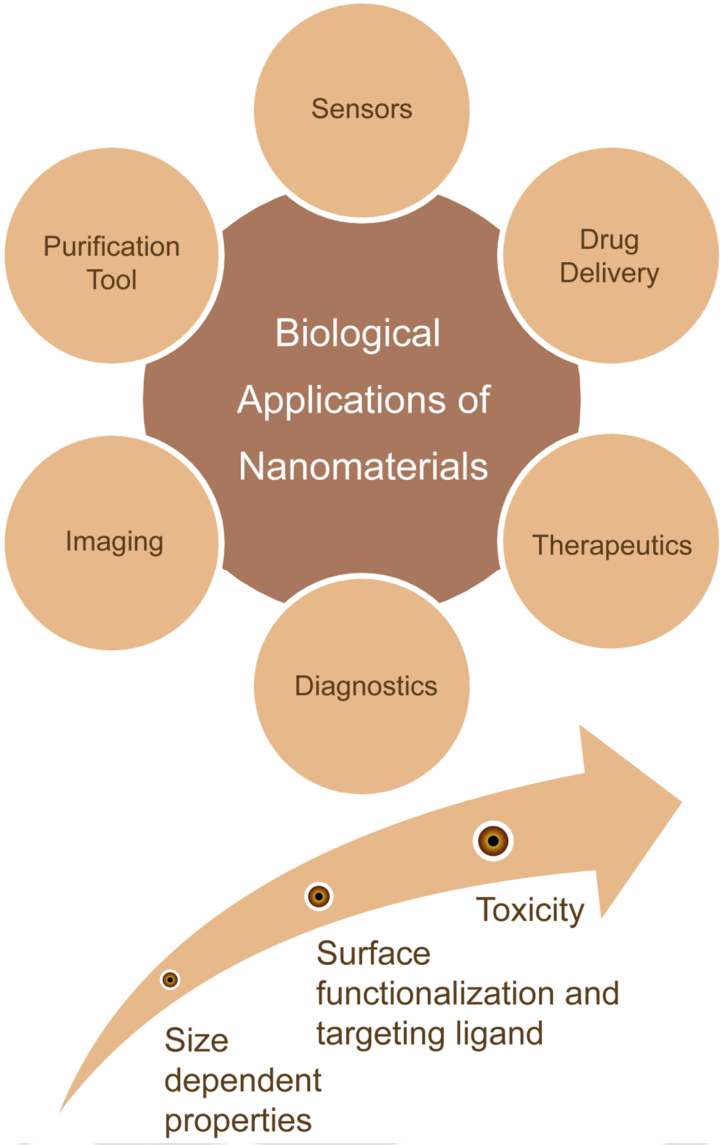

Figure 1.1. An overview of biological applications of nanomaterials and their cardinal features which influence biological applications.

that enable development of profound biological sensing systems. Considering the enormous scale of research in this emerging field, recent literature reports describe the potential nanoscale materials as sensors (Jain et al., 2008; Saha et al., 2012; Agasti et al., 2010; Alivisatos, 2004; Niemeyer, 2001).

An important application of nanomaterials has been in the field of drug-delivery. Some prominent examples of the use of nanomaterials in this field include nanoparticle-

based drug delivery has resulted in enhancing the solubility of poorly water-soluble drugs, enhanced half-life of drug systemic circulation by reducing immunogenicity, sustained and responsive drug release, targeted drug delivery and combination therapy (Zhang et al., 2008; Vigderman and Zubarev, 2013)

Recently nanomaterials are used for the noninvasive imaging of organs because it has a major impact in medicine due to their strongly enhanced LSPR. Noble metal nanoparticles scatter light very strongly at the LSPR frequency, making them promising tools for optical imaging and labeling of biological systems. Among different nanomaterials, quantum dots (QDs), with their unique optical and electrical properties are substantially used for biomedical imaging. Chan and Nie (1998) have reported imaging of tumors in live animals using QDs. In another study, Akerman et al. (2002) linked QDs to a peptide for labeling tumor vasculatures in live mice. Further, iron magnetic nanoparticles were used to track progenitor cells *in vivo* using magnetic resonance imaging (Lewin et al., 2000; Bulte et al., 2001). Liong and his groups synthesized iron oxide-mesoporous silica nanoparticles for magnetic resonance (MR) and fluorescence imaging (Liong et al., 2008). Chen et al. synthesized Fe_3O_4-containing mesoporous nanocapsules as contrast agents of MRI and for cell imaging (Chen et al., 2010). Fluorescent QDs hold great potential for molecular imaging *in vivo* as reviewed by different studies (Michalet et al., 2005; Medintz et al., 2005). El-Sayed and coworkers demonstrated diagnosis of cancer by imaging of the cancer biomarker epidermal growth factor receptor (El-Sayed et al., 2005).

Small dimensions of the nanostructured materials help them to use in molecular diagnostics. The nanotechnology based diagnostic basically carried out through nanochips and nanoarrays. Nam et al. has demonstrated that nanoparticle-based bio-bar-code approach to detect free prostate-specific antigen (PSA), at low attomolar concentrations (Nam et al., 2003). The photostability and narrow emission spectra of quantum dots make them desirable candidates for their use in FISH to study the expression of specific mRNA transcripts as demonstrated by Chan and coworkers. They revealed that the sensitivity of multiple-label FISH can increase by using quantum dots (Chan et al., 2005). Bio-barcode assays allow detection of very small amounts of proteins in body fluids that cannot be detected by conventional methods (Bao et al., 2006). Antibody-conjugated nanoparticles rapidly detect respiratory syncytial virus (RSV) and estimate relative levels of surface

protein expression (Agrawal et al., 2005). Single walled carbon nanotubes have been used as optical nanosensor for specific detection of glucose (Barone et al., 2005). In another study, nanoparticle-based bio-barcode assay was used to measure the amyloid β-derived diffusible ligands (ADDLs) in the cerebrospinal fluid (CSF) as a biomarker for Alzheimer's disease (Georganopoulou et al., 2005). The unique physio-chemical property of gold nanoparticles attributes them for the detection of biological molecules at low concentration (Wilson, 2008).

The convergence of nanotechnology and medicine, suitably called nanomedicine, can potentially advance the fight against a range of diseases (Sanhai et al., 2008). In particular, the application of nanomedicine for antibacterial therapy can help sustain the drug release over time, increasing its solubility and bioavailability, decreasing aggregation and improving efficacy (Swenson et al., 1990; Gelperina et al., 2005; Dillen et al., 2006). Liposomal encapsulation of gentamicin allows a significant reduction (50%) in the total treatment duration in disseminated *Mycobacterium avium* infections in mice as compared to the usual antimicrobial therapy (de Steenwinkel et al., 2007). It is important to mention that magnetic nanoparticles are used as hyperthermia agents *in vitro* and *in vivo* to treat prostate cancer. Gold nanomaterials have been extensively used in photothermal cancer therapy, radiofrequency therapy, rheumatoid arthritis therapy and antibacterial therapy (Boisselier and Astruc, 2009).

The ability to separate and identify different proteins accurately and efficiently out of a biological sample is of utmost importance for application in biomedicine, energy resources, environmental protection, and catalysis (Fu et al., 2008; Liu et al., 2009; Liu et al., 2009b). Monodispersed and functional immobilized metal affinity magnetic chondroitin sodium sulfate nanoparticles have been used for separate phosvitin phosphopeptides (PPPs) from aqueous solution of egg yolk polypeptides (Zhang et al., 2012). Thiol group functionalized silica-coated magnetic nanoparticles were used for rapid and selective magnetic field-based separation of mixed proteins (Lee et al., 2012). Silica-coated magnetic nanoparticles were used for effective protein separation through surface modification with various amino acid side chain-like functional groups such as thiol, disulfide, carbon chain carboxyl, amine and aldehyde (Lee et al., 2012b). Bao and his

groups have studied that bi-functional Au-Fe_3O_4 nanoparticle can used for separating proteins simply with the assistance of a magnet (Bao et al., 2007).

In the present Ph.D. thesis, a major emphasis has been on the use of gold nanoparticles for estimation of bacterial cells and development of antibacterial agents. In the following section a detailed overview of the synthesis, characteristic features and salient application potential of gold nanoparticles is presented.

1.2. Gold Nanoparticle

Gold nanoparticles hold considerable promise in biological applications owing to their unique optical properties. Modern applications of gold nanoparticles (AuNPs) are widespread over diverse specialized fields like sensing to imaging to cancer treatment and drug delivery (Saha et al., 2012; Agasti et al., 2010; Murphy et al., 2008; Jain et al., 2008; Lal et al., 2008; Xia et al., 2011; Lee et al., 2008; Daniel et al., 2004). Amongst various metal nanoparticles, gold nanoparticles have been shown to be generally more stable and hence suitable for biological applications. (El-Sayed, 2001). Furthermore, the advantage of gold nanoparticle in biodiagnostic over quantum dots and organic dyes is that gold nanoparticles are biocompatible, superior contrast agents for imaging and render unique surface-enhanced and refractive index-dependent spectroscopic properties.

1.2.1. Methods of synthesis

Faraday in 1857 described the formation of a deep red colloidal solution of gold which was obtained by the reduction of gold chloride by phosphorus. The synthesis of gold nanoparticles with diameters ranging from a few to several hundreds of nanometers can be accomplished through well-established reactions in aqueous solution as well as in organic solvents. In a prototype synthesis, gold salts are reduced by the addition of a reducing agent which leads to the nucleation of gold (Au) ions to nanoparticles. In addition, a stabilizing agent is also required which is either adsorbed or chemically bound to the surface of the Au nanoparticles. A plethora of synthetic protocols for AuNPs are available based on the use of the commercially available $HAuCl_4$ as the starting material in most of the reactions. A pioneering breakthrough achieved in the context of the synthesis of gold

nanoparticles was the citrate reduction method of Au^{3+} to Au^{0} in water which was invented by Turkevitch et al. in 1951. In 1994, Brust et al. investigated the synthesis of thiol-stabilized gold clusters of 2 nm size using a two-phase system wherein gold chloride was solvated in toluene by a phase-transfer reagent. In a separate study, Yu and his group demonstrated the synthesis of gold nanorods (10 nm) by electrochemical oxidation of a gold plate electrode in the presence of cationic, quaternary ammonium surfactants and under ultra-sonication (Yu et al., 1997). Additional studies on similar lines have also demonstrated growth of colloidal gold to produce monodisperse gold nanorods in high yield based on seeded growth (Jana et al., 2001; Nikoobakht and El-Sayed, 2003).

Silica-gold core-shell nanoparticles, or gold nanoshells, have been in focus due to their interesting optical properties and numerous biomedical applications. An interesting work by Oldenburg and coworkers demonstrated that near-infrared absorbing gold nanoshells could be prepared by electrostatic adsorbtion of small gold nanoparticles onto the surface of silica nanoparticles and subsequent formation of a conformal shell (Oldenburg et al., 1998). Gold-silver alloy nanocages and nanoframes with controllable pores on the surface have been synthesized via galvanic replacement reaction between truncated Ag nanocubes and aqueous $HAuCl_4$ (Chen et al., 2006; Skrabalak et al., 2008). Recently, Zhang and coworkers have developed a method to produce monodisperse gold nanocubes in high quantity by a seeded growth technique analogous to that used to produce nanorods, in the presence of cetyltrimethylammonium chloride (CTAC) instead of the conventional cetyltrimethylammonium bromide (CTAB) (Zhang et al., 2010).

1.2.2. Surface modification and bio-conjugation

In the context of application of AuNP in the field of biomedical sciences, selective interaction of AuNPs with cells or biological entities of interest is paramount. In this regard, the ability to functionalize AuNPs with the desirable ligands is critical. Gold nanoparticles are especially attractive to biochemists since the chemistry for functionalization of AuNPs with various ligands is well established and a plethora of protocols are available for tagging ligands onto AuNPs. A representative cartoon indicating the possibility of functionalization of AuNPs with various relevant ligands is indicated in Figure 1.2. Essentially, the functionalization could involve conjugation with

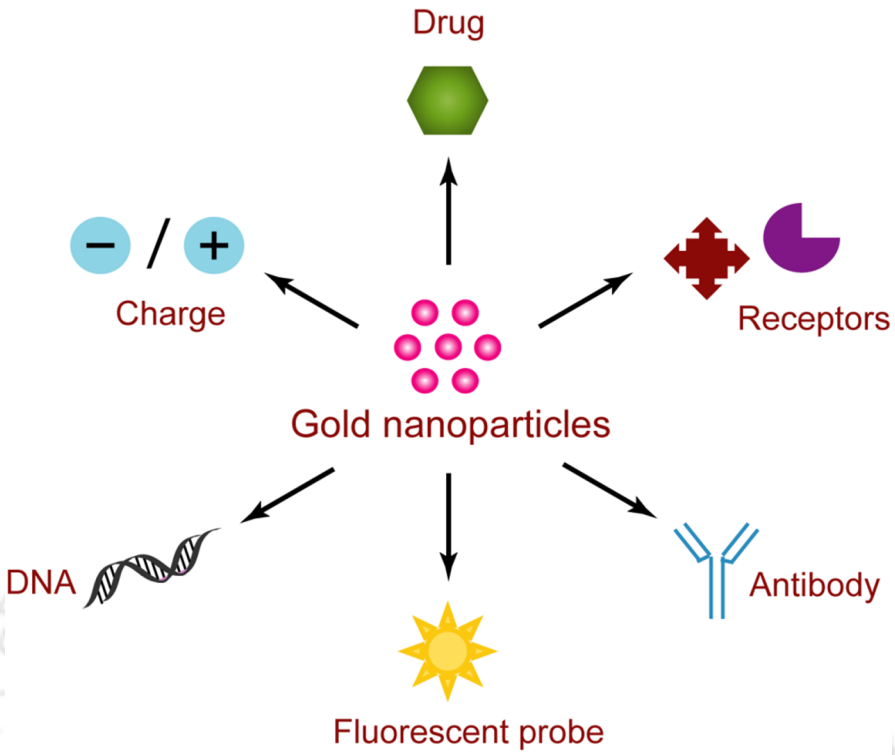

Figure 1.2. Functionalization of gold nanoparticles for various biological interactions.

drugs for development of therapeutics, receptors and macromolecules such as DNA for studying affinity based interactions for sensing and diagnostic applications, attachment of fluorescent probes for imaging applications and rendering charge to the nanoparticle for promoting charge-based interactions with either cell surface or biological macromolecules.

A large variety of molecules are used as functional linkers and passivating agents. Some of anchoring groups utilized for attachment of these linkers onto AuNP surface include thiolate, dithiolate, dithiocarbamate, amine, carboxylate, selenide, isothiocyanate, or phosphine moieties (Dreaden et al., 2012). While one end of these molecules is either adsorbed or chemically linked onto nanoparticle surface, the other end is free to orient towards the solution and provides stability to the system. Amongst various functional groups, the thiol moieties exhibit the highest affinity-based binding propensity onto gold surfaces by formation of the strong Au-sulfur bonds (Brust et al., 1994; Templeton et al., 2000; Flynn et al., 2003). One of the commonly employed surface ligand is thiolated polyethylene glycol (PEG-SH), which has been used for functionalization of AuNPs to

facilitate application in biomedical field. The hydrophilicity of the molecule allows facile dispersion of AuNPs which were conjugated with a wide range of lipophilic molecules (Dreaden et al., 2009). The strong Au-thiol interactions have also been exploited to synthesize gold nanoparticles with macromolecules such as proteins having free thiol groups. In an interesting study, AuNPs could be synthesized with the enzyme α-amylase with retention of enzymatic activity in the generated nanocomposite (Rangnekar et al 2007). Simple physical methods like hydrophobic-hydrophobic interactions and charge pairing have also been used to conjugate various biologically important molecules on AuNP surface. Kim and coworkers have demonstrated the potential of highly hydrophobic molecules (e.g. chemotherapeutics such as paclitaxel and doxorubicin) to be bound to gold nanoparticle conjugates through amphiphilic ligands (Kim et al., 2009). In another study, Brown and coworkers have demonstrated that a Pt (IV) prodrug form of cisplatin can be coordinated with the help of carboxylate-terminal ligands on AuNP surface, which enables intracellular transport and consequent activation of the prodrug (Brown et al., 2010).

1.2.3. Surface plasmon resonance

A typical suspension of gold nanoparticle appears ruby red in color, which has been explained on the basis of the scattering of an electromagnetic wave from the nanoparticles. The Mie theory of scattering (Mie, 1908) provides a basic explanation of to scattering is applicable to spherical particles of varying size and composed of an absorbing or non-absorbing material. Thus this theory is most useful in explaining the underlying principle of the optical properties of metallic spherical particles. In case of gold nanoparticles it well known that upon exposure to an electromagnetic radiation of a appropriate wavelength, the delocalized conduction electrons oscillate in harmony with respect to the positive nuclei and resonate at the same frequency as that of the incoming light. This phenomenon is known as the surface plasmon resonance (SPR) of the gold nanoparticles and is depicted in the cartoon shown in Figure 1.3.

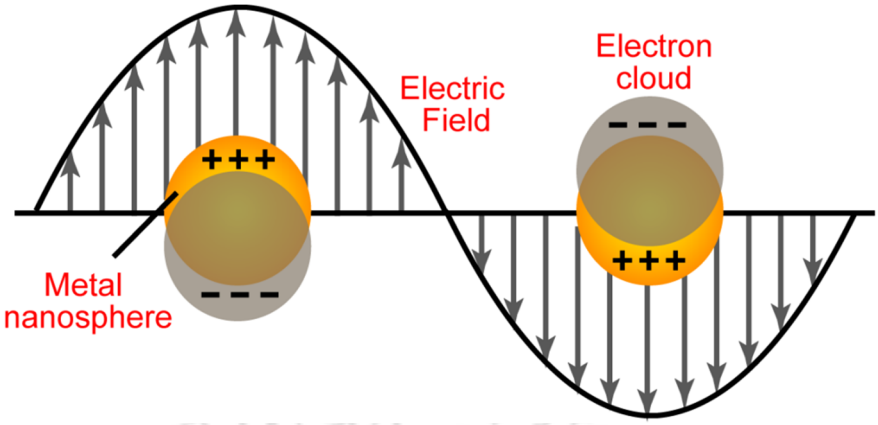

Figure 1.3. Collective oscillation of delocalized electrons in a metal nanosphere such as gold nanoparticle leads to the phenomenon of surface plasmon resonance (SPR).

The phenomenon of SPR is referred to as extinction which is sum of absorption and scattering. Furthermore, SPR also generates strong electric near fields in the vicinity of the surface of the particle. For metallic nanoparticles such as gold, silver and copper, SPR leads to strong absorption in the visible region. The surface plasmon absorption of AuNPs renders unique optical properties that can be exploited in a variety of applications for labeling, imaging and sensing which are relevant in the realm of diagnostics and therapies. In general, SPR response of gold nanostructures is dependent on a number of variables such as size, shape, and morphology of the nanostructure, as well as the dielectric constant of the environment (Kelly et al., 2003; Wiley et al., 2006; Cobley et al 2011). The tunable SPR of gold nanostructures in turn facilitates a number of sensor applications.

1.2.4. Biological applications of gold nanoparticle

The wide range of existing methods of synthesizing gold nanoparticles coupled with unique size-dependent properties, biocompatible chemistry and facile functionalization have facilitated a wide gamut of biological applications. The development of sensors, cancer therapeutics, bioimaging devices, drug delivery and controlled release systems are exemplary cases in point that vindicate the promise of gold nanoparticles in biology. An overview of some of the powerful applications of gold nanoparticles in biology and medicine is indicated in Table 1.1.

Table 1.1. Representative examples of application of gold-based nanomaterials in biology.

Nanomaterials	Application	Target	Reference
Gold nanoparticle	Drug delivery	Cancer cell	Zhang et al., 2011
Gold nanorods	Drug delivery	Dopaminergic neuronal (DAN) cells	Bonoiu et al., 2008
Gold nanoparticle	Drug delivery	MC-38 colon carcinoma tumors of mice	Paciotti et al., 2004
Chitosan-gold nanoparticle hybrid nanospheres	NIR photothermal therapy	LoVo cells	Guo et al., 2010
Gold nanoparticle	Biosensing	DNA	Maxwell et al., 2002
Gold nanoparticle	Biosensing	Cholesterol	Zhang et al., 2008
Gold nanocages	Imaging	Human mesenchymal stem cells	Zhang et al., 2013
Gold nanoparticle	Biosensing	DNA	Bu et al., 2013
Gold nanocages	Therapy	Cancer cells	Chen et al., 2007
Gold nanoparticles	Cancer therapy	MCF-7 breast cancer cells	Joshi et al., 2012
Gold nanoparticles	Drug delivery	Insulin Delivery	Joshi et al., 2006
Gold nanoparticles	Photothermal therapy	Cancer cells	Huang et al., 2010
Gold nanorods and Gold nanoparticles	Photodynamic and Photothermal therapy	Malignant cells	Kuo et al., 2012
Gold nanoparticles (37 nm)	Detection	Cancer Biomarker	Liu et al., 2008
Gold nanorods	Gene delivery	Plasmid DNA	Ramos and Rege, 2012
Gold nanoparticles	Gene delivery	Small interfering RNA (siRNA) and plasmid DNA	Guo et al., 2010
Gold nanoprobe	Detection	RNA	Conde et al., 2010
Gold nanoparticles	Detection	DNA	Elghanian et al., 1997

In the present Ph.D. thesis, the focus has been in the use of gold nanoparticles in the area of bacterial cell estimation and development of antibacterial agents. In the following section, a review of the pertaining issues regarding bacterial cell estimation and development of antibacterial agents as well as the application potential of gold-based nanomaterials in these focal themes is presented.

1.3. Estimation of bacterial cells

There is a constant impetus to develop rapid, sensitive and reliable methods of estimating bacterial cell numbers, owing to its significance especially in the context of clinical diagnosis, food safety, and environmental monitoring. In case of pathogenic bacteria, this requirement is even more critical, since the presence of even a single viable cell may have grave health implications. In the following section the pros and cons of a number of tools which aid in bacterial cell estimation is discussed. The limitations of these existing tools are indicated and the potential of nanomaterials in bacterial estimation is highlighted.

1.3.1. Culture and colony based methods

Conventional culture methods encompass the oldest and the most widely used techniques for either detection or estimation of bacterial cells. Culture methods have been used for detection of pathogenic bacteria such as *Listeria monocytogenes* (Artault et al., 2001; DeBoer and Beumer, 1999; Stephan et al., 2003), *Staphylococcus aureus, Salmonella* sp., *Escherichia coli,* (Ayçiçek et al., 2004), and *Yersinia enterocolitica* (Weagant, Feb 2008) etc. The major drawbacks of microbiological methods are that the methods are laborious and protracted. It is also important to mention that for different bacterial strains, specific media needs to be used in certain cases where viable but non-culturable cells (VNC) are present, this method has severe limitations.

1.3.2. Immunology-based methods

Immunology-based methods are powerful analytical tools for detection of wide variety of bacterial pathogen. Essentially based on antigen-antibody interactions, detection of bacterial cells, spores, viruses and toxins are possible. (Iqbal et al., 2000). Immunology-based methods have been used for the detection of *E. coli* , *Salmonella* and

L. monocytogenes (Abdel-Hamid et al., 1999b; Aldus et al., 2003; Chen and Durst, 2006; Magliulo et al., 2007; Sunwoo et al., 2006, Valdivieso-Garcia et al., 2003; Churchill et al., 2006; Yu et al., 2004b), *Campylobacte*r spp. (Hochel et al., 2007). For immune detection method for bacteria detection, conventional and heavy chain antibodies, polyclonal, monoclonal or recombinant antibodies are used. Monoclonal antibodies have been used to detect a wide range of pathogens in food such as *Listeria innocua* (Solve et al., 2000), *Escherichia coli* O157:H7 (Zhao and Liu, 2005), *Salmonella enterica* (Schneid et al., 2005 and *Shigella* (Warren et al., 2006).

The major drawbacks of immunoassay-based methods are low sensitivity, low affinity of the antibody to the pathogen or other analyte being measured and unwarranted interference from contaminants (Meng and Doyle, 2002). In combination with other methods like matrix-assisted laser desorption ionization-time of flight mass spectrometry (MALDI-TOF), pathogenic bacteria such as *L. monocytogenes* has been detected (Hibi et al., 2006).

1.3.3. Polymerase chain reaction (PCR)

Amongst nucleic acid based techniques, polymerase chain reaction (PCR) is a powerful tool which has been extensively used for estimation and detection of pathogenic bacteria. This method has superior sensitivity over other conventional methods with an ability to detect a single copy of a target DNA sequence. PCR-based methods have been employed in the detection of wide range of pathogens like *S. aureus*, *L. monocytogenes*, *Salmonella* spp., *Bacillus cereus*, *Escherichia coli* O157:H7, *Yersinia enterocolitica* (Velusami et al., 2010). The specificity, sensitivity, rapidity, accuracy and capacity to detect small amounts of target nucleic acid in a sample have been advocated as the main advantages of PCR-based techniques (Toze, 1999). In recent time's emergence of various formats of PCR such as multiplex and real-time PCR in conjunction with tremendous advancement in detection technologies has facilitated high sensitivity and specificity to bacterial cell estimation as reported extensively in literature (Mancini et al., 2010; Sibley et al., 2012; Jeng et al., 2012).

1.3.4. Limitation of current technologies

Conventional molecular diagnostic techniques are widely throughout the world to estimate or identify pathogenic agents with high degree of sensitivity and accuracy. However, most of these techniques are sophisticated and require personnel-expertise. Furthermore, the high cost and short shelve-life of some diagnostic reagents, such as enzymes, nucleic acids, hamper the application potential of molecular techniques. Requirement of an extensive sample preparation step in conjunction with protracted readout times further hinder the deployment of these techniques.

1.3.5. Estimation of bacteria by nanomaterials

The integration of nanotechnology approaches into biosensors holds great promise for addressing the analytical needs of developing diagnostics. Compared to the bulk materials nanomaterial offers larger surface-to volume ratios and superior electronic and optical properties. Due to their large surface area, nanomaterials allow a greater number of biomolecules to be immobilised and this consequently increases the number of interaction sites available for target detection. This attribute coupled with favorable electronic and optical properties, facilitate the use of nanomaterials in 'label-free' detection and in the development of biosensors with enhanced sensitivities and improved response times. The following section provides some prominent examples of the use of nanomaterials for estimation of bacterial cells.

1.3.5.1. Bacterial estimation by quantum dots

Quantum dots (QDs) are colloidal semiconducting fluorescent nanoparticles. QDs are more stable than conventional fluorescent dyes and hold unique size dependent fluorescence property. QDs have been conjugated by different approaches to of a wide range of bio-recognition elements and used a fluorescent probe for the detection of food borne pathogens such as *L. monocytogenes*, *C. jejuni*, *E. coli* O157:H7, *S. typhimurium*, *S. aureus* and *Shigella flexneri* (Vinayaka and Thakur 2010; Tully et al., 2006; Bruno et al., 2009; Hahn et al., 2005; Yang and Li, 2006; De Liu et al., 2007). Dudak and co-workers demonstrated simultaneous detection of *E. coli* and *S. enteritidis*, by coupling immunomagnetic separation with QD labeling. Target-specific antibodies coupled to QDs

with different emission wavelengths were used to label captured bacteria and the ranges for detection were found to be 5 x 10^2 to 5 x10^5 CFU/mL for *E. coli* and 4 x10^2 to 4 x10^5 CFU/mL for *S. enteritidis* (Dudak and Boyaci, 2009). Using an analogous system, Zhao and colleagues detected *S. typhimurium*, *Shigella flexneri*, and *E. coli* O157:H7, with a detection limit of 10^3 CFU/mL in a food matrix (Zhao et al., 2009). Su and Li demonstrated the use of magnetic beads coated with anti-*E. coli* O157 antibodies to selectively target bacteria and biotin conjugated anti-*E. coli* antibodies to form sandwich immune complexes for magnetic separation of bacteria which was followed by labeling with streptavidin-coated QDs for measuring the cell concentration (Su and Li, 2004). The detection limit was at least 100 times lower than that of Fluorescein isothiocyanate (FITC)-based method and the detection time was less than 2 h. In another study this group reported simultaneous detection of *E. coli* O157:H7 and *S. typhimurium* using semiconductor QDs with different emission wavelengths (525 nm and 705 nm) (Yang and Li, 2006). Mukhopadhyay et al. (2009) demonstrated the use of fluorescent mannose conjugated CdS QDs to detect *E. coli* at levels as low as 10^4 bacteria/ml of sample.

1.3.5.2. Bacterial estimation by gold nanoparticles

A colorimetric assays, based on AuNP aggregation was developed for monitoring *S. typhimurium* (Vidotti et al., 2011) and multiple drug-resistant *S. typhimurium* DT104 (Wang et al., 2010). These rapid simple detection methods could estimate 10^4 CFU/mL and 10^3 CFU/mL, respectively. In another study, the limit of detection of *S. typhimurium* DT104 was subsequently improved to a level of 10 CFU/mL using surface-enhanced Raman scattering (SERS) (Khan et al., 2011). Recent work using SERS with AgNPs as enhancing substrates has demonstrated estimation of single bacteria (Green et al., 2009). Yang et al. (2009) immobilized *Salmonella* spp. monoclonal antibodies on AuNPs and detection of *Salmonella* spp. in pork samples was accomplished using electrochemical impedance spectroscopy (EIS) technique. In another study, an array of gold NP-conjugated fluorescent polymer constructs were developed which achieved rapid detection and identification of nine different species of bacteria as well as three strains of *E. coli* (Phillips et al., 2008). A colorimetric gold-based nanocomposite biosensor using an enzymatic

amplification process to provide high sensitivity for detection of bacteria has also been reported recently (Miranda et al., 2011).

1.3.5.3. Magnetic nanoparticles in bacterial estimation

Magnetic nanoparticles and nanocomposites have emerged as key players in different niche areas like medical diagnostics and therapy, catalysis, environmental remediation, cell labeling and immunomagnetic separations. Iron oxide NPs, such as magnetite Fe_3O_4 or Fe_2O_3 have been well studied with great interest in isolating pathogens from food, blood, etc. using an external magnet and quantifying them with various analytical techniques. Varshney et al. used streptavidin-coated magnetic NPs and biotin labeled antibodies to detect *E. coli* O157:H7 (Varshney et al., 2005). About 94% of the bacteria could be captured in a range of initial bacterial count from 1.6×10^1 to 7.2×10^7 CFU/ml in 15 min without any enrichment. In another study, Cheng and coworkers determined the number of *E. coli* cells (20 CFU/ml) in a milk sample by biotin functionalized amine Fe_3O_4 NPs using the adenosine triphosphate (ATP) bioluminescence method in about 1 h (Cheng et al., 2009). NP-based immune-magnetic separation combined with real-time PCR *enabled estimation of L. monocytogenes*, in spiked milk sample. The detection limit was found to be 226 CFU/0.5 ml (Yang et al., 2007). *Mycobacterium avium* spp. paratuberculosis was detected and quantified in milk and blood through magnetic relaxation (Kaittanis et al., 2007). *Salmonella* bacteria were selectively captured from buffer solution or milk matrix by antibody-conjugated magnetic nanoparticles and separated by applying an external magnetic field. The detection limit of *Salmonella* in milk was found to be more than 100 CFU/ mL (Joo et al., 2012).

1.3.5.4. Carbon nanotubes in bacterial estimation

The physical and catalytic properties, high electrical conductivity, chemical stability, and mechanical strength make CNTs ideal for use in sensor. Potentiometric biosensors based on single-walled carbon nanotubes as ion-to-electron transducers and aptamers as recognition elements were used for real-time and label-free estimation of *S. aureus* at viable cell concentration of 0.2 to 10^3 CFU/mL (Zelada-Guillen et al., 2009; Zelada-Guillen et al., 2012). For immunomagnetic separation of *Escherichia coli* O157:H7, Lin et

al. used bovine serum albumin-functionalized multiple-walled carbon nanotubes with encapsulated ferromagnetic elements which conjugate with anti-*E. coli* antibodies (Lin et al., 2006). Elkin and his groups demonstrated that immuno-single walled carbon nanotube is capable of recognizing pathogenic *E. coli* O157:H7 cells through specific antibody-antigen interactions (Elkin et al., 2005).

A brief overview of various nanomaterials used in estimation of bacterial cells is provided in Table 1.2.

Table 1.2. Nanomaterials used for estimation of bacterial pathogens.

Nanomaterials	Pathogen	Detection method	Limit of detection	Reference
AuNP nanorod	*Escherichia coli* O157:H7	Two-Photon Rayleigh Scattering Spectroscopy	50 CFU/mL	Singh et al., 2009
AuNP nanodots	*Escherichia coli*	UV-visible spectroscopy	150 CFU/mL	Tseng et al., 2011
Silica nanoparticle	*Listeria monocytogenes*	Immunoassay	50 CFU/mL	Wang et al., 2010
AuNP	*Escherichia coli*	Dark-field light-scattering imaging	10^4 CFU/mL	Xu et al., 2012
Streptavidin-conjugated CdSe QDs	*Mycobacterium* spp.	Fluorescence spectroflurometer	10^4 bacteria/mL	Liandris et al., 2011
Quantum Dots	*Escherichia coli*	Antibody microarray	10 CFU/mL	Sanvicens et al., 2011
CdSe-ZnS quantum dot	*Escherichia coli* O157:H7	Immunomagnetic separation (IMS) and fluorescence spectroscopy	10^3CFU/mL	Su and Li, 2004
CdSe quantum dots	*Escherichia coli*, *S. aureus*	Fluorescence spectroscopy	10^2 CFU/mL	Xue et al., 2009

Nanomaterials	Pathogen	Detection method	Limit of detection	Reference
Quantum dots	*E. coli* O157:H7, *Salmonella Typhimurium*	Immunoassay	10^4 CFU/mL	Yang and Li, 2005
AuNP nanorod	*E. coli* O157: H7, *Salmonella Typhimurium*	UV-visible spectroscopy	10^2 CFU/mL	Wang and Irudayaraj, 2008
AuNP	*Escherichia coli* O157:H7	Immunoassay	6 CFU/strip in PBS buffer and 50 CFU/strip in milk	Lin et al., 2008
AuNP	*S. aureus*	Colorimetric assay	50 Cells/mL	Wang et al., 2012
AuNP	*Salmonella typhimurium* DT104	Colorimetric assay	10 CFU/mL	Khan et al., 2011
Gold-coated magnetic nanoparticles	*Escherichia coli*	Immunomagnetic separation (IMS) and surface-enhanced Raman scattering (SERS)	8 CFU/mL	Guven et al., 2011
AuNP	*Salmonella*	Electrochemical	143 cells/mL	Afonso et al., 2013
Carbon nanotube	*Salmonella enterica* serovar *Typhimurium*	Immunoassay	10^3 CFU/mL	Chunglok et al., 2011

1.4. Development of antibacterial agents

One of the critical issues in modern healthcare regime is the emergence of drug-resistant bacterial pathogens. These pathogens have evolved mechanisms to evade the action of most commercially available therapeutic antibiotics and this underscores the need for novel

and potent antibacterial agents. It is envisaged that the use of nanoscale materials as bactericidal agents represents a novel paradigm in antibacterial therapeutics. In the following section the concerns of antibiotic resistance and the potential of nanomaterials as potent antibacterial agents is highlighted

1.4.1. Antibiotic resistance

The perpetual development and increase of bacterial resistance to conventional antibiotics has led to a grave public health hazard. These pathogens have evolved effective approaches to counteract the biocidal action of antibacterial molecules. Some of the pathways for resistance development are: (i) modification of target through increment in numbers of target molecules or variation in target topology (ii) hydrolysis or structural alteration mediated enzymatic inactivation of antibiotic (iii) inhibited drug accumulation caused by a membrane-permeability barrier or increment in drug efflux and (iv) mutations in drug-activating enzymes (Nikaido, 2009; Allen et al., 2010). A cartoon indicating these underlying principles is depicted in Figure 1.4. There is an urgent need for innovation and invention of novel antibacterial agents with alternative and new modes of action.

1.4.2. Nanomaterials as antimicrobial agents

The challenge of combating drug-resistant bacteria demands a radical therapeutic approach and emphasizes the need to develop potent antibacterial agents, which are different from conventional antibiotics. In this context, it is envisaged that the use of nanoscale materials as bactericidal agents represents an attractive option. The high surface area to volume ratio and unique physicochemical properties of nanomaterials are amenable to enhanced antimicrobial activity. It has been suggested that bactericidal nanomaterials may be suitable in overcoming resistance and reducing toxicity effects commonly observed with conventional antibiotics (Huh et al., 2011). Nanoparticles (NPs) are effective as cargo for delivery of antimicrobial agents and it also provides important pharmacological benefits such as improved solubility and half-life of drug, sustained and stimuli-responsive drug release, site-targeted delivery and combination therapy (Zhang et al., 2010; Moghimi et al., 2005; Risbud et al., 2000; Alphandary et al., 2000).

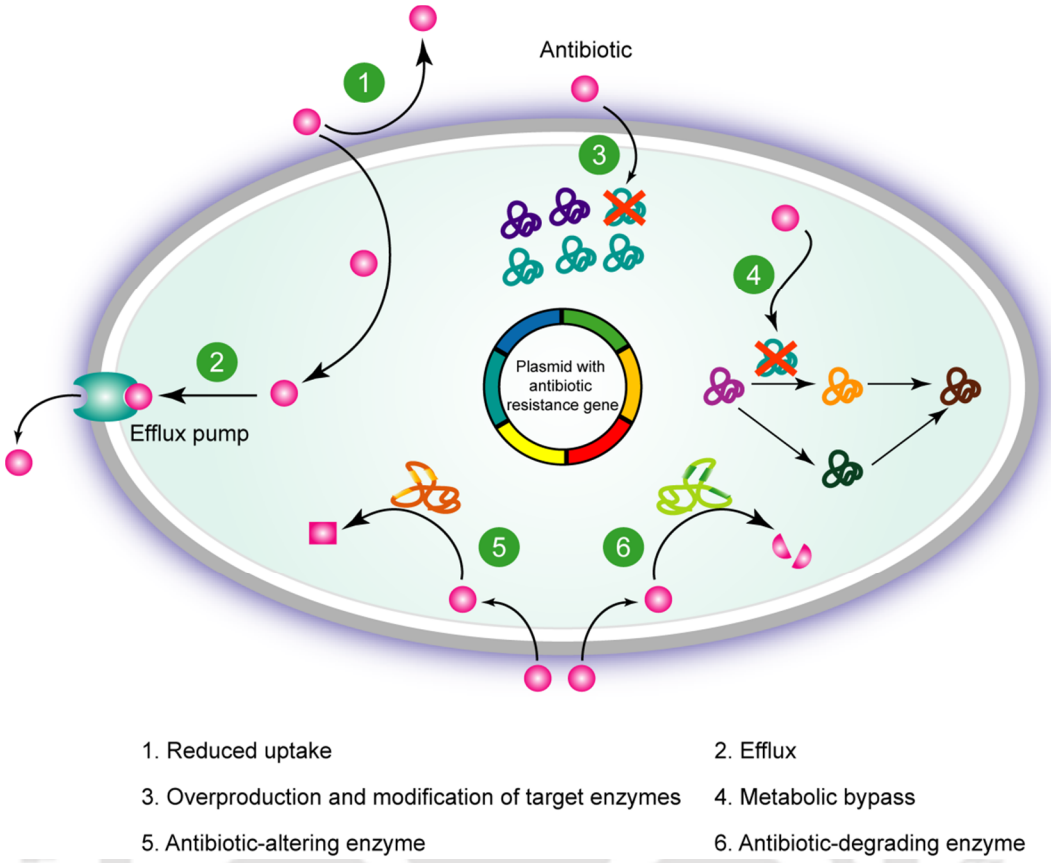

Figure 1.4. Mechanism of development of antibiotic resistance in pathogenic bacteria.

1.4.3. Antibacterial activity of silver nanoparticle

Silver has been known for its antimicrobial properties from ancient times. Silver either in metallic form or in ionic form demonstrates strong antibacterial activity which is both dose dependent (Shrivastava et al., 2007) and effective against a wide range of pathogens (Yamanaka et al., 2005; Lara et al., 2010; Shahverdi et al., 2007; Sarkar et al., 2007). Smetana et al. (2008) reported that silver nanoparticle (AgNP) of diameter less than 10 nm may attach to the sulfur containing proteins on bacterial cell wall causing rupture and eventual cell death. The activity of AgNP is also shape dependent as evidenced by a previous study where truncated AgNP displayed stronger antibacterial activity compared to spherical or rod shaped AgNP (Pal et al., 2007).

1.4.4. Antibacterial activity of copper nanoparticle

The antibacterial properties of copper has been widely utilized in advanced coating technologies, such as the design of materials for biomedical devices, hospital equipment, food processing and storage equipment, household materials, and antifouling paints (Avery et al., 1996; Stoimenov et al., 2002). Copper and its oxides are common biocides in a large number of commercial antifouling marine paints. Recent reports have shown that copper nanoparticle (Cu NP)/polymer composites exhibit antifungal and antibacterial properties (Cioffi et al., 2004; Cioffi et al., 2005a; Cioffi et al., 2005b; Ramstedt et al., 2007). Rastogi and Arunachalam demonstrated that bovine serum albumin-copper nanocomposites exhibit higher antimicrobial activity against gram-positive strains compared to gram-negative strains. The composite inhibited bacterial growth by damaging the bacterial cell membrane, leading to leakage of cytoplasmic content and cell death (Rastogi and Arunachalam, 2013). In another study, copper oxide nanoparticles synthesized by green synthesis method displayed antibacterial activity against both Gram-positive as well as Gram-negative pathogens and smaller size particles revealed higher antimicrobial activity (Padil and Černík, 2013). CuO nanocrystals have been shown to display concentration dependent antibacterial activity against *E. coli* by targeting the cell wall, eventually leading to cell death (Hassan et al., 2012).

1.4.5. Antibacterial action of zinc oxide nanoparticle

ZnO nanoparticles are believed to be nontoxic, biocompatible and have been also used as drug carriers, cosmetics, and fillings in medical materials, biocidal or disinfecting agent, anticancer agent (Rosi and Mirkin, 2005; Dutta et al., 2012). ZnO nanoparticles have been shown to exhibit bactericidal activity against *Campylobacter jejuni* and the antibacterial mechanism of ZnO nanoparticles was likely due to disruption of the cell membrane and oxidative stress (Xie et al., 2011). In another study, the antibacterial activity of ZnO nanoparticles against *Staphylococcus aureus* was dependent on the size of the nanoparticles and antibacterial activity was mainly due to the production of reactive oxygen species and the accumulation of nanoparticles in the cytoplasm or on the outer membrane (Raghupathi et al., 2011). Antibacterial potential of ZnO nanoparticles against

extended-spectrum β-lactamases-producing *Escherichia coli* and *Klebsiella pneumonia* has been reported by Ansari et al. (2012).

1.4.6. Chitosan-based nanocomposites as antibacterial agents

Chitosan, a positively charged polysaccharide biopolymer derived from chitin, is commonly found in shells of marine crustaceans and cell wall of fungi (Rabea et al., 2003). Chitosan exhibits a number of interesting biological properties such as antimicrobial activity, chelating and polycationic properties, biodegradability, biocompatibility (Das et al., 2013; Gan and Wang, 2007) and thus received great attention in the fields of medicine, food, chemicals, pharmaceuticals, and agriculture (Suginta et al., 2013). Porous chitosan/silver nanocomposite has been shown to exhibit superior antibacterial properties against Gram-negative bacteria as compared to Gram-positive bacteria (Das et al., 2013). Recently, Madhumathi et al. developed novel α- chitin/nanosilver composite scaffolds having excellent antibacterial activity against *S. aureus* and *E. coli* (Madhumathi et al., 2010). In another study, chitosan-Ag-nanoparticle composite was found to have significantly higher antimicrobial activity than its components at their respective concentrations against *Escherichia coli* (Sanpui et al., 2008). Chitosan thin films containing silver nanoparticle revealed antibacterial activity against gram-positive *S. aureus* and gram-negative *K. pneumoniae* and *E. coli* (Pinto et al., 2012).

A brief overview of various nanostructured materials used as antimicrobial agents is provided in Table 1.3.

Table 1.3. Various nanostructured materials used as antimicrobial agents.

Nanomaterials	Organism tested	MIC	Proposed mechanism	Reference
Gold nanoparticle	*E. coli*	4 µg/mL	Changes membrane potential, inhibit ATP synthase and inhibit the subunit of ribosome for tRNA binding	Cui et al., 2012
Copper iodide nanoparticle	DH5α *B. subtilis*	0.066 mg/mL 0.15 mg/mL	Membrane damage and ROS mediated DNA damage	Pramanik et al., 2012
CuO nanoparticles	*P. aeruginosa* *S. aureus*	28 ± 4 µg/mL 25 ± 4 µg/mL	Release of Cu^{2+} ions and oxidation of surface molecules of microbes	Azam et al., 2012
Copper nanoparticle	*E. coli*	3.0 µg/mL	Cell filamentation and inhibition of cell division	Chatterjee et al., 2012
Copper nanoparticle	*E. coli*	60 µg/mL	Formation of cavities/pits in the bacterial cell wall and reduction reaction at the bacterial cell wall	Raffi et al., 2010
Silica nanoparticle	*E. coli* *S. aureus*	2 µg/mL 1 µg/mL	Large surface area of the nano-size particles increase active sites to contact with bacteria for higher activity	Song et al., 2009
Silver nanoparticle	*E. coli*	50 µg/L	ROS generation	Zhang et al., 2013
Quantum dots	*E. coli*	200 nM	Oxidative damage caused by ROS	Lu et al., 2008
ZnO nanoparticle	*E. coli* O111	50 mg/L	Free zinc ions and labile zinc complex formation with biomecules	Li et al.,2011
ZnO nanoparticle	*S. aureus*	500 µg/mL	Hydrogen peroxide production	Seil and Webster, 2012
Silica nanoshells	*Escherichia coli* DH5α	0.75 µg/mL	Inhibition of DNA gyrase	Rosemary et al., 2006

Nanomaterials	Organism tested	MIC	Proposed mechanism	Reference
ZnO nanoparticles	*E. coli* *P. aeruginosa* *S. aureus*	500 µg/mL 500 µg/mL 125 µg/mL	Generation of ROS	Premanathan et al., 2011
Oleoyl-chitosan nanoparticles	*E. coli* *S. aureus*	125 mg/L	Destroying the integrity of bacterial cell membranes	Xing et al., 2008
Silver nanoparticle	*Bacillus subtilis* ATCC 6633	6.25 mg/L	Intracellular localization and biochemical changes relating to metal stress	Jain et al., 2009
Silver nanoparticle	*Staphylococcus aureus* CCM 3953	6.75 µg/mL	Cell membrane damage and interacting with phosphorus- and sulfur-containing compounds	Panacek et al., 2006
Silver nanoparticle	*Klebsiella pneumoniae*	27 µg/mL	Cell membrane damage and interacting with phosphorus- and sulfur-containing compounds	Panacek et al., 2006
Silver nanoparticle	*E. coli*	Reduced 70% with 10 µg/mL in agar	Membrane disruption, Ag ion interference with DNA replication	Sondi and Salopek-Sondi, 2004
Quantum dots	*E. coli*	1200 µg/mL	Generation of ROS	Luo et al., 2011
Chitosan nanoparticle	*E. coli K88* *S. typhimurium* ATCC 50013 *S. aureus* ATCC 25923	0.125 µg/mL 0.25 µg/mL 0.25 µg/mL	Disruption of cell membranes and the leakage of cytoplasm	Qi et al., 2004
Chitosan nanoparticle	*E. coli* *S. aureus*	117 µg/mL 234 µg/mL	Membrane disruption	Du et al., 2009
Copper nanoparticle	*Salmonella typhi* *E. coli* *S. aureus*	3.6 µg/mL 1.6 µg/mL 3.2 µg/mL	Dissipation of the proton motive force	Valodkar et al., 2012
Silver nanoparticle	*S. aureus* *E. coli*	180 µg/mL 15 µg/mL	Interaction of silver with the cell components	Taglietti et al., 2012

1.4.7. Nanoparticle-antibiotic combination therapy

Ruden et al. demonstrated the antimicrobial properties of silver ions and silver nanoparticles in combination with different antimicrobial peptides (AMPs) such as polymyxin B, gramicidin S. Silver nanoparticles together with polymyxin B, gramicidin S exhibit an additive effect whereas combination of silver nanoparticles and polymyxin B revealed synergy against gram-negative bacteria (Ruden et al., 2009). In another study, Park et al. (2011) described the antimicrobial activity of conjugates of the peptide antibiotic polymyxin B to Au nanoparticles and CdTe quantum dots. CdTe-polymyxin B conjugates were more toxic to *Escherichia coli* than polymyxin B alone. Vancomycin (Van)-functionalized Ag@TiO_2 nanoparticles revealed high UV light-driven bactericidal activity against Gram-positive bacteria and Au@Van nanoparticles exhibited enhanced activity against Van-resistant enterococci and Gram-positive bacteria (Wan et al., 2011; Gu et al., 2003). Recently, Allahverdiyev et al. reported interactions between nanoparticles and antibiotics, as well as other antibacterial agents to formulate new prospects for future studies (Allahverdiyev et al., 2011).

1.4.8. Anti-biofilm activity of nanoparticle

Biomedical devices and implants which are commonly used in the healthcare system are prone to bacterial colonization and leading to what is commonly known as biofilm. The ability of bacteria to develop antibiotic resistance and form biofilms is a major cause of medical implant-associated infections. Nanotechnology-driven approaches are expected to provide new opportunities for preventing and fighting biofilm-mediated infections. The surface functionalization of polyurethane and plastic catheters by silver nanoparticles (NPs) was shown to have anti-biofilm activity against a broad range of pathogenic strains (Roe et al., 2005). Lellouche et al. demonstrated the anti-biofilm activity of metal fluoride nanomaterials against two common nosocomial biofilm-forming pathogens, i.e. *Escherichia coli* and *Staphylococcus aureus* (Lellouche et al., 2009; Lellouche et al., 2012). Applerot et al. studied the anti-biofilm activity of a glass surface coated with zinc oxide (ZnO) nanoparticles against two common bacterial pathogens. The generation of hydroxyl radicals from the coated surface was implicated in the mode of action of the nanoparticles as an anti-biofilm agent (Applerot et al., 2012).

1.5. Mechanism of action of antibacterial nanomaterials

The precise pathways for nanoparticle mediated bactericidal activity are still emerging. In general, the composition, surface modification, intrinsic properties as well as the bacterial species itself play a role in the process of nanoparticle mediated bactericidal activity. The greater surface area to volume ratio of the nanoparticle compared to that of the bulk material is pivotal for nanoparticle activity against bacterial strains. Further, if the nanoparticle is positively charged it is able to interact electrostatically with the negatively charged bacterial membrane causing a subsequent disruption of the bacterial membrane (Thill et al., 2006). A large number of nanoparticles have been reported to act upon the bacterial membrane causing loss of cell viability. Likewise, nanoparticles of smaller size and positive zeta potential have been reported to be better antimicrobial agents. In another study, Sondi and coworkers (2004) reported that AgNP mediated bactericidal activity was not electrostatic interaction driven but rather dependent on the concentration of the nanoparticle itself. The silver nanoparticles were also reported to be involved with the formation of structures called “pits” in the cell wall of the bacteria. It has also been reported that Ag^{+} ions interact with thiol containing proteins causing their consequent inactivation (Hamm et al., 2012; Liau et al., 1997) Ag^{+} ions have also been reported to interfere with DNA replication process (Chadeau et al., 2012; Feng et al., 2000; Russell and Hugo, 1994). Nanoparticles are also known to induce the generation of reactive oxygen species (ROS) whereby peroxidation of membrane lipids may occur (Dutta et al., 2012). This assumption was validated by Liu et al. (2013), where they reported that silver decorated titania nanoparticles caused bactericidal effect through direct or indirect interaction with cell membrane causing lipid peroxidation, disruption of DNA replication and repair and inactivation of proteins important for respiratory process. An overview of various antibacterial mode of action of nanomaterials is indicated as a cartoon in Figure 1.5.

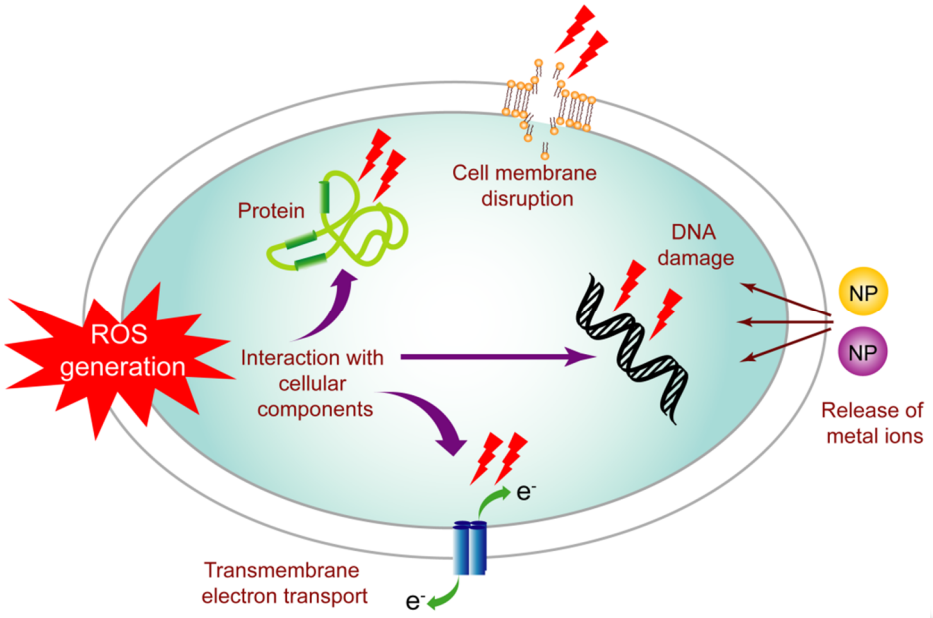

Figure 1.5. Mode of action of bactericidal activity of nanomaterials.

1.6. Toxicity of nanoparticles

The unique physicochemical properties of nanoparticles make them promising materials in the field of pharmaceutical, drug delivery, biomedical imaging, and bio sensing and food industries. However, biocompatibility, toxicity and the ability to penetrate cells are three critical factors which are very important for utility of nanoparticles in therapeutic applications. Nanoparticle may be toxic to the cells by releasing of toxic ions and nonspecifically binding to the biomacromolecules. Although nanomaterials are currently being widely used in modern technology, there is a dearth of information concerning the human health and environmental implications of manufactured nanomaterials. Among the various metal nanoparticles used in various field in biology and medicine, cytotoxic effects of these nanoparticle have been reported in eukaryotic systems. Recently, it was reported that single-wall nanotubes induce lung tissue damage in mice and causes acute lung toxicity by producing granulomas in rats at very high dose (Lam et al., 2004; Warheit et al., 2004). In another study it was shown that silver nanoparticles induce toxicity in neurons, which involves degradation of cytoskeleton components, perturbations of pre- and postsynaptic proteins, and mitochondrial dysfunction leading to cell death (Xu et al., 2013). It was reported that silver nanoparticle is cytotoxic to cultured keratinocytes,

fibroblasts, liver cells, alveolar macrophages and embryonic stem cells and embryonic fibroblasts (Ahamed et al., 2010). Silica nanoparticle exhibit dose and size dependent cytotoxicity towards human hepatoma HepG2 cells and in human embryonic kidney cells (Li et al., 2011; Wang et al., 2009). Toxicity of ZnO nanoparticle was also evaluated against primary mouse embryo fibroblast cells, human bronchial epithelial cells (BEAS-2B), RAW 264.7 and BEAS-2B cells (Yang et al., 2009; Heng et al., 2010; Xia et al., 2008). A recent study revealed that AuNPs caused oxidative stress in human lung fibroblasts after internalization and accumulation of AuNPs in human breast adenocarcinoma (MCF-7) cells resulted in mitochondrial depolarization and swelling (Li et al., 2010; Qiu et al., 2010).

Generation of reactive oxygen species (ROS) and oxidative stress appear to be two likely mechanisms of nanoparticle toxicity. ROS and oxidative stress stimulate a wide variety of physiologic and cellular events including stress, inflammation, DNA damage and apoptosis. Nanoparticles may generate ROS by various mechanism such as exposure of nanoparticle to an acidic environment such as the lysosome, either from the surface of the NPs or from leached ions, interaction of the nanoparticles with cellular organelles such as mitochondria, interaction of nanoparticles with redox active proteins such as NADPH oxidase, and interaction of nanoparticles with cell surface receptors and activation of intracellular signaling pathways (Soenen et al., 2011).

SCOPE AND SIGNIFICANCE OF THE PRESENT RESEARCH WORK

SCOPE AND SIGNIFICANCE OF THE PRESENT RESEARCH WORK

Based on the state of current knowledge on the use of nanomaterials in biology and medicine and the lacunae in the research area, the motivating factors for undertaking the present research project were identified. The rationale of the present research work is explained in the following sections:

Recent literature reports clearly validate the emerging trends in the area of nanomaterials and their applications in biology and medicine. One of the key issues in modern healthcare regime is the demand to develop rapid, sensitive and reliable methods of estimation of bacterial cells, especially in the context of clinical diagnosis. In this regard the advent of nanotechnology in recent years has ushered in great promise. Among the nanomaterials, gold nanoparticles (AuNPs) are particularly appealing in terms of their unique size-dependent properties, biocompatible chemistry and facile functionalization. It is envisaged that these favorable attributes can be exploited to develop rapid, cost effective, sensitive and high-throughput estimation of bacteria, with a future potential to develop miniaturized and automated sensitive devices for bacterial detection.

The emergence of drug-resistant pathogenic bacteria is a global healthcare problem of great concern. To counter this challenge, an innovative therapeutic approach is the need of the hour, for which development of novel and efficient bactericidal agents, radically different from conventional antibiotics is critical. The use of nanoscale materials as bactericidal agents represents a particularly innovative option. The high surface area to volume ratio of nanomaterials is suitable to achieve enhanced interactions with the target pathogen and their unique physicochemical attributes can be explored to generate potent bactericidal nanocomposites. Moreover, development of antibacterial nanocomposites which exhibit a membrane-targeted activity can perhaps defy the conventional drug-resistance mechanism rampant in bacterial pathogens. While working with new antibacterial nanocomposites a crucial aspect is to decipher the detailed mechanism of action of the developed nanomaterials on bacterial cells. An in-depth study revealing the fundamental basis of the interactions would facilitate the development of newer nanomaterials with potent therapeutic applications.

Finally there is an enormous window of opportunity to generate bactericidal nanocomposites which are highly selective to pathogenic bacteria with minimal cytotoxic effects. These nanocomposites would then enable the development of future designer therapeutics which can be specifically used to eliminate the target pathogen without causing any adverse effect on either host cells or the host gut commensal microbiota. In this direction, the use of safe antimicrobial peptides to develop bactericidal nanocomposites represents a particularly attractive option.

Essentially it is envisaged that the present investigation would enable the development of a comprehensive nanomaterial-based platform for rapid estimation of bacterial cell numbers for future sensing applications. Additionally, the nanomaterial-based bactericidal agents developed in the present work would serve as prototype studies to generate biocompatible and potent antibacterials with potential therapeutic implications.

SPECIFIC OBJECTIVES
OF THE RESEARCH WORK

SPECIFIC OBJECTIVES OF THE RESEARCH WORK

In the background of the literature reviewed in Chapter 1 and by identifying the scope and significance of the present research work, the following specific objectives were defined:

1. Development of a facile method of bacterial cell estimation based on poly-L-lysine (PLL) mediated aggregation of gold nanoparticles. A major goal of this project was to develop a method which is non-invasive with minimal sample handling steps, analytically simple, sensitive, applicable to a wide range of bacterial cells and with a future potential to develop a sensor device.

2. Studies on the bactericidal efficacy and membrane-directed activity of a gold nanoparticle-polythiophene (AuNP-PTh) composite. Development of membrane-targeting nanoscale antibacterials bear special merit since the probability of developing resistance against such bactericidal agents requires an extensive revamp of membrane components, which is a physiologically demanding task for the bacteria.

3. Studies on potential therapeutic applications of AuNP-PTh composite. This project entails three major goals: (a) Ascertain the utility of AuNP-PTh as an adjuvant to potentiate the action of therapeutic antibiotics in combinatorial assay (b) Determine the bactericidal efficacy against model gastro-intestinal pathogens in simulated gastric fluid (SGF) and (c) Evaluate the anti-biofilm activity of AuNP-PTh.

4. Generation of potent bactericidal nanocomposites based on safe antimicrobial peptides (AMPs). The FDA approved bacteriocin nisin which was chosen as a model AMP is known to loose its biological activity at physiological pH due to loss in solubility. In this project the essential aim was to develop a ‘soft tailoring’ strategy for nisin so as to improve its solubility and retain its biological activity at physiologically relevant pH. To achieve this goal the endeavor was to generate

nisin-organic acid complex and nisin-citrate stabilized AuNP composites and evaluate their antimicrobial activity at elevated pH.

5. The final objective was to advance the goal of generating safer bactericidal nanocomposites with natural AMPs. Herein, the idea was to test the feasibility of employing anionic nanoparticles to selectively capture the cationic bacteriocin pediocin, which is an AMP secreted by a food-grade lactic acid bacterium. A major endeavor in this project was to explore magnetic anionic nanoparticles as nano-baits for efficient capture of the bacteriocin from the culture filtrate and generate bactericidal nanocomposites.

Chapter 2

Estimation of Bacterial Cells Based on Poly-L-lysine Mediated Aggregation of Gold Nanoparticles

This chapter describes a rapid and sensitive estimation of viable bacterial cells in solution based on a systematic decrease in the degree of poly-L-lysine (PLL)-mediated aggregation of citrate-stabilized gold nanoparticles (AuNPs). This method is applicable to a wide range of bacterial strains with a sensitivity of 10 CFU.

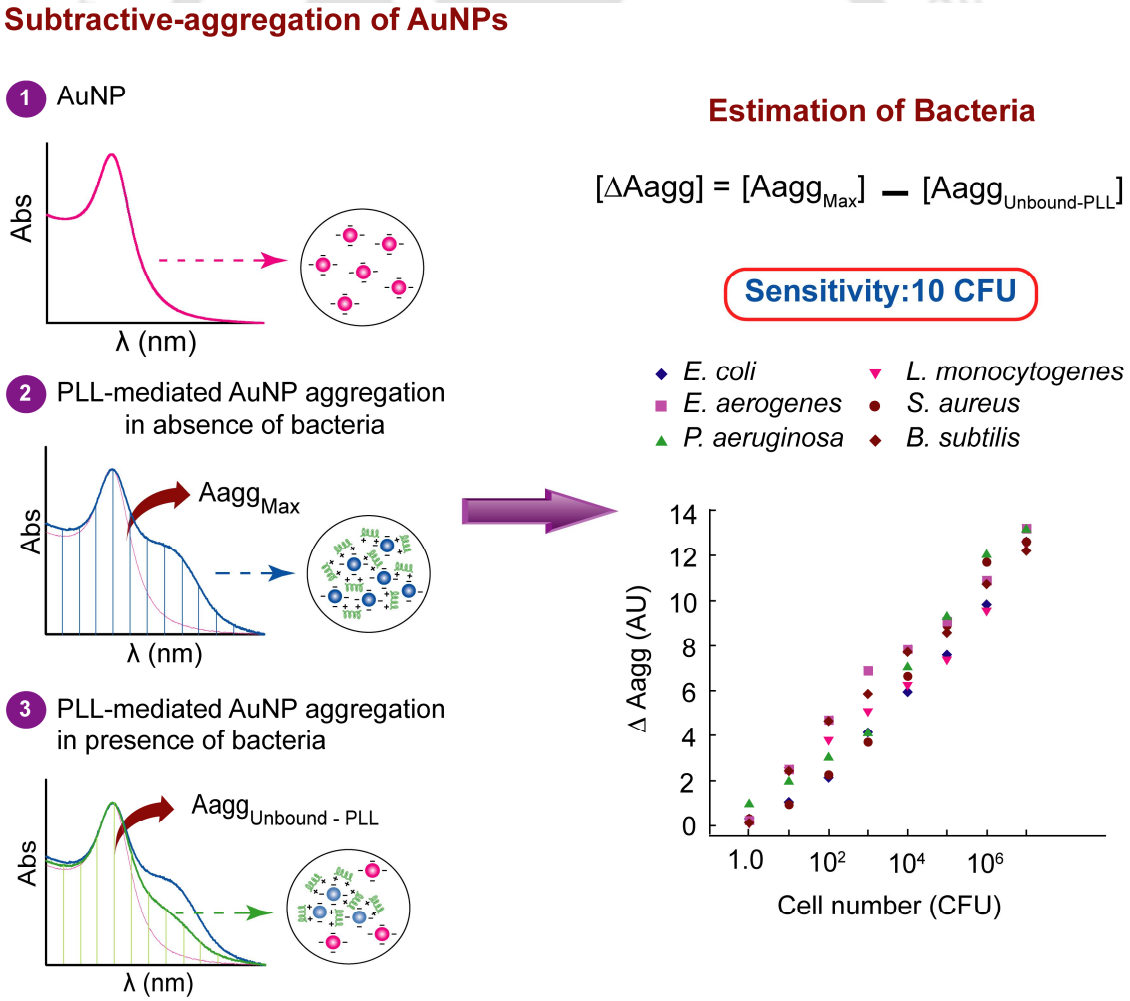

ABSTRACT

The investigation outlined in this chapter describes a new method for sensitive estimation of viable bacterial cells in solution based on a systematic decrease in the degree of poly-L-lysine (PLL)-mediated aggregation of citrate-stabilized gold nanoparticles (AuNPs). Quantification of cells was pursued by interacting bacterial cell suspensions with PLL and recovering the unbound PLL fraction which was subsequently used to promote aggregation of AuNPs. In the absence of any bacterial cells, AuNP-PLL interaction leads to maximum AuNP aggregation observed through a large broadening of the SPR peak of AuNPs. When bacterial cells in solution were used as a bait to sequester PLL, there was a decline in AuNP aggregation mediated by unbound PLL. This decline in AuNP aggregation, which accounted for bacterial cell number, can be referred as "subtractive-aggregation". For cell estimation a measure of subtractive-aggregation was obtained from the difference in area (ΔAagg) under the extinction curve between maximum aggregation ($Aagg_{Max}$) and aggregation due to unbound PLL ($Aagg_{Unbound\text{-}PLL}$) following initial interaction of bacterial cells with PLL. Using this method, cell numbers of a wide range of bacterial strains which included Gram-negative *Escherichia coli* MTCC 433, *Enterobacter aerogenes* MTCC 2822 and *Pseudomonas aeruginosa* MTCC 2488 as well as Gram-positive *Bacillus subtilis* MTCC 1305, *Staphylococcus aureus* MTCC 740 and *Listeria monocytogenes* Scott A could be estimated with a sensitivity of 10 colony forming units (CFU). Importantly, the method was specific for viable cells and a centrifugal filter device could be used to expedite the overall process and facilitate rapid estimation of bacterial cells in solution based on the same principle used herein. The application potential and reliability of the method was further validated in an antimicrobial susceptibility test, wherein estimation of viable cell numbers of target bacteria *Leuconostoc mesenteroides* NRRL B640 following treatment with the antimicrobial peptide nisin was on par with conventional plating. The developed method of bacterial cell estimation offers a distinct advantage over other conventional methods in terms of ease of operation, rapidity, high sensitivity and quantitative estimation of viable cells.

2.1. Introduction

There is a growing demand to develop rapid, sensitive and reliable methods of estimating bacterial cell numbers especially in the regime of clinical diagnosis, food safety, and environmental monitoring. In the context of pathogenic bacteria, this assumes even greater significance as the presence of even a single viable cell may entail serious health concerns. Conventional methods for estimating bacterial cells rely on standard microbiological tools such as plating in a specific growth media. This process is arduous and lacks sensitivity, and hence undesirable especially when rapid diagnosis is paramount. In recent times, nucleic acid-based methods such as polymerase chain reaction (PCR) and immunoassays have been developed to achieve high sensitivity and specificity (Mancini et al., 2010; Lauri and Mariani, 2009; Geng et al., 2004; Tokarskyy and Marshall, 2008; Mothershed and Whitney, 2006; de le Rica et al., 2009; Xu et al., 2012). However, these assays depend on critical selection of appropriate target genes and target antigens, which can be tricky and overall the methods are invasive, costly and protracted. New generation detection methods such as magneto-sensors, electrochemical impedance spectroscopy and quartz crystal microbalance biosensor have emerged as an alternate, which offers fast detection, great sensitivity and specificity (Lu et al., 2009; Maalouf et al., 2007; Shen et al., 2007; Joo et al., 2012; Pera et al., 2010; Tun et al., 2011). However, the relatively high degree of sophistication in instrumentation and personnel expertise required for implementing these tools may have to be addressed prior to their routine application.

The emergence of nanotechnology in recent years has ushered in great promise in the field of diagnostics and therapeutics. Nanoparticles (NPs) represent a particularly interesting platform, displaying unique size-dependent properties. Literature reports on the application of nanoscale materials in biology and medicine are abundant (Agasti et al., 2010; De et al., 2008). Amongst metal NPs, AuNPs have been particularly interesting and have rendered a wide array of biological applications (Sperling et al., 2008; Murphy et al., 2008; Cobley et al., 2011). Depending on their size, shape, degree of aggregation, and local environment, AuNPs exhibit a characteristic surface plasmon resonance (SPR), which can be exploited in developing a bio-responsive probe (Deka et al., 2008; Deka et al., 2009; Deka et al., 2010, Zhao et al., 2008; Huang et al., 2007; Jain et al., 2007; Dreaden et al., 2012). Nanoparticle-based detection systems for probing macromolecules such as proteins,

nucleic acids, and pathogens have been reported (Xia et al., 2010; Fournier-Wirth and Coste, 2010; Tong et al., 2013; Dykman and Khlebtsov, 2012; Chang et al., 2013; Liandris et al., 2011; Sundaram et al., 2013). Nanotechnology-based tools have also been implemented for detection of bacterial cells. For instance, magnetic glyco-nanoparticles have been used to specifically detect *E. coli* with a detection limit of 10^4 cells/mL (El-Boubbou et al., 2007). Rapid and specific detection of *Mycobacterium avium* spp. *paratuberculosis* was demonstrated on the basis of magnetic relaxation with antibody-functionalized superparamagnetic iron oxide nanoparticles, and detection of the pathogen was also demonstrated in a complex matrix like milk and blood (Kaittanis et al., 2007). In another study, magnetic nanoparticles functionalized with antibodies were used in combination with infrared fingerprinting to detect *E. coli* O157:H7 and *S. typhimurium* in food matrix (Ravindranath et al., 2009).

While specific detection of pathogenic bacteria is important and draws immense attention, there is a constant impetus to develop broad-affinity based methods which can provide a platform based on a universal principle and facilitate detection or estimation of cell numbers of a range of bacterial strains. In this regard, vancomycin-functionalized nanoparticles have been used as small molecule probe to detect various Gram-positive and Gram-negative bacteria (Kell et al., 2008). In another study, metal oxide coated magnetic NPs were allowed to interact with bacteria bearing lipopolysaccharide (LPS) via metal phosphate chelation followed by MALDI-MS analysis, which could identify potential biomarker ions for various Gram-negative pathogenic bacteria such as *Escherichia coli* O157:H7, *Shigella sonnei*, *Pseudomonas aeruginosa* and *Klebsiella pneumonia* (Chen et al., 2008).

Bacterial cells are known to be negatively charged and this characteristic trait is largely ascribed to the presence of either teichoic acid in Gram-positive bacteria or the outer membrane lipopolysaccharide (LPS) in Gram-negative bacteria (Berry et al., 2005; Wilson et al., 2001). In the context of developing a detection system which is versatile and universally applicable to a wide group of bacterial strains, the anionic charge characteristics of bacterial cell surface can be envisaged as an attractive option to mediate electrostatic interactions with an oppositely charged sensor probe. In a previous study the potential application of a fluorescent gold nanoparticle-polythiophene nanocomposite in

estimating various bacterial strains has been demonstrated. The quantification was based on loss of the fluorescence intensity of the positively charged nanocomposite upon interaction with negatively charged bacterial cell surface (Panda et al., 2008). Rapid and discriminatory identification of bacteria has been demonstrated using an array of AuNP-conjugated polymer constructs. The basis was the displacement of anionic conjugated polymer from cationic NPs by negatively charged bacterial surfaces (Phillips et al., 2008). In a recent study, glyco-dendronized poly-L-lysine (PLL) has been used to bind to cell-surface carbohydrate receptors and detect *E. coli* by microscopic analyses (Laurino et al., 2011).

In the present investigation a rapid and sensitive method of estimating bacterial cells in solution was developed for which the fundamental idea was to use the polycationic species PLL and set off aggregation of negatively charged citrate-stabilized AuNPs. PLL being polycationic, also has a propensity to interact electrostatically with bacterial cells. The approach for estimation of bacterial cell numbers was to initiate bacteria-PLL interactions, separate unbound PLL fraction and measure the extent of aggregation of AuNPs by the unbound fraction of PLL. This phenomenon is referred to as "subtractive-aggregation" wherein the extent of AuNP aggregation by unbound PLL provides a measure of bacterial cell numbers. The charge-based interaction of PLL with bacterial cells rendered a generality to the method resulting in estimation of cell numbers in solution for a wide variety of bacterial strains with a lower detection limit of 10 CFU. Interestingly, this charge-based interaction also allowed the method to be specific for viable bacterial cells. The utility and reliability of the subtractive-aggregation method in an antimicrobial susceptibility test is also demonstrated wherein the viable cell count obtained for target bacteria following treatment with a potent antimicrobial agent by both conventional plating as well as the present method were highly comparable.

2.2. Materials and Methods

2.2.1. Chemicals and growth media

Gold (III) chloride solution, ($HAuCl_4$), poly-L-lysine (PLL) hydrochloride (molecular weight ranging from 15,000-30,000), propidium iodide (PI) and nisin were procured from Sigma-Aldrich Chemicals, U.S.A. $HAuCl_4$ was obtained as a 30 wt % solution in dilute

HCl. Nutrient broth (NB), Brain-Heart Infusion (BHI) broth and deMan, Rogosa and Sharpe (MRS) broth were purchased from HiMedia, Mumbai, India. Tri-sodium citrate 2-hydrate was procured from Merck Chemicals, Mumbai, India.

2.2.2. Bacterial strains

The bacterial strains used in the present investigation consisted of Gram-positive strains of *Staphylococcus aureus* MTCC 740 (*S. aureus*), *Listeria monocytogenes* Scott A (*L. monocytogenes*), *Bacillus subtilis* MTCC 1305 (*B. subtilis*) and *Leuconostoc mesenteroides* NRRL B640 (*L. mesenteroides*) and the Gram-negative bacterial strains included *Escherichia coli* MTCC 433 (*E. coli*), *Pseudomonas aeruginosa* MTCC 2488 (*P. aeruginosa*) and *Enterobacter aerogenes* MTCC 2822 (*E. aerogenes*). *S. aureus* MTCC 740 and *L. monocytogenes* Scott A were propagated in BHI broth at 37^{o}C and 180 rpm for 12 h, whereas *B. subtilis* MTCC 1305, *E. coli* MTCC 433, *P. aeruginosa* MTCC 2488 and *E. aerogenes* MTCC 2822 were grown in NB medium at 37^{o}C and 180 rpm for 12 h. *L. mesenteroides* NRRL B640 was grown in MRS broth at 37^{o}C in a static incubator for 18 h.

2.2.3. Preparation of citrate-stabilized gold nanoparticle

The well established method of citrate reduction of $HAuCl_4$ was followed for synthesis of gold nanoparticles (AuNPs) as mentioned in an earlier study (Deka et al., 2009). As described in an earlier method. Briefly, a 10 mL aliquot of 1% (w/v) tri-sodium citrate 2-hydrate solution was added to 90 mL of MilliQ grade water and heated to boiling. Subsequently 1.0 mL of 1.72×10^{-2} M $HAuCl_4$ solution was added to the boiling solution and the mixture was refluxed for another 20 min till the solution turned ruby red in color indicating formation of AuNPs. Following synthesis, a 1.0 mL portion of the AuNP solution was taken in a cuvette and the UV-visible extinction spectrum was recorded (Cary 300, Varian, USA). An aliquot of the synthesized AuNP sample was also subjected to transmission electron microscope (TEM) analysis. (JEOL, JEM-2100F Transmission Electron Microscope, Japan)

2.2.4. Interaction of citrate-stabilized AuNPs and poly-L-lysine

A stock solution of PLL was prepared in MilliQ grade water at a concentration of 10^{-4} % (w/v). In a series of 2.0 mL microcentrifuge tubes, 1.5 mL portions of citrate-stabilized AuNP solution (0.25 nM) was taken to which various volumes of PLL (10 µL to 200 µL) was added. The addition of PLL to AuNP solution was pursued drop wise to achieve adequate mixing. The final volume of the mixture in every tube was adjusted to 1.9 mL with MilliQ grade water so as to achieve an approximate concentration of PLL in the range of 5.2 x 10^{-7}, 10.5 x 10^{-7}, 21 x 10^{-7}, 31.5 x 10^{-7}, 42 x 10^{-7}, 52 x 10^{-7}, 63 x 10^{-7}, 73.6 x 10^{-7}, 84 x 10^{-7}, 95 x 10^{-7} and 105 x 10^{-7} % w/v. In separate sets of samples, AuNPs and the indicated concentrations of PLL were interacted at room temperature for 15 min, 30 min and 60 min. The control samples consisting of 1.5 mL portion of citrate-stabilized AuNP solution and 0.4 mL of MilliQ grade water was also incubated under the same conditions. Following incubation at room temperature for the aforementioned time periods, UV-visible extinction spectrum of the samples was recorded at a wavelength set from 400-800 nm. The area under the UV-visible extinction spectrum was estimated using OriginPro 7.0 (OriginLab Corporation, MA, USA). All measurements were taken from three independent experimental samples. Aliquots of the sample from the series were also subjected to TEM analysis.

2.2.5. Studies on interaction of PLL and bacterial cells

The primary objective of this study was to ascertain the effect of concentration and interaction time of PLL with bacterial cells. Bacterial cells were harvested from a 1.0 mL aliquot of an overnight grown culture of Gram-negative *E. coli* MTCC 433 and Gram-positive *L. monocytogenes* Scott A by centrifugation at 8,000 rpm for 3 min. The cells were washed twice with sterile phosphate-buffered saline (PBS) to remove residual media components and then resuspended in 0.2 mL sterile PBS in separate tubes to achieve a cell number of 10^2, 10^4 and 10^6 CFU. Various volumes (10 µl – 200 µl) of PLL stock solution were added separately to 0.2 mL of bacterial cells and the final volume was made upto 0.4 mL with sterile PBS to achieve a PLL concentration range of 0.25 x 10^{-5}, 0.5 x 10^{-5}, 1.0 x 10^{-5}, 3.0 x 10^{-5}, 3.5 x 10^{-5}, 4.0 x 10^{-5} and 5.0 x 10^{-5} % w/v. The final bacterial cell concentrations in the samples were 10^2, 10^4 and 10^6 CFU per 0.4 mL. The samples were

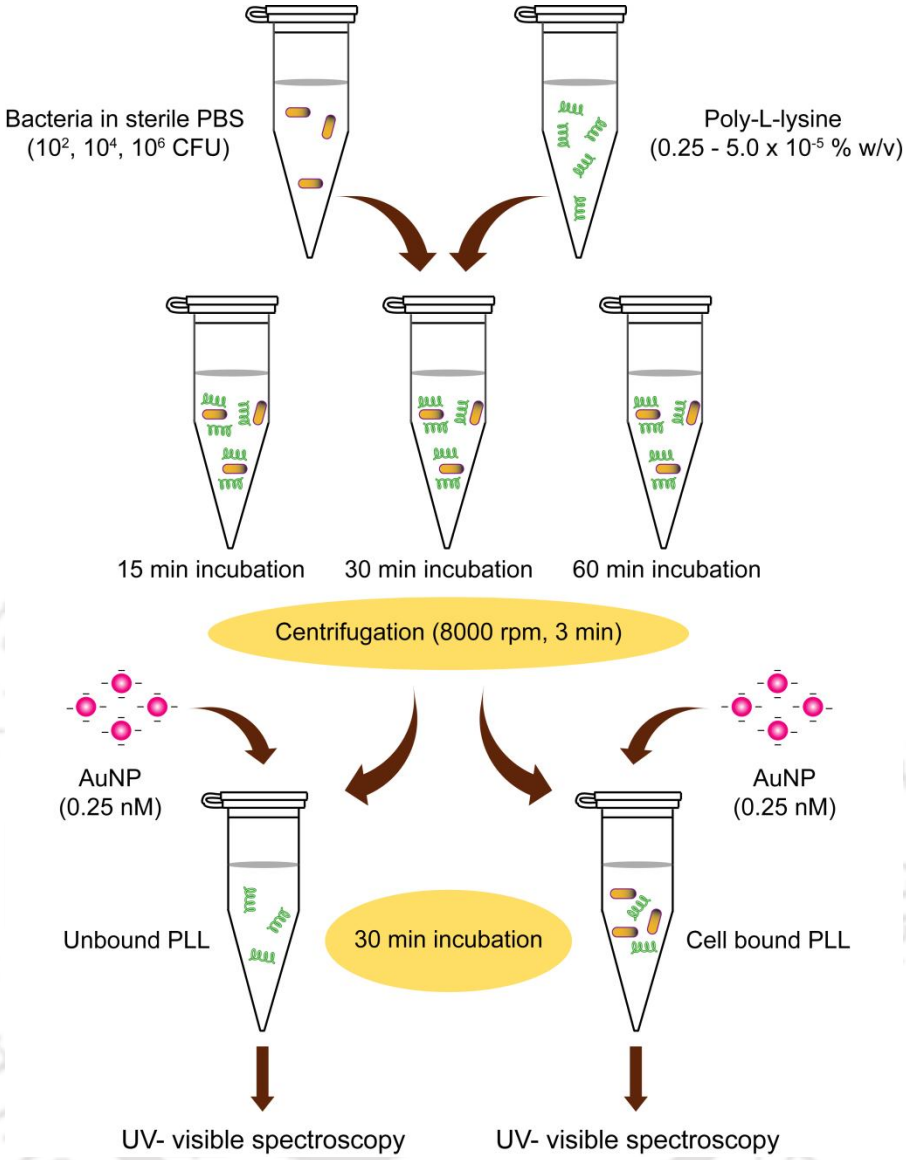

Figure 2.1. Schematic protocol to study interaction of PLL and bacterial cells.

incubated at room temperature under mild shaking condition for 15, 30 and 60 min. Subsequently the bacterial cells were separated by centrifugation at 8,000 rpm for 3 min and the recovered supernatant which was essentially unbound PLL (nearly 0.4 mL) was added drop wise to 1.5 mL citrate-stabilized AuNP taken in a fresh microcentrifuge tube and incubated at room temperature for 30 min. Likewise, the cell pellet which represented bacterial cells bound with PLL were resuspended in 0.4 mL sterile PBS and added separately to a 1.5 mL aliquot of citrate-stabilized AuNP and incubated at room

temperature for 30 min. UV-visible extinction spectrum of all the samples were recorded for three independent experimental samples and the area under each extinction spectrum was estimated. A schematic depicting the various steps of the experimental protocol to study PLL-bacterial cell interactions is indicated in Figure 2.1. Additional control experiments were also performed to study the effect of the order of addition of the three interacting components namely bacterial cells, PLL and AuNPs on the broadening of the extinction spectrum of AuNPs. The description of these experiments is provided in the following section.

2.2.6. Control experiments

The control experiments were conducted to study the effect of the order of addition of the three interacting components namely bacterial cells, PLL and AuNPs. All these experiments were conducted with bacterial cultures of *E. coli* MTCC 433 and *L. monocytogenes* Scott A.

In control experiment I, bacterial cells (in 0.2 mL sterile PBS) in the range of 10^2, 10^4 and 10^6 CFU were taken separately in tubes to which 0.2 mL of PLL solution was added to achieve a final PLL concentration of 3.5×10^{-5} % w/v in 0.4 mL. To this 1.5 mL of citrate-stabilized AuNP solution was added drop wise. The samples were mixed and incubated at room temperature under shaking condition for 30 min. Control samples were included devoid of either bacterial cells or PLL. UV-visible extinction spectrum of all the samples was recorded and the area under each extinction spectra was estimated as mentioned before.

In control experiment II, 0.2 mL of PLL solution was taken and added separately to 1.5 mL of citrate-stabilized AuNP solution. The mixtures were incubated at room temperature for 30 min following which 10^2, 10^4 and 10^6 CFU bacterial cells (in 0.2 mL sterile PBS) were added to the tubes separately and incubated at room temperature under mild shaking condition for 30 min. In the control samples, 0.2 mL of sterile PBS only (devoid of bacterial cells) was added to the tubes having pre-incubated PLL solution and citrate stabilized AuNP solution. UV-visible extinction spectrum of all the samples was recorded and the area under each extinction spectra was determined.

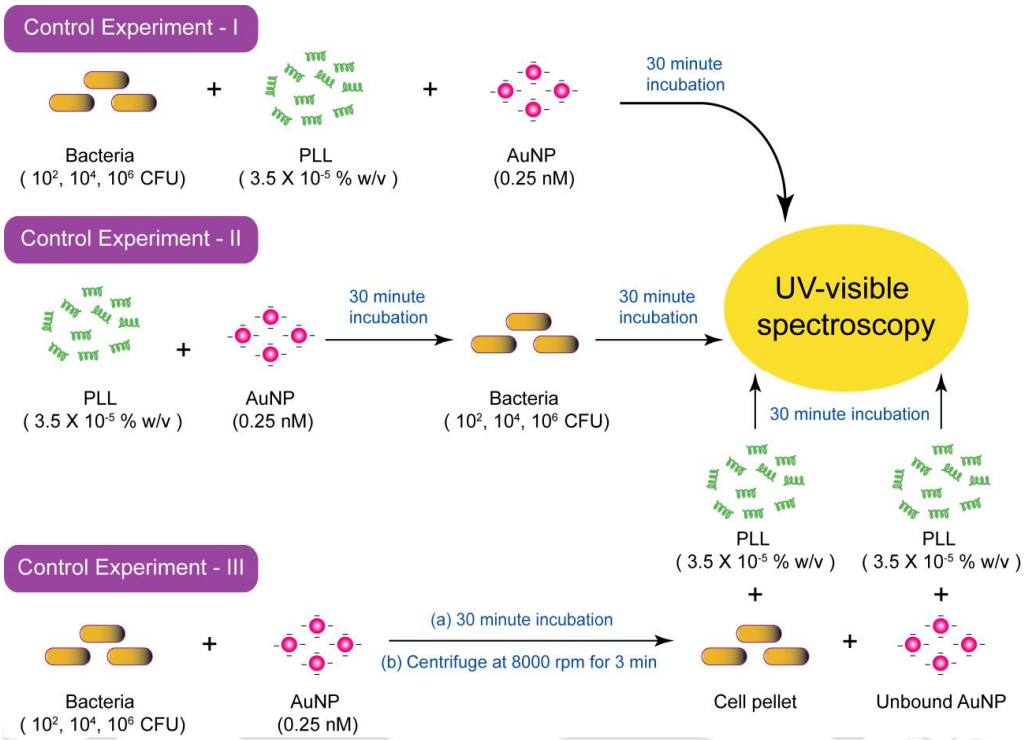

Figure 2.2. Schematic representation of control experiments to study interaction of PLL and bacterial cells.

In control experiment III, bacterial cells of varying concentrations (10^2, 10^4 and 10^6 CFU in 0.2 mL sterile PBS) were taken in separate tubes to which 1.5 mL AuNP solution was added. In the control sample, only 0.2 mL sterile PBS was added to 1.5 mL AuNP solution. All the samples were incubated for 30 min at room temperature under mild shaking condition. Subsequently, the samples were centrifuged at 8,000 rpm for 3 min. The supernatant from all the samples was recovered (nearly 1.7 mL) to which 0.2 mL of PLL was added. The samples were incubated at room temperature for 30 min and UV-visible extinction spectrum was recorded. Bacterial cell pellet recovered after centrifugation was also resuspended in 0.2 mL sterile PBS to which 0.2 mL of PLL was added to achieve a final concentration of 3.5 x 10^{-5} % w/v in 0.4 mL. To this 1.5 mL AuNP solution was added. The samples were incubated at room temperature for 30 min and UV-visible extinction spectrum was recorded. Area under each extinction spectra was determined for all samples. A schematic representing the various control experiments is indicated in Figure 2.2.

2.2.7. Effect of PLL on bacterial cell viability

A 0.2 mL aliquot of PLL (3.5 x 10^{-5} % w/v) was added to varying cell numbers (10^2, 10^4 and 10^6 CFU) of *E. coli* MTCC 433 and *L. monocytogenes* Scott A suspended in 0.2 mL sterile PBS and incubated at room temperature for 30 min and 60 min under mild shaking conditions. Following incubation, the samples were plated to determine the viable cell numbers. A control sample consisting of untreated bacterial cells was also included. Cell viability was also determined by inoculating both PLL-treated and untreated samples into culture media and monitoring the growth of the cells by measuring absorbance at 600 nm in a microtitre plate reader (Infinite M200, TECAN, Switzerland).

2.2.8. Estimation of bacterial cell numbers

For estimation of cell numbers, Gram-positive bacterial strains of *Staphylococcus aureus* MTCC 740, *Listeria monocytogenes* Scott A, *Bacillus subtilis* MTCC 1305 and Gram-negative strains of *Escherichia coli* MTCC 433, *Pseudomonas aeruginosa* MTCC 2488 and *Enterobacter aerogenes* MTCC 2822 were selected. Cells were harvested from a 1.0 mL aliquot of an overnight grown culture broth by centrifugation at 8,000 rpm for 3 min. The cells were washed twice with sterile PBS and then resuspended in 0.2 mL sterile PBS to achieve a logarithmic series of cell number in the range of 1.0-10^7 CFU. A 0.2 mL portion of PLL solution was added separately to the series of tubes with varying cell number to achieve a final PLL concentration of 3.5 x 10^{-5} % w/v in 0.4 mL. Thus the bacterial cell concentrations in the samples ranged from 1.0-10^7 CFU per 0.4 mL. The samples were incubated at room temperature under mild shaking condition for 30 min. Subsequently the bacterial cells were separated by centrifugation at 8,000 rpm for 3 min. The recovered supernatant consisting of unbound PLL was added to 1.5 mL of citrate-stabilized AuNP solution and incubated at room temperature for 30 min. Subsequently UV-visible extinction spectrum of all the samples were recorded as mentioned before and the area under each extinction spectrum was estimated. The control samples consisted of (i) bacterial solution or PLL alone (both were volume adjusted to 0.4 mL) added to 1.5 mL of AuNP solution and (ii) volume adjusted AuNP solution alone. The areas under UV-visible extinction spectrum were considered for calculating the difference between the areas due to maximum aggregation of AuNP by PLL alone ($Aagg_{Max}$) and aggregation of

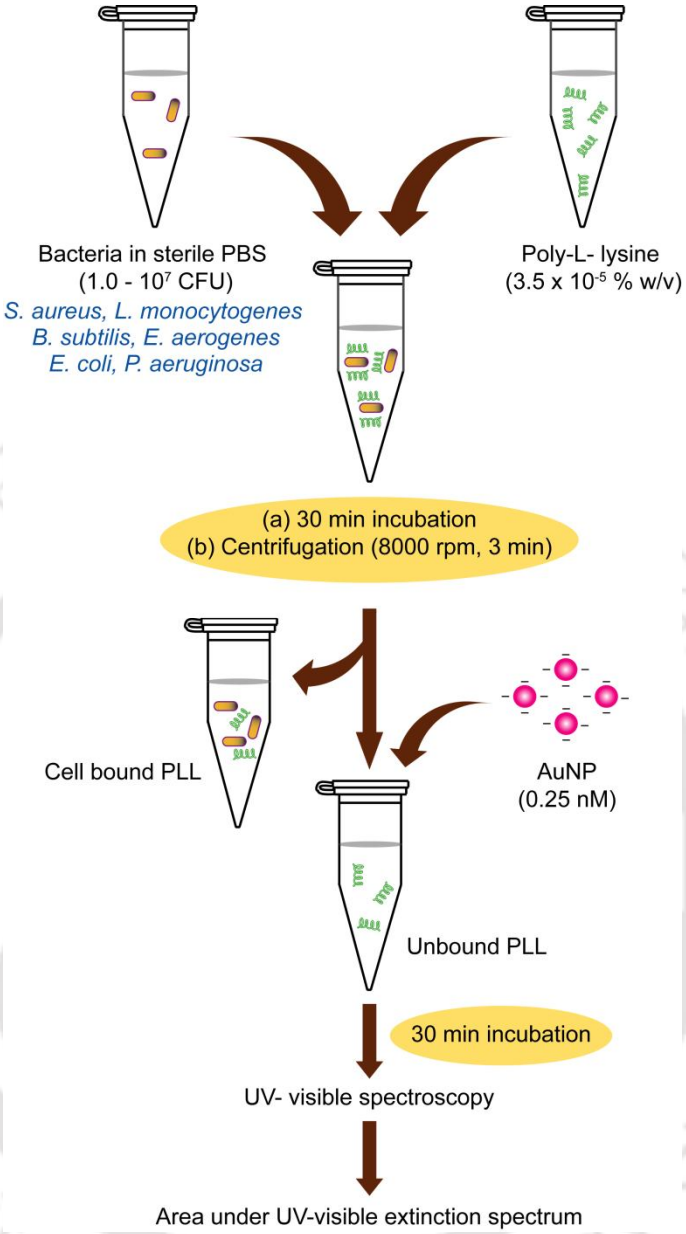

Figure 2.3. Schematic protocol for estimation of bacterial cells in solution based on PLL-mediated aggregation of AuNPs.

AuNP by unbound PLL ($Aagg_{Unbound\text{-}PLL}$) for every sample of the series ranging from 1.0-10^7 CFU. The difference in the areas gave a measure of subtractive-aggregation (ΔAagg) and a plot between ΔAagg and bacterial cell number was constructed. A two-way analysis of variance (ANOVA) followed by all pair wise multiple comparison (Holm-Sidak method) was performed using Sigma Plot version 11.0. A schematic indicating the

experimental protocol to estimate bacterial cell numbers in solution based on PLL-mediated aggregation of AuNPs is indicated in Figure 2.3.

2.2.9. Estimation of cell numbers in centrifugal device

Cells of *E. coli* MTCC 433 and *L. monocytogenes* Scott A were taken in the range of 1.0-10^7 CFU in 0.2 mL sterile PBS and interacted with 0.2 mL PLL (final concentration of 3.5 $x10^{-5}$ % w/v in 0.4 mL) in a microcentrifuge tube. Following 30 minutes of interaction, the contents of the tube were added to Costar Spin-X centrifuge tube having a 0.22 µm cellulose acetate membrane filter (Sigma-Aldrich, USA) and spun immediately at 8,000 rpm for 1 min. The bacterial cells with bound PLL were entrapped in the filter whereas the unbound PLL fraction (nearly 0.4 mL) was collected as flow through in the collection tube. As mentioned earlier, 1.5 mL AuNP solution was then added to the unbound PLL fraction and incubated for 30 minutes. Aggregation of AuNP was determined by recording the UV-visible extinction spectrum of the samples and determining the area under each spectrum. As mentioned earlier in section 2.2.8, bacterial cell numbers were estimated from the measure of subtractive-aggregation (ΔAagg). A schematic representing the protocol to estimate bacterial cell numbers in the centrifugal device is indicated in Figure 2.4.

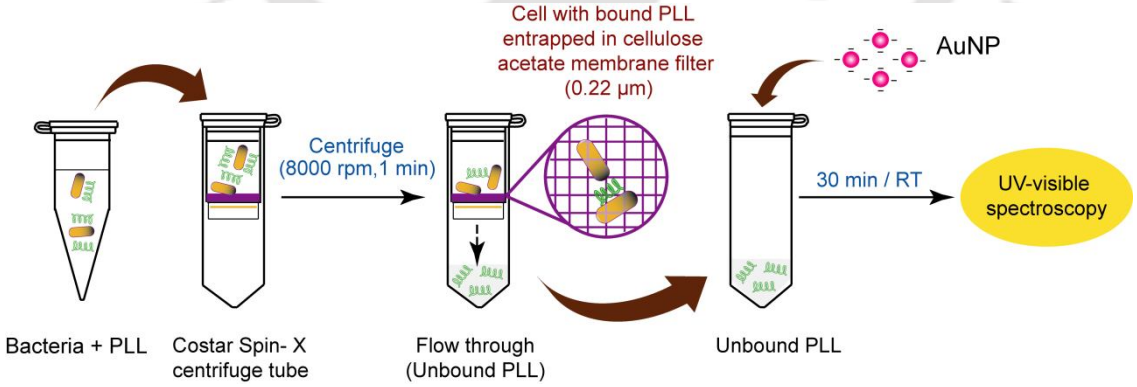

Figure 2.4. Schematic representation of estimation of bacterial cells in centrifugal device.

2.2.10. Interaction with heat-treated bacterial cells

In this set of experiments, varying cell numbers of *E .coli* MTCC 433 (10^2, 10^4 and 10^6 CFU) were taken in separate tubes in 500 µL of sterile PBS and subjected to heat treatment at 55°C, 65°C, 80°C for 30 min each and autoclaving at 121°C and 15lb/in^2 for 20 min. To verify bacterial cell death and membrane damage following various heat treatments, aliquots of the samples were (i) subjected to plating to determine viable cell numbers, (b) re-inoculated in fresh growth media to ascertain the effect of heat treatment on cell viability and (c) stained with propidium iodide (PI) to ascertain membrane damage in bacterial cells. The detailed description of staining of bacterial cells with PI is provided in section 2.2.11. Subsequently, 0.2 mL of PLL solution was added separately to heat-treated bacterial cells (in 0.2 mL sterile PBS) to achieve a final PLL concentration of 3.5 x 10^{-5} % w/v in 0.4 mL. The samples were incubated at room temperature under mild shaking condition for 30 min. The bacterial cells were then separated by centrifugation at 8,000 rpm for 3 min and the supernatant consisting of unbound PLL was added to 1.5 mL of AuNP solution and incubated at room temperature for 30 min. UV-visible extinction spectrum of all the samples were recorded and the area under the curve was used to estimate bacterial cell numbers by subtractive-aggregation as mentioned before in section 2.2.8. The control sample consisted of either heat-treated bacterial cells in solution or PLL alone (both were volume adjusted to 0.4 mL) added to 1.5 mL of AuNP solution. A schematic of the protocol of heat-treatment of bacterial cells and estimation of their cell numbers by subtractive-aggregation method is indicated in Figure 2.5.

2.2.11. Propidium iodide (PI) staining of heat-killed bacterial cells

A 1.5 mM stock solution of propidium iodide (PI) of relative molecular weight Mr 668 (Sigma-Aldrich, USA) was prepared in sterile MilliQ water. Following heat-treatment, bacterial cells were washed with sterile MilliQ water and PI was added to the cells at a final concentration of 30 µM. After 10 min of incubation in a circulating water bath incubator (Amersham, USA) set at 37°C, samples were centrifuged and washed in sterile MilliQ water to remove excess dye and the cells were resuspended in 1.0 mL of sterile MilliQ grade water. A 10 µl aliquot of the PI stained sample was spotted on a clean glass slide, air dried and observed under fluorescence microscope (Axioskop2MAT, Carl Zeiss,

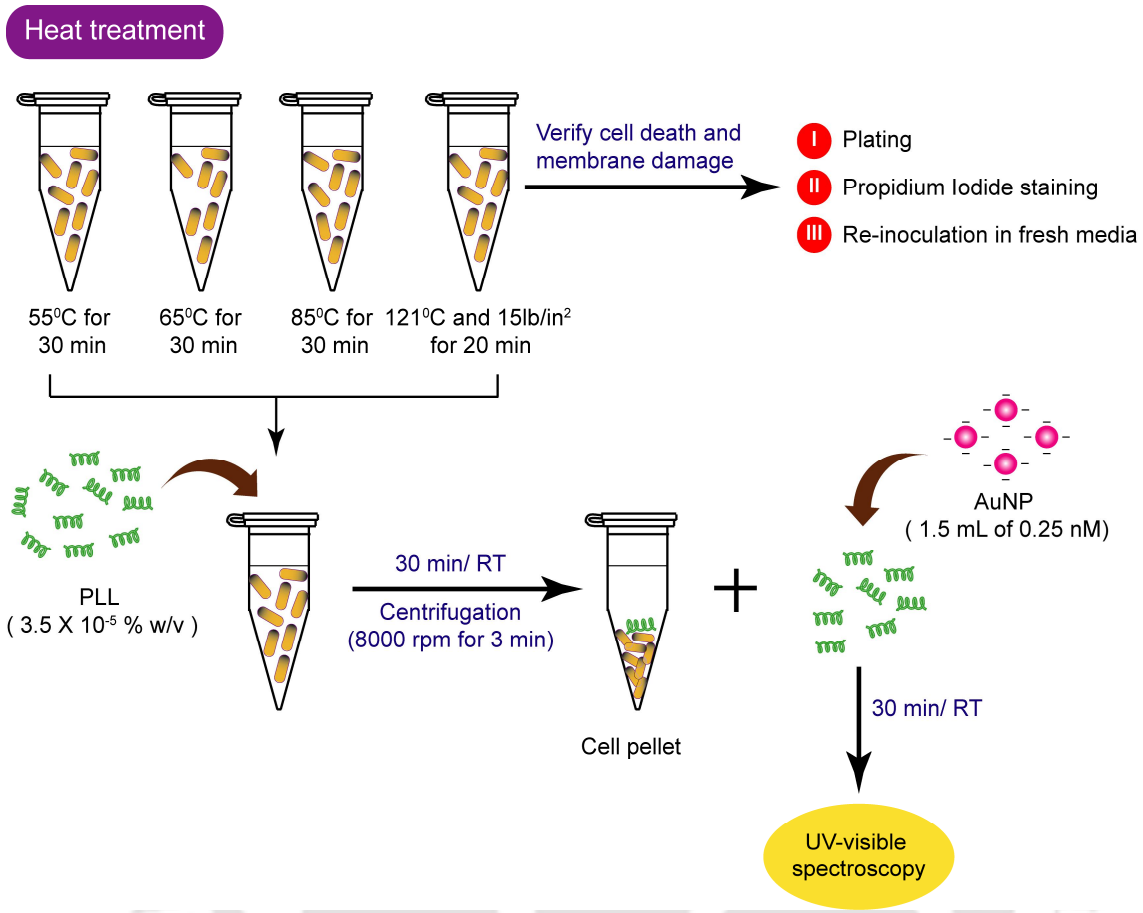

Figure 2.5. Protocol for heat-treatment of bacterial cells and estimation of cells based on PLL-mediated aggregation of AuNPs.

Oberkochen, Germany) with green light excitation at 495-570 nm and long pass filter above 617 nm.

2.2.12. Potential application in antimicrobial susceptibility test

The potential of the subtractive-aggregation method of bacterial cell estimation as a tool to determine viable cell numbers was determined following exposure of the cells to nisin, which is a well characterized antimicrobial peptide. Initially, the antimicrobial activity of nisin was verified against the target bacteria *L. mesenteroides* NRRL B640 by a conventional agar well diffusion assay as follows: A stock solution of nisin (10,000 IU/mL) was made in 0.75% NaCl (pH 5.3). The assay plate had a bottom layer of MRS medium (deMan-Rogosa and Sharpe) with agar (1.5% agar), which was overlaid with

MRS soft agar (0.8% agar) seeded with 10^6 cells of freshly grown target strain of *L. mesenteroides* NRRL B640. Requisite number of holes of 6 mm diameter was punched in the assay plate. To each well, 50 µl of test sample (1000 IU/mL, 800 IU/mL, 400 IU/mL, 200 IU/mL, 100 IU/mL, 50 IU/mL nisin and 0.75% NaCl, pH 5.3) was added. The plates were pre-incubated at 4°C for 3 h to facilitate diffusion of the sample followed by incubation at 37°C for 24 h. Nisin activity of the samples was determined by observing the zone of inhibition produced around the wells.

Estimation of cell numbers of *L. mesenteroides* NRRL B640 by subtractive-aggregation method following treatment with nisin was pursued as follows: Initially a calibration plot between subtractive-aggregation areas (ΔAagg) and varying cell numbers of *L. mesenteroides* NRRL B640 (1.0-10^7 CFU) was constructed by adopting the general method of bacterial cell estimation described in section 2.2.8. To ascertain the viability of *L. mesenteroides* NRRL B640 cells upon treatment with nisin, the target bacteria was initially propagated in MRS broth as described in section 2.2.2. The cells were harvested by centrifugation, washed with sterile PBS and a 1.0 mL aliquot of the cells (corresponding to 10^6 CFU) in sterile PBS were taken in several microcentrifuge tubes to which various volumes of nisin solution was added (10 µl, 20 µl, 40 µl, 80 µl) from a stock solution (10000 IU/mL) so as to achieve a final nisin concentration of 100, 200, 400 and 800 IU/mL, respectively. The cells were incubated for 12 h. Following, treatment with nisin, the cells were harvested by centrifugation and resuspended in 0.2 mL of sterile PBS. To this, 0.2 mL of PLL solution was added (3.5 x 10^{-5} % w/v) and the samples were incubated at room temperature for 30 min under mild shaking conditions. Subsequently, samples were centrifuged and 1.5 mL of citrate-stabilized AuNP solution was added to the supernatant and incubated further for 30 min at room temperature. UV-visible extinction spectrum of the samples was recorded and area under each spectrum was calculated. In case of nisin treated samples, cell numbers for *L. mesenteroides* NRRL B640 were ascertained using the previously generated calibration curve of subtractive-aggregation areas (ΔAagg) and varying cell numbers of *L. mesenteroides* NRRL B640 (1.0-10^7 CFU). To test the reliability and accuracy of the subtractive-aggregation method in estimating cell numbers, cells of *L. mesenteroides* NRRL B640 were treated with varying concentrations of nisin as described earlier and following treatment, the samples were serially diluted and

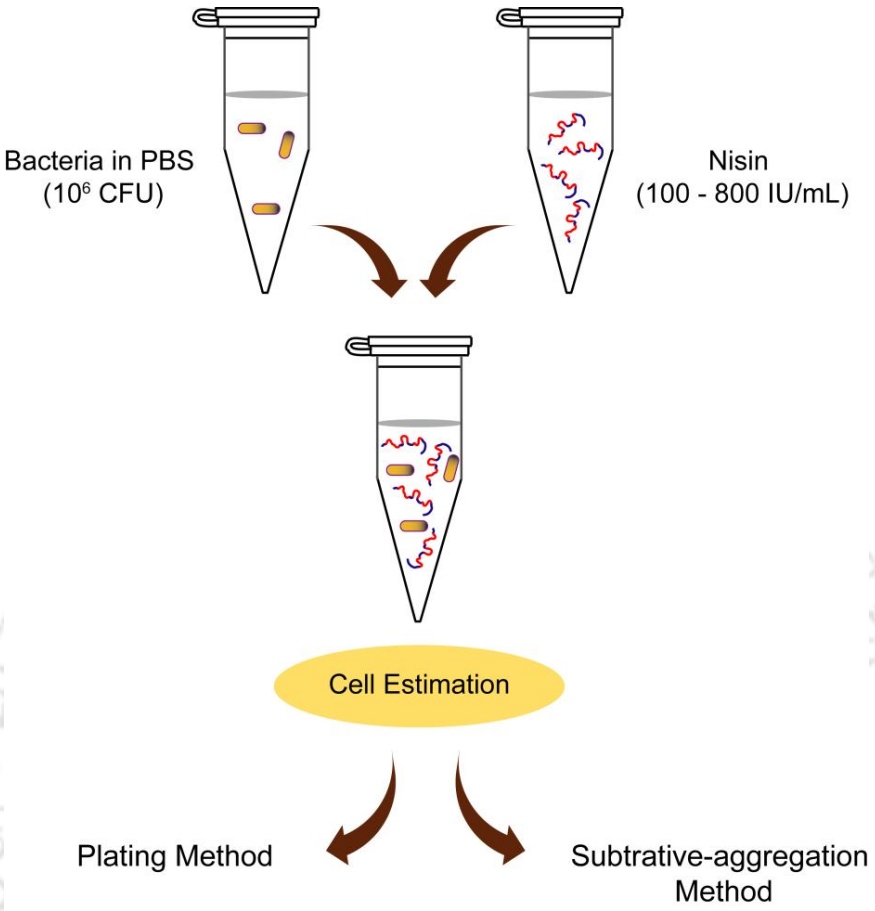

Figure 2.6. Schematic representation of estimation of bacterial cell numbers by plating and subtractive-aggregation method following treatment with nisin.

plated to determine viable cell number. A schematic of the protocol of estimation of bacterial cell numbers by subtractive-aggregation method following treatment with the antimicrobial peptide nisin is indicated in **Figure 2.6.**

2.3. Results and Discussion

2.3.1. Characterization of citrate-stabilized AuNPs

Citrate-stabilized AuNPs used in the present investigation was synthesized by following the well established citrate reduction method **(**Deka et al., 2009**)**. As evident from Figure 2.7a, a solution of the synthesized AuNPs exhibited a prominent extinction peak at 520 nm, which is the characteristic SPR band for AuNPs (Cobley et al., 2011). TEM analysis revealed that the AuNPs were well dispersed and spherical in shape (Figure 2.7b). The average particle size as determined using ImageJ software (http://rsb.info.nih.gov/ij) was observed to be 12.0 ± 2.0 nm (Figure 2.7c).

2.3.2. PLL-mediated aggregation of AuNPs

Aggregation of negatively charged citrate-stabilized AuNPs in presence of varying concentrations of the polycationic PLL was pursued by interacting varying concentrations of PLL and AuNPs in solution for 15, 30 and 60 min following which UV-visible spectral measurements were taken. Figure 2.8a indicates the UV-visible extinction spectra after 30 min of AuNPs and PLL interaction. It is clear from the figure that a distinct broadening of the extinction spectra of AuNPs was evident upon an increase in the concentration of PLL. It is also notable that beyond a PLL concentration of 84 x 10^{-7} % w/v there was only

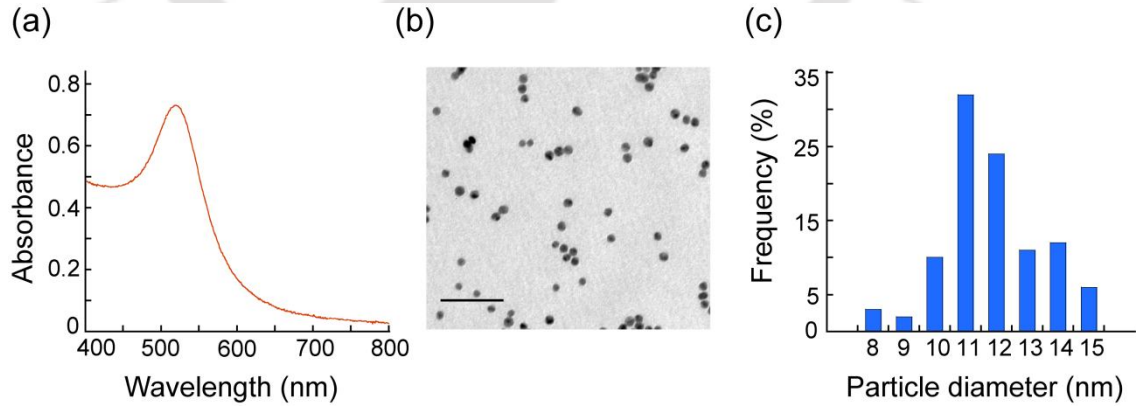

Figure 2.7. (a) UV-visible extinction spectra of citrate-stabilized AuNPs. **(b)** Transmission electron micrograph of AuNPs. The scale bar is 50 nm. **(c)** Particle size distribution of AuNPs using ImageJ software (http://rsb.info.nih.gov/ij).

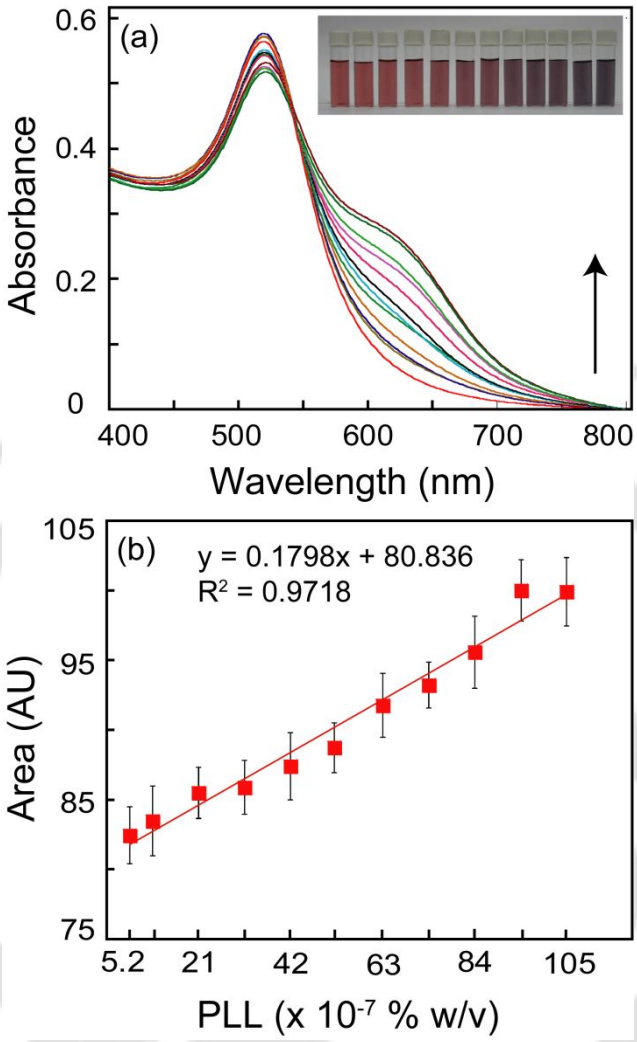

Figure 2.8. (a) UV-visible spectrum of citrate-stabilized AuNPs with increasing concentration of PLL. Spectral measurements were performed following 30 min of addition of PLL solution to AuNPs. The lowest trace (red color) is for the control sample consisting of AuNP alone. The subsequent traces were obtained with increasing concentration of PLL (0.25×10^{-5}, 0.5×10^{-5}, 1.0×10^{-5}, 3.0×10^{-5}, 3.5×10^{-5}, 4.0×10^{-5} and 5.0×10^{-5} % w/v) as indicated by arrow. Inset represents image of vials of AuNP solution in the presence of increasing concentration of PLL (left to right). **(b)** Area under the UV-visible spectrum for samples in (a) as a function of PLL concentrations.

marginal broadening probably indicating saturation. Further, there was no shift of the absorbance maximum in the samples, although at higher concentrations of PLL a hump

appeared at higher wavelength, which is a well-known phenomenon, associated with localized SPR spectra of AuNPs. With increasing concentration of PLL a change in the color of AuNP solution from ruby red to deep violet was also manifested (inset of Figure 2.8a). When the area under the UV-visible extinction spectrum was estimated, a systematic increase was observed as a function of PLL concentration with a saturation observed at PLL concentrations of 95 x 10^{-7} and 105 x 10^{-7} % w/v (Figure 2.8b). In order to study the effect of incubation time of PLL and AuNPs on spectral broadening, measurements were also taken after 15 min and 60 min interaction of PLL and AuNP (refer to Figure A2.1 in Appendix). It was observed that in case of samples wherein PLL and AuNPs were interacted for 15 min the extent of spectral broadening and the corresponding area under extinction spectrum (refer to Figure A2.1a and A2.1c in Appendix) was less than that for 30 min (Figure 2.8a and 2.8b) and 60 min (refer to Figure A2.1b and A2.1d in Appendix) interaction time, respectively. In the context of linear response of AuNP aggregation as a function of PLL concentration it was observed that the best response was obtained for 30 min interaction time (R^2 value of 0.97) followed by 60 min and 15 min interaction time (R^2 value of 0.96 and 0.95, respectively). Based on the results obtained in these experiments UV-visible spectral measurements were taken after 30 min incubation of PLL with AuNPs for all subsequent experiments.

Poly-L-lysine hydrochloride (molecular weight ranging from 15,000-30,000) renders a large number of positively charged residues, which can interact electrostatically with negatively charged citrate-stabilized AuNPs, resulting in a concentration-dependent aggregation of AuNPs. To ascertain this phenomenon, TEM analysis of citrate-stabilized AuNPs as well as AuNPs in presence of various concentrations of PLL was conducted. It is clear from Figure 2.9a that as synthesized citrate-stabilized AuNPs were spherical in shape and well dispersed. With addition of increasing concentration of PLL, a progressive increase in AuNP aggregation was manifested (Figure 2.9b-d). At lower concentrations of PLL (21 x 10^{-7} % w/v), isolated clusters of aggregated AuNPs could be observed along with a few dispersed particles (Figure 2.9b). With further increase in PLL concentration to 42 x 10^{-7} % w/v, the size of the clusters increased (Figure 2.9c). At high PLL concentration of 84 x 10^{-7} % w/v, bulk of the particles were involved in the formation of aggregates and the sizes of such aggregates were evidently larger than that obtained at lower

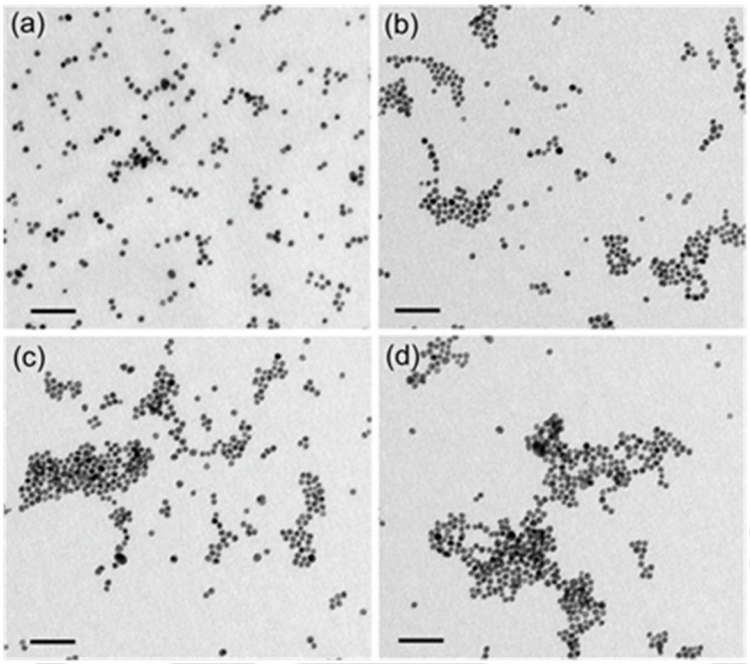

Figure 2.9. Transmission electron microscope (TEM) images of **(a)** as synthesized citrate-stabilized AuNPs, and **(b-d)** AuNPs in the presence of increasing concentration of PLL (21 x 10^{-7}, 42 x 10^{-7}, and 84 x 10^{-7} % w/v, respectively). Scale bar for all the images is 50 nm.

concentrations of PLL (Figure 2.9d). Representative higher magnification TEM images for select samples of PLL-aggregated AuNPs are also represented in Figure A2.2 in Appendix. Overall, the TEM experiments clearly revealed a progressive increase in the aggregation of AuNPs with increasing PLL concentration and this perhaps explains the broadening of UV-visible spectra observed in the samples, following interaction of PLL and AuNPs. In this context, measurement of particle size could also have been a good quantitative indicator of PLL-driven aggregation of AuNPs in solution.

2.3.3. PLL-bacterial cell interaction studies

The primary objective of the present work was to develop a fast, convenient and sensitive method of estimating bacterial cell numbers in solution. An important criterion in this endeavor was to develop a broad-based working principle so as to permit estimation of a wide range of bacterial cells. In this context the characteristics of the bacterial cell surface provided the critical lead. It is well known that the bacterial cell surface is negatively

charged at near neutral pH and this feature is largely attributed to the presence of teichoic acid in Gram-positive bacteria and lipopolysaccharide (LPS) in Gram-negative bacteria (Berry et al., 2005; Wilson et al., 2001). It can thus be conceived that a positively charged polymeric species like PLL would readily interact with the bacterial cell surface based on electrostatic interaction. If PLL is taken in stoichiometric excess, some fraction of the polymer would be bound to bacterial cells while the unbound fraction could then be separated and used for initiating aggregation of negatively charged citrate-stabilized AuNPs. It is also rational to comprehend that an increase in bacterial cell numbers in solution would result in greater sequestration of the positively charged PLL by negatively charged bacterial cells, leading to reduced amount of the polymer as unbound fraction and consequently the degree of aggregation of AuNPs by the unbound PLL would also decrease correspondingly. Hence a measure of the extent of aggregation of AuNPs by unbound PLL can be used as a tool to estimate bacterial cell numbers and this formed the basis of the present endeavor.

The concentration of PLL and its interaction time with bacterial cells are critical parameters which may influence the final estimation of cell numbers based on aggregation of AuNPs by unbound PLL. To address these issues, Gram-negative *E. coli* MTCC 433 and Gram-positive *L. monocytogenes* Scott A cells (10^2, 10^4 and 10^6 CFU each) were interacted with varying concentrations of PLL (0.25 - 5.0 x 10^{-5} % w/v) for various time periods and then the unbound fraction of PLL was used to initiate aggregation of AuNPs in solution. It is important to mention that the concentration of PLL used for these experiments (refer to section 2.2.5) were higher compared to earlier experiments where AuNP aggregation was pursued at different concentrations of PLL (refer to section 2.2.4), so as to ensure recovery of sufficient unbound PLL fraction. The salient observation in these experiments was that AuNP aggregation increased as a function of PLL concentration for both *E. coli* MTCC 433 as well as *L. monocytogenes* Scott A, as evident from the broadening of UV-visible extinction spectrum (Appendix, Figure A2.3 and A2.4) and corresponding increase in the area under the curve (Figure 2.10). This increase in area was observed across every cell number used in the experiments (10^2, 10^4 and 10^6 CFU) as well as the various interaction times between PLL and bacterial cells (15, 30 and 60 min). It can be presumed that with increasing PLL concentrations, the fraction of

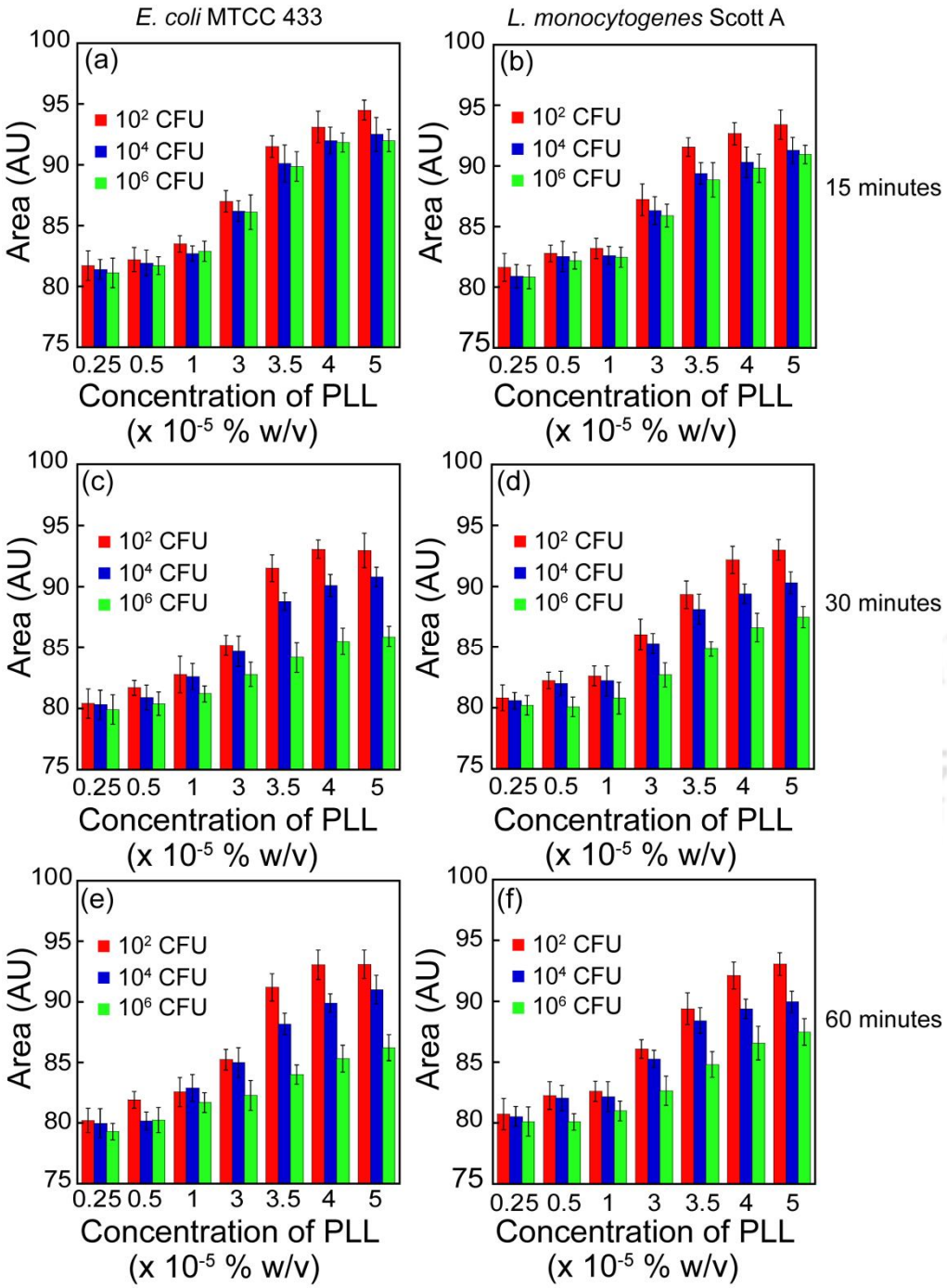

Figure 2.10. Area under UV-visible extinction spectrum following PLL interaction with varying bacterial cell number. PLL concentrations indicated in the plots represent the initial concentrations used for interaction with bacterial cells.

unbound PLL shows a corresponding increase and thus accounts for a systematic increase in AuNP aggregation and area under extinction spectrum. Quantitative differences in the area under extinction spectrum amongst samples representing various cell numbers (10^2, 10^4 and 10^6 CFU) were prominently manifested in case of 30 and 60 min of interaction between 3.5 x 10^{-5} % w/v PLL and bacterial cells. For instance, in case of *E. coli* MTCC 433, at a PLL concentration of 3.5 x 10^{-5} % w/v and 30 min interaction time **(**Figure 2.10c), difference in the areas under the curve correlated with differences in cell numbers (91.52, 88.8 and 84.2 AU, corresponding to 10^2, 10^4 and 10^6 CFU, respectively). This correlation between area under the curve and cell numbers was also consistent in case of *L. monocytogenes* Scott A (Figure 2.10d). It is also noteworthy that the calculated areas under extinction spectrum corresponded to the linear range of response of AuNP aggregation as a function of PLL concentration (refer to Fig. 2.8b). In case of 15 min interaction time between bacterial cells and PLL, the corresponding difference in area was only marginal (Figure 2.10a and 2.10b). It can be surmised that an extended interaction time between PLL and bacterial cells (30 and 60 min) resulted in quantitative sequestration of PLL from solution as a function of bacterial cell numbers and the degree of aggregation of AuNP by unbound PLL was inversely correlated with bacterial cell numbers. This fact was also substantiated by TEM analysis (Appendix, Figure A2.5), wherein both the number as well as sizes of AuNP aggregates appear to be larger for the sample with 10^2 CFU in comparison to the sample with 10^4 CFU of *E. coli* MTCC 433. When the initial PLL concentration was enhanced to 4.0 x 10^{-5} and 5.0 x 10^{-5} % w/v, the differences in the areas with respect to varying cell numbers were observed to reduce in magnitude, which perhaps indicates a saturation effect. Based on the results obtained, it is clear that an initial interaction time of 30 min between 3.5 x 10^{-5} % w/v PLL and bacterial cells was suitable to achieve quantitative cell estimation in the shortest time.

It is significant to mention that bacterial cell numbers could not be estimated by following aggregation of AuNPs by cell-bound PLL as the UV-visible extinction spectrum coincided with the control sample (AuNP alone), indicating lack of AuNP aggregation (Appendix, Figure A2.6). A pertinent objective of the present investigation was to ascertain the effect of the sequence of addition of the three interacting components namely bacterial cells, PLL and AuNPs for which various experiments were set up (refer to control

experiments in section 2.2.6). When varying concentrations of bacterial cells, PLL and AuNPs were incubated together for 30 min, bulk of the PLL was involved in causing rapid aggregation of AuNPs in solution and hence the UV-visible extinction spectrum (Appendix, Figure A2.7a and A2.7b) and areas under extinction spectrum for *E. coli* and *L. monocytogenes* failed to reflect differences in cell numbers (Appendix, Figure A2.8a and A2.8b). In another experiment, initial interaction of PLL and AuNPs resulted in substantial aggregation of AuNPs and a hump was observed at a higher wavelength in the extinction spectrum (Appendix, Figure A2.7c and A2.7d). Subsequent addition of *E. coli* MTCC 433 or *L. monocytogenes* Scott A failed to disrupt the PLL-AuNP complex, and thus the areas under extinction spectrum failed to reflect quantitative differences in cell numbers (Appendix, Figure A2.8c and A2.8d). Further, when varying concentrations of bacterial cells were initially interacted with AuNPs, binding of AuNPs by bacterial cells was minimal as both the bacterial cells as well as citrate-stabilized AuNPs possess negative charge. Thus when the unbound AuNPs were recovered and incubated with PLL, the extent of spectral broadening for AuNPs revealed no significant difference for varying cell numbers (Appendix, Figure A2.7e, A2.7f and Figure A2.8e, A2.8f). Based on the control experiments it was thus established that quantitative estimation of bacterial cell numbers in solution could be readily pursued by initially interacting PLL and bacterial cells followed by recovery of unbound PLL and measuring the extent of aggregation of AuNPs by the unbound PLL fraction.

2.3.4. Effect of PLL on cell viability

The initial interaction of PLL and bacterial cells was a key element in the present method of estimating bacterial cells. Hence, it was pertinent to investigate the effect of PLL on bacterial cell viability as there are reports suggesting that PLL may affect cell viability (Yoshida and Nagasawa, 2003; Conte et al., 2007). However, in the present investigation, the viability of bacterial cells was not affected. For instance, when approximately 6.6×10^6 CFU *E. coli* MTCC 433 per 0.4 mL sample volume was interacted with 3.5×10^{-5} % w/v PLL, the viable cell count obtained after 30 min and 60 min of interaction was determined to be 6.5×10^6 CFU. Similar observations were recorded for *L. monocytogenes* Scott A. Even at lower cell numbers (10^4 and 10^2 CFU), bacterial cell viability was unaffected by

PLL. Further when PLL-interacted cells were re-inoculated into fresh growth media and incubated overnight, high media turbidity resulted indicating cell growth. It may be mentioned that the concentration of PLL (3.5×10^{-5} % w/v) used for initial interaction with bacteria in the present investigation is significantly lower than the minimum inhibitory concentration (MIC) of PLL reported for various bacterial strains (Yoshida and Nagasawa, 2003; Conte et al., 2007). The fact that PLL did not affect cell viability renders the present method non-destructive to the samples. This is an additional advantage since PLL-bound bacterial cells can be plated to determine viable cell count and compared with the cell number estimations obtained by the AuNP aggregation method in order to validate the accuracy and reliability of the developed method of cell estimation.

2.3.5. Estimation of cell numbers of various bacterial strains by subtractive-aggregation

While developing a method of bacterial cell estimation in the present investigation, the wide scale applicability of the method for various types of bacterial strains encompassing both Gram-positive and Gram-negative bacteria and the sensitivity of the method were two key issues that needed to be addressed. To pursue these goals various Gram-positive and Gram-negative pathogenic bacteria were selected and their cell numbers were varied over a range of $1.0\text{-}10^7$ CFU. As observed earlier, the extent of broadening of the UV-visible extinction spectrum of AuNPs (Appendix, Figure A2.9) and the area under extinction spectrum (Appendix, Figure A2.10) revealed a systematic decrease in samples with increasing bacterial cell numbers. Interestingly this phenomenon was explicit for all the bacterial strains tested. The linear relationship between area under UV-visible extinction spectrum and bacterial cell numbers (Appendix, Figure A2.10) for all the tested bacterial strains was also substantiated by the equations indicated in Table A2.1 (refer to Appendix). Bacterial cells are negatively charged owing to the presence of either teichoic acid in Gram-positive bacteria or lipopolysaccharide in Gram-negative bacteria (Berry et al., 2005; Wilson et al., 2001). The large number of positive charge residues on PLL ensures an equivalent propensity of interaction with negatively charged cell surface of both Gram-positive and Gram-negative bacteria. This in turn results in equal proportion of unbound PLL recovered in all the samples, which probably explains the nearly equivalent levels of estimation across various bacterial strains. The minimal differences observed in the

broadening of UV-visible extinction spectrum and corresponding area under the spectrum could possibly be due to differences in charge characteristics of the cell surface as well as cell surface area which is likely to be encountered as a strain level difference. In other words, the differences in area under curve observed for different bacterial strains reflect their innate nature of difference which could be captured in this method. However, the linearity in the relationship for all the strains indicates a general nature of interaction between bacteria and PLL. It may be mentioned that the decrease in area under extinction spectrum from 1.0 to 10 CFU was nearly to the same extent as from 10 to 100 CFU. The plausible explanation is that at lower cell concentrations, PLL is in stoichiometric excess in solution and the difference in the amount of unbound PLL recovered when cell concentration increases from 1.0 to 10 CFU as well as 10 to 100 CFU is only minimal. Hence, similar extent of decrease in area under extinction spectrum is observed. However, as cell numbers increase beyond 100 CFU, quantitative sequestration of PLL takes place as a function of increasing cell number and the magnitude of decrease in area under extinction spectrum becomes more pronounced. It may be mentioned that the area under UV-visible extinction spectrum obtained for the lowest limit of detection i.e. for 10 CFU was close to 92.0 AU for *E. coli* MTCC 433 and was within the linear range of response of AuNP aggregation as a function of PLL concentration (refer to Figure 2.8b). This fact was also consistent with all other bacterial strains.

The present method of bacterial cell estimation provided an interesting mechanistic insight, which enabled sensitive estimation of bacterial cells in solution. In the absence of any bacterial cells, maximum AuNP aggregation by PLL was observed. Subsequently, when increasing concentration of bacterial cells in solution were used as a bait to sequester PLL, there was a progressive decline in AuNP aggregation. Essentially, bacterial cells effectively entrap PLL onto their surface by electrostatic interactions leading to a decrease in the availability of PLL in solution. Subsequently, when AuNPs are interacted with the unbound PLL fraction there is a systematic decrease in AuNP aggregation, which can account quantitatively for bacterial cell numbers. This decline in AuNP aggregation which correlates with increasing bacterial cell numbers can be referred to as “subtractive-aggregation”. The bacterial cell-PLL interaction in solution can be stated as follows:

$$[B] + [PLL] = [B\text{-}PLL] + [PLL]_{Unbound} \quad (1)$$

where [B] is bacterial cell concentration, [PLL] is the concentration of poly-L-lysine, [B-PLL] is bacteria-bound fraction of PLL and $[PLL]_{Unbound}$ is the free fraction of PLL in solution following interaction with bacteria. The maximum aggregation of AuNPs (agg_{Max}) in solution by PLL is achieved when the solution is devoid of any bacterial cells. The difference between maximum aggregation (aggMax) and aggregation due to unbound PLL ($agg_{Unbound\text{-}PLL}$) in presence of bacteria in solution represents subtractive-aggregation (Δagg) which can be stated as:

$$[\Delta agg] = [agg_{Max}] - [agg_{Unbound\text{-}PLL}] \quad (2)$$

A measure of subtractive-aggregation can be obtained from the difference in area (ΔAagg) under the UV-visible extinction spectrum for maximum aggregation ($Aagg_{Max}$) and aggregation by unbound PLL ($Aagg_{Unbound\text{-}PLL}$) and this can be stated as:

$$[\Delta Aagg] = [Aagg_{Max}] - [Aagg_{Unbound\text{-}PLL}] \quad (3)$$

A pictorial representation of the phenomenon of subtractive-aggregation is indicated in Figure 2.11.

Aggregation of AuNPs by unbound PLL fraction is largely influenced by the bacterial cell numbers which were initially interacted with PLL and thus from equation 3 it is quite evident that the subtractive-aggregation area (ΔAagg) essentially provides a measure of cell numbers. This fact is corroborated in the results depicted in Figure 2.12, wherein it is evident that cell numbers in the range of 10^1-10^7 CFU per 0.4 mL sample volume could be readily estimated on the basis of ΔAagg values. In case of 1.0 CFU, ΔAagg values for the bacterial strains were very low. A two-way analysis of variance (ANOVA) followed by all pair wise multiple comparison (Holm-Sidak method) revealed that with regard to difference in ΔAagg values amongst various bacterial strains across every cell number (CFU), the values obtained for *E. aerogenes* MTCC 2822 versus

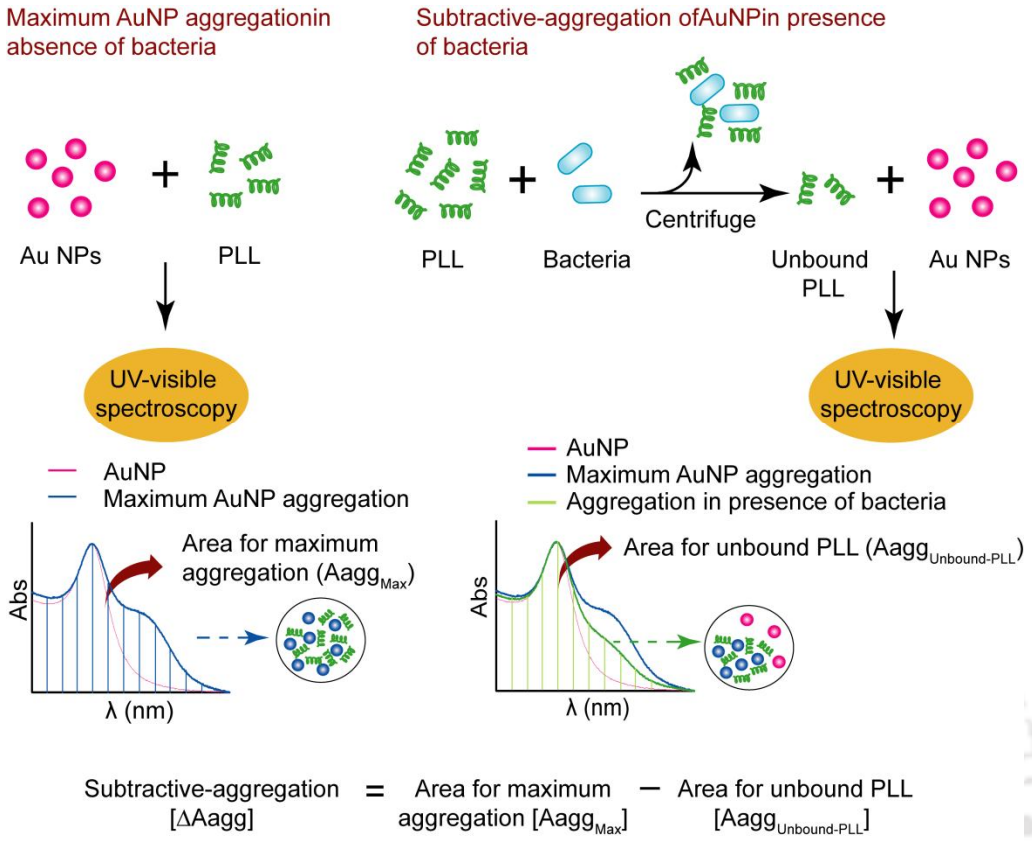

Figure 2.11. Schematic representation of subtractive-aggregation phenomenon.

E. coli MTCC 433 as well as *B. subtilis* MTCC 1305 versus *E. coli* MTCC 433 were statistically significant (*p* value <0.005). The relationship between subtractive-aggregation area and bacterial cell number can be represented by linear equations indicated in Table 2.1. These equations can be used to estimate cell numbers of the respective bacterial strains.

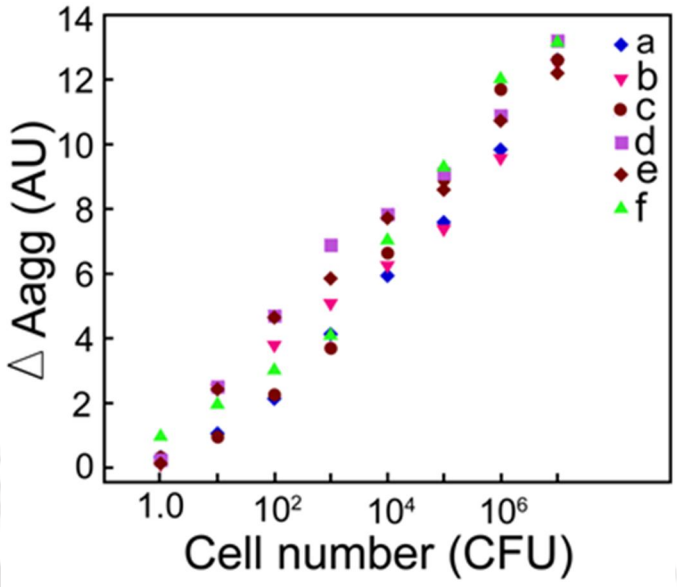

Figure 2.12. Plot for subtractive-aggregation (ΔAagg) versus bacterial cell numbers. **(a)** *Escherichia coli* MTCC 433, **(b)** *Listeria monocytogenes* Scott A, **(c)** *Staphylococcus aureus* MTCC 740, **(d)** *Enterobacter aerogenes* MTCC 2822, **(e)** *Bacillus subtilis* MTCC 1305 and **(f)** *Pseudomonas aeruginosa* MTCC 2488.

Table 2.1. Measurement of subtractive-aggregation as a function of bacterial cell numbers

Bacterial strains	**# Equation for subtractive-aggregation area (ΔAagg) versus cell number (CFU)**
Escherichia coli MTCC 433	$y = 1.762x - 2.475$ ($R^2 = 0.97$)
Pseudomonas aeruginosa MTCC 2488	$y = 1.873x - 1.928$ ($R^2 = 0.97$)
Enterobacter aerogenes MTCC 2822	$y = 1.746x - 0.932$ ($R^2 = 0.98$)
Listeria monocytogenes Scott A	$y = 1.598x - 1.357$ ($R^2 = 0.97$)
Bacillus subtilis MTCC 1305	$y = 1.665x - 0.952$ ($R^2 = 0.99$)
Staphylococcus aureus MTCC 740	$y = 1.936x - 2.824$ ($R^2 = 0.97$)

#ΔAagg = $Aagg_{Max} - Aagg_{Unbound\text{-}PLL}$. $Aagg_{Max}$ is obtained from area under the UV-visible extinction spectrum for AuNP aggregation by 3.5 x 10^{-5}% w/v PLL alone. $Aagg_{Unbound\text{-}PLL}$ is obtained from area under the UV-visible extinction spectrum for AuNP aggregation by unbound PLL following initial interaction of 3.5 x 10^{-5}% w/v PLL with varying cell numbers (1.0 – 10^7 CFU) of various bacterial strains.

2.3.6. Estimation of cell numbers in centrifugal device

It was observed that the overall time taken to estimate bacterial cell numbers for any given bacterial strain using the present method was around 45 min. In terms of rapidity of the process, the crux of the problem was the manual separation of unbound PLL following interaction with bacterial cells as this exercise demanded careful pipetting of small volumes from multiple samples (cell numbers ranging from 1.0-10^7 CFU) and was hence protracted. In order to expedite the process, the next endeavor was to explore the possibility of using a centrifugal device with a 0.22 µm membrane filter to separate bacterial cells following initial interaction with PLL. It was conceived that the use of such a device would facilitate entrapment of PLL-bound bacterial cells in the filter and unbound PLL could then be recovered as flow through, which eventually would avoid manual pipetting steps as well as reduce the overall estimation time. To this end, the initial interaction of bacterial cells (ranging from 1.0-10^7 CFU) with PLL was pursued in a separate microcentrifuge tube so as to avoid any non-specific binding of cells or PLL to the filter device of the centrifugal tube. Subsequently, unbound PLL fraction recovered as flow through from the centrifugal device was used for initiating aggregation of AuNPs. As evident from Figure A2.11a-b (refer to Appendix), with increase in cell numbers the extent of the spectral broadening for AuNPs diminished progressively. This correlation between cell number and spectral broadening was also observed in the area under extinction spectrum as indicated in Figure A2.11c (refer to Appendix). Quantitative estimations for maximum AuNP aggregation ($Aagg_{Max}$) as well as AuNP aggregation by unbound PLL ($Aagg_{Unbound\text{-}PLL}$) were also performed and from the subtractive-aggregation area cell numbers in the range of 10^1-10^7 CFU could be readily estimated (Appendix, Figure A2.11d). The results obtained with the centrifugal device have encouraging implications. The separation of bacterial cells following initial interaction with PLL and recovery of the unbound PLL fraction as flow through is accomplished in a single step involving a 1 min spin. As compared to the tedious process of manual separation of unbound PLL, the short duration of recovery of unbound PLL and the possibility of parallel processing of multiple samples could significantly reduce the overall estimation time of cell numbers.

2.3.7. Estimation of viable versus non-viable cells

For any cell estimation method, determination of viable cell count is a pertinent issue, which needs to be addressed. In order to test the potential of the present method of cell estimation to distinguish viable vis-a-vis non-viable cells, experiments were performed with cells subjected to various heat treatment. When 10^2 CFU of *E. coli* MTCC 433 were subjected to 55^{o}C for 30 min, the cells failed to survive the heat treatment as determined by plating, re-inoculation and subtractive-aggregation method (Table 2.2). When higher cell numbers (10^6 and 10^4 CFU) of *E. coli* MTCC 433 were subjected to the same condition, enumeration of cells which survived the heat treatment could be performed and interestingly, the cell numbers estimated by conventional plating and subtractive-aggregation method nearly coincided (Table 2.2), which reflected the reliability of the developed method in estimating viable cell numbers. For all other conditions of heat treatment (65^{o}C, 80^{o}C and autoclaving), cell numbers could not be estimated indicating cell death, and this fact was also verified by lack of growth in plating as well as re-inoculation experiments (Table 2.2). Following interaction of heat-killed cells (autoclaving) of *E. coli* MTCC 433 and *L. monocytogenes* Scott A with PLL, the UV-visible extinction spectrum of AuNPs interacted with unbound PLL failed to reveal any change in the extent of AuNP aggregation as compared to the sample representing maximum AuNP aggregation (AuNP aggregation in presence of PLL alone) and this trend was unequivocally observed for all cell numbers (Figure 2.13). It was also observed that cells subjected to heat treatment at 65^{o}C and 80^{o}C responded in a similar manner. Further, in the absence of PLL, heat-killed bacterial cells alone had no effect on the characteristic extinction spectra of AuNPs. To account for the lack of change in the extent of AuNP aggregation in case of heat-killed non-viable cells, it may be construed that PLL perhaps fails to bind to heat-killed cells. As a consequence, bulk of the PLL is recovered as unbound fraction and hence the aggregation observed in case of heat-killed cells is on par with that observed for PLL alone. Heat treatment at higher temperature presumably leads to outer membrane damage in bacterial cells. In that case, it is anticipated that the charge characteristics of such cells is likely to be lost. This would hamper the initial binding of PLL to bacterial cells, which is primarily driven by electrostatic interaction. To verify this

Table 2.2 Estimation of viable cell numbers of *E. coli* MTCC 433 by subtractive-aggregation method and conventional plating following various heat treatment.

Heat treatment	Initial cell number (log_{10} CFU)	#Cell number after treatment estimated by subtractive-aggregation (log_{10} CFU)	Cell number after treatment estimated by plating (log_{10} CFU)	Growth after re-inoculation into fresh media
55 °C/30 min	6.0	4.73 ± 0.09	4.59 ± 0.13	+
	4.0	2.45 ± 0.11	2.54 ± 0.12	+
	2.0	nd	nd	-
65°C/30 min	6.0	nd	nd	-
	4.0	nd	nd	-
	2.0	nd	nd	-
80°C/30 min	6.0	nd	nd	-
	4.0	nd	nd	-
	2.0	nd	nd	-
121 °C/20 min/ 15lb/in^2 (Autoclaving)	6.0	nd	nd	-
	4.0	nd	nd	-
	2.0	nd	nd	-

#Cell number for *E. coli* MTCC 433 was estimated by equation y = 1.762x – 2.475 where y is subtractive-aggregation area (ΔAagg) and x is cell number (CFU). nd: Cell viability was affected by heat treatment and hence could not be estimated by plating or subtractive-aggregation; (+) indicates turbidity in growth media after re-inoculation; (-) indicates lack of turbidity in growth media after re-inoculation.

hypothesis heat-treated bacterial cells were stained with propidium iodide (PI) which is an indicator of membrane damage. Viable cells with intact membrane prevent PI uptake whereas membrane compromised cells readily incorporate PI, which upon intercalation with cellular DNA exhibits enhanced fluorescence (Virto et al., 2005). Evidence for membrane damage in heat-killed (autoclaved) cells is clearly observed in Figure 2.14 wherein cells of *E. coli* MTCC 433 exhibit intense red fluorescence. Discrimination of viable and non-viable cells has been reported earlier using fluorescent probes based on cell viability markers such as membrane potential, intracellular esterase activity and membrane

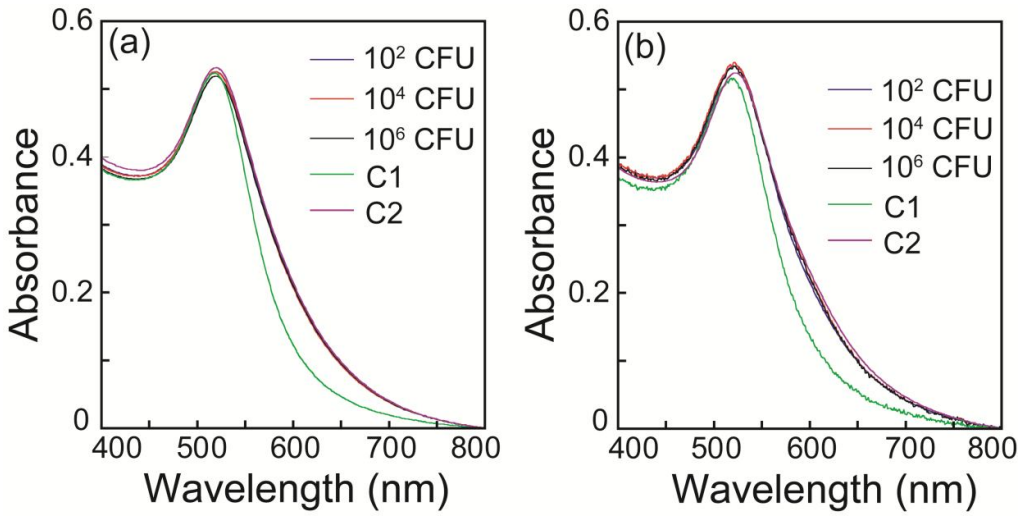

Figure 2.13. UV-visible extinction spectrum of AuNP in the presence of PLL following initial interaction of PLL with bacteria subjected to heat-killing by autoclaving. **(a)** *E. coli* MTCC 433, **(b)** *L. monocytogenes* Scott A. C1: AuNP alone (volume adjusted) and C2: AuNP interacted with 3.5 x 10^{-5} % w/v PLL.

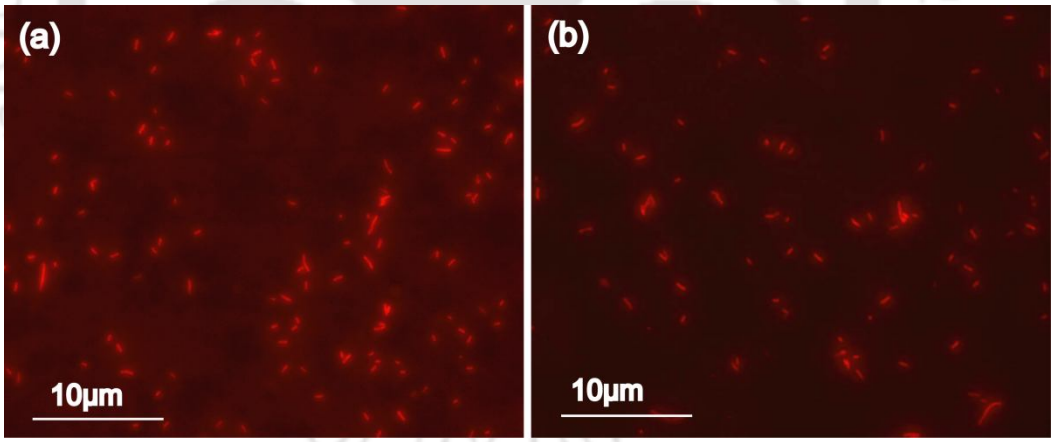

Figure 2.14. Propidium iodide stained cells of *E. coli* MTCC 433 subjected to heat killing by autoclaving. **(a)** 10^4 CFU and **(b)** 10^2 CFU.

integrity (Amor et al., 2002; Papadimitriou et al., 2006; Hoefel et al., 2003; Bunthof et al., 2001). These probes have been used alone or in combination to differentiate live and dead cells quantitatively. Although the probes render considerable sensitivity and differentiating

ability, they are used in conjunction with specialized techniques such as flow cytometry, which requires careful standardization and interpretation of results. In comparison, the present method of estimating viable cells by measuring AuNP aggregation is essentially label free, rapid and relatively simple in terms of mode of operation.

2.3.8. Application studies

It was encouraging to observe that the present method of bacterial cell estimation clearly provided a measure of viable cell numbers on the basis of subtractive-aggregation of AuNPs. The final endeavor of this investigation was to determine the application potential of the method in estimating viable bacterial cell numbers following exposure of target bacteria to an antimicrobial agent. For these studies, nisin was selected as a model antimicrobial peptide and the effect of various concentrations of the peptide on the viability of the target strain *Leuconostoc mesenteroides* NRRL B640 was studied. Nisin is a lantibiotic and a widely used food preservative, which is known to act on the membrane and disrupt membrane potential of target bacterial strains (Cotter et al., 2005; Zendo et al., 2010). Initial experiments based on agar well diffusion assay revealed that *L. mesenteroides* NRRL B640 was susceptible to nisin, as evident from the zone of growth inhibition (Appendix, Figure A2.12) and hence suitable to be used as a target bacteria. Subsequently, experiments were conducted with known cell numbers of *L. mesenteroides* NRRL B640 (1.0 -10^7 CFU) and AuNP aggregation by unbound PLL was studied by observing the broadening of the UV-visible extinction spectrum of AuNPs and determining area under the curve as well as subtractive-aggregation area for every sample as a function of cell numbers. It was observed that the overall trend of broadening of extinction spectrum of AuNPs, the area under each UV-visible extinction spectrum as well as subtractive-aggregation areas (ΔAagg) obtained for *L. mesenteroides* NRRL B640 (Appendix, Figure A2.13a-c) were largely consistent with the results observed earlier for other bacterial strains (refer to Figure A2.9 and Figure A2.10 in Appendix and Figure 2.12).

Following treatment with varying levels of nisin, viable cell numbers of *L. mesenteroides* NRRL B640 ascertained by both plating method as well as AuNP subtractive-aggregation was compared. Treatment of *L. mesenteroides* NRRL B640 with

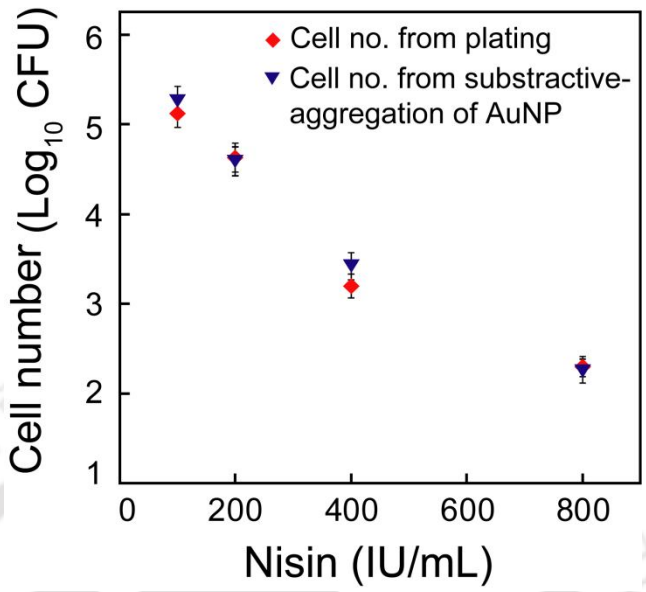

Figure 2.15. Estimation of cell numbers for *L. mesenteroides* NRRL B640 following treatment with the antimicrobial peptide nisin.

increasing concentration of nisin resulted in a progressive decline in the viability of the cells. Conventional plating method revealed that following exposure to a nisin concentration of 100, 200 and 400 IU/mL for 12 h, the viable cell count of the target strain reduced to 5.12, 4.63 and 3.20 log10 CFU per mL, respectively, as compared to the untreated cells where the cell number was nearly 6.0 log10 CFU per mL (Figure 2.15). At the highest nisin concentration of 800 IU/mL there was a dramatic decrease in viability of the cells resulting in a cell count as low as 2.3 log10 CFU per mL (Figure 2.15). When the cell numbers were estimated by the subtractive-aggregation method, the results largely coincided with that of the plating method (Figure 2.15). By using the equation indicated in Figure A2.13c (refer to Appendix), the cell numbers calculated by the subtractive-aggregation method amounted to 5.25, 4.59, 3.42 and 2.25 log10 CFU per mL, when L. mesenteroides NRRL B640 cells were treated with 100, 200, 400 and 800 IU/mL nisin, respectively. Upon exposure to an antimicrobial agent like nisin it may be assumed that both viable as well as nisin-affected non-viable cells would be present in the sample and the proportion of nisin-affected non-viable cells would be high in number with increasing

concentration of nisin. It is significant to mention that the present method of viable cell estimation by Au NP subtractive-aggregation provided an accurate estimation of viable cells even in the midst of nisin- affected non-viable target cells present in the same sample. This feature renders the method on par with conventional plating for estimating viable cell numbers. However, the rapidity of the present method provides a distinct advantage over plating which is usually arduous and protracted.

2.4. Significant Findings

In the present study, a polycationic species PLL was used to initiate aggregation of citrate-stabilized AuNPs, which in turn facilitated the development of a convenient tool for rapid estimation of bacterial cell numbers in solution. The salient features of the developed method are as follows:

1. The method is applicable to a wide range of bacterial strains and offers high sensitivity with a detection limit of 10 CFU and can estimate viable cell numbers with a high degree of accuracy.
2. The method is operationally simple, devoid of any conjugation chemistry and is essentially non-destructive.
3. The significance of the method is enhanced owing to the distinct possibility of translating the concept from laboratory bench to the development of a miniaturized centrifugal device for rapid estimation of bacterial cells.
4. The application potential of the subtractive-aggregation method of estimating viable bacterial cells was also verified through reliable estimation of viable cells in an antimicrobial susceptibility test using a prototype antimicrobial agent. This method could perhaps be extended to screen other antimicrobial agents and candidate drugs in future.
5. The reliability of the method in estimating viable cell numbers in solution augers well for its future application potential in the domain of pathogen detection, and microbiological quality control. For practical applications, development of appropriate strategies for sample preparation and sequestration of bacterial cells from complex matrix could significantly expand the application potential of the developed method.

The developed method of bacterial cell estimation essentially exploits surface charge interactions between PLL and AuNPs and thus promotes aggregation of AuNPs, which could be used as a handle to estimate cell numbers. It was envisaged that potent antibacterial nanocomposites can perhaps be developed by exploring an analogous principle of charge-based interactions between anionic bacterial cells and cationic nanocomposites. The motivating factor was that the charge-based interaction would enable a multivalent affinity effect, which could eventually contribute to heightened antibacterial activity.

Based on this premise, in the next chapter, the antibacterial activity of a cationic gold nanoparticle-polythiophene composite is described and a detailed study on its membrane-directed mode of action is presented.

Chapter 3

Antibacterial Activity and Mode of Action of Gold Nanoparticle-Polythiophene (AuNP-PTh) Composite

Chapter 3 describes the antibacterial activity of gold nanoparticle-polythiophene composite against pathogenic bacterial strains. Fluorescence-based assay revealed that composite causes membrane damage and membrane depolarization which leads to cell death. An in vitro XTT-based assay revealed that AuNP-PTh composite was non-totoxic to human adenocarcinoma HT-29 cells.

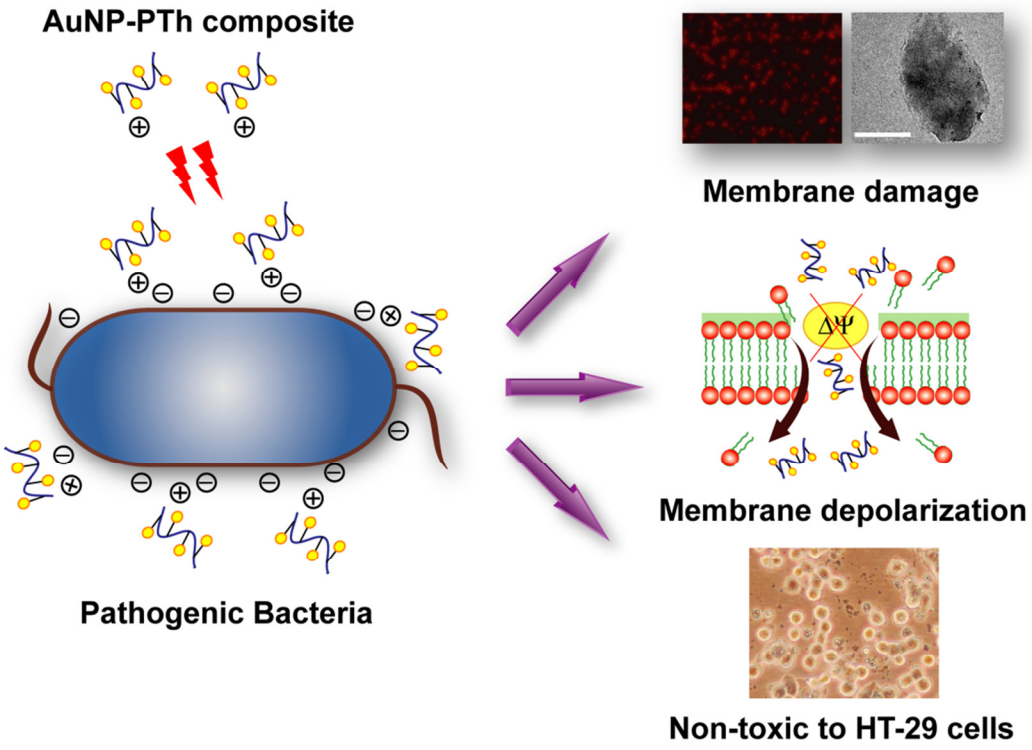

ABSTRACT

The use of nanoscale materials as bactericidal agents holds considerable therapeutic promise for amelioration of drug-resistant pathogenic bacteria. In this chapter, the antimicrobial activity and mode of action of a gold nanoparticle-polythiophene (AuNP-PTh) composite against common pathogenic bacteria is reported. Conventional antibacterial assay revealed that the nanocomposite was broad-spectrum in its bactericidal activity, with a minimum bactericidal concentration (MBC) of 112 µM against both *E. coli* MTCC 433 and *L. monocytogenes* Scott A. Fluorescence-based experiments conducted with the dyes cFDA-SE and PI indicated a dose-dependent loss in target cell viability and membrane damage in AuNP-PTh treated cells. These results were further validated by fluorescence microscopy and transmission electron microscope (TEM) analysis. Pretreatment of bacterial cells with the proton ionophore CCCP followed by exposure to AuNP-PTh nanocomposite suggested that the bactericidal activity of the nanocomposite was independent of the transmembrane potential of target bacteria. Experiments conducted with membrane potential sensitive dye $DiSC_3 5$ clearly indicated that treatment of bacterial cells with AuNP-PTh composite resulted in membrane depolarization. An *in vitro* XTT-based assay revealed that AuNP-PTh composite was non-cytotoxic to human adenocarcinoma HT-29 cells. It is envisaged that the membrane-directed activity of AuNP-PTh nanocomposite holds considerable therapeutic implications since an intact and functional membrane is paramount to the survival of bacteria and development of resistance is less likely in the event of extensive membrane damage.

3.1. Introduction

The emergence of drug-resistant pathogenic bacteria is a burgeoning issue of grave concern in modern healthcare regime. The drug-resistant pathogens are armed with an arsenal of resistance mechanisms such as enhanced drug impermeability, enzyme-catalyzed target modifications, drug inactivation and others, which empower them to evade the action of several therapeutically relevant drugs such as antibiotics. (Thomson and Bonomo, 2005; Morar and Wright, 2010; Gootz, 2010; Wright, 2011). Treatment of infections caused by drug-resistant bacteria calls for a radical therapeutic approach and underlines the need to develop potent antibacterial agents. However, in recent years, the progress achieved in discovery and development of novel antibiotics to combat these emerging pathogens has been below par and this fact has been highlighted in many reports (Song, 2008; Coates et al., 2002). In the quest for novel bactericidal agents, the current interest is in molecules with a mechanism of action that does not readily favor development of resistance. In this context, the use of nanoscale materials as bactericidal agents can be considered as a particularly innovative option. The high surface area to volume ratio and unique physicochemical features of nanomaterials are suitable to achieve enhanced antimicrobial activity. It has been suggested that antimicrobial nanomaterials may be favorable in overcoming resistance and reducing toxicity effects commonly associated with conventional antibiotics (Huh and Kwon, 2011).

The use of nanoparticles (NPs) as cargo for effective delivery of antimicrobial agents provides significant benefits such as improved solubility and prolonged half-life of drug, sustained and stimuli-responsive drug release, site-targeted delivery and combined delivery of multiple drugs for synergistic activity (Zhang et al., 2010; Moghimi et al., 2005; Risbud et al., 2000; Alphandary et al., 2000; Rogueda and Traini, 2007; Zhang et al., 2008; Cheow et al., 2010). Metal nanoparticles have been largely exploited as antimicrobial agents. For instance, the antimicrobial property of silver nanoparticle (Ag NP) has been extensively reported (Gogoi et al., 2006; Sondi and Salopek-Sondi, 2004; Furno et al., 2004; Ip et al., 2006). Amongst other metal-based nanomaterials, gold nanoparticle (AuNP) has been found to be particularly appealing and has been exploited in various biological applications (Sperling et al., 2008; Murphy et al., 2008; Boisselier and Astruc, 2009; Cobley et al., 2011; Dreaden et al., 2012; Dykman and Nikolai Khlebtsov,

2012) The favorable attributes of AuNPs such as chemical stability, non-toxicity and facile surface functionalization render unique opportunities for developing novel bactericidal agents (Tom et al., 2004; Gu et al., 2003; Norman et al., 2008; Pissuwan et al., 2009; Petros and DeSimone, 2010; Goodman et al., 2004). Nanoscale materials and composites based on the polymeric entities such as chitosan and other synthetic polymers and its derivatives have also been extensively characterized for their antimicrobial properties (Qi et al., 2004; Xing et al., 2009; Rhim et al., 2006; Alonso et al., 2012; Song et al., 2012). A large number of studies have highlighted the antimicrobial mechanism of nanoscale materials. Based on the findings of these studies, the antibacterial activity of nanomaterials have been attributed to bacterial cell wall or membrane damage, interference of energy transduction process, inhibition of vital enzymes and DNA synthesis, production of reactive oxygen species (ROS), change in membrane potential and inhibition of ATP synthase activities (Pal et al., 2007; Huang et al., 2008; Lu et al., 2008; Hetrick et al., 2008; Cui et al., 2012).

To combat the challenge posed by drug-resistant pathogenic bacteria, the current motivation is in the development of bactericidal nanoscale materials with a mode of action that can contravene the resistance mechanism of target pathogens. In this regard, nanomaterials that target the bacterial membrane can be conceived to be an attractive option since the probability of developing resistance against such bactericidal agents would require an extensive restoration of membrane components, which is a physiologically demanding task for the bacteria (Bambeke et al., 2008; Hurdle et al., 2011). In the present study, the antimicrobial activity of a water soluble gold nanoparticle-polythiophene (AuNP-PTh) composite against pathogenic bacteria is reported. The membrane-targeting activity of the nanocomposite is elucidated by fluorescence-based experiments and transmission electron microscope (TEM) analysis. Evaluation of the *in vitro* cytotoxic effect of the nanocomposite on a model human cell line is also reported in this study.

3.2. Materials and Methods

3.2.1. Materials

$HAuCl_4$ (30 wt % solution in dilute HCl), thiophene (99+%), polymyxin B, valinomycin, 5 (and 6)-carboxyfluorescein diacetate succinimidyl ester (cFDA-SE), propidium iodide (PI), 1-N-phenylnaphthylamine (NPN), carbonyl cyanide m-chlorophenylhydrazone (CCCP), 3,3'-dipropylthiadicarbocyanine iodide ($DiSC_35$), Dulbecco's Modified Eagles medium (DMEM), penicillin, streptomycin and XTT-based *in vitro* toxicology assay kit were obtained from Sigma-Aldrich Chemicals, USA. Fetal calf serum (FCS) was obtained from PAA Laboratories, USA. Dimethyl sulfoxide (DMSO) and glutaraldehyde were purchased from Merck, Mumbai, India. HEPES buffer was procured from Sisco Research Laboratories (SRL), Mumbai, India. Nutrient broth (NB) and Brain-Heart Infusion (BHI) broth were purchased from HiMedia, Mumbai, India.

3.2.2. Bacterial strains and growth conditions

The bacterial strains used in the present investigation included Gram-positive *Bacillus subtilis* MTCC 1305 (*B. subtilis*), *Listeria monocytogenes* Scott A (*L. monocytogenes*) and *Staphylococcus aureus* MTCC 96 (*S. aureus*) and Gram-negative *Escherichia coli* MTCC 433 (*E .coli*), *Enterobacter aerogenes* MTCC 2822 (*E. aerogenes*), *Yersinia enterocolitica* MTCC 859 (*Y. enterocolitica*) and *Pseudomonas aeruginosa* MTCC 2488 (*P. aeruginosa*). *B. subtilis* MTCC 1305, *E. coli* MTCC 433, *E. aerogenes* MTCC 2822 and *P. aeruginosa* MTCC 2488 were grown in Nutrient Broth (NB) at 37°C and 180 rpm for 12 h, whereas *S. aureus* MTCC 96, *Y. enterocolitica* MTCC 859 and *L. monocytogenes* Scott A were propagated in Brain-heart Infusion (BHI) broth at 37°C and 180 rpm for 12 h.

3.2.3. Gold nanoparticle-polythiophene (AuNP-PTh) composite

AuNP-PTh composite was synthesized by a previously described method (Panda et al., 2008). In brief, homogenous mixture of thiophene (30 mM) was prepared by addition of required amount of thiophene to 10 mL of MilliQ grade water followed by sonication in a 35 kHz ultrasonicator. Subsequently, 30 µL of $HAuCl_4$ from a stock solution of 1.72×10^{-2} M was added and this mixture was incubated in a mechanical shaker operating at 100 rpm and 25°C for a period of 24 h. After incubation, the solution had changed from dark purple

color to a colorless solution with a pH ~ 3.5. The concentration of the protonated species in the composite was considered as the concentration of the composite. (Panda et al., 2008). Prior to every experiment AuNP-PTh solution was prepared fresh and the stock solution was stored in 4^{o}C in a refrigerator.

3.2.4. Antibacterial activity of AuNP-PTh composite

Antibacterial activity of AuNP-PTh was determined against common pathogenic bacteria which included Gram-positive *B. subtilis* MTCC 1305, *L. monocytogenes* Scott A and *S. aureus* MTCC 96 and Gram-negative *E. coli* MTCC 433, *E. aerogenes* MTCC 2822 and *Y. enterocolitica* MTCC 859. The target pathogens were grown in requisite media (Nutrient broth and Brain-heart Infusion broth) incorporated with varying concentrations of AuNP-PTh (45, 75 and 150 µM) for 24 h at 37^{o}C. The growth of nanocomposite-treated cells was monitored by measuring absorbance at 600 nm in a spectrophotometer (Cary 300, Varian) and was expressed as percentage growth compared to control (untreated cells). To ascertain the dose-dependent effect of AuNP-PTh treatment on cell viability, varying concentrations of AuNP-PTh (15-150 µM) was added to target cells (10^6 CFU/mL) of *E. coli* MTCC 433 and *L. monocytogenes* Scott A suspended in sterile phosphate buffered saline (PBS) and incubated at 37^{o}C and 180 rpm. The viable cell numbers (Log_{10} CFU/mL) were determined intermittently by serial dilution and plating.

3.2.5. Minimum bactericidal concentration (MBC) of AuNP-PTh

Varying concentrations of AuNP-PTh (15-150 µM) was added to target bacterial cells (10^6 CFU/mL) suspended in sterile PBS and incubated at 37^{o}C and 180 rpm. Following 12 h incubation, an aliquot of the sample was re-inoculated into fresh growth media and cell growth was monitored by measuring absorbance at 600 nm after 24 h. The minimum bactericidal concentration (MBC) of AuNP-PTh was defined as the lowest concentration of the nanocomposite, which prevented the growth of treated cells following re-inoculation as ascertained by an absorbance reading of < 0.1 at 600 nm. The MBC value was calculated from three independent experiments, each having three replicas. Data analysis and calculation of standard deviation was performed with Microsoft Excel 2010 (Microsoft Corporation, USA).

3.2.6. Binding affinity of AuNP-PTh for bacterial cells

Fluorescence emission spectra of varying concentrations of AuNP-PTh (2.0-100 µM) were recorded in a spectrofluorimeter (FluoroMax-3, HORIBA) at an excitation wavelength of 345 nm and emission wavelength of 435 nm. A calibration curve of fluorescence intensity (at 435 nm) as a function of concentration of AuNP-PTh solution was generated. For binding studies of the nanocomposite onto bacterial cells, varying concentrations of AuNP-PTh (3.75, 7.5, 15, 30, 45, 60 and 75 µM) was added to cells of *E. coli* MTCC 433 and *L. monocytogenes* Scott A (10^6 CFU/mL each) suspended in sterile 0.85% saline and incubated at 37^{o}C and 180 rpm. Following 30 min of incubation, cells were separated by centrifugation and AuNP-PTh fluorescence emission intensity in cell free supernatant was measured at 435 nm and used to determine the concentration of unbound or free AuNP-PTh from the previously generated calibration curve. The concentration of bound AuNP-PTh was determined from the difference of initial AuNP-PTh concentration used to interact with bacterial cells and the concentration of unbound nanocomposite. A plot of bound AuNP-PTh as a function of initial nanocomposite concentration and a Scatchard plot (Bound/free versus Bound) was generated. The slope of the Scatchard plot was used to calculate the dissociation constant (K_d) of AuNP-PTh.

3.2.7. Mechanism of action of AuNP-PTh

A series of experiments were conducted to probe the mode of action of AuNP-PTh on bacterial cells. Gram-negative *E. coli* MTCC 433 and Gram-positive *L. monocytogenes* Scott A were selected as target pathogenic bacteria and the experiments encompassed the following: (a) cFDA-SE assay, (b) PI uptake assay, (c) Fluorescence microscope analysis, (d) NPN assay, (e) Transmission electron microscope (TEM) analysis, (f) Effect of membrane potential on the antimicrobial activity of AuNP-PTh and (g) $DiSC_35$-based membrane depolarization assay. A detailed description of the protocols for the aforementioned experiments is provided in the following section.

3.2.7.1. cFDA-SE assay

A stock solution of cFDA-SE (500 µM) was prepared in ethanol and stored at -20^{o}C. Cells of *E. coli* MTCC 433 and *L. monocytogenes* Scott A were grown overnight, washed twice

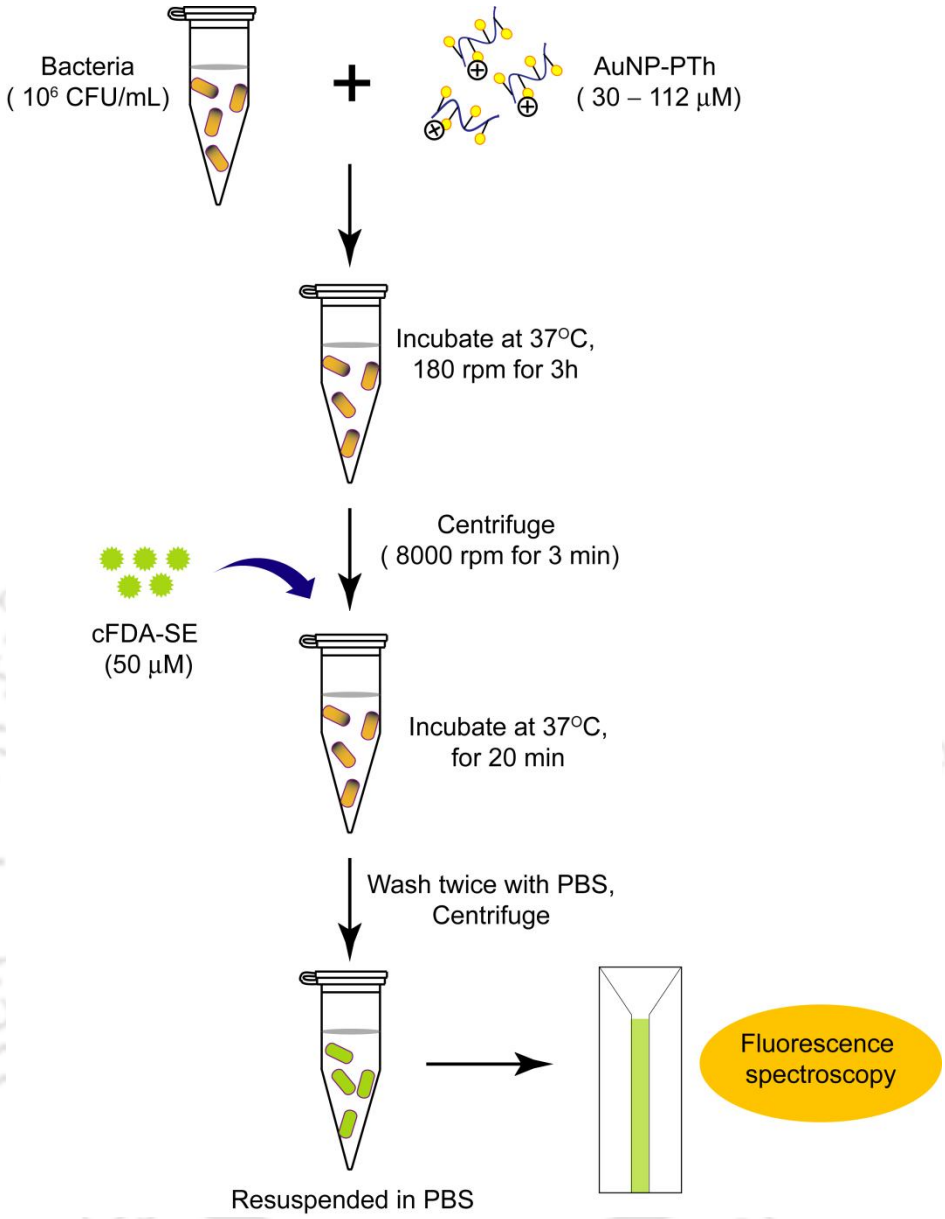

Figure 3.1. Schematic representation of experimental protocol for cFDA-SE assay.

with sterile PBS and resuspended in 1.0 mL of the same buffer. Varying concentrations of AuNP-PTh (30-112 µM) were added to the target bacteria suspensions (10^6 CFU/mL) and incubated at 37°C and 180 rpm. Control samples consisting of untreated cells of the target pathogens were also included. Following 3 h of incubation cells from both treated as well as control samples were pelleted by centrifugation and washed twice with sterile PBS. The cells were then resuspended in 1.0 mL of sterile PBS and labeled with cFDA-SE (final

concentration of 50 µM) at 37°C for 20 min by following the method described previously (Lee et al., 2004). The labeling reaction was terminated by pelleting the cells by centrifugation and washing the cells twice with sterile PBS to remove excess cFDA-SE molecules. The cells were finally suspended in 1.0 mL of sterile PBS and fluorescence measurements for three independent experimental samples were conducted in a spectrofluorimeter (FluoroMax-3, HORIBA) at an excitation wavelength of 488 nm and emission wavelength of 518 nm. A schematic of the cFDA-SE assay is indicated in Figure 3.1.

3.2.7.2. PI uptake assay

A stock solution of PI (1.5 mM) was prepared in sterile MilliQ water and stored at 4^{o}C. Overnight grown cells of *E. coli* MTCC 433 and *L. monocytogenes* Scott A were washed twice with sterile PBS and resuspended in 1.0 mL of the same buffer. Varying concentrations of AuNP-PTh (30-112 µM) were added to target bacteria suspensions (10^6 CFU/mL) and incubated at 37^{o}C and 180 rpm. In parallel sets, control samples consisting of untreated cells of the target pathogens were also included. Following 3 h of incubation cells were pelleted by centrifugation, washed with sterile PBS to remove excess AuNP-PTh. The cells were resuspended in 1.0 mL of sterile PBS and PI was added to both treated cells as well as control samples (final concentration of 30 µM) for cell labeling as described in a previously reported method (Bunthof et al., 2001). After 30 min of incubation in a circulating water bath incubator (Amersham) set at 37^{o}C, samples were centrifuged and washed with sterile distilled water to remove excess dye. The cells were resuspended in 1.0 mL of sterile PBS and fluorescence was measured in a spectrofluorimeter (FluoroMax-3, HORIBA) at an excitation wavelength of 535 nm and emission wavelength of 617 nm. Fluorescence measurements were taken for three independent experimental samples. A schematic of the PI uptake assay is indicated in Figure 3.2.

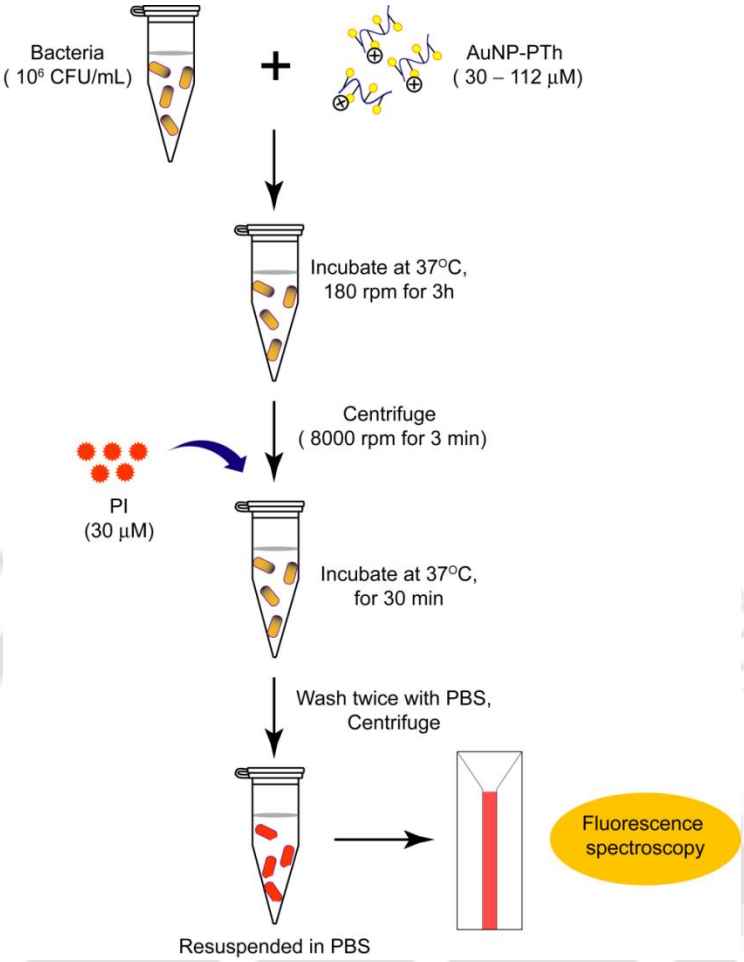

Figure 3.2. Schematic representation of experimental protocol for propidium iodide (PI) uptake assay.

3.2.7.3. Fluorescence microscopy

Varying concentrations of AuNP-PTh (30-112 µM) were added to *E. coli* MTCC 433 and *L. monocytogenes* Scott A cell suspensions in sterile PBS (10^6 CFU/mL) and incubated at 37°C and 180 rpm. Following incubation of 3 h, cells were washed twice with sterile PBS to remove excess AuNP-PTh and both the treated and control cells were labeled with cFDA-SE and PI as mentioned previously in section 3.2.7.1 and 3.2.7.2., respectively. The stained cells were fixed in 2.5% glutaraldehyde and washed twice with sterile PBS. A 10 µl aliquot of the fixed sample was spotted on a clean glass slide, air dried and observed under fluorescence microscope (Eclipse Ti-U, Nikon) with a filter that allowed blue light

excitation for cFDA-SE and green light excitation for PI stained cells. Images of the treated and control cells were recorded.

3.2.7.4. NPN assay

A stock solution of NPN (500 µM) was made in acetone. *E. coli* MTCC 433 and *L. monocytogenes* Scott A cells were grown in respective medium at 37°C in a shaker incubator till mid-logarithmic phase (A_{600} of 0.5). The cells were centrifuged, washed twice with 5mM HEPES buffer (pH 7.4) and resuspended in the same buffer. A 1.0 ml aliquot of cells was taken in separate cuvettes to which NPN (final concentration of 10 µM) and varying concentrations of AuNP-PTh (10, 30, 60 and 112 µM) was added. Increase in fluorescence intensity of NPN was measured as a function of time following addition of AuNP-PTh. For the NPN assay, cells treated with polymyxin B (1.0 µg/mL) was used as positive control as mentioned in a previous study (Schurek et al., 2009; Zhang et al., 2000). Fluorescence measurements were performed in a spectrofluorimeter (FluoroMax-3, HORIBA) at an excitation and emission wavelength of 350 nm and 420 nm, respectively. Fluorescence measurements were taken for three independent samples. A schematic of the NPN assay is indicated in Figure 3.3.

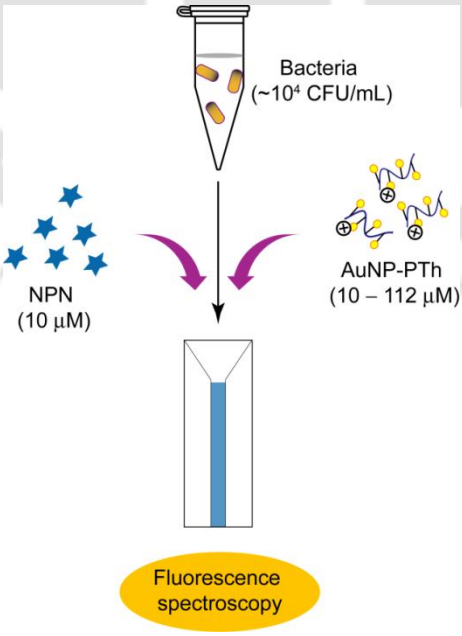

Figure 3.3. Schematic representations of the protocol for NPN assay.

3.2.7.5. Transmission electron microscope (TEM) analysis

L. monocytogenes Scott A cells were grown overnight, washed twice with sterile PBS and resuspended in the same buffer. Separate aliquots of cells (approximately 10^6 CFU/mL) were treated with AuNP-PTh (75 µM) for 3 h and 6 h at 37°C. Control samples consisted of untreated cells suspended in sterile PBS. Treated and control cells were washed once with sterile PBS followed by a wash with sterile MilliQ grade water and then resuspended in sterile MilliQ grade water. An aliquot of each sample (2.0 µl) was spotted on carbon coated TEM grid (Pacific Grid, USA), air-dried in laminar hood and examined in a transmission electron microscope (Jeol JEM 2100, Japan) operating at 200 kV and their images were recorded.

3.2.7.6. Effect of membrane potential on the antibacterial activity of AuNP-PTh

A stock solution of CCCP (10 mM) was made in ethanol and stored in -20°C. Cells of *E. coli* MTCC 433 were pre-treated with the uncoupler CCCP to collapse the transmembrane proton motive force as described earlier (Mangoni et al., 2003). CCCP treated and untreated cells (approximately 10^6 CFU/mL) were taken in sterile PBS and incubated with varying concentrations of AuNP-PTh (60 and 112 µM) for 6 h at 37°C. Bactericidal effect of AuNP-PTh on CCCP treated and untreated cells were determined by plating the samples at regular time intervals and determining the viable cell count. A schematic of the CCCP-based assay is indicated in Figure 3.4.

3.2.7.7. Membrane depolarization assay

A stock solution of $DiSC_35$ (3.0 mM) was made in ethanol and stored at -20°C. Cells of *E. coli* MTCC 433 and *L. monocytogenes* Scott A were grown till mid-logarithmic phase (A_{600} = 0.4 - 0.5). The cells were harvested by centrifugation, washed with a buffer solution (5 mM HEPES buffer, 5 mM glucose, pH 7.2) and resuspended in the same buffer to an A_{600} of 0.05. The cell suspensions were incubated with $DiSC_35$ (0.4 µM) for 1 h at 37°C followed by addition of KCl (100 mM). The cell suspensions (1.0 mL) were subsequently placed in a cuvette to which varying concentrations of AuNP-PTh (60 and 112 µM) was added and fluorescence readings of the samples were recorded intermittently

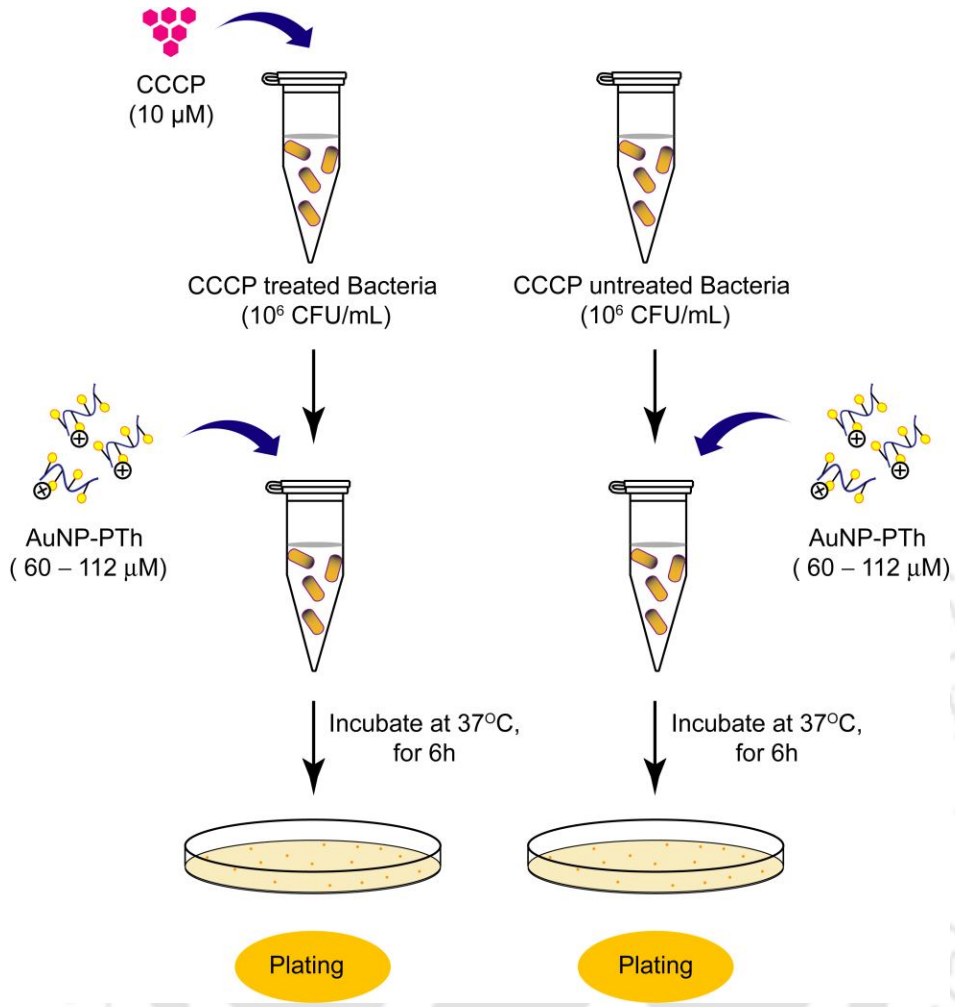

Figure 3.4. Schematic representation of experimental protocol for CCCP assay.

in a spectrofluorimeter (FluoroMax-3, HORIBA) set to an excitation wavelength of 622 nm and emission wavelength of 670 nm. For the membrane depolarization assay, cells treated with valinomycin (30 µM) were used as positive control as described in an earlier study (Vooturi et al., 2009). Fluorescence measurements were taken for three independent experimental samples. A schematic of the $DisC_35$-based membrane depolarization assay is indicated in Figure 3.5.

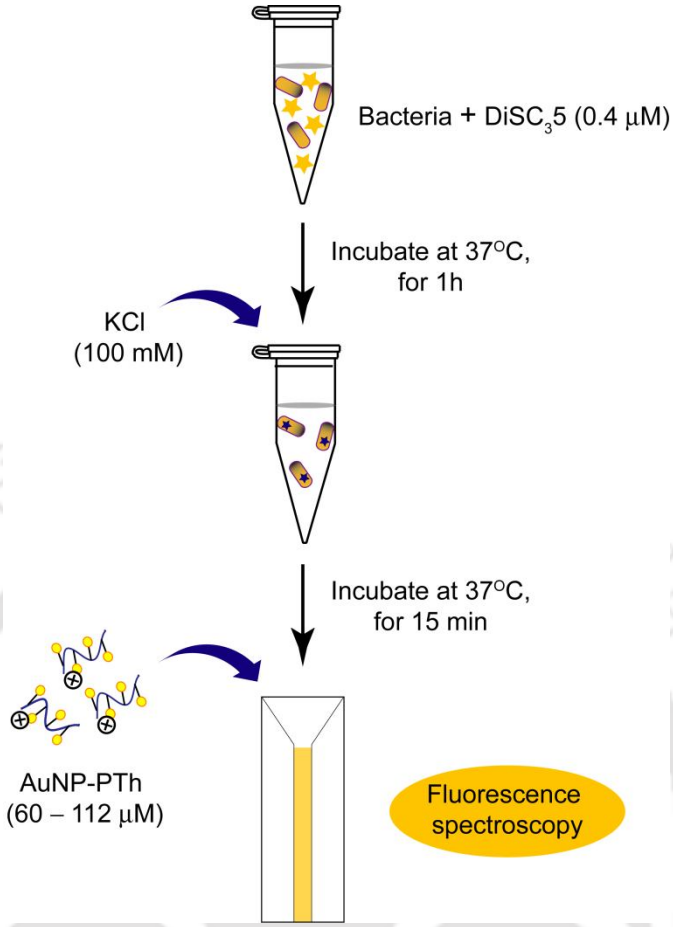

Figure 3.5. Schematic representation of $DisC_35$-based membrane depolarization assay.

3.2.8. Cytotoxicity assay

The cytotoxic effect of AuNP-PTh on human adenocarcinoma cells line (HT-29) was ascertained by a standard XTT assay. Prior to the cytotoxicity assay, HT-29 cells were initially grown in 25 cm^2 tissue culture flask in Dulbecco's Modified Eagle Medium (DMEM) supplemented with 10% (v/v) fetal bovine serum (FBS), penicillin (100 µg/mL) and streptomycin (100 µg/mL) at 37°C under a humidified atmosphere of 5% CO_2 in an incubator (HERA cell 150 CO_2 incubator, Thermo Scientific, USA). For cytotoxicity assay, cells were trypsinized and subsequently seeded onto 96-well tissue culture plates at a density of 10^4 cells per well and incubated with varying concentrations of AuNP-PTh (30, 60 and 112 µM) made in DMEM for a period of 24 h and 48 h in a CO_2 incubator as mentioned previously. Subsequently, the media was carefully aspirated and fresh DMEM

containing XTT solution (0.2 mg/mL) was added to the wells. The plates were further incubated for 3 h at 37^{o}C and then the absorbance of the samples was measured in a microtitre plate reader (Infinite M200, TECAN, Switzerland) at 450 nm. For each concentration of AuNP-PTh, the XTT assay was performed in six sets. Data analysis and determination of standard deviation was performed with Microsoft Excel 2010 (Microsoft Corporation, USA). In the XTT assay, the absorbance obtained for solvent control samples (cells treated with DMSO alone) was considered to represent 100% cell viability, whereas the absorbance for AuNP-PTh-treated cells were compared to that obtained for solvent control cells in order to determine % cell viability. The statistical significance of the results obtained in the XTT assay was determined by performing an analysis of variance (ANOVA) using Sigma plot version 11.0.

3.3. Results and Discussion

3.3.1. Bactericidal activity of AuNP-PTh

Gold nanoparticle-polythiophene composite used in the present investigation is readily soluble in water (Panda and Chattopadhyay, 2007). In a previous study, it was reported that electrostatic interactions mediated by the protonated form of AuNP-PTh in conjunction with weak van der Waals forces likely promote the binding of AuNP-PTh with negatively charged bacterial cells and there was a preliminary indication of the antimicrobial activity of the nanocomposite upon prolonged incubation with bacterial cells (Panda et al., 2008) The general proclivity of AuNP-PTh to readily adsorb onto bacterial cell surface and the initial hint of its antimicrobial activity was encouraging. Hence it was worthwhile to probe the bactericidal potency of AuNP-PTh in detail and decipher its mode of action against pathogenic bacteria. The bactericidal activity of various concentrations of AuNP-PTh against common Gram-positive and Gram-negative pathogenic bacteria is represented in Figure 3.6. As evident from the figure, treatment of the target pathogenic bacteria with 45 µM AuNP-PTh resulted in considerable inhibition of their growth. For instance the % growth of *L. monocytogenes* Scott A was around 34% as compared to the untreated control cells, whereas in case of *E. aerogenes* MTCC 2822, the % growth was observed to be around 42% when compared to the control untreated cells (Figure 3.6). It was also observed that a dose-dependent growth inhibition was explicit for all the tested pathogens,

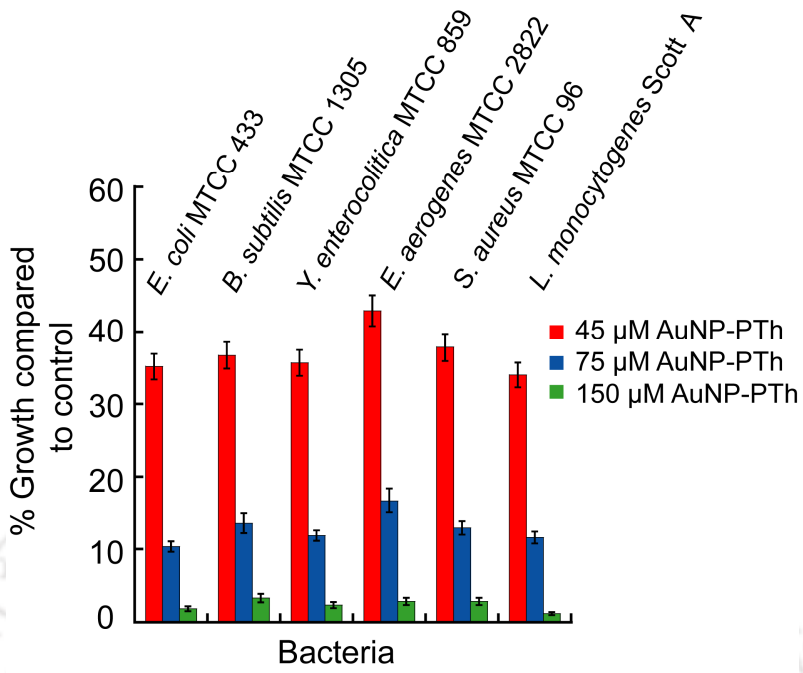

Figure 3.6. Antibacterial activity of AuNP-PTh composite against common pathogenic bacteria.

which suggested a broad-spectrum bactericidal activity of AuNP-PTh. At the highest AuNP-PTh concentration of 150 µM, there was a prominent inhibitory effect, resulting in annihilation of the bacterial pathogens. It may be mentioned here that AuNP-PTh could inhibit the growth of the pathogen *S. aureus* MTCC 96, which was earlier tested to be a presumptive methicillin-resistant *S. aureus* (MRSA) strain (Vudumula et al., 2012). MRSA strains are known to be drug-resistant and have been associated with serious infections (Kaye and Kaye, 2000; Chatterjee and Otto, 2013). In the light of the current efforts towards discovering potent antibacterial agents against MRSA, (Bambeke et al., 2008; Livermore, 2004; Jacqueline et al., 2013; Hurdle et al., 2011; Garcia-Lara et al., 2005) the ability of AuNP-PTh to eradicate a presumptive MRSA holds encouraging therapeutic prospects.

The bactericidal potency of AuNP-PTh was also tested by determining the loss of viability of target cells suspended in sterile PBS. The rational of these experiments was that since sterile PBS is a nutrient-free medium that is unlikely to support rapid growth of bacterial cells, the outcome of the antibacterial assay with AuNP-PTh against target pathogens suspended in sterile PBS would not be influenced by the ability of the bacterial strains to proliferate. To pursue this goal, cells of *E. coli* MTCC 433 and *L. monocytogenes*

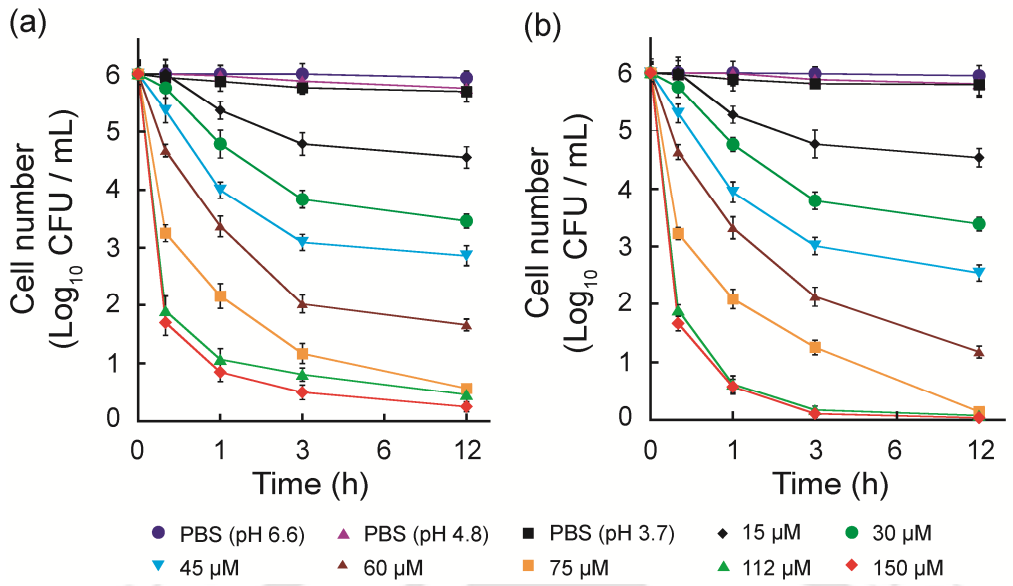

Figure 3.7. Effect of varying concentrations of AuNP-PTh on the viability of **(a)** *E. coli* MTCC 433 and **(b)** *L. monocytogenes* Scott A. The pH of AuNP-PTh solution at a concentration range of 15-150 µM varied from 4.8-3.7.

Scott A (10^6 CFU/mL each) were suspended in sterile PBS and treated with varying concentrations of AuNP-PTh (15 -150 µM). It was observed that an increase in AuNP-PTh concentration and interaction time lead to a corresponding decline in the viability of the target pathogens (Figure 3.7). At high AuNP-PTh concentrations of 112 and 150 µM, the reduction in cell viability was quite rapid and following 12 h of interaction, the target cell populations were virtually eradicated with the viable cell counts reaching below 1.0 Log_{10} CFU (Figure 3.7). It may be mentioned here that with increasing concentration of AuNP-PTh (15-150 µM), the pH of PBS solution in which the target cells were suspended varied from 4.8-3.7. From Figure 3.7, it can be observed that cell viability of target pathogens in various pH-adjusted PBS solutions remained unaffected which strongly indicated that the loss in viability of target pathogens on exposure to AuNP-PTh was not influenced by pH. The minimum bactericidal concentration (MBC) of AuNP-PTh for both *E. coli* and *L. monocytogenes* was determined to be 112 µM. In the context of the bactericidal activity of AuNP-PTh, particle size of the nanocomposite is likely to have a major impact. In an earlier study it was demonstrated by dynamic light scattering (DLS) experiments that AuNP-PTh composite particles were sub-micrometer in size, with majority of the particles

displaying a size distribution ranging from 100-300 nm. Further it was also reported that the nanocomposite with smaller particle size demonstrated an increased propensity to interact with bacterial cells (Panda et al., 2008). The smaller size particles present in AuNP-PTh composite are likely to display strong interaction with bacterial cells owing to a larger surface area available for effective contact with the cells. Given the superior interaction with bacterial cells, the smaller size particles present in the AuNP-PTh nanocomposite conceivably play a significant role in potentiating the bactericidal activity of AuNP-PTh.

3.3.2. Binding affinity of AuNP-PTh on bacterial cells

AuNP-PTh nanocomposite was fluorescent and in an earlier study it was shown that the emission intensity of the composite was concentration-dependent (Panda et al., 2008). This finding suggested that binding of AuNP-PTh onto bacterial cells could perhaps be pursued through fluorescence measurements of the nanocomposite. A dose-dependent binding of AuNP-PTh nanocomposite onto target bacterial cells was evident in the present study (Figure 3.8, inset) and a Scatchard plot obtained from AuNP-PTh fluorescence measurements (Figure 3.8) revealed that the binding affinity of AuNP-PTh nanocomposite for *E. coli* MTCC 433 and *L. monocytogenes* Scott A was comparable, with K_d values of 12.0 x 10^{-3} M and 8.09 x 10^{-3} M, respectively. The nearly similar affinity of AuNP-PTh nanocomposite for both the bacterial strains indicates the generality of AuNP-PTh-bacteria interaction and this fact perhaps explains the broad-spectrum bactericidal activity of the composite.

3.3.3. Mode of action of AuNP-PTh nanocomposite

3.3.3.1. Membrane-directed activity

In order to probe the mechanism of action of AuNP-PTh on pathogenic bacteria, fluorescent dyes which could specifically track membrane damage were used. Target cells of *E. coli* MTCC 433 and *L. monocytogenes* Scott A were treated with varying concentrations of AuNP-PTh for 3h followed by measurements of uptake of the fluorescent dyes cFDA-SE and PI. cFDA-SE is a membrane-permeable dye and hence

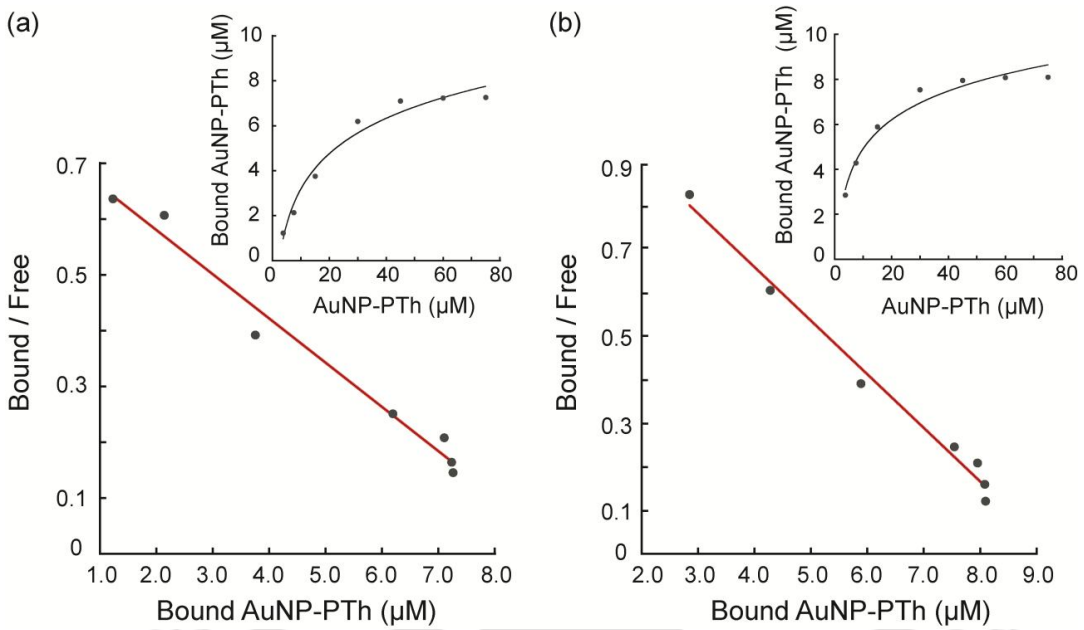

Figure 3.8. Scatchard plot for determination of binding affinity of AuNP-PTh for **(a)** *E. coli* MTCC 433 and **(b)** *L. monocytogenes* Scott A. Inset indicates concentration-dependent binding of AuNP-PTh on bacterial cells.

readily taken up by cells. Following uptake, the intracellular esterase activity prevalent in viable cells leads to cleavage of ester bond of the dye and consequently the fluorescent form of the dye accumulates in the cell and is conjugated to intracellular and cell-surface proteins, which prevents passive leakage of the dye from cells (Hoefel et al., 2003). Hence the magnitude of cFDA-SE fluorescence is a direct measure of cell viability. When the target cells of *E. coli* MTCC 433 and *L. monocytogenes* Scott A were treated with AuNP-PTh for 3h, there was a progressive decrease in cFDA-SE fluorescence for the cells with increase in the nanocomposite concentration from 30 µM to 112 µM (Figure 3.9a). It may be mentioned here that the effect of pH on cFDA-SE assay was verified by the inclusion of the control samples C1 and C2. The pH of the samples C1 (pH 6.6) and C2 (pH 3.7) correspond to the pH of an AuNP-PTh solution of 30 µM and 112 µM, respectively. It was observed that in case of the pH control samples C1 and C2, the change in cFDA-SE fluorescence intensity for both the target bacteria was negligible (Figure 3.9a), which strongly suggested that the assay was not affected by pH.

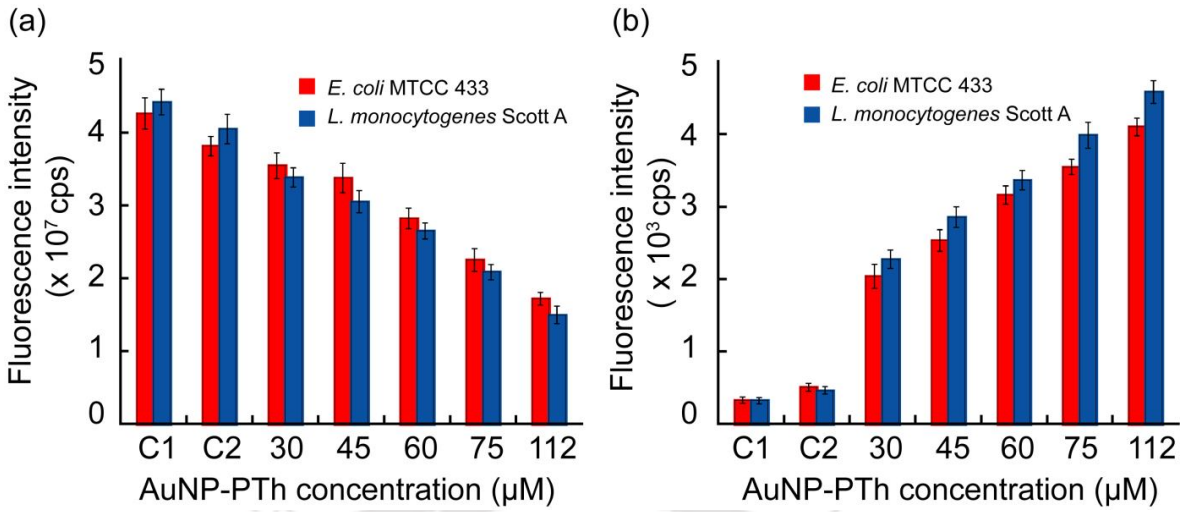

Figure 3.9. Fluorescence measurements of **(a)** cFDA-SE and **(b)** PI uptake in AuNP-PTh treated pathogenic bacteria. C1 and C2 are control samples of PBS with pH adjusted to 6.6 and 3.7, respectively.

Given the fact that cFDA-SE fluorescence is essentially based on intracellular esterase activity of viable cells, the results obtained in cFDA-SE assay suggested that the proportion of viable cells declined with increase in AuNP-PTh concentration, clearly indicating a dose-dependent effect, which was also observed earlier (Figure 3.7). As reported in an earlier study, the cationic AuNP-PTh nanocomposite likely adsorbs onto anionic bacterial cells through electrostatic interactions (Panda et al., 2008) and following adsorption, it was anticipated that the nanocomposite perhaps induces membrane damage in bacterial cells. To ascertain membrane damage in AuNP-PTh treated cells, a PI uptake assay was performed. PI is a membrane-impermeant dye which is taken up by cells only if the membrane is damaged and following uptake, the dye binds to single- and double-stranded nucleic acids through intercalation, which results in enhanced fluorescence (Virto et al., 2005). Treatment of target cells of *E. coli* MTCC 433 and *L. monocytogenes* Scott A with increasing concentrations of AuNP-PTh resulted in a progressive increase in the uptake of PI (Figure 3.9b), which clearly suggested a dose-dependent membrane damage in nanocomposite-treated cells.

Fluorescence microscope studies with AuNP-PTh treated cells indicated a marked decline in the number of cFDA-SE stained target cells and a corresponding increase in the

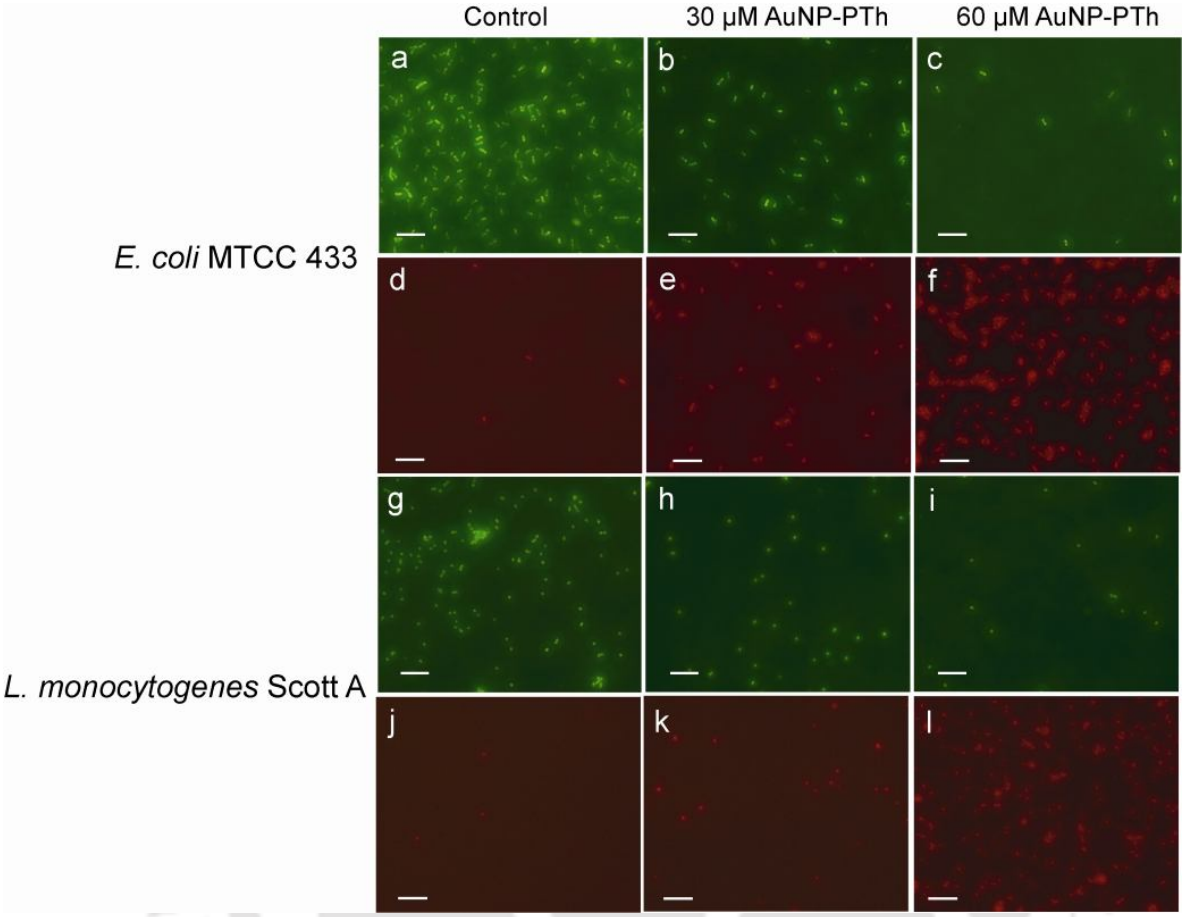

Figure 3.10. Fluorescence microscopic images of control and AuNP-PTh treated cells of **(a-f)** *E. coli* MTCC 433 and **(g-l)** *L. monocytogenes* Scott A labeled with cFDA-SE **(Panels a-c and g-i)** and PI **(Panels d-f and j-l).** Scale bar for all the images is 10 µm.

number of PI stained cells, with increase in AuNP-PTh concentration (Figure 3.10). This dose-dependent effect was consistent with the results obtained earlier in the solution-based fluorescence experiments (Figure 3.9a and Figure 3.9b).

The membrane-permeabilization activity of AuNP-PTh against pathogenic bacteria was evaluated by 1-N-phenylnaphthylamine (NPN) uptake assay. NPN is an uncharged lipophilic dye, which fluoresces weakly in aqueous environment, but its fluorescence greatly increases in nonpolar or hydrophobic environment such as the cell membrane. However, when bacterial cells are treated with an antimicrobial agent, which promotes

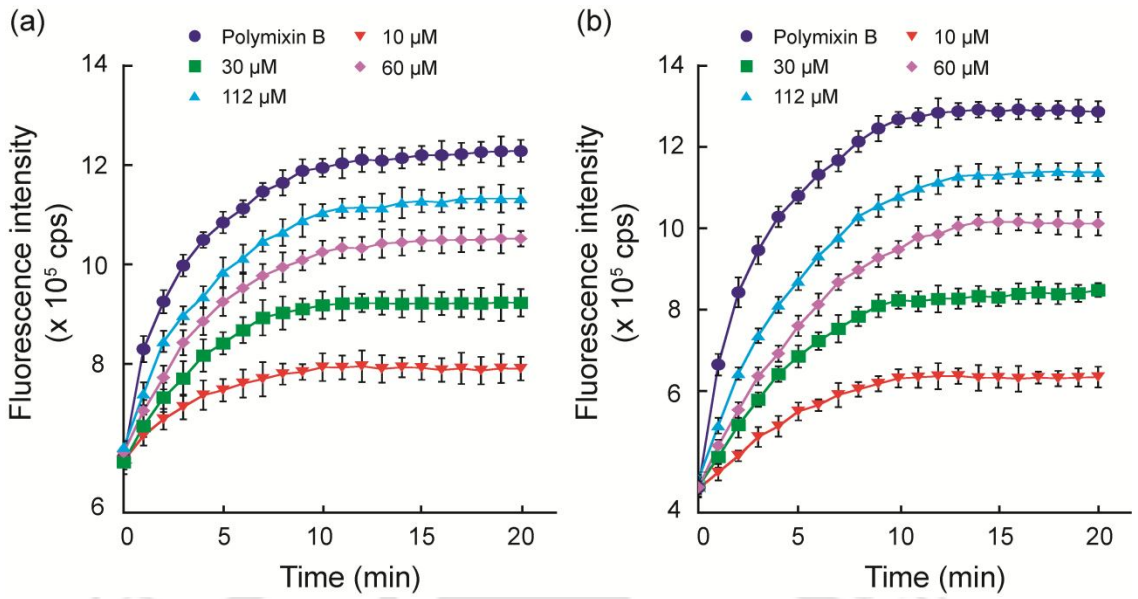

Figure 3.11. NPN uptake assay for determination of membrane permeabilization in **(a)** *E. coli* MTCC 433 and **(b)** *L. monocytogenes* Scott A cells treated with varying concentrations of AuNP-PTh. Cells treated with 1.0 µg/ mL polymyxin B was used as positive control.

membrane-permeabilization, NPN gains access to the hydrophobic core of the membrane from aqueous medium and as a consequence of the hydrophobic ambience, its fluorescence intensity is now enhanced (Halander and Mattila-Sandholm, 2000). In the present investigation, an NPN- based membrane-permeabilization assay was conducted for *E. coli* MTCC 433 and *L. monocytogenes* Scott A cells treated with varying concentrations of AuNP-PTh (10 µM-112 µM). A time-dependent increase in NPN fluorescence followed by a plateau indicated progressive membrane permeabilization in AuNP-PTh-treated cells and the extent of membrane damage was also observed to be dose-dependent (Figure 3.11). For every sample, it was observed that there was a progressive increase in NPN fluorescence till around 10 min of assay time, which indicated progressive membrane permeabilization in AuNP-PTh-treated cells (Figure 3.11a and Figure 3.11b). A plateau effect was observed beyond 10 min of assay time, which indicated a saturation effect. Further, it was observed that the increase in fluorescence intensity of NPN was more pronounced at higher AuNP-PTh concentrations, which suggested that the extent of membrane permeabilization in target bacterial cells was dose-dependent.

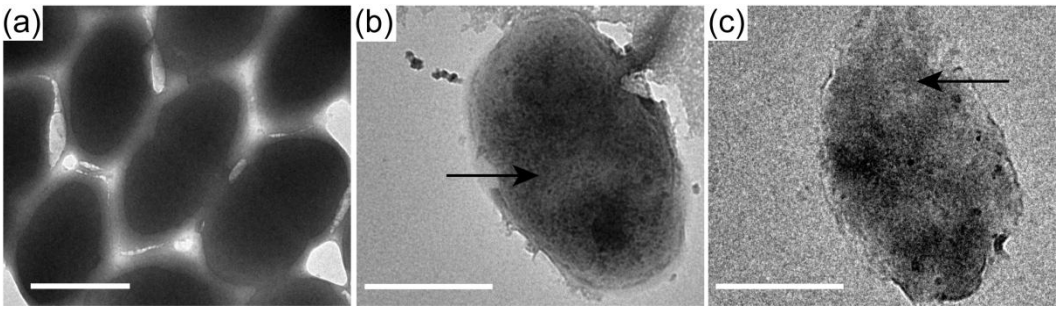

Figure 3.12. Transmission electron microscope images of **(a)** untreated cells of *L. monocytogenes* Scott A and **(b-c)** cells of *L. monocytogenes* Scott A treated with 75 µM AuNP-PTh for 3 h and 6 h, respectively. Arrow in Panel d and e indicates loss of electron density in cell treated with AuNP-PTh. Scale bar is 0.5 µm.

Evidence for membrane damage in AuNP-PTh-treated cells was also obtained by transmission electron microscope (TEM) analysis. Loss in membrane integrity was observed for *L. monocytogenes* Scott A cells treated with 75 µM AuNP-PTh for 3h (Figure 3.12b). Further, when the cells of *L. monocytogenes* Scott A were subjected to the nanocomposite treatment for a longer time (6 h), this effect was observed to be more prominent (Figure 3.12c). In contrast, the untreated control cells revealed an intact membrane and morphology typically associated with *L. monocytogenes* cells (Figure 3.12a). Leakage of intracellular constituents as a consequence of extensive membrane damage also resulted in a decrease in intracellular electron density in AuNP-PTh-treated cells (indicated by an arrow in Figure 3.12b and Figure 3.12c).

3.3.3.2. Effect of target cell membrane potential on the antibacterial activity of AuNP-PTh

The findings of cFDA-SE assay, PI assay and TEM analysis strongly suggested a membrane-directed bactericidal activity of AuNP-PTh nanocomposite. The next endeavor was to investigate the effect of target cell membrane potential on the antimicrobial activity of AuNP-PTh. This objective was pertinent given that that the antibacterial activity of several membrane-acting antimicrobial agents have been attributed to a functional transmembrane potential (Ψ) in target bacterial cells (Yeaman and Yount, 2003; Breukink and de Kruijff, 1999; Epand et al., 2010; Kaplan et al., 2011). To pursue this goal, cells of

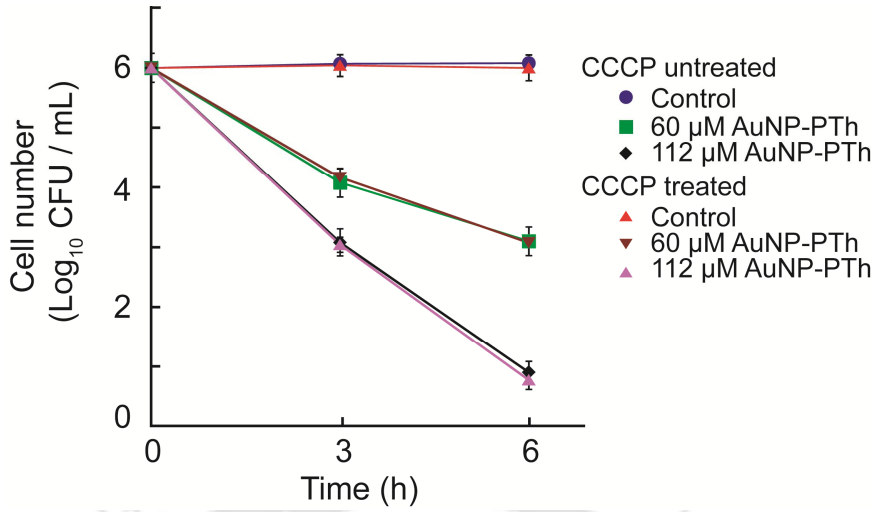

Figure 3.13. Effect of membrane potential on the antibacterial activity of AuNP-PTh on *E. coli* MTCC 433.

E. coli MTCC 433 were pre-treated with carbonyl cyanide m-chlorophenyl hydrazone (CCCP), which promotes the collapse of the transmembrane proton motive force and subsequently the cells were treated with varying concentrations of AuNP-PTh. As evident from Figure 3.13, the viability of CCCP-untreated and CCCP-treated control cells essentially remained unaffected for the period of the experiment (6 h) and the viable cell counts were nearly equivalent (around 6.0 Log_{10} CFU/ mL) for both these samples. However, in case of AuNP-PTh treated bacterial cells, a marked decrease in cell viability was observed for both CCCP-treated and untreated cells and this reduction in cell viability could be correlated with the dose of AuNP-PTh used against the target cell. Further, it was also observed that the extent of loss in cell viability was akin for both CCCP-treated and untreated cells, which suggested that the bactericidal activity of AuNP-PTh was independent of the transmembrane potential of the target bacterial cells. Amongst various attributes of pathogenic bacteria, variations in their membrane electrochemistry and membrane energetic are often observed as a strategy to escape the host defense mechanisms (Yeaman and Yount, 2003). In this regard, the membrane potential-independent bactericidal activity of AuNP-PTh holds significant therapeutic implications especially for elimination of pathogenic bacteria, which may present an altered membrane electrochemistry.

3.3.3.3. Effect of AuNP-PTh on the membrane potential of target cells

An important endeavor of the present investigation was to validate whether treatment of bacterial cells with AuNP-PTh resulted in collapse of the transmembrane potential. In these experiments, 3, 3'-dipropylthiadicarbocyanine iodide ($DiSC_35$), a membrane potential-sensitive probe was employed. It is well established that in bacterial cells with a functional membrane potential gradient ($\Delta\Psi$), there is an accumulation of $DiSC_35$ in the cytoplasmic membrane of energized cells, and consequently the fluorescence of the dye is quenched. Subsequently, if the membrane potential gradient in these cells is perturbed as a result of treatment with an antimicrobial agent, the dye is released into solution, which is manifested as an increase in fluorescence intensity (Lowery et al., 2009; Torrent et al., 2008). In the present study, treatment of $DiSC_35$-loaded cells of *E. coli* MTCC 433 and *L. monocytogenes* Scott A with varying concentrations of AuNP-PTh resulted in a significant enhancement of fluorescence till around 12 min of the assay time followed by a plateau, which suggested that the nanocomposite could readily dispel the membrane potential in target cells (Figure 3.14). A dose-dependent collapse in the transmembrane potential of AuNP-PTh-treated bacterial cells was also evident in the experiments (Figure 3.14).

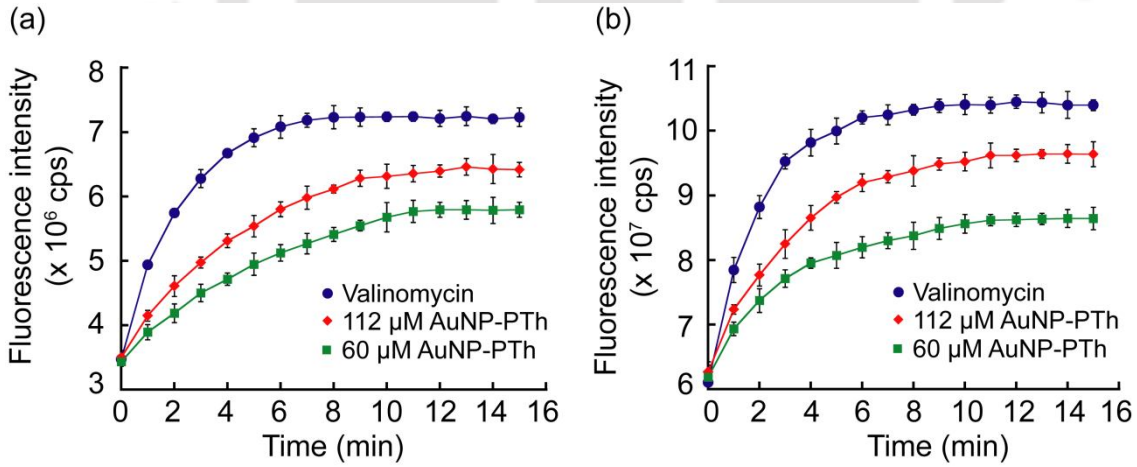

Figure 3.14. Membrane depolarization determined by $DiSC_35$ fluorescence in **(a)** *E. coli* MTCC 433 and **(b)** *L. monocytogenes* Scott A cells treated with AuNP-PTh. Cells treated with 30 µM valinomycin were used as positive control.

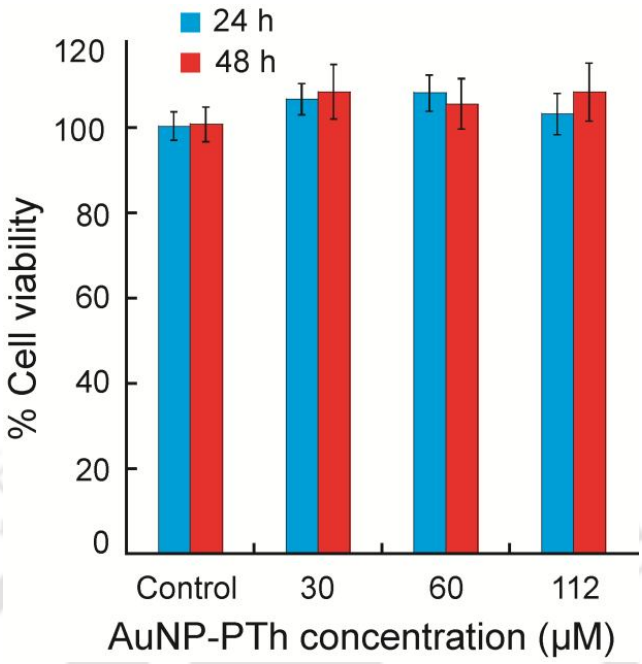

Figure 3.15. Cytotoxicity assay to determine % viability of HT-29 cells following treatment with varying concentrations of AuNP-PTh. Each data point represents mean ± standard deviation from six samples.

3.3.4. Cytotoxic effect of AuNP-PTh

Antibacterial nanomaterials are conceivably efficient to achieve sustained therapeutic effects as they are likely to be retained for a longer time in the body as compared to other therapeutic agents such as antibiotics (Drbohlavova et al., 2013). However, the toxic effect of nanomaterials upon long-term exposure is a critical issue which must be addressed in order to achieve safe therapeutic applications (Brayner, 2008; Karlsson et al., 2008; Love et al., 2012). Hence in the present investigation it was pertinent to ascertain the cytotoxic effect of varying concentrations of AuNP-PTh for which HT-29 cells (adenocarcinoma cells) were chosen as model human cell line and a standard XTT-based colorimetric assay was pursued. The result of the XTT assay is shown in Figure 3.15. As evident from the figure AuNP-PTh treatment for various time periods (24h and 48 h) failed to exhibit any deleterious effect on the viability of HT-29 cells and this result was noted even at an AuNP-PTh concentration of 112 μM, which is equivalent to the MBC of the nanocomposite. Bacterial cells are known to be negatively charged owing to the presence

of teichoic acid in Gram-positive bacteria and lipopolysaccharide in Gram-negative bacteria (Weidenmaier and Peschel, 2008; Gutsmannn and Seydel, 2010). On the other hand, mammalian cells are mostly neutral at physiological pH as their cytoplasmic membrane is composed of zwitterionic phospholipids (Yeaman and Yount, 2003). The protonated form of AuNP-PTh in conjunction with weak van der Waals force are factors which enhance the affinity of the nanocomposite for negatively charged bacterial cells (Panda et al., 2008) and this perhaps accounts for the selective antibacterial activity.

3.4. Significant Findings

The present study highlights the antibacterial activity of a water soluble gold nanoparticle-polythiophene (AuNP-PTh) composite against common pathogenic bacteria. The important findings of the study are as follows:

1. AuNP-PTh composite readily inhibited the growth of common Gram-positive and Gram-negative pathogenic bacteria and thus displayed a broad-spectrum bactericidal activity.
2. Fluorescence-based assays in conjunction with transmission electron microscope analysis established the membrane-directed bactericidal activity of AuNP-PTh. It is envisaged that the membrane-targeting activity would enhance the therapeutic value of AuNP-PTh since the probability of developing resistance against such bactericidal agents requires a revamp of membrane components in target pathogens, which is a physiologically demanding task for the bacteria.
3. Interestingly, AuNP-PTh composite also displayed high bacterial selectivity and was non-cytotoxic to human HT-29 cells in an *in vitro* assay. The high bacterial selectivity and lack of cytotoxicity on human cells augers well for future therapeutic application of the nanocomposite.

   The profound membrane-directed bactericidal activity of AuNP-PTh and the non-cytotoxic nature of the nanocomposite are significant motivating factors to probe the therapeutic potential of the nanocomposite. In the next chapter, the potential of AuNP-PTh to sever the outer membrane defense barrier in Gram-negative

pathogenic bacteria and potentiate the activity of an antibiotic in combination therapy is demonstrated. Further, the therapeutic prospect of the nanocomposite to inhibit the growth of model gastrointestinal pathogens in simulated gastric fluid (SGF) and its bactericidal activity against biofilm formed by pathogenic bacteria is also highlighted in the following chapter.

Chapter 4

Potential Therapeutic Applications of Gold Nanoparticle-Polythiophene (AuNP-PTh) Composite

This chapter describes the three important therapeutic applications of gold nanoparticle-polythiophene composite. The nanocomposite enhanced the efficacy of antibiotics against the target bacterial strains, revealed antimicrobial activity in simulated gastric fluid (SGF) and displayed strong anti-biofilm activity alone or in combination with tobramycin.

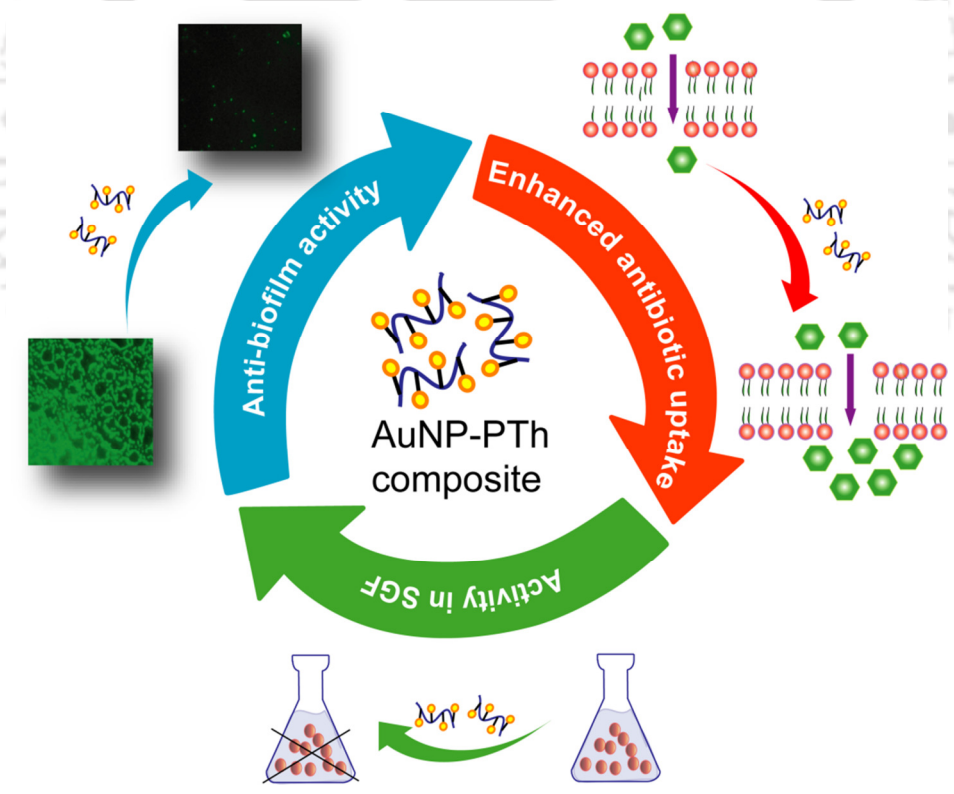

ABSTRACT

In this chapter the potential therapeutic applications of the membrane-targeting AuNP-PTh nanocomposite is reported. The bactericidal efficacy of therapeutic antibiotics erythromycin and polymyxin B in combination with AuNP-PTh nanocomposite was tested against Gram-negative and Gram-positive pathogenic bacteria, respectively. The outcome of these experiments clearly indicated that the extent of growth inhibition of the target pathogens was significantly higher when the cells were subjected to a combined treatment of AuNP-PTh and the antibiotics erythromycin or polymyxin B, as compared to either AuNP-PTh or antibiotic alone. An eightfold reduction in the MIC of erythromycin and polymyxin B was observed against target pathogens in combination with 45 µM AuNP-PTh and a synergy was observed with regard to the interaction between the nanocomposite and the antibiotics. Interestingly, AuNP-PTh nanocomposite could also exhibit bactericidal activity in an acidic niche and rendered a significant decrease in % viability of *E. coli* MTCC 433 and *L. monocytogenes* Scott A cells suspended in simulated gastric fluid (SGF). In a separate set of experiment, it was observed that treatment of *P. aeruginosa* biofilm with increasing concentration of AuNP-PTh nanocomposite resulted in a corresponding reduction in biofilm biomass and polysaccharide liberation as estimated by crystal violet and Congo red staining, respectively. Fluorescence microscope analysis and Field emission scanning electron microscope (FESEM) provided evidence for the anti-biofilm activity of AuNP-PTh nanocomposite. The ability of AuNP-PTh nanocomposite to potentiate the activity of tobramycin against *P. aeruginosa* biofilm in combination treatment is also demonstrated in the present work.

4.1. Introduction

Pathogenic bacteria are highly versatile in life-style and possess various adaptive strategies in order to foil the host defense mechanisms or the action of antimicrobial agents. In case of Gram-negative pathogenic bacteria, the outer membrane is a major hindrance to the action of therapeutic antibiotics (Nikaido, 2003; Bolla et al., 2011; Saha et al., 2008; Delcour, 2009). In this regard, nanoscale antibacterial agents that can breach this defense barrier and facilitate the uptake of antibiotics may hold special merit as an adjuvant in antibiotic-mediated therapy (Fayaz et al., 2010; Vigderman, and Zubarev, 2013; Allahverdiyev et al., 2011). Gastrointestinal pathogens are capable of surviving in the highly acidic environment of the stomach (Hong et al., 2012; Merrell and Camilli, 2002). Further, elimination of gastrointestinal pathogens is challenging since therapeutic agents such as antibiotics may suffer a loss of activity in an acidic environment (Lamp et al., 1992; Mercier et al., 2002; George and Abraham, 2006). This calls for development of robust antibacterials that can retain their bactericidal activity in the gastric milieu.

With regard to infections caused by pathogenic bacteria, the formation of bacterial biofilm is of great concern as they are largely involved in chronic and nosocomial infections (Parsek and Singh, 2003; Costerton et al., 1999; Mah and O'Toole, 2001; Majumdar and Padiglione, 2012). Besides, bacteria in biofilms are known to display a much higher tolerance to antibiotic than planktonic cells (Ceri et al., 1999; Drenkard, 2003; Fux et al., 2005; Stewart et al., 2000). During biofilm formation bacteria liberates an extracellular matrix or EPS (extracellular polymeric substance), which is presumed to play a significant role for development of resistance to antibiotics (Costerton et al., 1999; Flemming and Wingender, 2010). Biocidal agents based on nanomaterials bear considerable potential in combating the challenge of biofilms formed by pathogenic bacteria. Benzyl penicillin-encapsulating cationic liposomes and magnesium fluoride nanoparticles have been shown to demonstrate anti-biofilm activity (Kim and Jones, 2004; Lellouche et al., 2009). Recent studies have also revealed that silver-coated magnetic nanoparticles and zinc oxide nanoparticles have been utilized in elimination of biofilm and prevention of biofilm formation on coated surfaces (Mahmoudi and Serpooshan, 2012; Applerot et al., 2012).

The strong membrane-directed antibacterial activity of AuNP-PTh nanocomposite (reported in Chapter 3) opened up a window of opportunity to explore the potential of the nanocomposite in confronting some of the aforementioned adaptive attributes of pathogenic bacteria. In the present chapter, the potential of AuNP-PTh nanocomposite as an adjuvant to potentiate the activity of prototype therapeutic antibiotics in combination therapy is demonstrated. Further, the therapeutic prospect of the nanocomposite to inhibit the growth of model gastrointestinal pathogens in simulated gastric fluid (SGF) and its bactericidal activity against bacterial biofilm directly or in combination with an antibiotic is also highlighted.

4.2. Materials and Methods

4.2.1. Materials

$HAuCl_4$ (30 wt % solution of $HAuCl_4$ in dilute HCl; 99.99%), thiophene (99 + %), polymyxin B, valinomycin, 5 (and 6)-carboxyfluorescein diacetate succinimidyl ester (cFDA-SE), propidium iodide (PI), erythromycin, pepsin, Congo red and tobramycin were obtained from Sigma-Aldrich Chemicals, USA. The growth media used for culturing the bacterial strains and crystal violet was procured from HiMedia, Mumbai, India.

4.2.2. Bacterial strains and growth conditions

The bacterial strains used in the present investigation consisted of Gram-positive *Listeria monocytogenes* Scott A (*L. monocytogenes*), *Enterococcus faecalis* MTCC 439 (*E. faecalis*) and *Staphylococcus aureus* MTCC 96 (*S. aureus*) and Gram-negative *Escherichia coli* MTCC 433 (*E. coli*), *Yersinia enterocolitica* MTCC 859 (*Y. enterocolitica*) and *Pseudomonas aeruginosa* MTCC 2488 (*P. aeruginosa*). *E. coli* MTCC 433 and *P. aeruginosa* MTCC 2488 were grown in Nutrient Broth (NB) at 37^{o}C and 180 rpm for 12 h, whereas *S. aureus* MTCC 96, *E. faecalis* MTCC 439, *Y. enterocolitica* MTCC 859 and *L. monocytogenes* Scott A were propagated in Brain-heart Infusion (BHI) medium at 37^{o}C and 180 rpm for 12 h.

4.2.3. Gold nanoparticle-polythiophene (AuNP-PTh) composite

AuNP-PTh composite solution was prepared by the following the method described earlier in section 3.2.3 and the concentration of the protonated species in the composite was considered for determining the concentration of the composite (Panda et al., 2008).

4.2.4. Minimum inhibitory concentration (MIC) of erythromycin, polymyxin B and tobramycin

MIC of erythromycin was determined against Gram-negative bacteria *E. coli* MTCC 433 and *Y. enterocolitica* MTCC 859 while MIC of polymyxin B was determined against Gram-positive *S. aureus* MTCC 96 and *E. faecalis* MTCC 439. MIC of tobramycin was determined against *P. aeruginosa* MTCC 2488. The target bacterial strains were inoculated at 1% level into microtitre wells having the requisite growth medium and grown overnight at 37^{o}C and 130 rpm in presence of varying concentrations of either erythromycin (5.0-320 µg/mL), polymyxin B (5.0-320 µg/mL) or tobramycin (0.078-2.5 µg/mL). The growth of the bacterial strains was ascertained by measuring absorbance at 600 nm in a microtitre plate reader (Infinite M200, TECAN, Switzerland). MIC of the antibiotics was recorded as the lowest antibiotic concentration which resulted in an absorbance reading of <0.1 at 600 nm (A_{600} = <0.1), indicating lack of cell growth. The MIC values for erythromycin, polymyxin B and tobramycin were calculated from three independent experiments, each having three replicas. Data analysis and calculation of standard deviation was performed with Microsoft Excel 2010 (Microsoft Corporation, USA).

4.2.5. Bactericidal activity of erythromycin and polymyxin B in combination with AuNP-PTh composite

The bactericidal activity of erythromycin in combination with AuNP-PTh nanocomposite was tested against Gram-negative bacteria *E. coli* MTCC 433 and *Y. enterocolitica* MTCC 859. In a separate experiment, the antibacterial activity of polymyxin B was ascertained against Gram-positive bacteria *S. aureus* MTCC 96 and *E. faecalis* MTCC 439. Initially a 10 µL aliquot of bacterial cell suspension (10^6 CFU of the respective target bacteria suspended in sterile PBS) were inoculated into sterile microtitre plate wells having

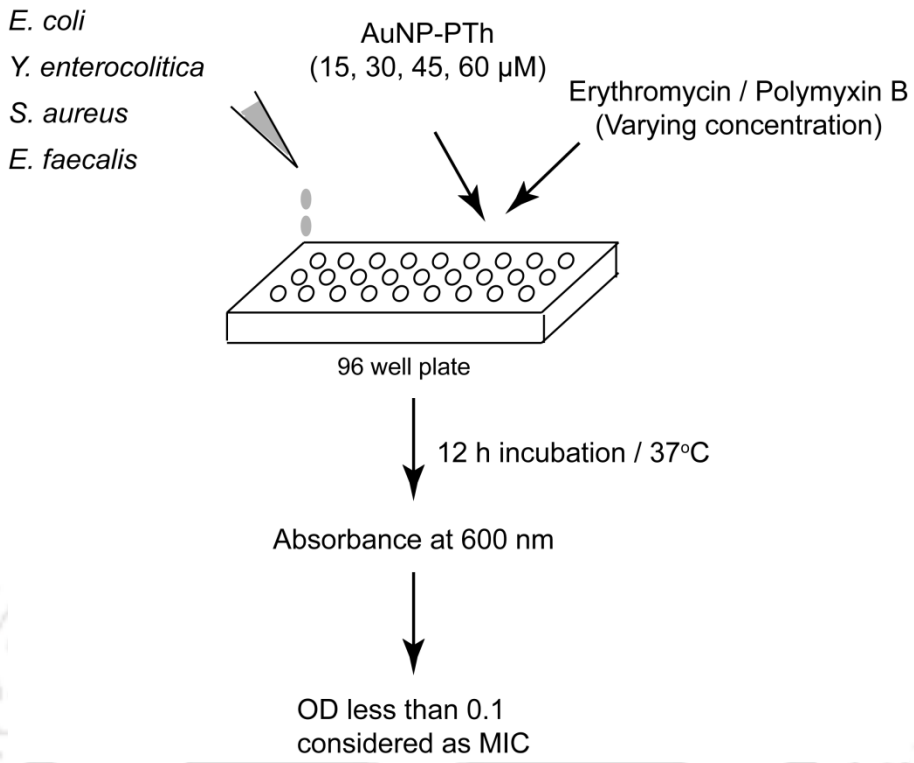

Figure 4.1. Schematic representation of experimental protocol to study the combination effect of antibiotics and AuNP-PTh on target bacterial cells.

requisite growth media (100 µL) incorporated with a serial two fold dilution (5.0 - 320 µg/mL) of either erythromycin or polymyxin B (5.0 - 40 µg/mL). For every concentration of erythromycin or polymyxin B, varying concentrations of AuNP-PTh (15, 30, 45 and 60 µM) was used in combination and the cells were incubated at 37°C and 180 rpm for 6 h. Growth of bacterial cells was estimated by measuring absorbance at 600 nm in a microtitre plate reader (Infinite M200, TECAN, Switzerland) and expressed as percentage growth inhibition compared to untreated cells (cells grown in the absence of antibiotics and AuNP-PTh). For every sample, three independent experiments were performed, each having three replicas. Fold decrease in the MIC of erythromycin and polymyxin B for cells treated with AuNP-PTh in combination was also determined. Data analysis and calculation of standard deviation was performed with Microsoft Excel 2010 (Microsoft Corporation, USA). A schematic indicating the salient steps of the experimental protocol to study the combination effect of antibiotics and AuNP-PTh on target bacterial cells is shown in Figure 4.1.

The interaction of AuNP-PTh and the antibiotics erythromycin or polymyxin B was quantified and expressed as the fractional inhibitory concentration (FIC) index which was determined using the expression:

$FIC = [A] / MIC_A + [B] / MIC_B$

where MIC_A and MIC_B represent the MIC of drug A (erythromycin or polymyxin B) and drug B (AuNP-PTh), respectively, and [A] and [B] are the MIC of drug A and drug B when used in combination. The interaction was interpreted as synergy (FIC ≤0.5), addition (FIC >0.5 to 1.0), indifference (FIC >1.0 to <4.0) and antagonism (FIC ≥ 4.0) following the method described earlier (Giacometti et al., 2000).

4.2.6. Antibacterial activity of AuNP-PTh in simulated gastric fluid

E. coli MTCC 433 and *L. monocytogenes* Scott A were grown in the respective growth medium overnight under the conditions described previously in section 3.2.2. Cells were harvested by centrifugation from a 1.0 mL aliquot of the overnight grown culture, washed twice in sterile 0.85% saline to remove media ingredients and finally the cells (10^6 CFU) were resuspended in 0.5 mL of simulated gastric fluid (SGF), which was prepared according to method described earlier (Charteris et al., 1998). The pH of SGF was adjusted to 2.5 with HCl. Subsequently, the cells were treated in SGF with varying concentrations of AuNP-PTh (30, 60 and 112 µM) at 37^{o}C for 2 h. The control sample consisted of cells suspended in SGF alone under the same conditions. During incubation, the samples were withdrawn periodically and plated to determine percentage viability of cells as compared to control (cells suspended in SGF alone). All experiments were performed in triplicates and a one way analysis of variance (ANOVA) was performed using Sigma Plot version 11.0.

4.2.7. Anti-biofilm activity of AuNP-PTh composite

4.2.7.1. Estimation of biofilm biomass

Biofilm of *P. aeruginosa* MTCC 2488 was grown in sterile 96 well microtitre plate by following a standard method described earlier (Musken et al., 2010). After 24 h of biofilm growth, the spent media was carefully aspirated and fresh growth media having varying concentrations of AuNP-PTh (30, 60 and 112 µM) were added to biofilms in the well.

Following 24 h of incubation, the media was aspirated and the wells were washed thrice with sterile MilliQ water (200 µl) to remove non-adherent bacterial cells. The wells were air dried for 45 min and a 1% (v/v) crystal violet solution (150 µl) was added to each well and incubated for 45 min to stain the biofilm biomass. Subsequently, the wells were washed thrice with sterile water (200 µl) to remove excess stain. The dye incorporated by the biofilm was solubilized with 95% ethanol (200 µl). The solubilized dye solution from each well was transferred into fresh well and the biofilm biomass was estimated by measuring the absorbance of the solution at 590 nm in a microtiter plate reader (Infinite M200, TECAN, Switzerland). All experiments were performed in triplicates and a one way analysis of variance (ANOVA) was performed using Sigma Plot version 11.0.

4.2.7.2. Congo red binding assay

Biofilm of *P. aeruginosa* MTCC 2488 was grown in sterile 96 well microtitre plate and treated with varying concentrations of AuNP-PTh nanocomposite (30, 45, 60 and 112 µM) for 24 h as described previously in section 4.2.7.1. Following treatment with the nanocomposite, the media was aspirated and the wells were washed with sterile MilliQ water (200 µL) to remove non-adherent bacteria. The wells were air dried for 45 min and stained with 1% Congo red dye (prepared in sterile MilliQ water) for 1 min (Izano et al., 2008) and then rinsed and dried. The bound Congo red dye was solubilized with 200 µL of DMSO and its absorbance was measured at 490 nm in a microtiter plate reader (Infinite M200, TECAN, Switzerland). All experiments were performed in triplicates and a one way analysis of variance (ANOVA) was performed using Sigma Plot version 11.0.

4.2.7.3. Fluorescence microscope analysis

Biofilm of *P. aeruginosa* MTCC 2488 was grown in sterile 96 well microtitre plate and treated with varying concentrations of AuNP-PTh nanocomposite (30, 60 and 112 µM) for 24 h as described previously in section 4.2.7.1. Following 24 h of treatment, the media was removed and the wells were washed thrice with sterile MilliQ water (200 µl) to remove non-adherent bacteria. AuNP-PTh-treated as well as control biofilm samples in multiple wells were labeled separately with cFDA-SE and PI following the method described earlier in section 3.2.7.1. and 3.2.7.1. The stained biofilms were observed under a fluorescence

microscope (Eclipse Ti-U, Nikon) with a filter that allowed blue light excitation for cFDA-SE and green light excitation for PI stained cells. Images of the treated and control biofilms were recorded.

4.2.7.4. Field emission scanning electron microscope (FESEM)

P. aeruginosa MTCC 2488 biofilm was grown on a cover slip by following the standard method (Musken et al., 2010). A representative biofilm sample was treated with 112 µM of AuNP-PTh nanocomposite for 6 h. Subsequently, the composite-treated as well as control biofilm samples were washed thrice with filter-sterilized PBS and finally with sterile MilliQ water. The samples were than air-dried in a laminar hood and examined in a field emission scanning electron microscope (Zeiss Sigma, USA) and their images were recorded.

4.2.7.5. Anti-Biofilm activity of AuNP-PTh nanocomposite and tobramycin in combination

Biofilm of *P. aeruginosa* MTCC 2488 was grown in 96 well microtitre plate as described earlier in section 4.2.7.1. The biofilm was then treated with various combinations of tobramycin (0.078-1.25 µg/mL) and AuNP-PTh composite (15, 30, 45, 60 µM). In parallel wells, the biofilm was also treated separately with either tobramycin (0.078-1.25 µg/mL) or AuNP-PTh composite (15, 30, 45, 60 µM). The treated and control biofilm samples were incubated at 37^{o}C in a humid chamber for 24 h. The biofilm biomass was estimated by crystal violet staining method as described earlier in section 4.2.7.1. The results were expressed as percentage growth inhibition compared to untreated biofilm samples. All experiments were performed in triplicates and a one way analysis of variance (ANOVA) was performed using Sigma Plot version 11.0.

4.3. Results and Discussion

4.3.1. Antibacterial activity of erythromycin and polymyxin B in combination with AuNP-PTh nanocomposite

It is largely advocated that the outer membrane in Gram-negative pathogenic bacteria acts as a strong permeability barrier to the passage of antibacterial agents and thus empowers the bacteria to resist the action of therapeutic antibiotics (Nikaido, 2003; Bolla et al., 2011; Saha et al., 2008). For instance, it has been reported that the uptake of a hydrophobic antibiotic such as erythromycin may be reduced due to the presence of the outer membrane permeability barrier in Gram-negative bacteria (Hancock, 1997). In order to facilitate the uptake of antibiotic and enhance its bactericidal efficacy, various approaches have been adopted such as the use of membrane-permeabilizing agents to weaken the outer membrane, application of lipopolysaccharide (LPS) destabilizing agents and inhibition of the efflux pump (Costerton et al., 1999; Alakomi et al., 2006; Helander et al., 1998; Bolla et al., 2011). In the previous study highlighted in chapter 3, it was observed through NPN assay that AuNP-PTh nanocomposite caused extensive membrane-permeabilization in Gram-negative *E .coli* MTCC 433 (refer to Figure 3.11a). Hence it was conceived that treatment of a Gram-negative pathogenic bacteria with AuNP-PTh could perhaps weaken the outer membrane and in turn facilitate enhanced uptake of a hydrophobic antibiotic. To test this premise, the bactericidal efficacy of the hydrophobic antibiotic erythromycin was tested against model Gram-negative pathogenic bacteria in combination with varying concentrations of AuNP-PTh nanocomposite. As shown in Figure 4.2, the inhibition observed with treatment of the target pathogens with increasing concentrations of AuNP-PTh nanocomposite (15, 30 and 45 µM) alone varied from 4%-29% for *E. coli* MTCC 433 and 4%-35% for *Y. enterocolitica* MTCC 859, respectively. On the other hand, treatment of *E. coli* MTCC 433 and *Y. enterocolitica* MTCC 859 with 10 µg/mL erythromycin alone lead to 34%-37% growth inhibition. Interestingly, a significant increase in the growth inhibition of the pathogens was observed with a combined treatment of AuNP-PTh and erythromycin, as compared to either AuNP-PTh or antibiotic alone (Figure 4.2). For instance, the inhibition observed with a combination of 45 µM AuNP-PTh nanocomposite and 10 µg/mL erythromycin was around 85% for *E. coli* MTCC 433 and 80% for *Y. enterocolitica* MTCC 859, respectively (Figure 4.2).

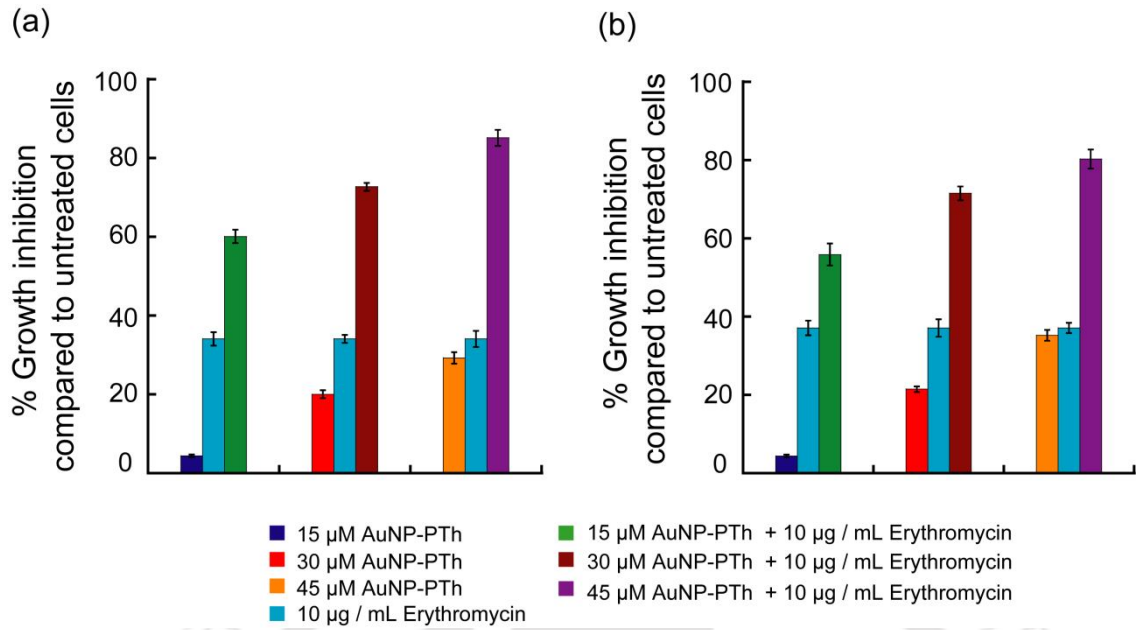

Figure 4.2. Effect of combined treatment of AuNP-PTh nanocomposite and erythromycin on the growth of **(a)** *E. coli* MTCC 433 and **(b)** *Y. enterocolitica* MTCC 859.

The enhanced growth inhibition of the tested pathogenic bacteria in case of combination treatment with AuNP-PTh and erythromycin was also observed for various antibiotic concentrations (refer to Appendix, Figure A4.1). It is significant to mention here that the concentration of AuNP-PTh chosen for these experiments (15, 30 and 45 µM) was significantly lower than its MBC (112 µM). Interestingly, the MIC of erythromycin was reduced two-fold in combination with 15 µM AuNP-PTh and at the highest concentration of AuNP-PTh nanocomposite (45 µM) in combination, the reduction in MIC of erythromycin was a substantial eightfold (Table 4.1). From a therapeutic point of view, this observation is encouraging as it indicates the possibility of minimizing the dose of the antibiotic to eliminate the pathogen and thus addresses the growing concern related to excessive use of antibiotic in combating pathogenic bacteria. The ability of AuNP-PTh nanocomposite to potentiate the action of erythromycin at low concentrations highlights the therapeutic potential of the nanocomposite as an adjuvant in combination therapy.

Table 4.1. Fold reduction in MIC of erythromycin in combination with AuNP-PTh and determination of fractional inhibitory concentration (FIC) index.

Target bacteria	AuNP-PTh (µM)	Folds reduction in MIC of erythromycin	FIC index[a]	Effect[b]
E. coli MTCC 433	15	2	0.6	A
	30	4	0.5	S
	45	8	0.5	S
Y. enterocolitica MTCC 859	15	2	0.3	S
	30	2	0.5	S
	45	8	0.5	S

[a] Fractional inhibitory concentration (FIC) index was assessed as described in section 4.2.5. [b] A: Addition; S: Synergy.

The nature of interaction between AuNP-PTh nanocomposite and erythromycin was ascertained by determining the fractional inhibitory concentration (FIC) index against the target bacteria *E. coli* MTCC 433 and *Y. enterocolitica* MTCC 859. In case of *E. coli* MTCC 433 it was observed that in combination with increasing concentrations of AuNP-PTh nanocomposite there was a reduction in the MIC of erythromycin and the nature of the interaction was additive at lower concentration of the nanocomposite (15 µM) and synergistic at higher concentrations of the nanocomposite (30 µM and 45 µM) as indicated in Table 4.1. The reduction in MIC of erythromycin was also noted for *Y. enterocolitica* MTCC 859 and the interaction was synergistic at all the tested nanocomposite concentration (Table 4.1). The manifestation of a synergy effect suggested that AuNP-PTh nanocomposite perhaps initiates membrane damage in target pathogens, which in turn may augment the accessibility of the internal target for erythromycin, resulting in enhanced killing of the pathogens.

The therapeutic antibiotic polymyxin B is largely known for its potent activity against Gram-negative pathogenic bacteria while Gram-positive bacteria are mostly resistant (Zavascki et al., 2007). Based on the strong membrane-targeting activity of AuNP-PTh nanocomposite, it was construed that the nanocomposite could perhaps be explored to boost the activity of polymyxin B against Gram-positive pathogens. To test

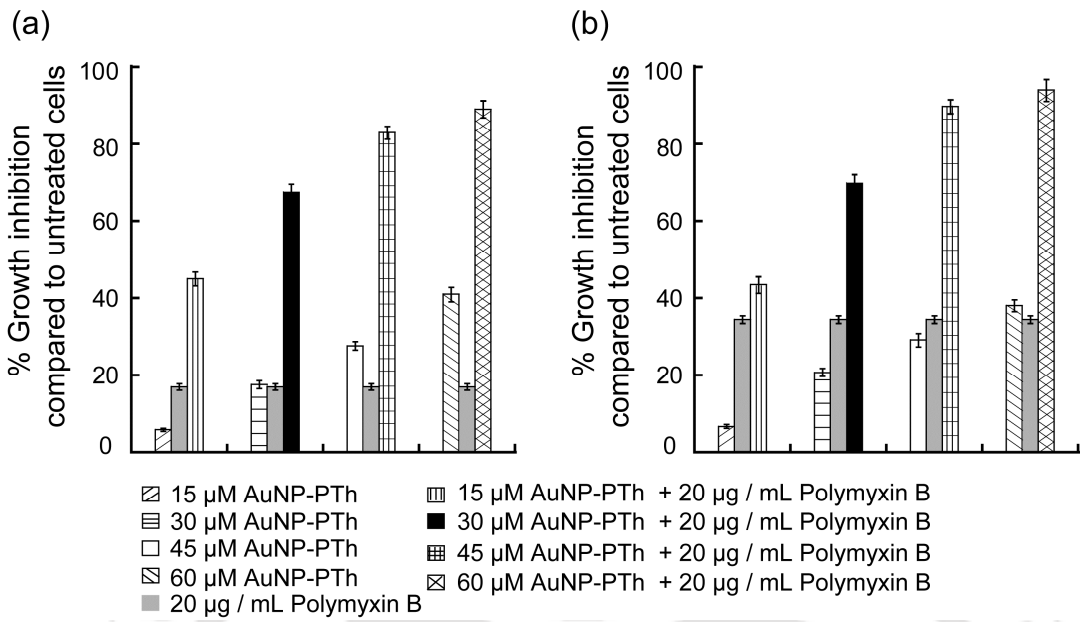

Figure 4.3. Effect of combined treatment of AuNP-PTh nanocomposite and polymyxin B on the growth of **(a)** *S. aureus* MTCC 96 and **(b)** *E. faecalis* MTCC 439.

this premise, the bactericidal activity of polymyxin B was ascertained in combination with varying concentrations of AuNP-PTh nanocomposite. As evident from Figure 4.3, treatment of *S. aureus* MTCC 96 with 20 µg/mL polymyxin B could bring about only 17% growth inhibition of the target pathogen, whereas in case of *E. faecalis* MTCC 439 around 34% growth inhibition was observed when treated with the same concentration of polymyxin B. However, a significant increase in the growth inhibition of the pathogens was observed when the cells were subjected to a combined treatment of AuNP-PTh nanocomposite and polymyxin B, as compared to either AuNP-PTh nanocomposite or antibiotic alone. As evident from Figure 4.3, this effect became more prominent by increasing the dose of AuNP-PTh nanocomposite in combination with 20 µg/mL of polymyxin B. Growth inhibition of the pathogen was also observed for various other concentrations of polymyxin B in combination with the nanocomposite (refer to Appendix, Figure A4.2). The nature of interaction between AuNP-PTh and polymyxin B was ascertained through fractional inhibitory concentration (FIC) index, which was

Table 4.2. Fold reduction in MIC of polymyxin B in combination with AuNP-PTh and determination of fractional inhibitory concentration (FIC) index.

Target bacteria	AuNP-PTh (µM)	Folds reduction in MIC of Polymyxin B	FIC index[a]	Effect[b]
S. aureus MTCC 96	15	4	0.3	S
	30	8	0.5	S
	45	8	0.5	S
E. faecalis MTCC 439	15	2	0.6	A
	30	4	0.5	S
	45	4	0.5	S

[a] Fractional inhibitory concentration (FIC) index was assessed as described in section 4.2.5. [b] A: Addition; S: Synergy.

estimated for both *S. aureus* and *E. faecalis* (Table 4.2). In case of *S. aureus* MTCC 96, a substantial reduction in the MIC of polymyxin B was evident with increasing concentrations of AuNP-PTh nanocomposite and the nature of interaction was synergy. In case of *E. faecalis* MTCC 439, the interaction of AuNP-PTh nanocomposite and the antibiotic was addition at the lowest nanocomposite concentration whereas at higher nanocomposite concentration the interaction was synergy (Table 4.2).

4.3.2. Antibacterial activity of AuNP-PTh nanocomposite in simulated gastric fluid (SGF)

Pathogenic bacteria are highly enduring and have the ability to survive in various harsh environment. In this regard the ability of gastrointestinal pathogens to survive in the harsh acidic environment prevalent in the stomach. Although human gastric fluid has been acknowledged as a defense barrier against enteric pathogens owing to its highly acidic pH, (Tamplin, 2005) many bacterial enteric pathogens are endowed with evolved mechanisms to survive in the acidic milieu of the stomach prior to colonization of the small intestine (Foster, 1999; Foster, 2004; Cotter et al., 2000; Bavaro, 2009; Amieva and El-Omar, 2008; Richard and Foster, 2004). An additional challenge in the elimination of acid-resistant pathogenic bacteria is that therapeutic agents such as antibiotics may suffer a loss of activity in acidic environment (Lamp et al., 1992; Mercier et al., 2002). It may be

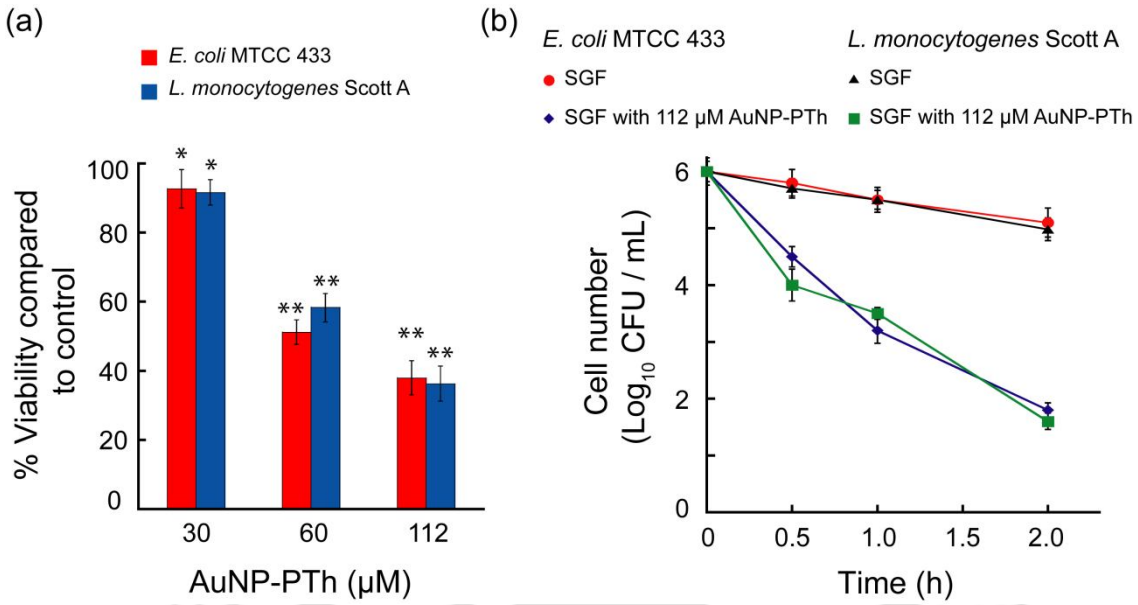

Figure 4.4. (a) Viability of target pathogenic bacteria treated with AuNP-PTh in simulated gastric fluid. Statistically significant values derived by ANOVA are indicated by asterisk marks. * indicates *p* value <0.05 and ** indicates *p* value <0.001. **(b)** Time-dependent effect of AuNP-PTh treatment on *E. coli* MTCC 433 and *L. monocytogenes* Scott A cells in simulated gastric fluid (SGF).

mentioned here that with increasing concentration of AuNP-PTh (15-150 µM), the pH of PBS solution in which the target cells were suspended varied from 4.8-3.7. In the previous chapter (refer to Figure 3.7) it was observed that viable cell populations of bacterial pathogens were reduced on exposure to AuNP-PTh solution (15-150 µM), whose pH was in the acidic range (4.8-3.7) and it was also evident that the acidic pH per se did not account for the loss in viability of target pathogens on exposure to the AuNP-PTh nanocomposite. Hence it was conceived that AuNP-PTh could be a potential antibacterial agent to target acid-resistant bacteria. To evaluate the bactericidal efficacy of AuNP-PTh in an acidic niche, cells of *E. coli* MTCC 433 and *L. monocytogenes* Scott A were suspended in simulated gastric fluid (SGF) having a pH of 2.5 and treated with varying concentrations of AuNP-PTh nanocomposite for 2h. As evident from Figure 4.4a, a decrease in % viability of cells treated with AuNP-PTh was observed for both the pathogens and this reduction in viability was also observed to be dose-dependent and statistically significant based on ANOVA. A time-dependent decrease in cell viability

upon treatment with AuNP-PTh (112µM) in SGF was also observed (Figure 4.4b). There was only a one log reduction in the cell viability when the target bacterial cells were suspended in SGF alone for 2 h (Figure 4.4b). This suggested that the decrease in viability of AuNP-PTh-treated target pathogens in SGF was not influenced by pH. In the present set of experiments the target pathogens suspended in SGF were subjected to the bactericidal action of AuNP-PTh for 2 h. This time period is relevant considering that bacteria in food is likely to be subjected to a pH of 2.5 for approximately 2 h in the gastric environment (Gordon et al., 1993).

4.3.3. Anti-biofilm activity of AuNP-PTh nanocomposite

Bacterial biofilms have been associated with several chronic infections such as bacterial endocarditis and cystic fibrosis (Parsek and Singh, 2003; Tré-Hardy et al., 2009; Fernández-Olmos et al., 2012). Opportunistic pathogens such as *Pseudomonas aeruginosa*, *Staphylococcus epidermidis* and *Staphylococcus aureus* are acknowledged as clinically most significant organisms that form biofilms. Owing to the significance of biofilms in human health and the high resistance of biofilms towards the action of antimicrobial agents, (Mah and O'Toole, 2001; Davies, 2003; Donlan and Costerton, 2002; Amini et al., 2011) there is considerable motivation in the development of bactericidal agents with anti-biofilm activity (Mahmoudi and Serpooshan, 2012). In the present study it was observed that AuNP-PTh nanocomposite displayed profound membrane-directed activity and could readily sensitize pathogenic bacteria to the action of antibiotic. It was thus envisioned that the nanocomposite could perhaps be explored as an anti-biofilm agent. To this end experiments were conducted to evaluate the effects of varying concentration of AuNP-PTh on *P. aeruginosa* biofilm. Treatment of *P. aeruginosa* biofilm with increasing concentration of AuNP-PTh nanocomposite resulted in a corresponding decrease in biofilm biomass as estimated by crystal violet staining (Figure 4.5a) and a reduction in elaboration of extracellular polysaccharide as ascertained by Congo red staining (Figure 4.5b). A one way ANOVA revealed that the reduction in biofilm biomass upon treatment with AuNP-PTh nanocomposite was significant (p value < 0.001) compared to untreated biofilm. Likewise, the reduction in the elaboration of extracellular polysaccharide on treatment of *P. aeruginosa* biofilm with AuNP-PTh nanocomposite was also statistically

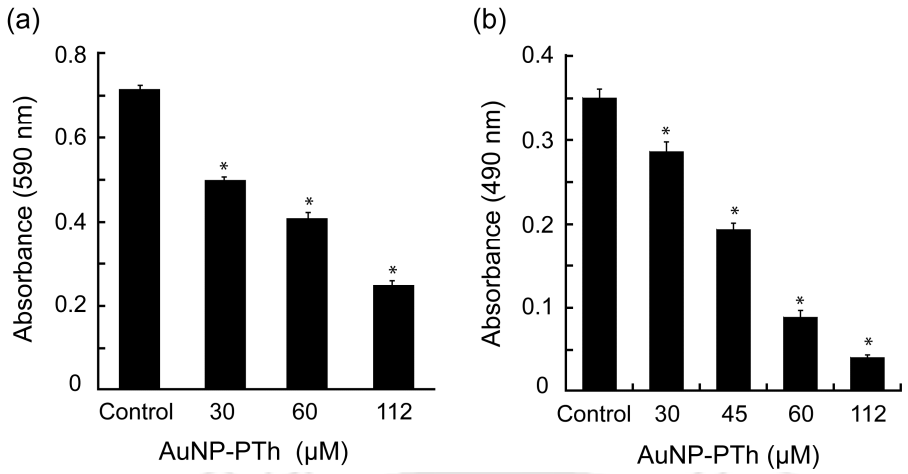

Figure 4.5. Anti-biofilm activity of AuNP-PTh nanocomposite ascertained by **(a)** estimation of *P. aeruginosa* MTCC 2488 biofilm biomass by crystal violet absorbance method and (**b)** Congo red binding assay. Statistically significant values derived by ANOVA are indicated by asterisk marks. * indicates *p* value <0.001.

significant. Given the pivotal role of extracellular polysaccharides in constituting the structural framework of biofilms, protection against physical stress, such as shear and resistance against the action of antimicrobial agents such as antibiotics (Mah and O'Toole, 2001; Stewart, 2001) the ability of AuNP-PTh nanocomposite to influence polysaccharide production in biofilms has significant therapeutic implications.

Fluorescence microscope analysis revealed a structured network of cFDA-SE stained *P. aeruginosa* cells suggesting the presence of a metabolically active biofilm, since cFDA fluorescence is an index of intracellular esterase activity of viable cells (Figure 4.6, panel a). Treatment of biofilm with 112 μM AuNP-PTh resulted in a drastic reduction of bacterial biofilm which manifested as sparse distribution of cFDA stained cells (Figure 4.6, panel b). Further, AuNP-PTh treated biofilm exhibited prominent PI staining, which clearly suggested the presence of membrane damage in nanocomposite-treated biofilm (Figure 4.6, panel d). These results indicated that AuNP-PTh could pervade across the extracellular matrix of *P. aeruginosa* biofilm to reach the embedded microcolonies and bring about copious membrane damage to the cells. Biofilms of pathogenic bacteria are known to be resistant to the action of antibiotics (Keren et al., 2004; Fux et al., 2005) and

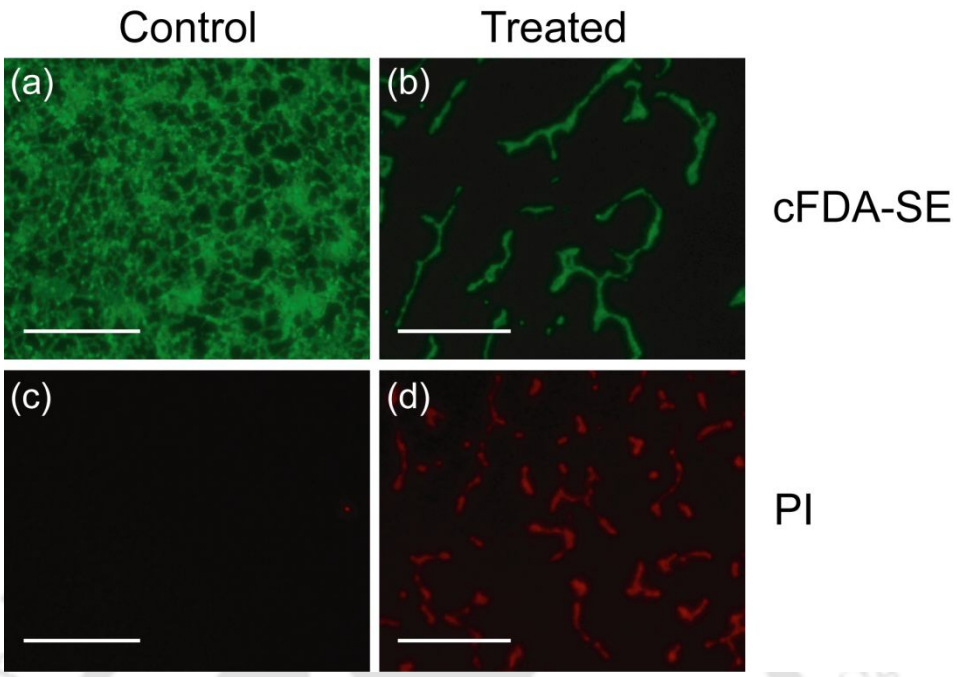

Figure 4.6. Fluorescence microscope analysis of *P. aeruginosa* MTCC 2488 biofilm treated with 112 µM AuNP-PTh nanocomposite. Biofilm was visualized by **(a-b)** cFDA-SE staining and **(c-d)** PI staining. Scale bar for the images is 100 µm.

in this context, the ability of AuNP-PTh to infiltrate and eradicate bacterial biofilm holds special therapeutic interest.

Evidence for anti-biofilm activity of AuNP-PTh nanocomposite was further strengthened by FESEM analysis. As evident from Figure 4.7a, in case of untreated biofilm of *P. aeruginosa* MTCC 2488, the shape of the cells were quite distinct and the cells appeared to be enveloped by a slimy layer, which presumably is the polysaccharide elaborated by the biofilm. On the other hand, in the nanocomposite- treated samples, the biofilm architecture was apparently disintegrated and damaged cells with irregular shape were observed (Figure 4.7b).

To further explore the anti-biofilm activity of AuNP-PTh nanocomposite, experiments were conducted to ascertain the effect of sub-MIC levels of the nanocomposite on the action of tobramycin, an antibiotic which is known to exhibit anti-biofilm activity against *P. aeruginosa* (Musken et al., 2010, Tré-Hardy et al., 2009; Kim et al., 2008). The representative results of the experiments are shown in Figure 4.8. It can be

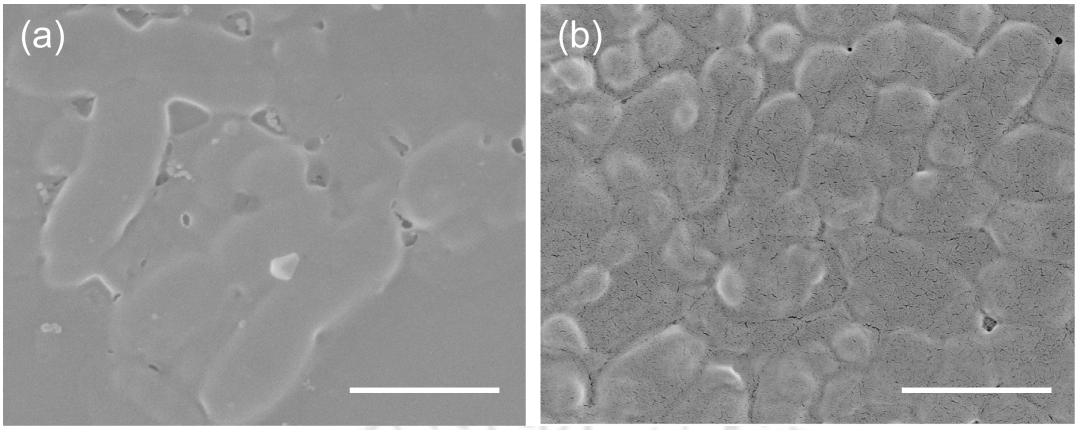

Figure 4.7. Field emission scanning electron microscope (FESEM) analysis of **(a)** untreated and **(b)** AuNP-PTh nanocomposite treated biofilm of *P. aeruginosa* MTCC 2488. Scale bar for the images is 1.0 µm.

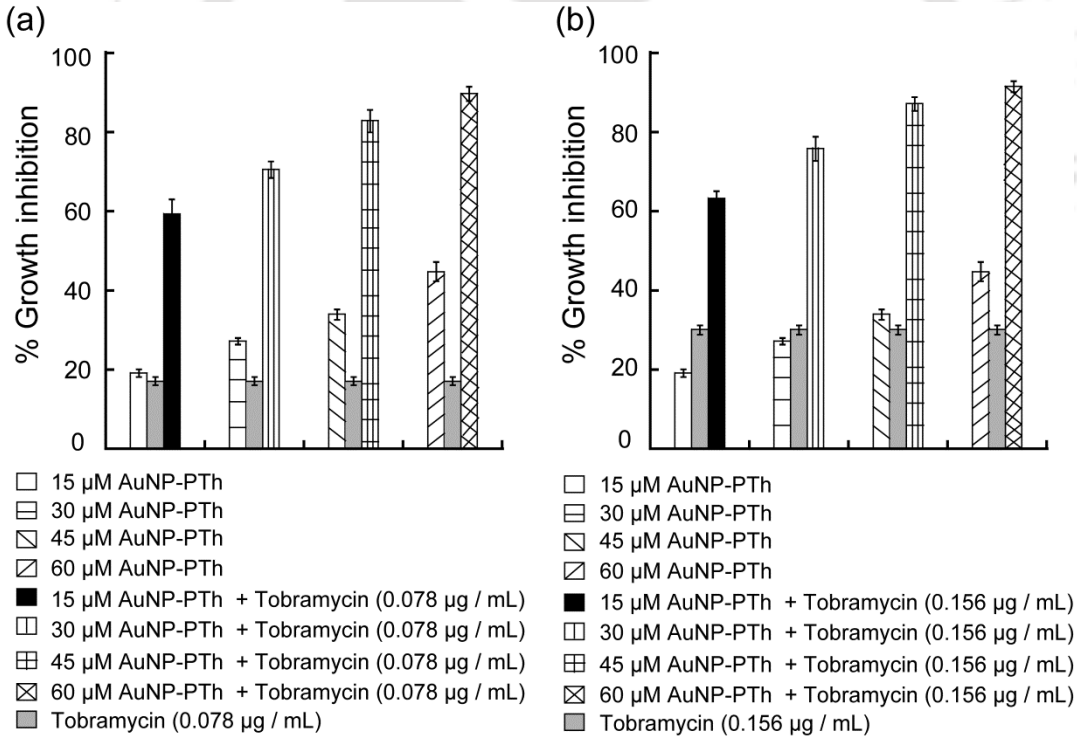

Figure 4.8. Effect of combined treatment of AuNP-PTh nanocomposite and tobramycin on the growth of *P. aeruginosa* MTCC 2488 biofilm.

observed from the figure that treatment of *P. aeruginosa* MTCC 2488 biofilm with 0.078 and 0.156 µg/mL tobramycin resulted in about 17% and 30% growth inhibition, respectively. Interestingly, in a combinatorial assay, a progressive increase in the growth inhibition of biofilm was observed with increase in the concentration of AuNP-PTh nanocomposite. For instance, there was more than 90% growth inhibition of *P. aeruginosa* biofilm at a tobramycin concentration of 0.156 µg/mL in combination with 60 µM composite (Figure 4.8b). It is significant to mention here that the concentrations of AuNP-PTh composite and tobramycin used for the combinatorial assays were below their respective MIC values for the target pathogen. The ability of low levels of AuNP-PTh nanocomposite to potentiate the action of tobramycin reflects the therapeutic merit of the nanocomposite as an adjuvant in combination therapy for eradication of *P. aeruginosa* biofilm. Further, it also offered the opportunity to reduce the levels of tobramycin to be used for effective elimination of the biofilm. This is significant given that therapeutic applications of tobramycin at high concentrations may lead to unwarranted side effects (Thomsen and Friis, 1979).

4.4. Significant Findings

The present study essentially demonstrates the therapeutic potential of AuNP-PTh nanocomposite in combination therapy with antibiotics, elimination of model gastrointestinal pathogens in a simulated gastric fluid and eradication of bacterial biofilms. The key findings of the study are as follows:

1. The membrane-directed activity of AuNP-PTh composite could be successfully explored in sensitizing target pathogenic bacteria and enhancing the efficacy of the model therapeutic antibiotics erythromycin and polymyxin B. A synergistic interaction was observed when the antibiotics were used in combination with higher concentration of AuNP-PTh nanocomposite.
2. AuNP-PTh nanocomposite could readily eliminate model gastrointestinal pathogenic bacteria in simulated gastric fluid (SGF). It is also to be noted that the bactericidal activity of AuNP-PTh was retained in a highly acidic environment of the SGF and there was no interference from the SGF components, indicating that

the nanocomposite was robust. This is an encouraging therapeutic attribute of the nanocomposite and in future it would be interesting to validate these findings in *in vivo* infection models of gastrointestinal pathogens.

3. Experimental results revealed that AuNP-PTh nanocomposite alone or in combination with tobramycin could substantially eradicate bacterial biofilm. This finding auger well for future therapeutic application of the nanocomposite to curb *in vivo* models of biofilm infection.

There is a considerable demand for the development of new nanoscale materials as antibacterials which would not only be potent against pathogenic bacteria but would also be safe and non-cytotoxic. In this direction, the study on the antibacterial activity of AuNP-PTh nanocomposite highlighted in chapter 3 and chapter 4 is a case in point. In line with the enormous scope of using nanomaterials in combination with biomolecules in order to develop innovative, novel and safer therapeutic antibacterials, the generation of nisin-gold nanoparticle composite and its retention of antimicrobial activity at elevated pH is reported in the next chapter.

Chapter 5

Generation of a Bactericidal Nanocomposite Based on Nisin with Retention of Activity at Elevated pH

This chapter describes a soft-tailoring strategy for retaining the biological activity of the antimicrobial peptide nisin at elevated pH. Nisin-organic acid complex and nisin-gold nanoparticle composite was generated, which displayed the characteristic nisin activity even at elevated pH, in contrast to nisin alone.

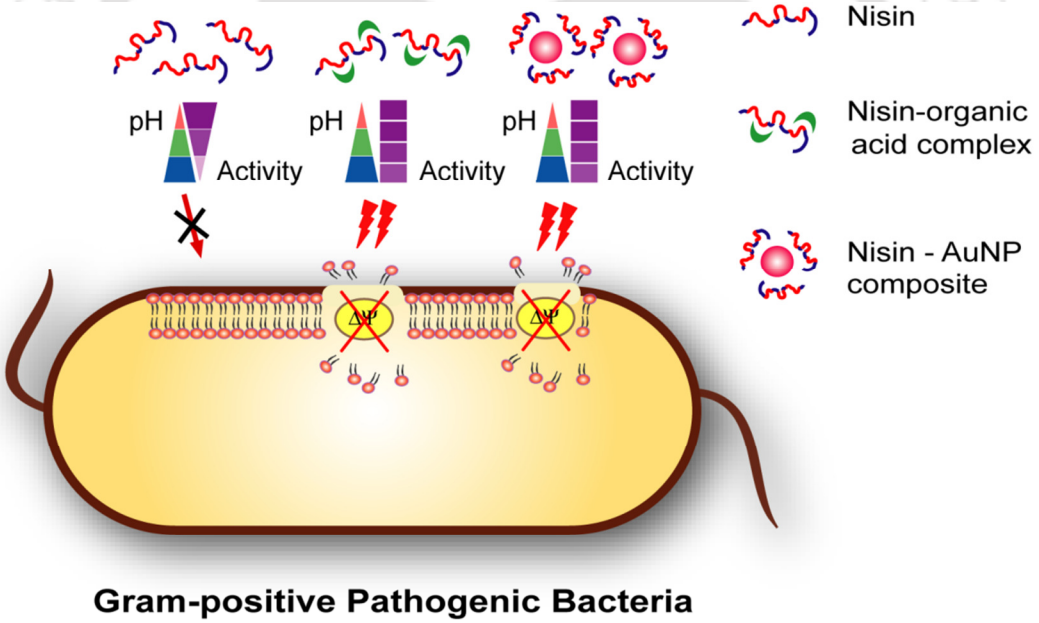

ABSTRACT

Nisin is an FDA approved antimicrobial peptide that holds considerable prospect in healthcare applications. However, the low solubility and loss of biological activity of nisin at physiological pH is a major impediment. To circumvent this problem, it was envisaged that nisin can perhaps form hydrogen bonds with biocompatible organic acids in solution even at elevated pH to generate nisin-organic acid complex (N-OAC), which could lead to improved solubility of the peptide and retention of its activity. Nisin was interacted with a set of biocompatible organic acids such as citric acid (CA), lactic acid (LA), ascorbic acid (AA), oxalic acid (OA) and gallic acid (GA) in order to generate nisin-organic acid complex (N-OAC) in solution. The formation of N-OAC was evidenced by FTIR analysis. Conventional agar well diffusion assay, cFDA-SE leakage assay and PI uptake assay revealed that all the generated N-OACs displayed antibacterial activity and the signature membrane-directed activity of nisin at elevated pH, in contrast to nisin alone. A CD spectrum of nisin-citric acid (nisin-CA) complex at pH 7.0 and pH 8.0 revealed an overall conservation of the spectral pattern of nisin, which perhaps explains the retention of nisin activity at elevated pH. Recovery of the bioactive nisin-organic acid complex from solution poses a practical problem. To overcome this impasse, nisin-citrate stabilized AuNP (N-AuNP) composite was generated, wherein hydrogen bond formation between nisin and citrate-stabilized AuNPs could render enhanced solubility and retention of nisin activity at elevated pH. Formation of N-AuNP composite was studied by UV-visible extinction spectrum and TEM analysis and manifestation of characteristic nisin activity in N-AuNP composite at elevated pH was verified by fluorescence-based assays in solution as well as fluorescence microscope analysis. An *in vitro* MTT-based assay suggested that both nisin-CA complex and N-AuNP composite were non-toxic to human adenocarcinoma HT-29 cells.

5.1. Introduction

The advent of drug-resistant pathogenic bacteria is a global healthcare problem of great concern (Nikaido, 2009; Fischbach and Walsh, 2009). To combat this challenge, an innovative therapeutic approach is the need of the hour, for which development of novel and efficient bactericidal agents, radically different from conventional antibiotics is critical. In this context, a desirable endeavour would be to generate novel antimicrobial agents that are potent and non-toxic to human cells and displaying a mechanism of action that does not favor development of resistance in the target bacteria. Conceivably, membrane-targeting antimicrobial agents hold considerable therapeutic promise since the probability of developing resistance against them would require extensive restoration of membrane components, which can be an uphill task for the bacteria (Bambeke et al., 2008; Hurdle et al., 2011). Amongst the known membrane-acting antimicrobial agents, cationic antimicrobial peptides (AMPs) are attractive and hold considerable potential as therapeutic agents (Zasloff, 2002; Mangoni et al., 2003; Hancock and Chapple, 1999; Brogden, 2005).

Lantibiotics constitute a group of ribosomally synthesized and post-translationally modified antimicrobial peptides (AMPs), which are typically recognized by the presence of several unusual amino acids like lanthionine, methyllanthionine, 2,3-didehydroalanine, 2,3-didehydrobutyrine (Chatterjee et al., 2005; Willey et al., 2007). Lantibiotics have been in focus owing to their significant activity against Gram-positive pathogenic bacteria, and a large number of fundamental studies have contributed significantly in unraveling the structure-function relationship, enzymology, biosynthetic regulation and protein engineering of these molecules (Chatterjee et al., 2005; van Kraaiji et al., 1999; McAuliffe et al., 2001; Willey and van der Donk, 2007). Nisin is a prototype lantibiotic and a Generally Recognized As Safe (GRAS) peptide and FDA approved natural food preservative (Breukink and de Kruijff, 1999; Lubelski et al., 2008; Chen and Hoover, 2003; Cotter et al., 2005.; Sobrino-Lopez and Martin-Belloso, 2008). Studies have shown that nisin acts on the membrane of target bacteria and exerts its bactericidal activity by pore formation and disruption of cell wall synthesis by specific binding to lipid II, which is an essential precursor in peptidoglycan synthesis (Bonelli et al., 2006; Breukink et al., 1999; Hasper et al., 2006; Hsu et al., 2004; Wiedemann et al., 2001).

In recent times there has been a growing interest in application of nisin particularly in healthcare. Recognition of this window of opportunity is based on emerging literature reports, which suggest activity of nisin against drug-resistant pathogens (Brumfitt et al., 2002; Mota-Meira et al., 2000; Piper et al., 2009; Severina et al., 1998). However, low solubility and instability of nisin at physiological pH and above (Liu and Hansen, 1990; Rollema et al., 1995) is a major impediment to this prospect. Protein engineering in recent years has provided prominent examples of enhancing the functionality of nisin through controlled genetic manipulations (Rollema et al., 1995; Field et al., 2010; Field et al., 2012). Although genetic engineering has the potential to render tremendous structural diversity to antimicrobial peptides and facilitate their rational screening as antimicrobials, the process can be quite strenuous. To circumvent the problem of low solubility and loss of activity of nisin at high pH, a facile method of generating nisin-organic acid complex (N-OAC) and nisin-gold nanoparticle (N-AuNP) composite is described in this chapter, wherein the characteristic nisin activity is retained even at elevated pH.

5.2. Materials and Methods

5.2.1. Chemicals

Nisin, potassium bromide (IR grade), 5 (and 6)-carboxyfluorescein diacetate succinimidyl ester (cFDA-SE), propidium iodide (PI), carbonyl cyanide m-chlorophenylhydrazone (CCCP) and 3,3'-dipropylthiadicarbocyanine iodide ($DiSC_35$) were obtained from Sigma-Aldrich Chemicals, USA. Glutaraldehyde, tri-sodium citrate 2-hydrate and organic acids which included citric acid (CA), lactic acid (LA), ascorbic acid (AA), oxalic acid (OA) and gallic acid (GA) were purchased from Merck, Mumbai, India. HEPES buffer was procured from Sisco Research Laboratories (SRL), Mumbai, India. Dulbecco's Modified Eagles medium (DMEM), penicillin, streptomycin and MTT reagent were obtained from Sigma-Aldrich Chemicals, USA. Fetal calf serum (FCS) was obtained from PAA Laboratories, USA.

5.2.2. Bacterial strains and growth conditions

The bacterial strains used in the present investigation comprised of *Micrococcus luteus* ATCC 9341 (*M. luteus*) and *Listeria monocytogenes* Scott A (*L. monocytogenes*). The

growth media used for propagating the bacterial strains were purchased from HiMedia, Mumbai, India. Prior to experiments, the bacterial strains were propagated in Brain-Heart Infusion (BHI) broth at 37^{o}C and 180 rpm for 12 h.

5.2.3. Preparation of nisin solution

A 10 mg/mL stock solution of nisin (equivalent to 10,000 IU/mL) was prepared in 0.75% NaCl solution (pH 5.5 adjusted with 0.1 N HCl). The stock solution was filter-sterilized using a 0.22 µm membrane filter (Pall Life Sciences, USA) and stored in -20^{o}C.

5.2.4. Preparation of nisin-organic acid (N-OAC) complex

Initially a 6.8 mM stock of all the organic acids (citric acid, lactic acid, ascorbic acid, oxalic acid and gallic acid) was prepared in sterile MilliQ water. To prepare N-OAC complex, the respective stock solutions of nisin and various organic acids were mixed in appropriate proportions to yield a solution wherein the final acid concentration was 3.4 mM and nisin concentration was 50 IU/mL, 100 IU/mL and 200 IU/mL, respectively. The pH of the solution was adjusted to various levels as per experimental requirements with either 0.1 N HCl or 0.1 N NaOH. Subsequently the contents of the solution were allowed to mix thoroughly in a shaking incubator at room temperature (25^{o}C) for 2 h to facilitate formation of nisin-organic acid complex. The complex solutions were always prepared fresh prior to experiments unless stated otherwise.

5.2.5. FT-IR analysis of nisin-organic acid complex

FT-IR spectra of N-OAC complex samples (corresponding to 200 IU/mL nisin concentration) were recorded in KBr pellet at 4 cm^{-1} resolution in a spectrometer (Spectrum One, Perkin-Elmer). Five scans were performed for every sample in the range of 4000 to 450 cm^{-1}. A background spectrum for pure KBr was also measured.

5.2.6. Circular Dichroism (CD) spectra of nisin-citric acid (nisin-CA) complex

For CD spectra analysis, separate aliquots of nisin solution (pH 5.5 and pH 8.0, each corresponding to 200 IU/ml nisin concentration) and nisin-CA complex solution (pH 7.0 and pH 8.0, each corresponding to 200 IU/mL nisin concentration) were prepared in 10

mM phosphate buffer of respective pH. The CD spectra of each of these samples were recorded between 240 and 190 nm on a J-815 spectropolarimeter (JASCO) with a 1 mm path length cuvette at 25^{o}C. CD spectra of the respective buffers were also recorded and subtracted from the sample readings to eliminate the background signal. For every sample, eight scans were recorded and averaged in order to improve the signal-to-noise ratio. Data were digitally acquired every 1 nm and the obtained spectra was smoothed using the instruments in-built program.

5.2.7. Preparation of nisin-gold nanoparticle (N-AuNP) composite

Synthesis of citrate-stabilized gold nanoparticles (AuNPs) was accomplished by the method described earlier in 2.2.3. For studying nisin-AuNP interaction in solution, citrate-stabilized AuNP solution (0.25 nM) was taken in a series of microcentrifuge tubes, to which varying volumes of nisin stock solution was added drop wise to achieve adequate mixing and to attain a final nisin concentration of 25 IU/mL, 50 IU/mL, 100 IU/mL, 150 IU/mL, 200 IU/mL and 300 IU/mL. Following incubation at room temperature for 30 min, UV-visible extinction spectrum of the samples was recorded in a spectrophotometer at a wavelength set from 400-800 nm. All measurements were taken from three independent experimental samples. Aliquots of the sample from the series were also subjected to TEM analysis.

The N-AuNP composite was prepared by interacting AuNP solution with nisin stock solution as mentioned previously so as to achieve a final nisin concentration of 50 IU/mL, 100 IU/mL and 200 IU/mL. Following incubation of nisin and AuNP solution for 30 minutes, the solution was centrifuged at 15,000 rpm for 20 min. The pellet representing nisin-AuNP composite was resuspended in sterile MilliQ water. UV-visible extinction spectrum and TEM analysis of N-AuNP composite was pursued as mentioned earlier. Subsequently the pH of the composite was adjusted separately to 5.5, 7.0 and 8.0 for further experiments.

5.2.8. Agar well diffusion assay

Agar well diffusion assay was conducted to ascertain the antimicrobial activity of nisin, N-OAC complex solutions, N-AuNP composite, various organic acids and citrate-stabilized

AuNP solution. As per requirement of various experiments, pH of the samples was adjusted to various levels. The assay plates had a bottom layer of BHI agar (1.5% agar), which was overlaid with BHI soft agar (0.8% agar) seeded with 10^6 cells of freshly grown target cells of *M. luteus* ATCC 9341. Requisite number of holes of 6.0 mm diameter was punched in all the assay plates. To each well, 30 µl of test sample was added. The plates were pre-incubated at 4°C for 3 h to facilitate diffusion of the sample followed by incubation at 37°C for 24 h. The antimicrobial activity of the samples was determined by observing the zone of inhibition produced around the wells.

5.2.9. cFDA-SE leakage assay

Target cells of *M. luteus* ATCC 9341 were labeled with 5 (and 6)-carboxyfluorescein diacetate succinimidyl ester (cFDA-SE) as follows: Overnight grown cells of *M. luteus* ATCC 9341 were harvested by centrifugation at 8,000 rpm for 5 min. The cell pellet was washed twice with sterile phosphate buffer saline (PBS) and labeled with cFDA-SE (final concentration of 50 µM) at 37°C for 20 min. The labeling reaction was terminated by pelleting the cells followed by washing of cells twice with sterile PBS to remove excess cFDA-SE molecules. The labeled cells (approximately 10^6 CFU/mL) were treated with nisin, N-OAC complex and N-AuNP composite solutions of varying concentration and pH at 37^{o}C and 180 rpm for 3 h. In case of control samples, pH adjusted buffer solutions, various organic acid solutions or citrate-stabilized AuNPs were added to labeled cells and incubated under the same conditions. Subsequently all the samples were centrifuged at 8,000 rpm for 10 min. Leakage of carboxyfluorescein from cells was determined by measuring fluorescence of the cell free supernatant at an excitation wavelength of 488 nm and emission wavelength of 518 nm in a spectrofluorimeter (FluoroMax-3, HORIBA). The fluorescence measurements were recorded after subtracting the fluorescence of effluxed dye from control samples (cFDA-SE labelled cells in sterile PBS). Fluorescence measurements were taken for three independent experimental samples. The fluorescence intensity of effluxed cFDA obtained for samples treated with nisin solution of varying concentration and pH 5.5 was expressed as maximum nisin activity (100%). The fluorescence intensity of effluxed cFDA obtained for samples treated with nisin-organic

acid complex and nisin-AuNP composite solutions was compared with that obtained for nisin of corresponding concentration and pH 5.5 and expressed as % nisin activity.

5.2.10. Determination of minimum inhibitory concentration (MIC)

Target bacterial cells of *M. luteus* ATCC 9341 were inoculated at 1% level in microtitre wells having the requisite growth medium and grown overnight at 37^{o}C and 130 rpm in presence of varying concentrations of nisin, N-OAC complex and N-AuNP composite solutions (2.5-640 IU/mL nisin concentration) adjusted to various pH (5.5, 7.0 and 8.0). Bacterial cell growth was determined by measuring absorbance at 600 nm in a microtitre plate reader (Infinite M200, TECAN, Switzerland). MIC of the antimicrobial agents was recorded as the lowest concentration which resulted in OD_{600} reading of <0.1, indicating lack of cell growth. The MIC values were calculated from three independent experiments, each having three replicas. Data analysis and calculation of standard deviation was performed with Microsoft Excel 2010 (Microsoft Corporation, USA).

5.2.11. Cell viability assay

Approximately 10^6 CFU/mL of target pathogens *M. luteus* ATCC 9341 and *L. monocytogenes* Scott A (in sterile PBS) were interacted with nisin, N-OAC complex and N-AuNP composite solutions whose pH was adjusted to various levels. The nisin concentration in the samples corresponded to 200 IU/mL. Viable cell numbers (Log_{10} CFU) were determined at regular intervals by serial dilution and plating.

5.2.12. PI uptake assay

A 1.5 mM stock solution of PI was prepared in sterile MilliQ water and stored at 4°C. Approximately 10^6 CFU/mL of the target bacteria *M. luteus* ATCC 9341 (in sterile PBS) was treated with nisin, N-OAC complex and N-AuNP composite solutions of varying concentration and pH at 37^{o}C and 180 rpm for 3 h. In case of control samples, pH adjusted buffer solution, citric acid solution or citrate-stabilized AuNPs were added to cells and incubated under the same conditions. Subsequently, cells were washed with sterile PBS and PI was added to both treated cells and control samples at a final concentration of 30 μM. After 30 min of incubation in a circulating water bath incubator (Amersham) set at

37°C, samples were centrifuged and washed in distilled water to remove excess dye. The cells were resuspended in sterile PBS and fluorescence was measured in a spectrofluorimeter (FluoroMax-3, HORIBA) at an excitation wavelength of 535 nm and emission wavelength of 617 nm. Fluorescence data for each sample was normalized with the optical density at 617 nm. The values obtained for control samples were subtracted from all experimental values. Fluorescence measurements were taken for three independent samples. The fluorescence intensity of PI obtained for samples treated with nisin solution of varying concentration and pH 5.5 was expressed as maximum nisin activity (100%). The fluorescence intensity of PI obtained for samples treated with nisin-CA complex and N-AuNP composite solutions was compared with that obtained for nisin of corresponding concentration and pH 5.5 and expressed as % nisin activity.

5.2.13. Fluorescence microscopy

Approximately 10^6 CFU/mL of target bacteria *M. luteus* ATCC 9341 (in sterile PBS) was treated with nisin, nisin-CA complex and N-AuNP composite solutions (each corresponding to 200 IU/mL nisin concentration) of varying pH (5.5 and 8.0) at 37^{o}C and 180 rpm for 3 h. In case of control sample, pH adjusted buffer was added to cells and incubated under the same conditions. Subsequently, cells were washed twice with sterile PBS and both the treated and control cells were labeled with cFDA-SE and PI as mentioned previously. The stained cells were then fixed in 2.5% glutaraldehyde and washed twice with sterile PBS. A 10 µl aliquot of the fixed sample was spotted on a clean glass slide, air dried and observed under fluorescence microscope (Eclipse Ti-U, Nikon) with a filter that allowed blue light excitation for cFDA-SE and green light excitation for PI stained cells. Images of the treated and control cells were recorded.

5.2.14. Effect of membrane potential on antimicrobial activity

M. luteus ATCC 9341 cells were pre-treated with CCCP to collapse the transmembrane proton motive force as described previously (Mangoni et al., 2003). Approximately 10^7 CFU/mL CCCP treated and untreated cells (control) were suspended in sterile PBS and incubated with nisin (200 IU/mL, pH 5.5 and 8.0), nisin-CA complex (corresponding to 200 IU/mL nisin concentration, pH 8.0) and N-AuNP composite (corresponding to 200

IU/mL nisin concentration, pH 8.0) for 3 h and 6 h at 37°C. Survival of treated and control cells were compared by plating the samples and determining the viable cell count.

5.2.15. Membrane depolarization assay

M. luteus ATCC 9341 cells were grown till mid-logarithmic phase (OD_{600} = 0.4-0.5). The cells were harvested by centrifugation, washed with a buffer solution (5 mM HEPES buffer, 5 mM glucose, pH 7.2) and suspended in the same buffer to an OD_{600} of 0.05. The cell suspensions were incubated with 0.4 μM $DiSC_35$ for 1h at 37°C followed by the addition of 100 mM KCl. The cell suspension (1.0 mL) was placed in separate cuvettes to which nisin (200 IU/mL, pH 5.5 and 8.0), nisin-CA complex (corresponding to 200 IU/mL nisin concentration, pH 8.0) and N-AuNP composite (corresponding to 200 IU/mL nisin concentration, pH 8.0) solution was added and the fluorescence readings were monitored periodically in a spectrofluorimeter (FluoroMax-3, HORIBA) at an excitation wavelength of 622 nm and emission wavelength of 670 nm.

5.2.16. Storage studies

Nisin (200 IU/mL, pH 5.5), nisin-CA complex (corresponding to 200 IU/mL nisin concentration, pH 5.5, 7.0 and 8.0) and N-AuNP composite (corresponding to 200 IU/mL nisin concentration, pH 5.5, 7.0 and 8.0) solutions were stored at 4°C and room temperature (25°C) for a period of seven days. Samples were periodically withdrawn during storage (1, 3, 5 and 7 days) and their antimicrobial activity was tested by interacting with 10^6 CFU/mL *M. luteus* ATCC 9341 cells for 3 h at 37°C and 180 rpm. Subsequently the samples were surface plated on BHI-agar plate and viable cell numbers were enumerated after overnight incubation at 37°C. In case of control samples, target cells were treated with freshly prepared nisin solution (200 IU/mL, pH 5.5) and cell viability was determined as mentioned previously. The viable cell numbers obtained from treated samples were compared with control samples and the results were expressed as % activity compared to control.

5.2.17. Cytotoxicity assay

Cytotoxicity of purified nisin, nisin-citric acid complex and nisin-AuNP composite were assessed on human HT-29 colon adenocarcinoma cells by a standard MTT assay following the manufacturer instruction (Sigma-Aldrich, MO, USA). Dulbecco's Modified Eagle Medium (DMEM), penicillin, streptomycin and trypsin-EDTA solution were obtained from Sigma-Aldrich Chemicals, USA. Fetal bovine serum (FBS) was procured from PAA Laboratories, USA. HT-29 cells were initially grown in 25 cm^2 tissue culture flask by following the method described earlier in section 3.2.8. Prior to performing the cytotoxicity assay, cells were trypsinized and subsequently seeded onto 96-well tissue culture plates at a density of 10^4 cells per well and incubated with varying concentrations of purified nisin, nisin-CA complex and N-AuNP composite made in DMEM for a period of 24 h in a CO_2 incubator with 5% CO_2. Following incubation, the growth media was removed and fresh DMEM containing MTT solution was added. The plate was incubated for 3 h at 37°C. Subsequently, the supernatant was removed, the insoluble colored formazan product was solubilized in DMSO, and its absorbance was measured in a microtitre plate reader (Infinite M200, TECAN, Switzerland) at 550 nm. The assay was performed in six sets for each concentration of purified nisin, nisin-citric acid complex and nisin-AuNP composite. Data analysis and determination of standard deviation was performed with Microsoft Excel 2010 (Microsoft Corporation, USA). In the MTT assay, the absorbance obtained for solvent control samples (cells treated with DMSO alone) was considered to represent 100% cell viability, whereas the absorbance for other treated cells were compared to that obtained for solvent control cells in order to determine % cell viability.

5.3. Results and Discussion

5.3.1. Preparation and characterization of nisin-organic acid complex

Nisin is a cationic peptide with an amino acid composition, which indicates the presence of a large number of hydrogen bond donor as well as acceptor groups (Chatterjee et al., 2005; Willey and van der Donk, 2007). The structure of nisin is indicated in Figure 5.1.On the other hand, biocompatible organic acids such as citric acid (CA), lactic acid (LA), oxalic acid (OA), ascorbic acid (AA) and gallic acid (GA) used in the present study also bear relevant functional groups to form hydrogen bonds. The structure of the organic acids used in the present study is indicated in Figure 5.2. It was conceived that the organic acids could readily associate as cognate partners in solution with nisin through hydrogen bonds, which in turn may lead to enhanced solubility of nisin. Further, even at elevated pH, the organic acids would be deprotonated (pKa <5.5) and can still form hydrogen bonds (Figure 5.3) and ensure solubility of nisin, which may result in retention of nisin activity in solution**.** Following interaction of nisin with various organic acids in solution, the formation of nisin-organic acid complex (N-OAC) was verified by FTIR analysis by observing changes in C=O stretching frequency of the organic acids (Max and Chapados,

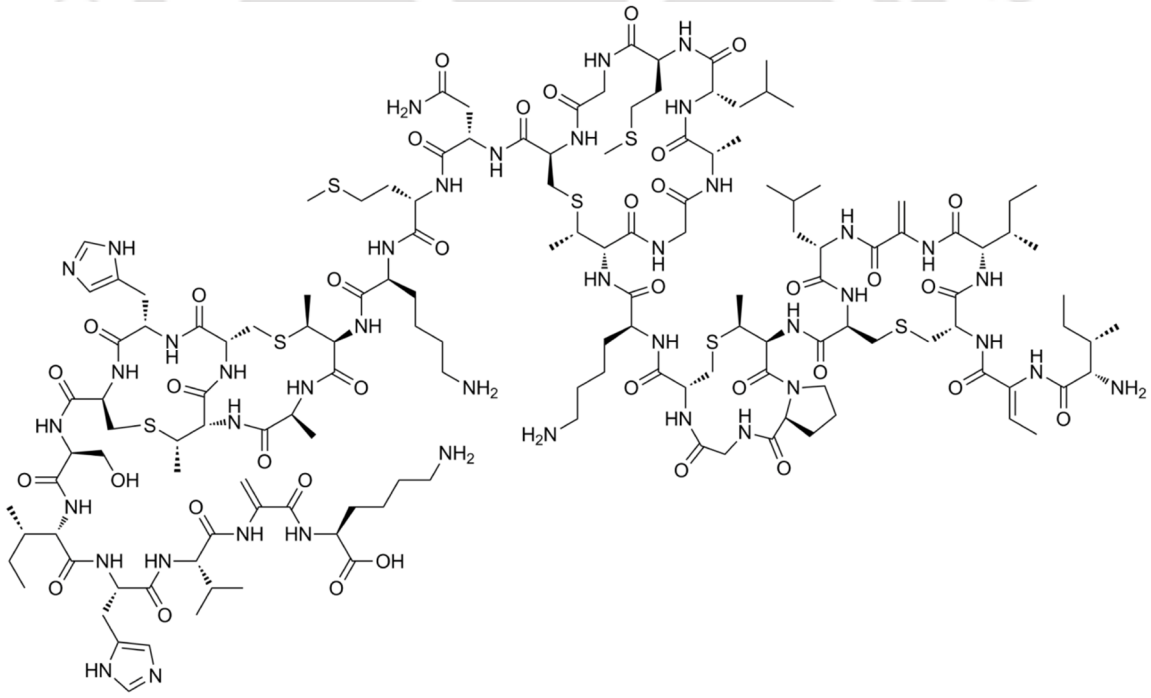

Figure 5.1. Structure of nisin.

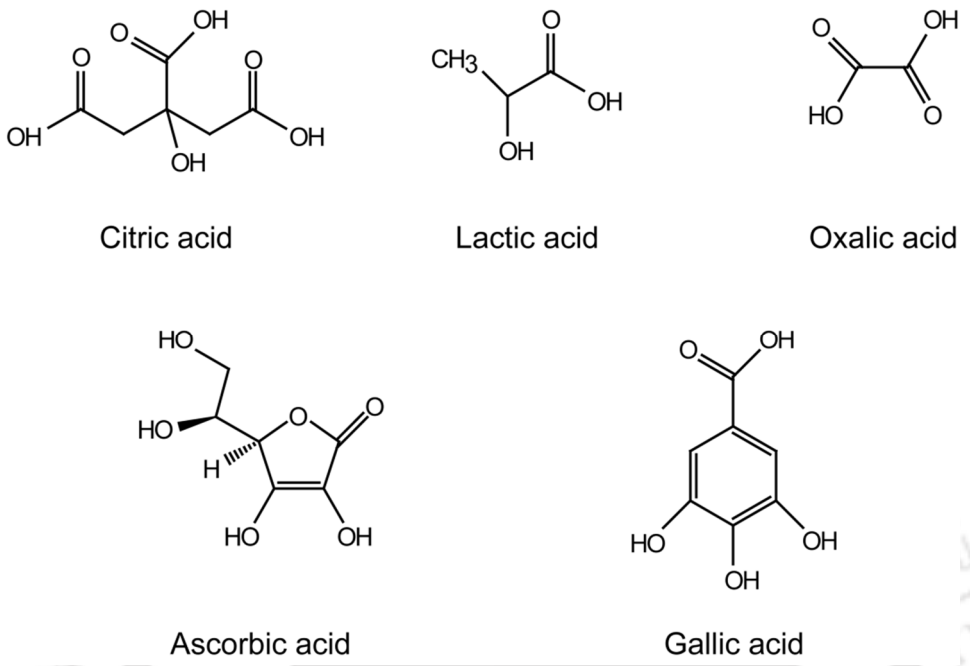

Figure 5.2. Structure of organic acids used in the present study.

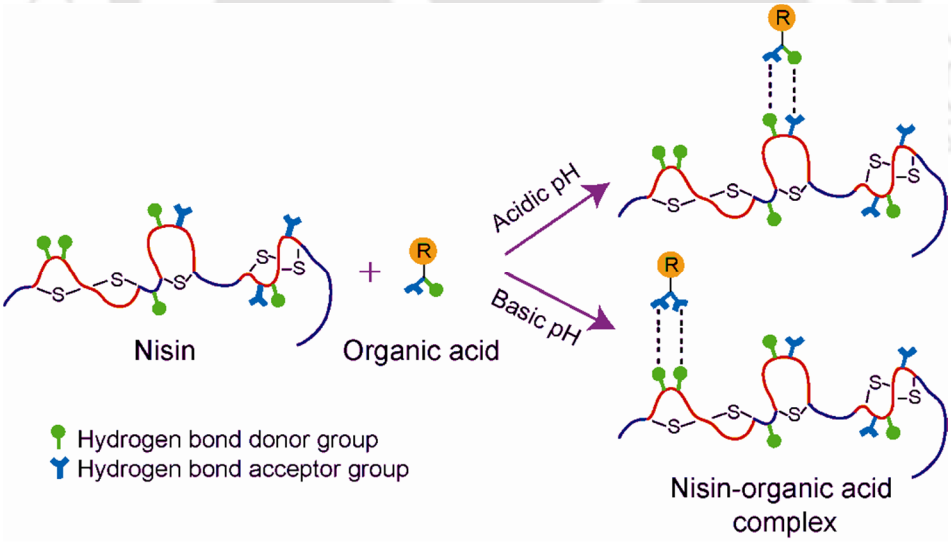

Figure 5.3. Hydrogen bond formation between nisin and organic acids may lead to increased solubility and retention of nisin activity at various pH.

2004; Regmi et al., 2012; Nakamoto, 1997). The C=O stretching frequency of citric acid shifted from 1660 cm^{-1} to 1720 cm^{-1}, which suggested formation of nisin-CA complex (Figure 5.4). Changes in the C=O stretching frequency was also observed for complex formation of nisin with other organic acids. (refer to Figure A5.1 in Appendix).

5.3.2. Antibacterial effect of nisin and nisin-organic acid complex

Nisin is a food-grade peptide which enjoys a Generally Recognized As Safe (GRAS) status and is used as a natural food preservative in processed cheese, milk, dairy products and canned foods (Sobrino-Lopez and Martin-Belloso, 2008). It has been well established that nisin exhibits highest solubility and stability at low pH and is known to loose its biological activity at high pH. The principal reason for this instability has been associated with the reactivity of the unsaturated amino acids, which can undergo a variety of addition reactions as there is a high possibility for modification of dehydro residues by nucleophiles which are present at alkaline pH (Rollema et al., 1995). Organic acids have a long history of use as food preservative and antimicrobial agent and can also increase the shelf-life of food ingredients (Jo et al., 2007; Mani-López et al., 2012). Based on the high isoelectric point of nisin (pI > 8.5) (Ryder et al., 2010) and the low pKa values for organic acids commonly

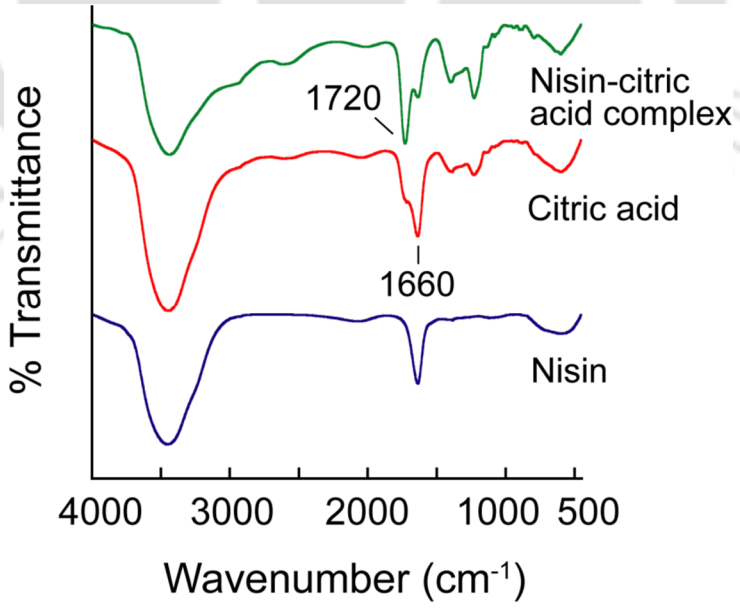

Figure 5.4. FTIR analysis of nisin-citric acid complex.

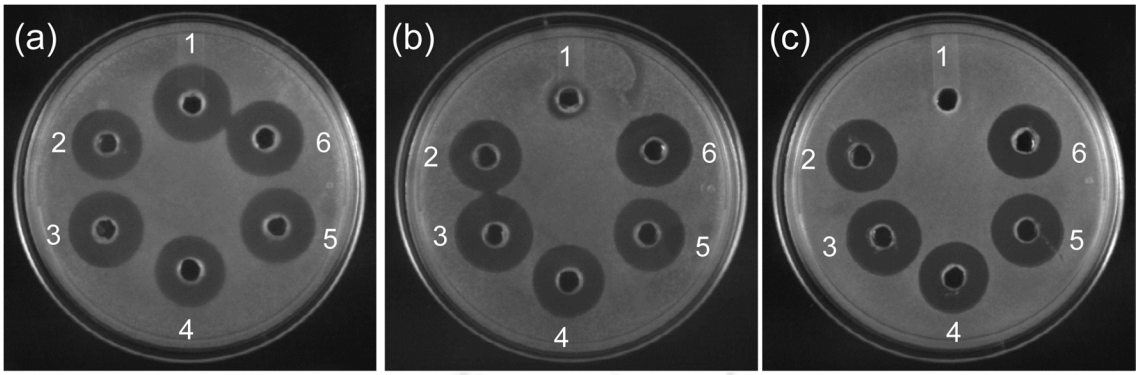

Figure 5.5. Antimicrobial activity of nisin-organic acid complex at **(a)** pH 5.5, **(b)** pH 7.0 and **(c)** pH 8.0 tested against *Micrococcus luteus* ATCC 9341. The samples tested were: 1. Nisin , 2. Nisin-lactic acid complex, 3. Nisin-citric acid complex, 4. Nisin-gallic acid complex, 5. Nisin-ascorbic acid complex, 6. Nisin-oxalic acid complex.

used in food system it was conceived that nisin-organic acid interactions could lead to stable and soluble adducts. To ascertain the bactericidal activity of nisin, *Micrococcus luteus* was used as a test strain in the present study, based on the well documented high sensitivity of this indicator bacterium to nisin (Nykanen et al., 1998; Dutreux et al., 2000; Sebti et al., 2003). In the present study different organic acids such as citric acid, ascorbic acid, oxalic acid, lactic acid and gallic acid were used to make complex with the nisin molecule and the bactericidal effect of nisin-organic acid complex was tested at different pH. An agar well diffusion assay against the target bacteria *Micrococcus luteus* ATCC 9341 revealed that nisin alone was active at pH 5.5 only (Figure 5.5, well no. 1). Interestingly all the nisin-organic acid complexes having 200 International Unit/mL (IU/mL) final nisin concentration exhibited prominent zone of inhibition at pH 5.5, pH 7.0 and pH 8.5 (Figure 5.5, well nos. 2-6).

However, when the organic acids alone were tested for antimicrobial activity at the specified pH values, no zone of inhibition (refer to Figure A5.2 in Appendix) was obtained, which suggested that the bactericidal effect of various nisin-organic acid complexes against *M. luteus* at different pH could plausibly be attributed to nisin activity and was not a pH effect.

5.3.3. Fluorescence-based assessment of antibacterial activity of nisin-organic acid complex

It has been reported in the literature that nisin induces pore formation in bacterial cell membranes (van Heusden et al., 2002; van Kraaij et al., 1998). To ascertain this phenomenon, target cells of *M. luteus* ATCC 9341 were treated with various concentrations of nisin and nisin-citric acid complex and membrane damage in treated cells was ascertained by cFDA-SE dye leakage assay and by measuring uptake of PI. These assays which essentially indicate membrane damage and pore formation in bacterial membrane (Vudumula et al., 2012; Singh et al., 2012) revealed a remarkable reduction in membrane-directed activity of nisin with increase in pH, whereas nisin-citric acid (N-CA) complex retained its activity even at higher pH (Figure 5.6), supporting earlier results of agar well diffusion assay (Figure 5.5). Similar results were also obtained with other nisin-organic acid complexes (refer to Figure A5.3 in Appendix).

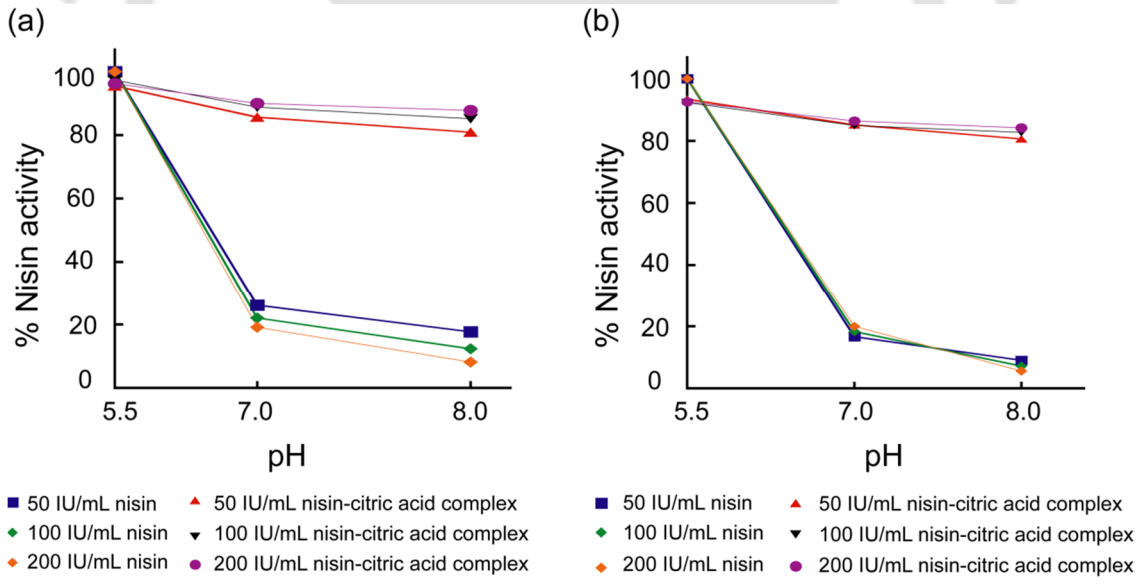

Figure 5.6. (a) cFDA-SE dye leakage assay in *M. luteus* ATCC 9341 cells treated with nisin-citric acid complex, **(b)** PI uptake assay to study the effect of nisin-citric acid complex at different pH on *M. luteus* ATCC 9341.

5.3.4. MIC and time-kill curves with nisin-citric acid complex

The MIC of nisin-citric acid complex determined against *M. luteus* ATCC 9341 was recorded as 60 IU/mL at pH 5.5, which was equivalent to nisin at pH 5.5. At the higher pH values of 7.0 and 8.0, the MIC value for nisin-CA complex against the target bacteria was marginally higher and recorded as 80 IU/mL. The antimicrobial activity of nisin-CA complex at various pH was further evaluated by determining the loss of cell viability. As evident from Figure 5.7, there was a dramatic loss in cell viability of both the target pathogens when subjected to treatment with nisin or nisin-CA complex at pH 5.5. Following 6 h of treatment, the cells were virtually eliminated and the viable cell numbers reduced to nearly 1.0 Log_{10} CFU. In case of nisin-CA complex at higher pH (pH 7.0 and 8.0), the overall pattern of loss in cell viability was similar, albeit at a slightly lesser magnitude (Figure 5.7).

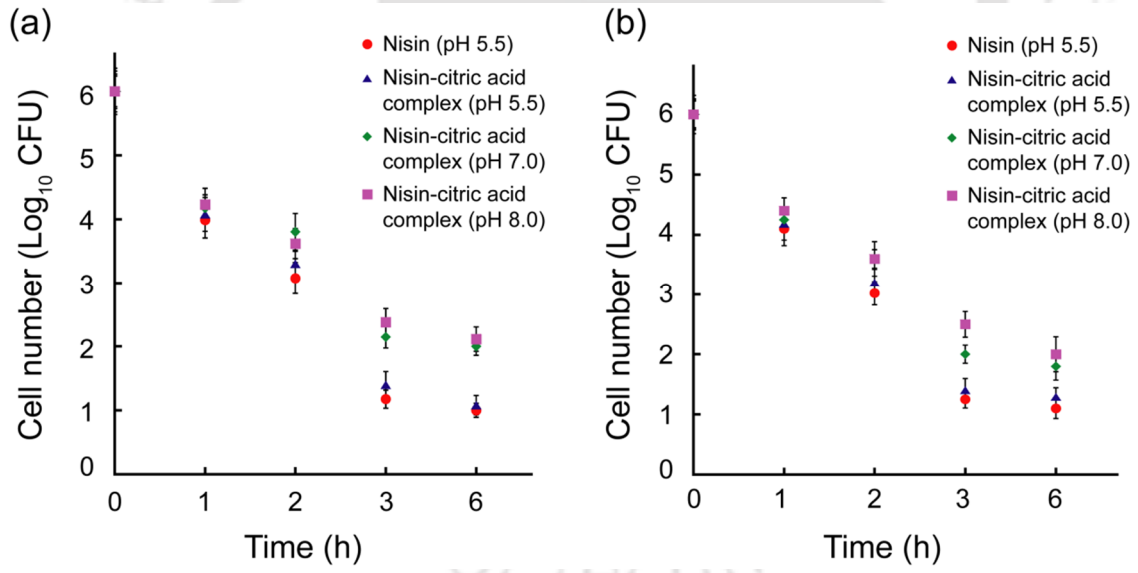

Figure 5.7. Effect of nisin-citric acid complex on the viability of **(a)** *M. luteus* ATCC 9341 and **(b)** *L. monocytogenes* Scott A at various pH.

5.3.5. CD spectra of nisin-citric acid complex

The aforementioned results clearly indicated the retention of nisin activity in the nisin-organic acid complexes at elevated pH, in contrast to nisin alone. This suggested that

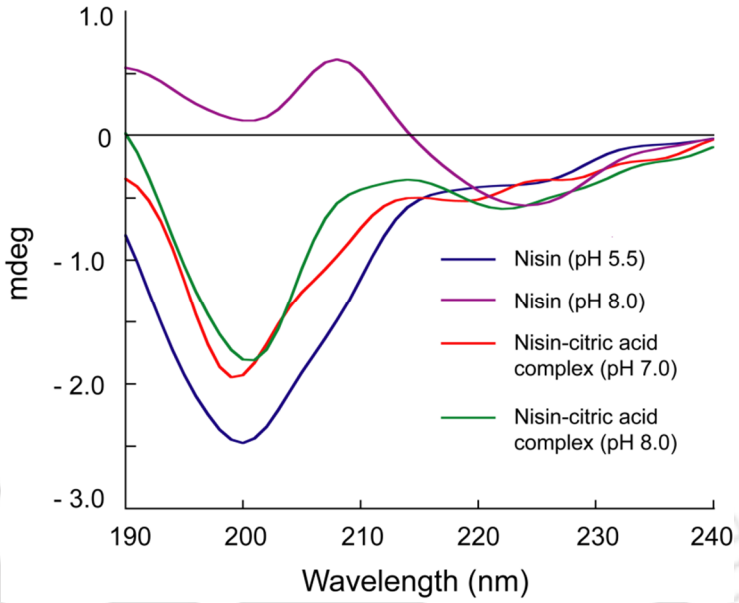

Figure 5.8. Circular dichroism spectra of nisin and nisin-citric acid complex at various pH.

formation of the organic acid complex not only enhanced the solubility and stability of nisin, but it also probably retained the native structure of the peptide upon complex formation. To verify this hypothesis, CD spectra of nisin-citric acid complex was pursued. The CD spectra of nisin alone exhibited a prominent peak at 200 nm and a small peak at 226 nm at pH 5.5 (Figure 5.8). It was noted that in case of nisin-citric acid complex, only a minor shift in ellipcity was observed along with a substantial conservation of CD spectral pattern associated with nisin. In case of elevated pH, peaks were obtained at 200 nm and 220 nm for nisin-citric acid complex at pH 7.0 while at pH 8.0, peaks were observed at 201 nm and 222 nm (Figure 5.8). Essentially the CD spectra results suggested minimal structural perturbations of nisin in citric acid complex, which perhaps accounted for the retention of nisin activity at elevated pH.

5.3.6. Generation of nisin-AuNP composite and determination of antibacterial activity

Retention of nisin activity even at elevated pH in various organic acid complexes was an interesting result. However, recovery of the bactericidal nisin-organic acid complex from solution poses a practical problem. To overcome this, it was conceived that interaction of the cationic peptide nisin with negatively charged citrate-stabilized AuNPs in solution may

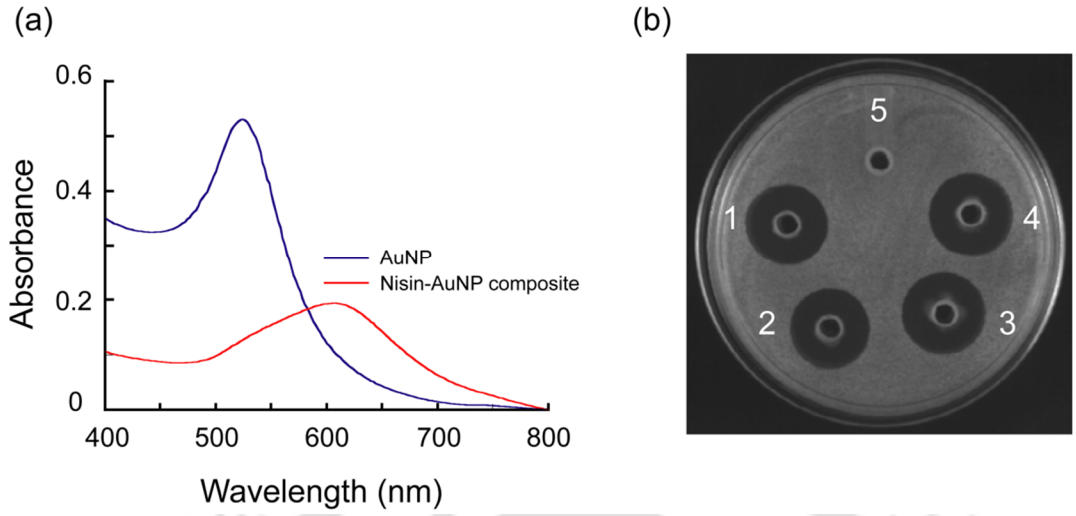

Figure 5.9. (a) UV-visible extinction spectrum of citrate-stabilized AuNP and nisin-AuNP composite, **(b)** Antimicrobial activity of nisin-AuNP composite against *M. luteus* ATCC 9341. 1. Nisin (pH 5.5), 2. Nisin-AuNP composite (pH 5.5), 3. Nisin-AuNP composite (pH 7.0), 4. Nisin-AuNP composite (pH 8.0), 5. Citrate-stabilized AuNP.

lead to the formation of a nisin-AuNP (N-AuNP) composite, through electrostatic interaction and this composite could then be recovered from solution by a simple centrifugation step. It was also envisaged that similar to nisin-citric acid complex, hydrogen bond formation between nisin and citrate-stabilized AuNPs may also lead to improved solubility and retention of nisin activity at elevated pH. This tenet is represented in Figure 5.3. To test this hypothesis, citrate stabilized AuNPs (average particle size of 12.0 ± 2.0 nm) were interacted with varying concentrations of nisin in solution and the UV-visible extinction spectrum of the solution was recorded. Incubation of AuNPs with increasing concentration of nisin resulted in a dose-dependent broadening of the extinction spectra of AuNPs and a red shift in absorbance maxima of AuNPs (refer to Figure A5.4, Appendix). Broadening of the extinction spectra of AuNPs in presence of nisin suggested aggregation, which was evidence in TEM analysis (refer to Figure A5.4, Appendix).

Following formation of nisin-AuNP composite and recovery of the same, UV-visible extinction spectrum of the composite was studied. As evident from Figure 5.9a, UV-visible extinction spectrum of only citrate-stabilized AuNPs revealed a characteristic extinction peak at around 520 nm, which is the signature surface plasmon resonance (SPR)

band of AuNPs. UV-visible extinction spectrum of N-AuNP composite (200 IU/mL nisin concentration) revealed a distinct shift in absorbance maxima (Figure 5.9a), which indicated aggregation of AuNPs. This phenomenon of aggregation was also explicit in TEM analysis of the nisin-AuNP composite (refer to Figure A5.5 in Appendix). The bactericidal activity of nisin-AuNP composite was tested by agar well diffusion against *M. luteus* ATCC 9341. Based on the zone of inhibition in the assay plate, it was observed that nisin-AuNP composite displayed activity against the target pathogen at pH 5.5, 7.0 and 8.0 akin to nisin at pH 5.5, whereas AuNP alone failed to display any bactericidal activity (Figure 5.9b). Further, the bactericidal activity of nisin-AuNP composite was also observed over a wide range of pH (3.0-8.0) and this activity was on par with the activity observed for nisin-citric acid complex (refer to Figure A5.6. in Appendix). In the context of these observations, control experiments indicated the lack of any pH effect as well as AuNPs alone in the observed bactericidal activity of nisin-AuNP composite (refer to Figure A5.7. in Appendix).

5.3.7. MIC and time-kill curves

The MIC of nisin-AuNP composite was recorded as 80 IU/mL at pH 5.5, pH 7.0 and pH 8.0 against *M. luteus* ATCC 9341. This was marginally higher than the MIC obtained for nisin at pH 5.5 against the same target bacteria and was comparable with the MIC value for nisin-citric acid complex at the higher pH values of 7.0 and 8.0. The time-kill curves indicated substantial loss in cell viability of both the target pathogens *M. luteus* ATCC 9341 and *L. monocytogenes* Scott A when subjected to treatment with N-AuNP composite. The essential feature observed in the time-kill curves for nisin-citric acid complex and the overall pattern of loss in cell viability was similar in case of treatment with N-AuNP composite, albeit at a slightly lesser magnitude (Figure 5.10).

5.3.8. Fluorescence-based assessment of antibacterial activity of nisin-AuNP composite

Given that nisin is known to act on the membrane and induce pore formation in target bacteria (van Heusden et al., 2002; van Kraaij et al., 1998), the next endeavour was to determine the effect of nisin-AuNP composite treatment on target cells of *M. luteus* ATCC 9341 by cFDA-SE dye leakage assay and by measuring uptake of PI. As evident from

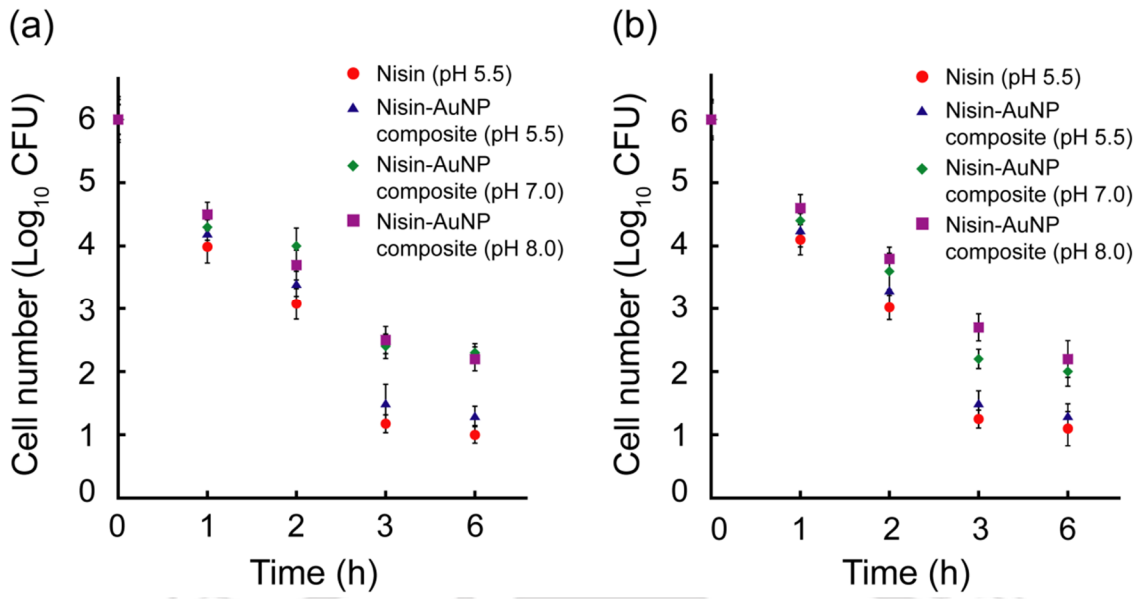

Figure 5.10. Effect of nisin-citric acid complex on the viability of (a) *M. luteus* ATCC 9341 and (b) *L. monocytogenes* Scott A at various pH.

Figure 5.11, cFDA-SE leakage assay and PI uptake assay revealed that N-AuNP composite displayed prominent activity against *M. luteus* ATCC 9341 at pH 5.5, 7.0 and 8.0, similar to the results obtained earlier with nisin-CA complex (Figure 5.6).

5.3.9. Membrane-directed activity of nisin-citric acid complex and nisin-AuNP composite

To further investigate the effect of bacterial transmembrane potential (Ψ) on the antimicrobial activity of nisin-citric acid complex and nisin-AuNP composite, cells of *M. luteus* ATCC 9341 were pre-treated with uncoupler carbonyl cyanide m-chlorophenyl hydrazone (CCCP) to collapse the transmembrane proton motive force. A progressive loss in cell viability was observed with time when the cells were treated with nisin-CA complex and N-AuNP composite, (Figure 5.12a). However, it is significant to mention that in the case of nisin-citric acid complex and nisin-AuNP composite treated cells, the loss in cell viability was comparable for both CCCP-treated and CCCP-untreated cells (Figure 5.12a), which suggested that the bactericidal activity of nisin-CA complex and N-AuNP composite was not affected by CCCP-induced membrane depolarization. Treatment of $DiSC_35$-loaded cells of *M. luteus* ATCC 9341 with nisin-citric acid complex and nisin-AuNP composite

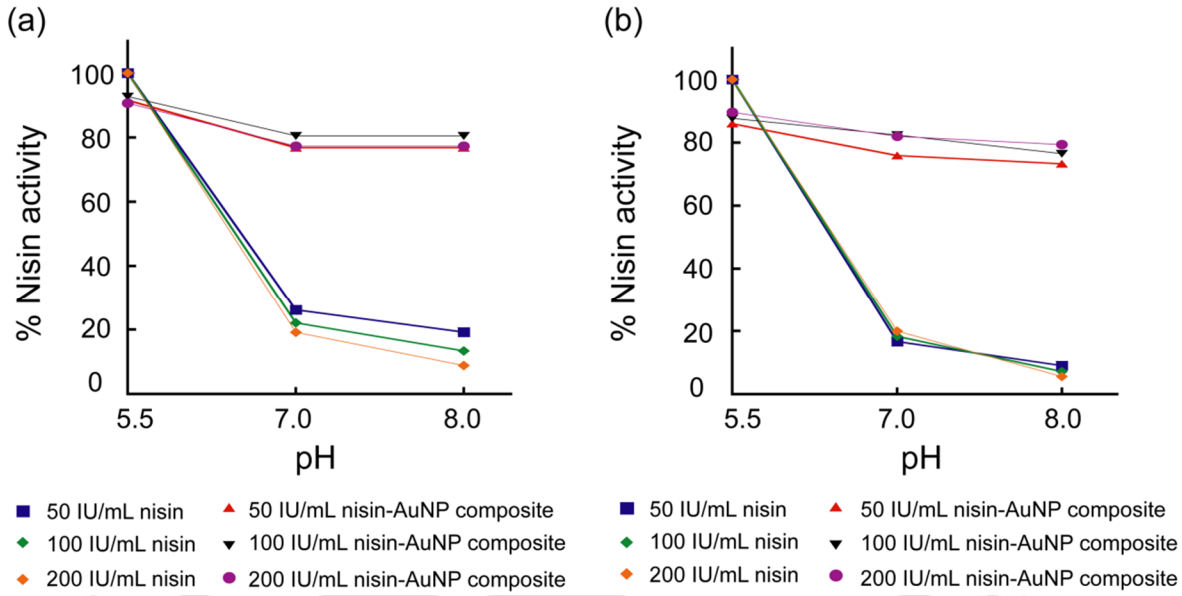

Figure 5.11. (a) cFDA-SE leakage assay in *M. luteus* ATCC 9341cells treated with nisin-AuNP composite at different pH, **(b)** PI uptake assay to study the effect of nisin-AuNP composite at different pH on *M. luteus* ATCC 9341.

resulted in a rapid increase in the fluorescence emission of the probe, which suggested that both nisin-CA complex as well as N-AuNP composite could dissipate the membrane potential in target cells even at an elevated pH within a short span of time **(**Figure 5.12b). Further evidence for membrane- directed antibacterial activity of nisin-CA complex and N-AuNP composite was obtained through fluorescence microscope analysis. Fluorescence microscopy with cFDA-SE and PI revealed that the population of cFDA-SE stained cells of *M. luteus* ATCC 9341 was diminished and the corresponding PI stained cells were increased, which clearly suggested membrane damage in treated cells (Figure 5.13).

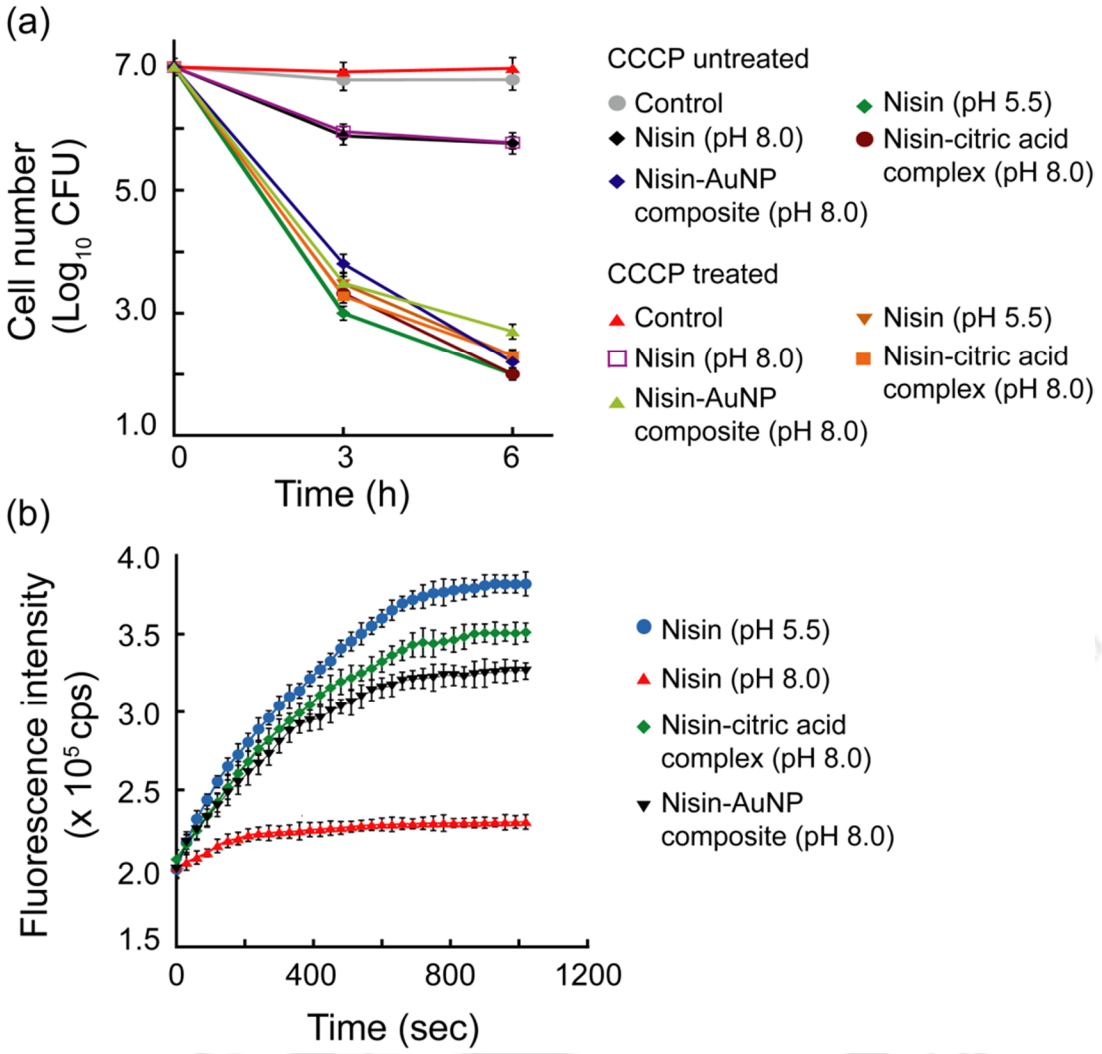

Figure 5.12. (a) Effect of membrane potential on the bactericidal activity of nisin, nisin-citric acid complex and nisin-AuNP composite on *M. luteus* ATCC 9341. **(b)** Membrane depolarization assay of *M. luteus* ATCC 9341 cells ascertained by $DiSC_35$ fluorescence.

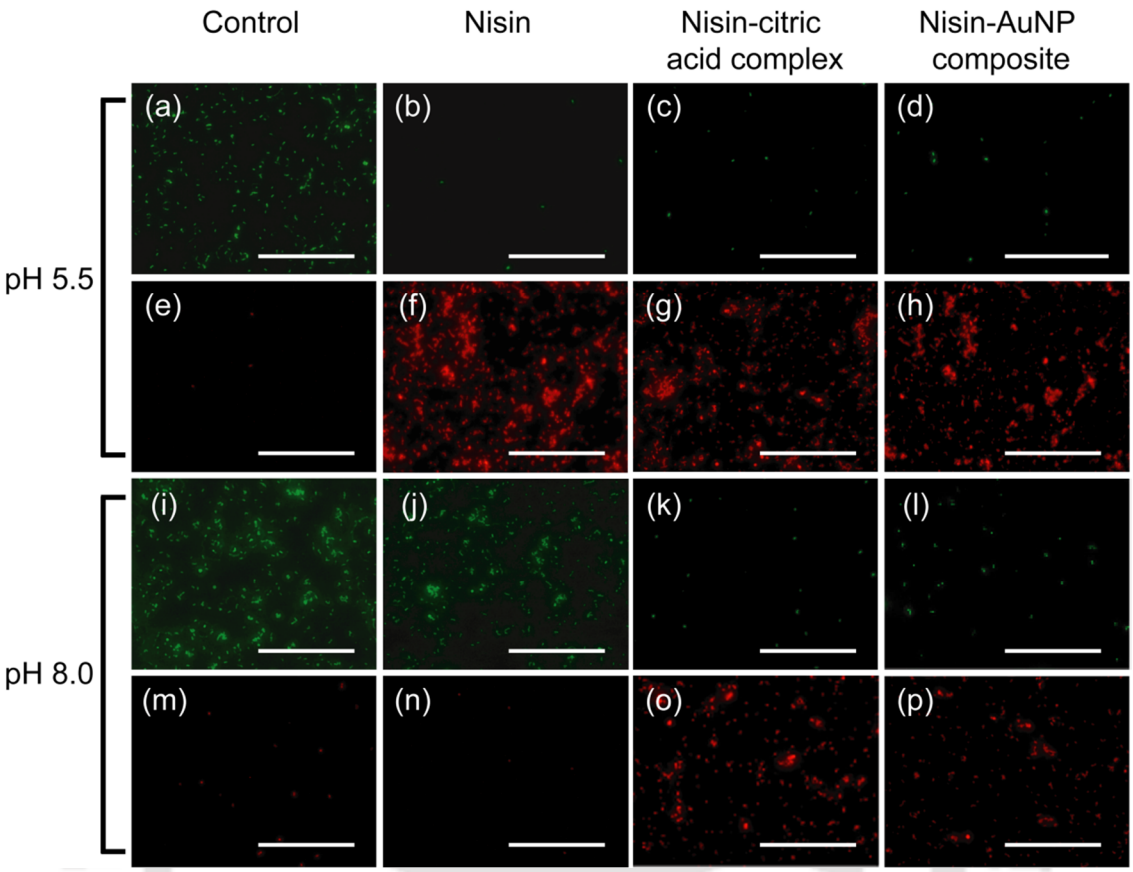

Figure 5.13. Fluorescence microscopic images of *M. luteus* ATCC 9341 cells treated with nisin, nisin-citric acid complex and nisin-AuNP composite at various pH. Green cells indicate viable cells labeled with cFDA-SE **(Panel a-d and i-l)** and red cells indicate membrane damaged cells labeled with PI **(Panel e-h and m-p).** Control samples indicate untreated bacterial cells (negative control). Scale bar for all the images is 50 µm.

5.3.10. Storage studies

Nisin-CA complex and N-AuNP composite exhibited substantial retention of bactericidal activity (90%) at elevated pH upon storage for 7 days at 4^{o}C. The magnitude of the antibacterial activity was comparable with that of nisin (pH 5.5) stored under similar conditions (Figure 5.14a). These results were encouraging and indicated that the developed nisin-CA complex and N-AuNP composite was quite stable. The stability of the nisin-citric acid complex and nisin-AuNP composite was slightly diminished when stored at room temperature (25^{o}C) as evident from the slight reduction in the antimicrobial activity to around 70% (Figure 5.14b).

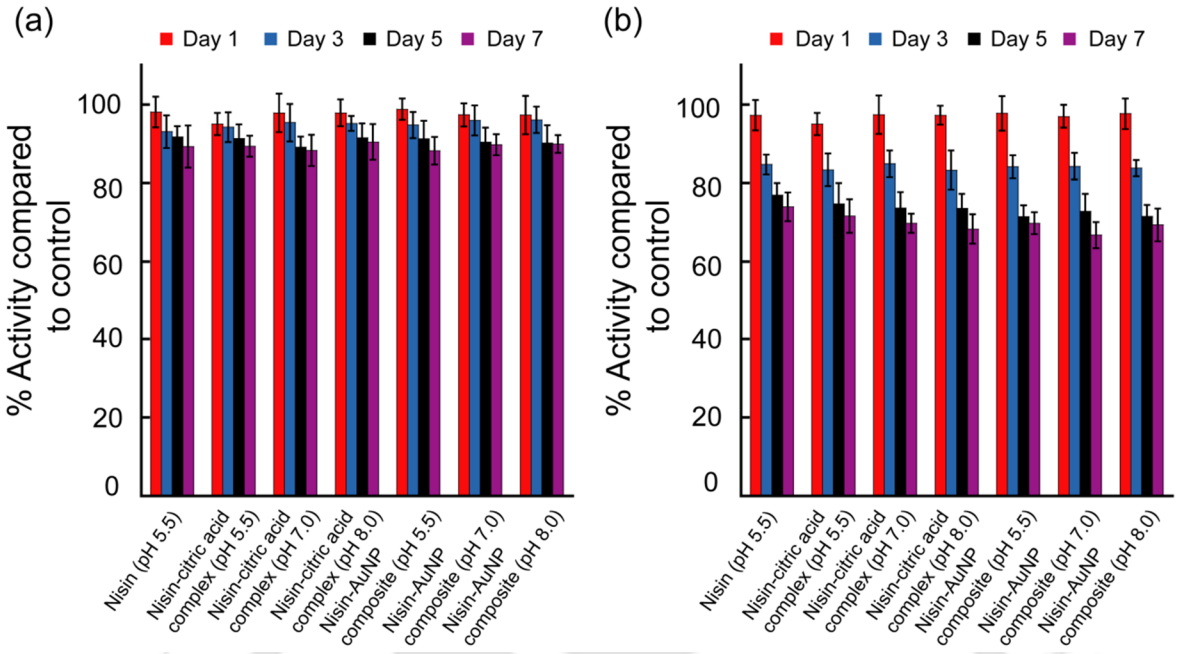

Figure 5.14. Antimicrobial activity of nisin, nisin-citric acid complex and nisin-AuNP composite stored at **(a)** 4°C and **(b)** room temperature (25°C).

5.3.11. Cytotoxic effect

The potential cytotoxic effect of purified nisin, nisin-CA complex and N-AuNP composite was determined against HT-29 cells (human adenocarcinoma cell line) by MTT-based colorimetric assay. As evident from Figure 5.14, purified nisin, nisin-CA complex and N-AuNP composite (corresponding to 100 IU/mL and 200 IU/mL nisin in each) failed to exert any adverse effect on the viability of HT-29 cells The lack of cytotoxic effect on model human cells is an interesting finding and enhances the therapeutic merit of the developed nanocomposite.

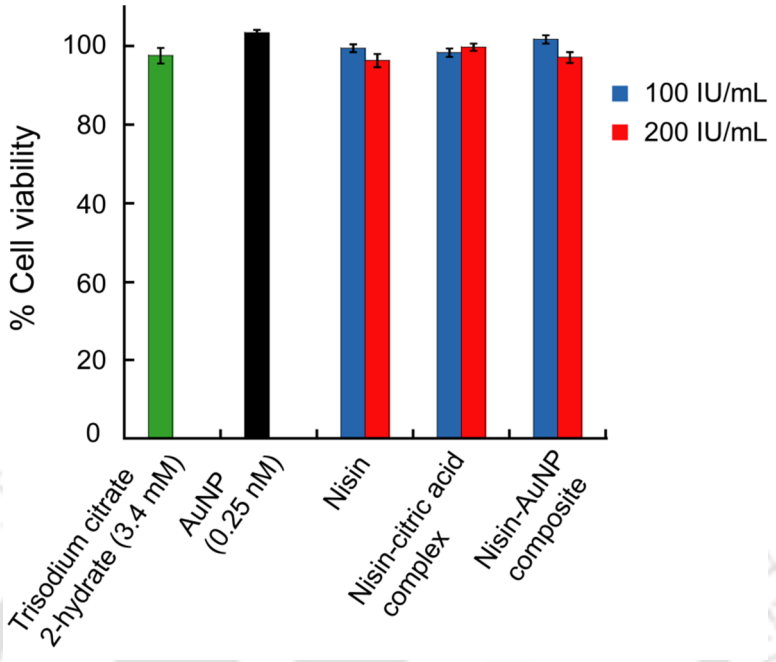

Figure 5.15. MTT assay to ascertain the *in vitro* cytotoxic effect of nisin, nisin-citric acid complex and nisin-AuNP composite on HT-29 cells.

5.4. Significant Findings

The present study essentially demonstrates a 'soft-tailoring' strategy to retain biological activity of the potent antimicrobial peptide nisin at physiologically relevant pH. The salient findings of the study are as follows:

1. Nisin is an antimicrobial peptide with GRAS status and a long history of safe use as food preservative. Owing to its profound membrane-targeting activity, there is a distinct possibility of expanding the application domain of nisin, especially in the healthcare regime. However, a serious impediment to this exciting prospect is the low solubility and loss of biological activity of nisin at physiological pH and above. In this study, a simple method of generating nisin-organic acid complex and nisin-gold nanoparticle composite is described, wherein the characteristic nisin activity is manifested even at elevated pH.

2. Based on the fact that nisin can readily form hydrogen bonds with organic acids in solution, which may lead to improved solubility of the peptide, nisin-organic acid complex was generated with a judicious choice of biocompatible organic acids. Interestingly, there was retention of nisin activity in the organic acid complexes even at elevated pH, in contrast to nisin alone.
3. The merit of generating N-OAC complex was vindicated by the fact that the structure of nisin was well conserved in the complex even at elevated pH as evidenced by CD spectra results for nisin-citric acid complex.
4. Recovery of the bioactive N-OAC complex from solution poses a practical problem. To tide over this impasse, nisin-citrate stabilized gold nanoparticle (AuNP) composite was generated, which could be recovered from solution by a simple centrifugation step. Interestingly, nisin-citrate stabilized AuNP composite displayed the signature antimicrobial activity of the peptide even at elevated pH.
5. The storage studies indicated that both nisin-CA complex as well as N-AuNP composite was robust and displayed considerable retention of activity upon storage at 4^{o}C as well as room temperature for a period of 7 days.
6. MTT-based cytotoxicity assay suggested that nisin, N-OAC complex and N-AuNP composite were non-toxic to HT-29 cells.

It is envisaged that the bioactive N-AuNP composite which displayed high antibacterial selectivity and was non-toxic to model human cells could enable interesting healthcare applications. However, based on literature reports which seem to suggest that the antimicrobial spectrum of nisin may have an effect on commensal gut microbiota, the next endeavor was to advance the study and select an antimicrobial peptide whose bactericidal spectrum was more restricted and suitable for potential therapeutic applications. In the next chapter, this premise is addressed by using anionic nanoparticles and generating a nanocomposite with the bacteriocin pediocin, which is an antimicrobial peptide secreted by a food-grade lactic acid bacteria.

Chapter 6

Selective Capture of Pediocin Secreted by Food-grade Lactic Acid Bacteria for Development of Bactericidal Nanocomposites

A robust nanoplatform based on anionic and magnetic nanoparticles enabled single-step selective capture of bacteriocin from food-grade lactic acid bacteria with concurrent generation of potential therapeutic antibacterial nanocomposites. Following magnetic separation and desorption of pediocin from IONP-pediocin nanocomposite, the recovered IONP could be recycled for subsequent round of pediocin capture.

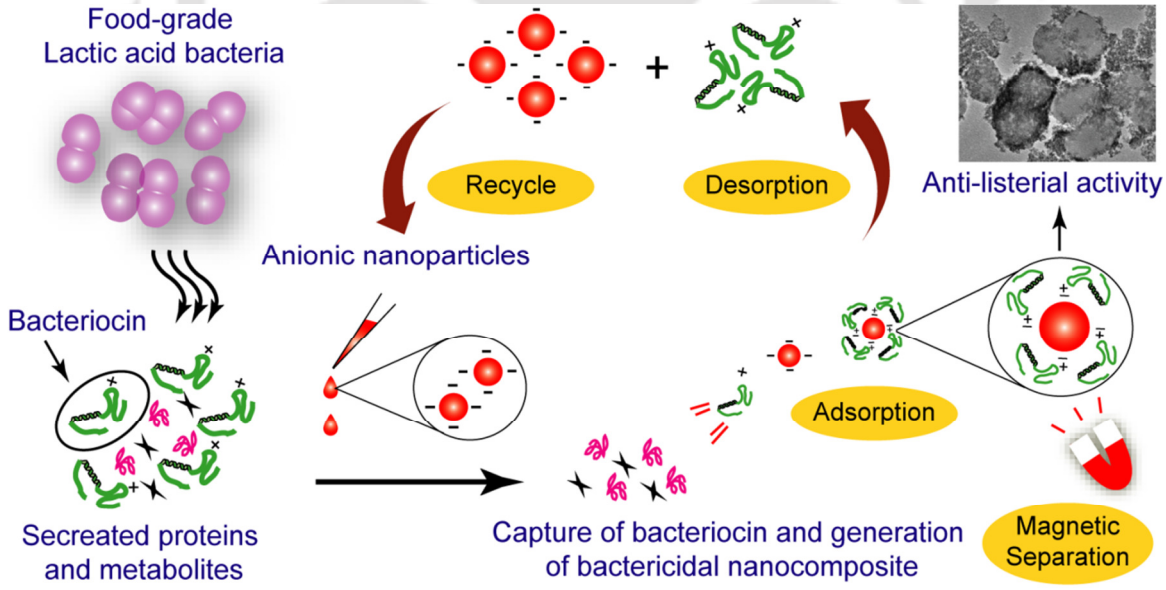

ABSTRACT

The present study highlights an efficient method of generating bactericidal nanocomposites with a natural antimicrobial peptide (AMP). Anionic nanoparticles were employed to selectively capture the cationic molecule pediocin, which is an AMP secreted by a food-grade lactic acid bacteria (LAB). Pediocin is a prototype Class IIa bacteriocin, which is heat-stable, active over a wide pH range and displays strong anti-listerial activity. Given the potent membrane-directed activity of pediocin and its reduced likelihood to impact commensal microbiota, there is a growing interest in exploiting the bactericidal activity of pediocin for therapeutic applications. Based on this premise, antibacterial nanocomposites were generated through charge-based capture and separation of secreted pediocin at pH 7.0 from the culture filtrate of the producer LAB by biocompatible anionic nanoparticles such as citrate-stabilized gold nanoparticles (AuNPs), silica nanoparticles (SNPs) and iron oxide nanoparticle (IONPs). The composites exhibited an antimicrobial spectrum and membrane-directed activity typically associated with pediocin. At pH 2.0, pediocin could be desorbed from the composites, with the highest desorption efficiency obtained for IONP. Efficient recovery of IONP-pediocin nanocomposite was achieved through a facile magnetic separation and following desorption, the recovered IONP could be recycled for subsequent round of pediocin adsorption. The steady state adsorption isotherm of pediocin with IONPs followed a Langmuir isotherm model. In case of IONP, a 16-fold purification of pediocin could be achieved and HPLC profile of the desorbed pediocin revealed a similar retention time as pediocin purified by an established cell-adsorption method. An *in vitro* MTT-based assay suggested that purified pediocin and all the pediocin-nanocomposites were non-toxic to cultured human adenocarcinoma HT-29 cells.

6.1. Introduction

Antibiotic-resistant pathogenic bacteria have emerged as a nemesis of modern healthcare. Despite the critical demand of new antibacterials, (Fischbach and Walsh, 2009; Wise Piddock, 2010) the fight against these life threatening pathogens is plagued by the sluggish progress in the discovery of new antibiotics (Gwynn et al., 2010; Livermore, 2011; Silver, 2011). In addition, the indiscriminate use of antibiotics can in turn fuel the evolution of multi-drug resistance in pathogenic bacteria (Lofmark et al., 2006). Hence there is an urgent need of a prudent therapeutic approach and potent antibacterials, which are fundamentally different from conventional antibiotics. In this context, bacteriocins, which are natural antimicrobial peptides (AMPs) secreted by lactic acid bacteria (LAB), can be considered as promising therapeutic antibacterials. A key concern regarding the deployment of antibiotics is their adverse effect on commensal gut microbiota (Willing et al., 2011; Blaser, 2011). In contrast, the restricted antimicrobial spectrum of bacteriocins from LAB ensures minimal collateral damage on commensal microbiota (Cotter et al., 2013; Drider et al., 2006), which in turn reduces the threat of infection by opportunistic pathogens (Sekirov et al., 2010; Preidis et al., 2011). The optimism associated with bacteriocins from LAB has gained momentum with emerging reports on their potential as new therapeutic agents against human pathogens, (Cotter et al., 2005) apart from their conventional food applications (Cleveland et al., 2001; Deegan et al., 2006; Chen and Hoover, 2003; Cotter et al., 2005).

To harness the true potential of bacteriocins as antibacterial therapeutics, it is imperative to develop a delivery system that is biocompatible, renders stability and can provide the bacteriocin in a bioactive form. In this regard, use of nanoscale materials to develop bactericidal agents is a judicious choice as highlighted in literature reports (Norman et al., 2008; Pissuwan et al., 2009; Huh and Kwon, 2011; Vigderman and Zubarev, 2013). A rational approach towards developing a bacteriocin-based nanocomposite is to interact purified bacteriocins from LAB with the chosen nanomaterial. However, this exercise can be quite challenging. The crux of the problem is purification and recovery of secreted bacteriocins from LAB, which involves arduous techniques such as salt precipitation, chromatographic tools or a cell-adsorption method (Drider et al., 2006; Carolissen-MacKay et al., 1997; Beaulieu et al., 2006; Yang et al., 1992; Halami et

al., 2005). Given that bacteriocin secreted by LAB is cationic in nature, (Drider et al., 2006) it is envisaged that anionic nanoparticles (NPs) could provide a viable solution to this impediment by enabling a one-step selective capture of bacteriocin through electrostatic interactions resulting in concurrent generation of a bactericidal nanocomposite. This precept formed the rationale of the present study.

The well studied and FDA approved bacteriocin nisin (Cotter et al., 2005; Chatterjee et al., 2005; Willey and van der Donk, 2007) holds considerable promise against clinically relevant drug-resistant pathogens (Brumfitt et al., 2002; Mota-Meira et al., 2000; Piper et al., 2009) However, the potential antagonism of nisin against common human intestinal microbiota (Blay et al., 2007) necessitates the search for alternate bacteriocins. In the present study, this issue is addressed through the prudent choice of pediocin (P), a potent bacteriocin produced by the food-grade LAB *Pediococcus pentosaceus* CRA51 (Singh et al., 2012). Pediocin is favorable in terms of its antimicrobial spectrum against important human Gram-positive gastrointestinal pathogens (Papagianni and Anastasiadou, 2009) and lack of activity against most gut bacteria (Blay et al., 2007; Bernbom et al., 2009). In the present study, gold nanoparticle (AuNP), silica nanoparticle (SNP) and iron oxide nanoparticle (IONP) were chosen as the anionic NPs to selectively capture pediocin from the cell-free culture filtrate with concomitant generation of a nanoparticle-pediocin (NP-P) composite. The bactericidal activity, storage studies and determination of the cytotoxic potential of the developed nanocomposites is reported in the present study.

6.2. Materials and Methods

6.2.1. Materials

Ferrous sulfate ($FeSO_4$, $6H_2O$) and ferric nitrate [$Fe(NO_3)_3$], ammonium hydroxide, ethanol, isopropyl alcohol, triethyl amine and tri-sodium citrate 2-hydrate were procured from Merck, India. $HAuCl_4$ (17 wt % solution of $HAuCl_4$ in dilute HCl; 99.99%), tetraethylorthosilicate (TEOS), sodium dodecyl sulphate (SDS), potassium bromide (IR grade), 5 (and 6)-carboxyfluorescein diacetate succinimidyl ester (cFDA-SE), 3,3'-dipropylthiadicarbocyanine iodide ($DiSC_35$), Dulbecco's Modified Eagle Medium (DMEM), penicillin, streptomycin and trypsin-EDTA solution were obtained from Sigma-Aldrich Chemicals, USA. Fetal bovine serum (FBS) was procured from PAA

Laboratories, USA. HEPES buffer and trifluoroacetic acid (TFA) was obtained from Sisco Research Laboratories (SRL), Mumbai, India.

6.2.2. Bacterial strains and growth conditions

The growth media used for propagating the bacterial strains were purchased from HiMedia, Mumbai, India. In the present investigation, *Pediococcus pentosaceus* CRA51 was chosen as the bacteriocin producing lactic acid bacteria (LAB) based on the potential of this strain to produce the anti-listerial bacteriocin pediocin (Singh et al., 2012). *Pediococcus pentosaceus* CRA51 was propagated in deMan, Rogosa and Sharpe (MRS) broth at 37^{o}C under static conditions for 18 h. The pathogenic bacterial strains used in the present investigation comprised of *Listeria monocytogenes* Scott A, *Staphylococcus aureus* MTCC 96 and *Enterococcus faecalis* MTCC 439. *L. monocytogenes* Scott A, *S. aureus* MTCC 96 and *E. faecalis* MTCC 439 were propagated in Brain-heart Infusion (BHI) broth at 37^{o}C and 180 rpm for 12 h.

6.2.3. Synthesis of citrate-stabilized gold nanoparticle (AuNP)

Citrate-stabilized AuNPs were synthesized by citrate reduction of $HAuCl_4$ as described earlier in section 2.2.3. UV-visible extinction spectrum of a 1.0 mL aliquot of AuNP solution was recorded (Cary 300, Varian, USA) and a separate aliquot of the synthesized AuNP sample was also subjected to transmission electron microscope (TEM) analysis.

6.2.4. Synthesis of silica nanoparticle (SNP)

SNPs were prepared by following a standard method of hydrolysis and condensation of TEOS in absolute ethanol with ammonium hydroxide as the base catalyst (Kim et al., 2007). For the synthesis, 4.2 g of TEOS was mixed with ethanol to a final volume of 50 ml. In a separate set, 2.5 g of ammonium hydroxide was mixed with deionized water and the volume was adjusted up to 50 ml with ethanol. The TEOS-ethanol solution was gently added to ammonium-water-ethanol solution with intermittent mixing. The resultant solution was incubated at 25°C for 1 h. Subsequently the solution was centrifuged at 20,000 rpm for 1 h to recover silica nanoparticles which were then washed with isopropyl alcohol (IPA) to remove excess TEOS. Finally, silica nanoparticles were dried in an air

circulating oven at 110 °C for 24 h. The synthesized SNPs were subjected to transmission electron microscope (TEM) analysis.

6.2.5. Synthesis of iron oxide nanoparticle (IONP)

IONPs were synthesized using an earlier reported method (Saha et al., 2011). Briefly, $FeSO_4$ and $Fe(NO_3)_3$ solution (0.1 M each) were mixed in a 1:1 ratio and stirred for 30 min. Following that, 3.0 mM SDS was added and the solution was stirred for a period of 30 min. Triethyl amine (~5% v/v) was then added drop wise under vigorous stirring for an additional 2 h. The pH of this system was maintained at ~2.0-3.0 before adding the base. Homogeneity of the solution was ensured by continuous stirring. The resulting suspension which was initially dark brown in color turned complete black after a period of 4 h of mixing. Centrifugation at 15,000 rpm for 15 min yielded the black suspension as a pellet. The pellet was resuspended in MilliQ water by sonication followed by several rounds of washing by MilliQ water and methanol to remove excess base and other impurities. Finally, the suspension was vacuum dried overnight to obtain IONPs. The synthesized IONPs were subjected to transmission electron microscope (TEM) analysis.

6.2.6. Cell-free culture filtrate (CF) of Pediococcus pentosaceus CRA51

Pediococcus pentosaceus CRA51 was grown in 100 mL MRS broth in static condition at 37^{o}C for 18 h. The cell-free culture filtrate was recovered by centrifugation at 10,000 rpm for 10 min at 4°C. The pH of the culture filtrate was adjusted to 7.0 with 2.0 N NaOH, followed by filter sterilization using a 0.22 µm membrane filter (Millipore, India) and the culture filtrate was stored at 4^{o}C and used within 24 h in each experiment. Pediocin titer in the cell-free culture filtrate was determined against *Listeria monocytogenes* Scott A by a spot-on-lawn assay, and the activity was expressed as arbitrary units per ml (AU/ mL) as mentioned in an earlier study (Singh et al., 2012).

6.2.7. Interaction of nanoparticles (NPs) and cell-free culture filtrate (CF) of Pediococcus pentosaceus CRA51 for generation of nanoparticle-pediocin (NP-P) composites

In case of gold nanoparticle-pediocin (AuNP-P) composite formation, 10 ml of cell-free culture filtrate was taken in separate sets to which varying volumes of 0.32 nM AuNP

solution (10 mL and 20 mL) was gently added. The solutions were then incubated for either 30 minutes or 60 minutes at room temperature under mild shaking. The solution was then centrifuged at 10,000 rpm for 10 minutes. The supernatant was aspirated and collected separately and the pellet representing AuNP-P composite was resuspended in 5.0 mL of sterile MilliQ water.

In case of silica nanoparticle-pediocin (SNP-P) and iron oxide nanoparticle-pediocin (IONP-P) composite formation, requisite volume of the respective nanoparticle solutions were added from the stock solutions (10.0 mg/mL each prepared in sterile MilliQ water) to separate 10 ml aliquots of cell-free culture filtrate so as to achieve a final nanoparticle concentration of 0.1 mg/mL, 0.25 mg/mL, 0.5 mg/mL and 1.0 mg/mL, respectively. The solutions were then incubated for either 30 minutes or 60 minutes at room temperature under mild shaking. Following incubation, the solution was centrifuged at 10, 000 rpm for 10 minutes. The supernatant was aspirated and collected separately and the respective pellets of SNP-P and IONP-P composites were resuspended in 5.0 mL of sterile MilliQ water. Pediocin activity in AuNP-P, SNP-P and IONP-P composites and the respective supernatants was ascertained by the spot-on-lawn assay as mentioned before (Singh et al., 2012).

6.2.8. FT-IR analysis of nanocomposites

FT-IR spectra of AuNP-P, SNP-P and IONP-P composite (corresponding to 200 AU/mL pediocin in each) was recorded in KBr pellets at 4 cm^{-1} resolution in a spectrometer (Spectrum One, Perkin-Elmer). Eight scans were performed for every sample in the range of 4000 to 450 cm^{-1}. A background spectrum for pure KBr was also measured.

6.2.9. Purified pediocin

Purification of pediocin from *Pediococcus pentosaceus* CRA51 was accomplished by a cell-adsorption method (Halami et al., 2005). Pediocin titer in the purified sample was determined against *Listeria monocytogenes* Scott A by a spot-on-lawn assay, and the activity was expressed as arbitrary units per ml (AU/ mL) as mentioned in an earlier study (Singh et al., 2012). The purified pediocin sample was used as a reference control in various experiments.

6.2.10. Bactericidal activity of AuNP-P, SNP-P and IONP-P composites

The antibacterial activity of the generated AuNP-P, SNP-P and IONP-P nanocomposites was ascertained by the following methods:

6.2.10.1. Agar well diffusion assay

Assay plates were prepared with a bottom layer of BHI agar (1.5% agar), which was overlaid with BHI soft agar (0.8% agar) seeded with 10^6 cells of freshly grown target cells of *Listeria monocytogenes* Scott A. Requisite number of holes of 6.0 mm diameter was punched in all the assay plates. To each well, 30 µl of AuNP-P, SNP-P and IONP-P composite solution and recovered supernatant following separation of the composites was added. Control samples consisted of cell-free culture filtrate and all three NP solutions. The plates were pre-incubated at 4°C for 3 h to facilitate diffusion of the sample followed by incubation at 37°C for 24 h. The antibacterial activity of the samples was determined by observing the zone of inhibition produced around the wells.

6.2.10.2. Time-kill curve

Approximately 10^6 CFU/mL of *L. monocytogenes* Scott A (in sterile PBS) were interacted with AuNP-P, SNP-P and IONP-P composite solutions (corresponding to 200 AU/mL pediocin in each) for a period of 6 h and viable cell numbers (Log_{10} CFU/mL) were determined at regular intervals by serial dilution and plating. For comparison, time kill curves were also generated with purified pediocin.

6.2.10.3. cFDA-SE leakage assay

L. monocytogenes Scott A cells were labeled with cFDA-SE by the method described earlier in section 3.2.7.1. Approximately 10^6 CFU/mL cFDA-SE labeled cells of the target pathogen were treated AuNP-P, SNP-P and IONP-P composite solutions (corresponding to 100 AU/mL and 200 AU/mL pediocin in each) at 37^{o}C and 180 rpm for 3 h. In a parallel set cells were also treated under the same conditions with equivalent concentration of purified pediocin. Subsequently all the samples were centrifuged at 8,000 rpm for 10 min. Leakage of cFDA from cells was determined by measuring fluorescence of the cell free

supernatant at an excitation wavelength of 488 nm and emission wavelength of 518 nm in a spectrofluorimeter (FluoroMax-3, HORIBA). The fluorescence measurements were recorded after subtracting the fluorescence of effluxed dye from control samples (cFDA-SE labeled cells suspended in sterile PBS). Fluorescence measurements were taken for three independent experimental samples.

6.2.10.4. Membrane depolarization assay

A stock solution of $DiSC_35$ (3.0 mM) was made in ethanol and stored at -20°C.Cells of *L. monocytogenes* Scott A were grown till mid-logarithmic phase (OD_{600} = 0.4-0.5). The cells were harvested by centrifugation, washed with a buffer solution (5.0 mM HEPES buffer, 5.0 mM glucose, pH 7.2) and suspended in the same buffer to an OD_{600} of 0.05. The cell suspensions were incubated with 0.4 µM $DiSC_35$ for 1h at 37°C followed by addition of 100 mM KCl. A 1.0 mL aliquot of the cell suspension was placed in separate cuvettes to which AuNP-P, SNP-P and IONP-P composite solutions (corresponding to 200 AU/mL pediocin in each) were added and the fluorescence readings were monitored periodically in a spectrofluorimeter (FluoroMax-3, HORIBA) at an excitation wavelength of 622 nm and emission wavelength of 670 nm. Cell suspension treated with an equivalent concentration of purified pediocin was also taken in parallel set. Cells treated with valinomycin (30 µM) were used as positive control in the assay.

6.2.10.5. Transmission electron microscope analysis

L. monocytogenes Scott A cells (approximately 10^6 CFU/mL in sterile PBS) were treated with IONP-P composite (corresponding to 200 AU/mL pediocin) for 6 h at 37°C. Control samples consisted of cells suspended in sterile PBS and treated with IONP solution alone under the same conditions. The treated and control cells were washed once with sterile PBS and once with sterile MilliQ water and then resuspended in sterile MilliQ water. A 2.0 µl aliquot of each sample was spotted on carbon coated TEM grid (Pacific Grid, USA), air-dried in laminar hood and examined in a transmission electron microscope (Jeol JEM 2100, Japan) operating at 200 kV and their images were recorded.

6.2.10.6. Antimicrobial spectrum

The antimicrobial spectrum of AuNP-P, SNP-P and IONP-P composites was determined against target cells of *L. monocytogenes* Scott A, *S. aureus* MTCC 96 and *E. faecalis* MTCC 439 by essentially following the method of an agar well diffusion assay as described earlier.

6.2.11. Desorption studies

For the desorption study, 5.0 mL of AuNP-P, SNP-P and IONP-P composite solutions were taken. Pediocin activity in each nanocomposite was initially ascertained by the spot-on-lawn assay as described earlier (Singh et al., 2012). To initiate desorption of pediocin, the pH of each nanoparticle-pediocin composite solution was adjusted to 2.0 with 0.1N HCL and incubated for 30 min in shaking condition at room temperature. Subsequently the composite solutions were centrifuged at 12,000 rpm for 10 min at 4^{o}C. The pH of the recovered supernatant was adjusted to 7.0 with 0.1 N NaOH and this sample was regarded as the desorbed pediocin. Pediocin activity in the desorbed sample was determined by the spot-on-lawn assay and expressed as % activity of desorbed pediocin as compared to the respective nanoparticle-pediocin composites.

6.2.12. Preparation and magnetic separation of IONP-pediocin composite

Requisite volume of IONP solution was added from the stock solution (10.0 mg/mL prepared in sterile MilliQ water) to 10 ml aliquot of cell-free culture filtrate so as to achieve a final nanoparticle concentration of 0.5 mg/mL. The solution was then incubated for 30 minutes at room temperature under mild shaking. The solution was then allowed to stand and a horse-shoe magnet was placed in the vicinity of the tube. After 10 min, the supernatant was aspirated and the pellet representing IONP-P composite was resuspended in 5.0 mL of sterile MilliQ water. Pediocin activity in IONP-P composite was ascertained by the spot-on-lawn assay as described earlier (Singh et al., 2012). A membrane depolarization assay and agar well diffusion assay was performed with both the supernatant as well as the magnetically recovered IONP-P composite solution by following the methods described earlier.

6.2.13. Multiple cycles of adsorption-desorption of pediocin with IONP

Preparation and magnetic separation of IONP-pediocin composite was accomplished as described previously. Desorption of pediocin from magnetically separated IONP-P composite was pursued at pH 2.0 and the recovered IONP was again used for another round of pediocin adsorption using cell-free culture filtrate and magnetic separation of IONP-P composite. Likewise a total of 5 successive adsorption-desorption cycles coupled with magnetic separation was pursued. After every round of adsorption, pediocin activity in IONP-P composite was determined (Singh et al., 2012) and expressed as % activity in IONP-P composite as compared to cell-free culture filtrate used a source of pediocin for the adsorption studies.

6.2.14. Adsorption isotherm studies

Initially the protein concentration in the cell-free culture filtrate of the producer LAB *Pediococcus pentosaceus* CRA51 as well as purified pediocin obtained by cell-adsorption method was determined by Bradford reagent (Sigma-Aldrich, USA) following the manufacturer instructions. To pursue the adsorption isotherm studies, in a total working volume of 1.0 mL, varying volumes of cell-free culture filtrate and purified pediocin (protein concentrations ranging from 5.0 mg/L to 80 mg/L in each) were added to a fixed concentration of IONP (0.5 mg/mL). The samples were then incubated for 30 minutes at room temperature under mild shaking. Following incubation, the samples were centrifuged at 10, 000 rpm for 10 minutes. The supernatant which consisted of un-adsorbed sample was aspirated and the protein concentration in this sample was ascertained by the Bradford reagent. The adsorption capacity, q_e (mg/g) was determined as mentioned previously (Saha et al., 2011). All experiments were carried out in triplicates and the data was presented as mean with standard deviation.

6.2.15. Reverse phase HPLC

Preparation and magnetic separation of IONP-P composite and desorption of pediocin from magnetically separated IONP-P composite was pursued at pH 2.0 as described earlier. A 20 µL of desorbed pediocin (pH adjusted to 7.0) as well as pediocin purified by the cell-adsorption method were subjected to RP-HPLC (PerkinElmer Analytical HPLC system,

USA) using an analytical RP-HPLC column (Brownlee Analytical C_{18}, 5 µm, 250 x 4.6 mm) with series 200 HPLC pump and series 200 UV/vis detector. The flow-rate was maintained at 1.0 ml/min and the solvents used were solvent A (0.1% TFA in MilliQ water) and solvent B (0.1% TFA in acetonitrile). The run consisted of 0 to 5 minutes 5 % solvent A and from 5 to 25 minutes a gradient of 5% to 95% solvent B. The eluted fraction was collected manually from multiple runs and vacuum evaporated in a SpeedVac concentrator (Eppendorf). The dried preparations were resuspended in sterile MilliQ water and pediocin activity of the samples was ascertained by the spot-on-lawn assay, an agar well diffusion assay, cFDA-SE leakage assay and membrane depolarization assay as described earlier.

6.2.16. Storage studies

AuNP-P composite, SNP-P composite, IONP-P composite, pediocin purified by cell adsorption method and desorbed pediocin from IONPs (corresponding to 200 AU/mL pediocin in each), were stored at 4^{o}C and room temperature (25^{o}C) for a period of seven days. Samples were withdrawn intermittently during storage (1, 3, 5 and 7 days) and their antibacterial activity was tested by interacting with 10^6 CFU/mL *L. monocytogenes* Scott A cells for 6 h at 37^{o}C and 180 rpm. Following treatment, the samples were surface plated on BHI-agar plate and viable cell numbers were enumerated after overnight incubation of the plates at 37^{o}C. In case of control samples, target cells were treated with freshly prepared AuNP-P composite, SNP-P composite, IONP-P composite, pediocin purified by cell adsorption method and desorbed pediocin from IONPs (corresponding to 200 AU/mL pediocin in each) and cell viability was determined as mentioned previously. The viable cell numbers obtained from treated samples were compared with control samples and the results were expressed as % activity compared to control.

6.2.17. Cytotoxicity assay

Cytotoxicity of purified pediocin, AuNP-P, SNP-P and IONP-P composites was assessed on human HT-29 cells by a standard MTT assay following the manufacturer instruction (Sigma-Aldrich, MO, USA). HT-29 cells were initially propagated in 25 cm^2 tissue culture

flask in Dulbecco's Modified Eagle Medium (DMEM) supplemented with 10% (v/v) fetal bovine serum (FBS), penicillin (100 µg/mL) and streptomycin (100 µg/mL) at 37°C under a humidified atmosphere of 5% CO_2. Prior to MTT assay, cells were seeded onto 96-well tissue culture plates (10^4 cells per well) and incubated with varying concentrations of purified pediocin, AuNP-P, SNP-P and IONP-P composites (corresponding to 250 AU/mL, 500 AU/mL, 1000 AU/mL and 2000 AU/mL pediocin in each) made in DMEM, for a period of 24 h in a CO_2 incubator. The control samples consisting of cells treated with DMSO were also included in parallel sets. Following 24 h of incubation, the media was gently aspirated and fresh DMEM containing MTT solution was added to the wells. The plates were again incubated for 4 h at 37°C. Following incubation, the supernatant was removed and the insoluble formazan product was solubilized in DMSO and its absorbance was measured in a microtitre plate reader (Infinite M200, TECAN, Switzerland) at 550 nm. For every test sample, MTT assay was performed in six sets for each tested concentration. Data analysis and determination of standard deviation was performed with Microsoft Excel 2010 (Microsoft Corporation, USA). The absorbance obtained for control samples represented 100% cell viability, whereas the absorbance for the treated cells were compared to the control samples to determine % cell viability.

6.2.18. Determination of minimum inhibitory concentration (MIC)

MIC of the purified pediocin, AuNP-P, SNP-P and IONP-P composites were determined against *Listeria monocytogenes* Scott A, *Staphylococcus aureus* MTCC 96 and *Enterococcus faecalis* MTCC 439. The bacterial cultures were inoculated at 1% level in microtitre plate wells having the requisite growth medium and grown overnight at 37°C and 180 rpm in presence of varying concentrations of the tested samples. The growth of the bacterial strains was determined by measuring absorbance at 600 nm using a microtitre plate reader (Infinite M200, TECAN, Switzerland). MIC of the samples was recorded as the lowest concentration which resulted in OD_{600} reading of <0.1, indicating lack of cell growth. The mean MIC values were calculated from three independent experiments, each having three replicas.

6.3. Results and Discussion

6.3.1. Capture of pediocin from cell-free culture filtrate and generation of nanoparticle-pediocin (NP-P) composite

Given the high isoelectric point of pediocin, (Rodríguez et al., 2002) it was conceived that interaction of anionic NPs with cell-free culture filtrate of the producer LAB at pH 7.0 would result in charge-based selective capture of the cationic pediocin resulting in concurrent formation of nanoparticle-pediocin (NP-P) composite in solution, which could then be easily separated from other secreted metabolites present in the culture filtrate by centrifugation. This tenet which formed the rationale of the present study is depicted in Figure 6.1.

In the present study, gold nanoparticle (AuNP), silica nanoparticle (SNP) and iron oxide nanoparticle (IONP) were chosen as the anionic NPs, based on their well documented biological applications (Saha et al., 2012; Bae et al., 2012; Lauren et al., 2008). The individual nanoparticles (NPs) were synthesized by following well established protocols.

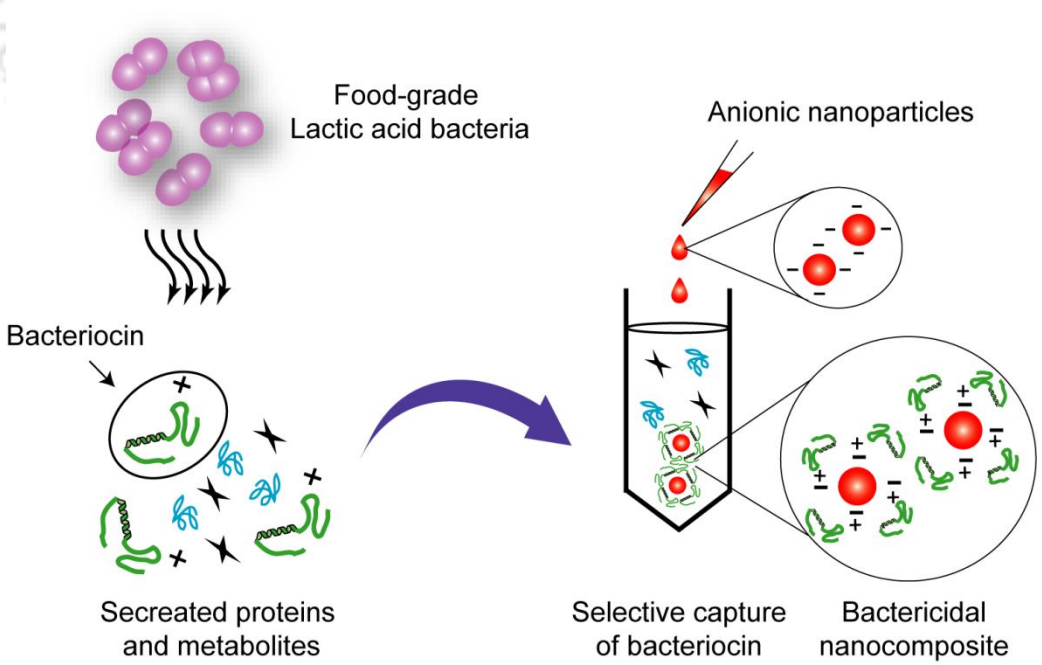

Figure 6.1. Selective capture of bacteriocin by anionic nanoparticles with concurrent generation of bactericidal nanocomposites.

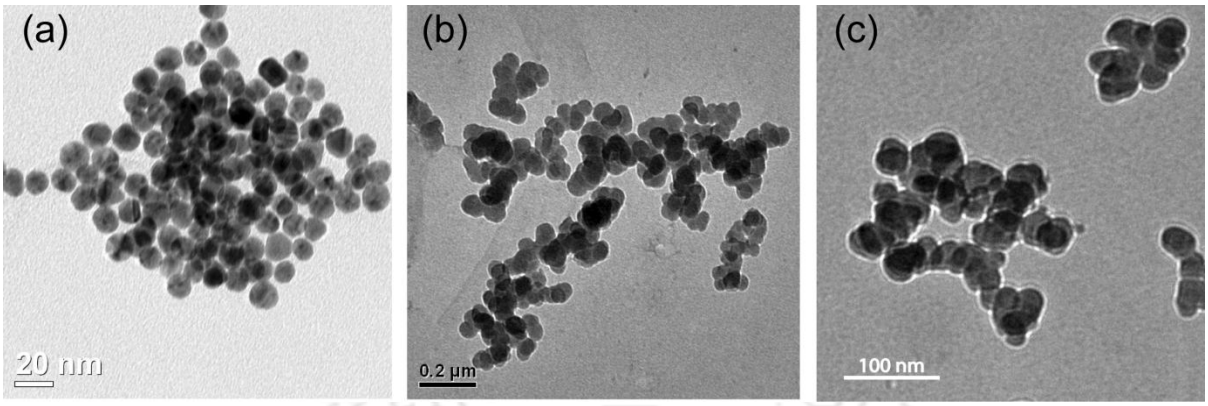

Figure 6.2. Transmission electron microscope images of **(a)** citrate-stabilized gold nanoparticle (AuNP), **(b)** silica nanoparticle (SNP) and **(c)** iron oxide nanoparticle (IONP). The average particle size of the nanoparticles was: AuNP (12.0 ± 2.0 nm), SNP (40-60 nm) and IONP (20-40 nm).

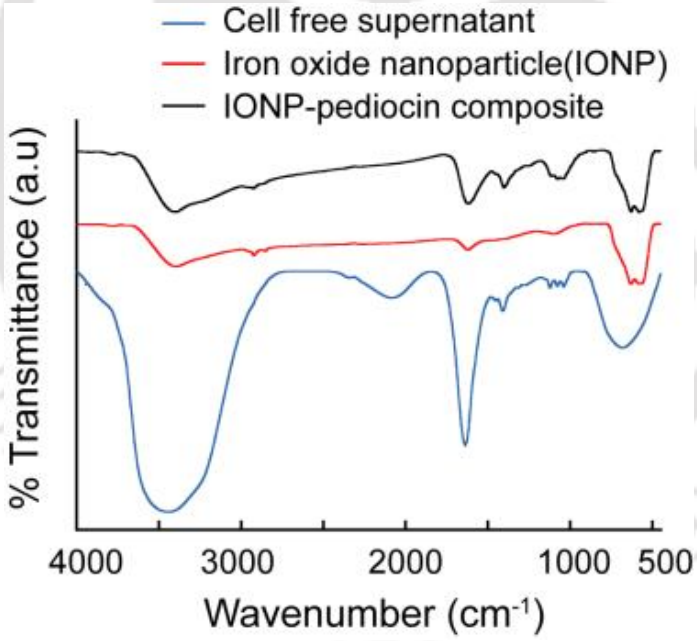

Figure 6.3. FTIR analysis of IONP-pediocin composite.

A representative TEM image of the nanoparticles is indicated in Figure 6.2. The average particle size of AuNPs, SNPs and IONPs were observed to be 12.0 ± 2.0 nm, 40-60 nm and 20-40 nm, respectively. The NPs were interacted with the cell-free culture filtrate and then

the NP-P composites were separated by centrifugation. The formation of NP-P composites were studied by FTIR analysis. A representative result of the FTIR analysis is depicted in Figure 6.3. It is evident from the figure that the characteristic amide stretching frequencies (1650 cm^{-1} and 1420 cm^{-1}) of cell-free supernatant was retained in the iron oxide-pediocin (IONP-P) composite, which suggested the presence of the peptide on the surface of IONPs. Similar observations were also made for gold nanoparticle-pediocin (AuNP-P) and silica nanoparticle-pediocin (SNP-P) composites (refer to Figure A6.1 in Appendix).

6.3.2. Bactericidal activity of nanoparticle-pediocin (NP-P) composite

Antibacterial activity of the generated NP-P composites was initially ascertained by a conventional agar well diffusion assay. Representative results of the initial experiments conducted with various proportions of culture-filtrate and NPs are indicated in Figures A.6.2-A6.4 (Appendix). The minimum concentration of NPs and time of interaction which enabled efficient capture of pediocin from the culture filtrate was determined by observing for the presence of zone of inhibition in the NP-P composite samples and a corresponding lack of zone of inhibition in the respective supernatants following separation of NP-P composites. From the results indicated in Figures A.6.2-A6.4 (Appendix), it was evident that the minimum concentration of the respective NPs and minimum time of interaction required to generate the NP-P composites were as follows: (i) For AuNP-P composite: 10 mL of cell-free culture filtrate and 20 mL of 0.32 nM AuNPs interacted for 30 min, (ii) For SNP-P composite: 10 mL of cell-free culture filtrate interacted with SNPs (final concentration 0.5 mg/mL) for 30 min and (iii) For IONP-P composite: 10 mL of cell-free culture filtrate interacted with IONPs (final concentration 0.5 mg/mL) for 30 min. All the subsequent experiments to generate the respective NP-P composites were conducted with the aforementioned proportions and interaction time. A representative result which demonstrates prominent anti-listerial activity of all the NP-P composites, manifested as large zones of inhibition around the well of the tested samples is indicated in Figure 6.4, well nos. 2-4. It may be mentioned that these zones of inhibition were equivalent to that observed for the cell-free culture filtrate (Figure 6.4, well no. 1). It is also to be noted that none of NPs alone exhibited any antibacterial activity (Figure 6.4, well nos. 5-7). Time-kill curves indicated that the NP-P composites had an adverse effect on the viability

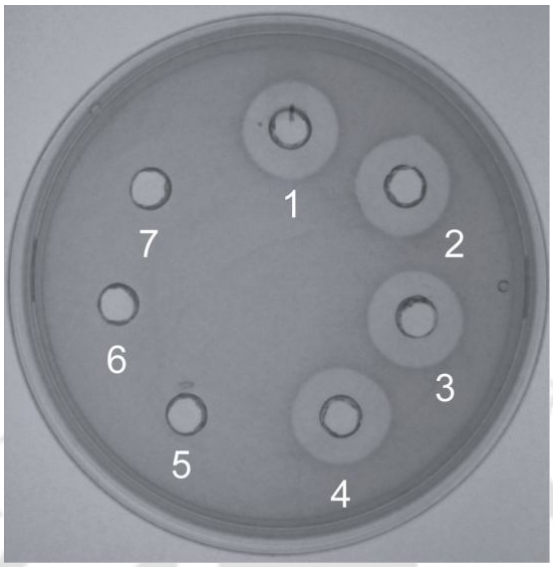

Figure 6.4. Agar well diffusion assay to test the antibacterial activity of various nanoparticle-pediocin composites against *Listeria monocytogenes* Scott A. **(1)** cell-free culture supernatant of *Pediococcus pentosaceus* CRA51, **(2)** AuNP-pediocin composite, **(3)** SNP-pediocin composite, **(4)** IONP-pediocin composite, **(5)** AuNP, **(6)** SNP and **(7)** IONP.

of *L. monocytogenes* Scott A and following 6 h of treatment with the nanocomposites (200 AU/mL pediocin in each), the viable cell number dropped drastically from an initial 6.0 Log_{10} CFU to around 2.0 Log_{10} CFU (Figure 6.5a). cFDA-SE leakage assay indicated that NP-P composites rendered membrane damage in *L. monocytogenes* Scott A and the magnitude of cFDA efflux from the NP-P composites was comparable to purified pediocin of equivalent concentration and the activity was dose-dependent (Figure 6.5b). Treatment of *L. monocytogenes* Scott A cells with NP-P composites also lead to rapid dissipation of membrane potential as evident from the $DiSC_35$ assay (Figure 6.6). Thus, the ability to dissipate the transmembrane potential in target cells, which is a signature activity of pediocin (Singh et al., 2012). was also retained in the NP-P composites. This suggested that the present method of capture of pediocin by NPs followed by concurrent generation of NP-P composites perhaps did not cause any significant perturbation of the native structure of pediocin and hence the activity was retained. Potent bactericidal activity of NP-P composite was also observed in transmission electron microscope (TEM) analysis.

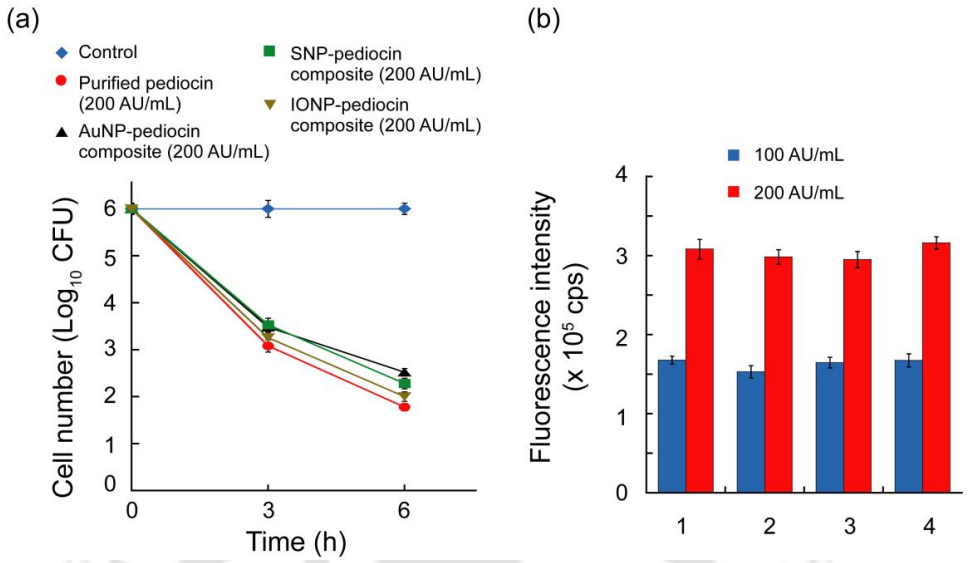

Figure 6.5. (a) Time-kill curves of purified pediocin, AuNP-pediocin composite, SNP-pediocin composite and IONP-pediocin composite against *L. monocytogenes* Scott A. **(b)** cFDA-SE leakage assay with (1) purified pediocin, (2) AuNP-pediocin composite, (3) SNP-pediocin composite and (4) IONP- pediocin composite against *L. monocytogenes* Scott A. Pediocin activity (AU/mL) in each of these samples is indicated.

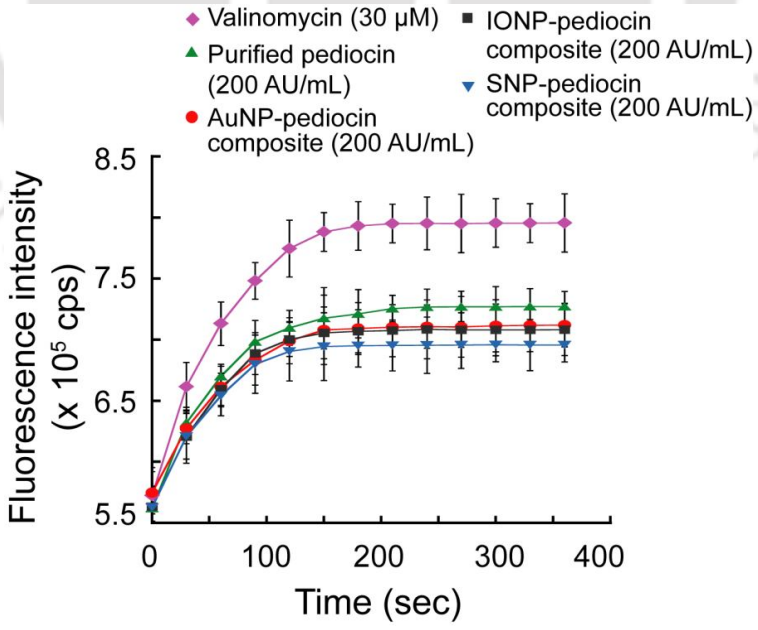

Figure 6.6. DiSC$_3$5-based membrane depolarization assay of *L. monocytogenes* Scott A cells treated with nanoparticle-pediocin composites.

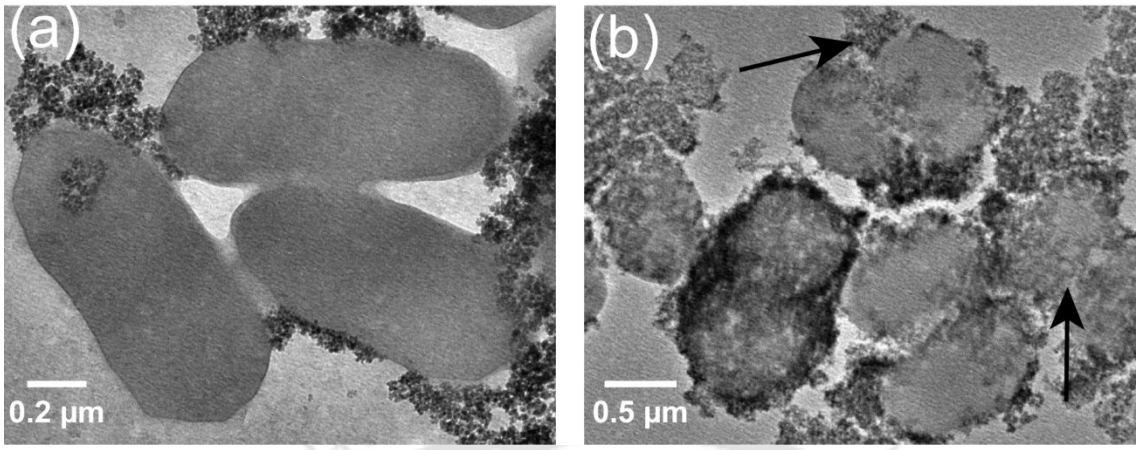

Figure 6.7. Transmission electron microscope images of *L. monocytogenes* Scott A cells treated with **(a)** IONP and **(b)** IONP-pediocin composite. Arrow indicates damaged cells.

A representative result indicated that IONP-treated cells of *L. monocytogenes* Scott A cells retained their characteristic morphology (Figure 6.7a) whereas the IONP-P-treated cells revealed prominent morphological perturbations (Figure 6.7b). Interestingly, all the NP-P composites exhibited antibacterial activity against model pathogens (Figure 6.8).

6.3.3. Desorption of pediocin from nanoparticle-pediocin (NP-P) composite

The one-step capture of pediocin through electrostatic interaction of the bacteriocin and anionic NPs also rendered the interesting possibility of desorption of the bacteriocin. The desorption studies with the NP-P composites were conducted at pH 2.0 so as to disrupt the charge-based interaction between the bacteriocin and the NPs. The activity obtained for desorbed pediocin from AuNP-P composite was negligible as compared to that obtained for SNPs and IONPs (Figure 6.9), suggesting negligible desorption of pediocin from AuNP-P composite. Presence of four cysteines in pediocin (Rodríguez et al., 2002) renders the possibility of strong Au-thiol interactions (Brust et al., 1994) apart from charge-based interactions and perhaps prevented desorption of pediocin by mere change of pH.

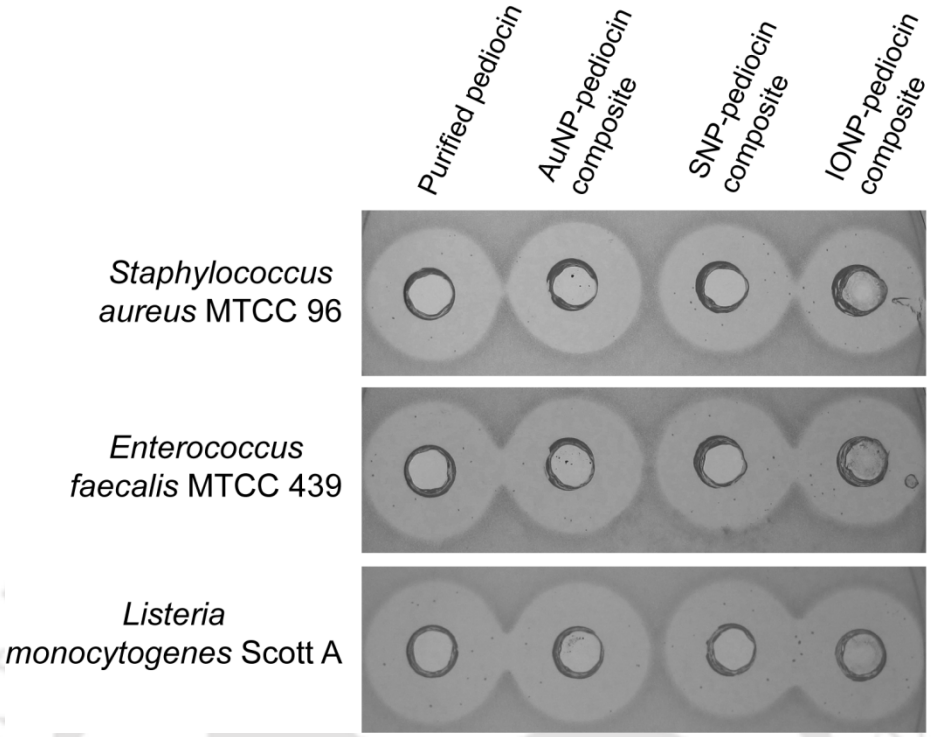

Figure 6.8. Antimicrobial spectrum of purified pediocin, AuNP-pediocin composite, SNP-pediocin composite and IONP-pediocin composite determined by an agar well diffusion assay.

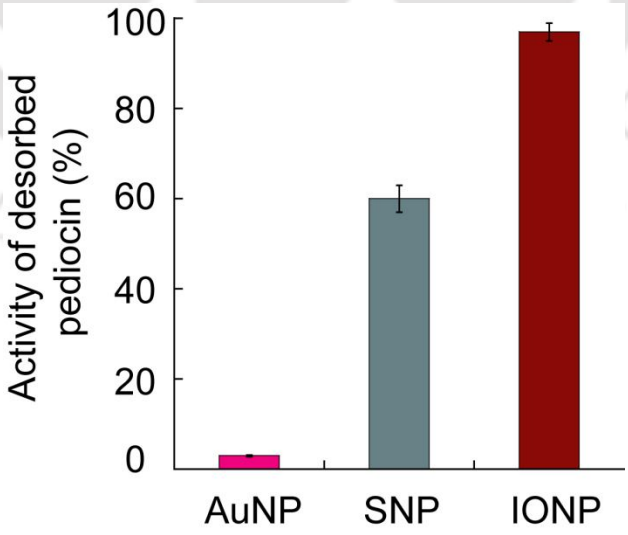

Figure 6.9. Activity of pediocin desorbed from anionic nanoparticles.

6.3.4. Magnetic separation of IONP-P composite and multiple adsorption-desorption cycles

Following capture of pediocin by IONPs, efficient recovery of IONP-P composite was also achieved through magnetic separation (Figure 6.10a) in lieu of a centrifugation step and the membrane-depolarization activity typically associated with pediocin was observed for the recovered composite (Figure 6.10b). Desorption of pediocin from IONP-P composite was achieved at pH 2.0 and the recovered IONP was recycled to explore multiple cycles of pediocin adsorption-desorption to ascertain the feasibility of repeated magnetic separation and re-usability of IONPs. The activity obtained for IONP-P composite using recycled IONPs was as high as 80% even in the third cycle of adsorption and decreased thereafter to around 50% after 5 cycles of adsorption (Figure 6.11). These results indicated the benefit of using IONPs, which could be salvaged and reused as a capture probe. Adsorption studies with IONPs suggested that the steady state adsorption isotherm obtained for cell-free culture supernatant as well as purified pediocin followed a Langmuir isotherm model (refer to Figure A6.5 and Table A6.1 in Appendix) and thus suggested adsorption at specific homogeneous sites on IONPs and a monolayer adsorption process (Saha et al., 2011).

6.3.5. Purification of pediocin using IONPs and HPLC

Recovery of IONP-P composite by magnetic separation followed by desorption at pH 2.0 resulted in 16-fold purification of pediocin (refer to Table A6.2 in Appendix). A similar HPLC profile and retention time suggested that the homogeneity of desorbed pediocin from IONPs was on par with purified pediocin (Figure 6.12). The HPLC eluted fraction of desorbed pediocin from IONPs exhibited anti-listerial activity in an agar well diffusion assay (Figure 6.12). Further, the HPLC eluted fraction also exhibited the characteristic membrane-directed activity in a cFDA leakage assay (Figure 6.13a) and membrane depolarization in target bacteria (Figure 6.13b), akin to purified pediocin.

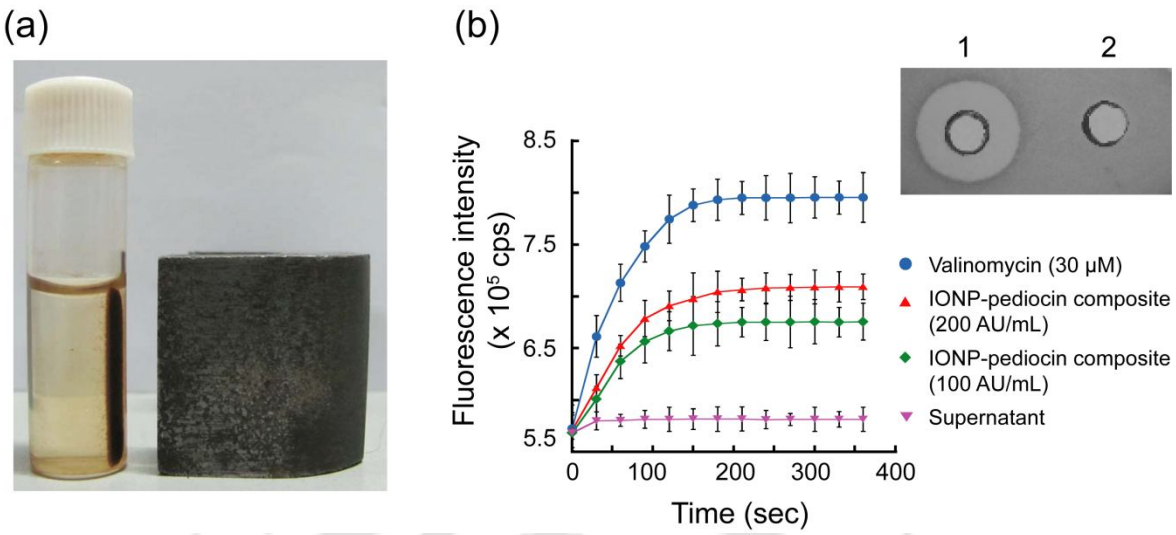

Figure 6.10. (a) Image of a vial showing separation of IONP-pediocin composite using a horse-shoe magnet. The IONP-pediocin composite is visible as a brownish-black deposit on the right side wall of the vial. **(b)** $DiSC_35$-based membrane depolarization assay of *L. monocytogenes* Scott A cells treated with magnetically separated IONP-pediocin composite and the supernatant following magnetic separation. Inset indicates agar well diffusion assay against *L. monocytogenes* Scott A with (1) magnetically separated IONP-pediocin composite (corresponding to 200 AU/mL pediocin) and (2) supernatant.

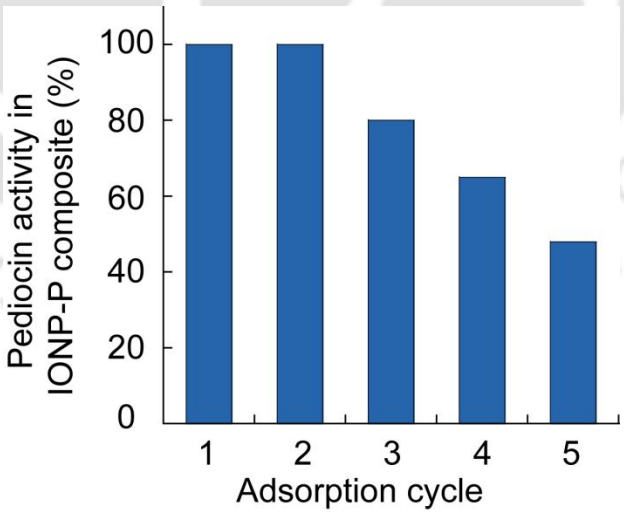

Figure 6.11. Pediocin activity in IONP-P composite in successive adsorption cycles following magnetic separation of IONP-pediocin composite and desorption of pediocin.

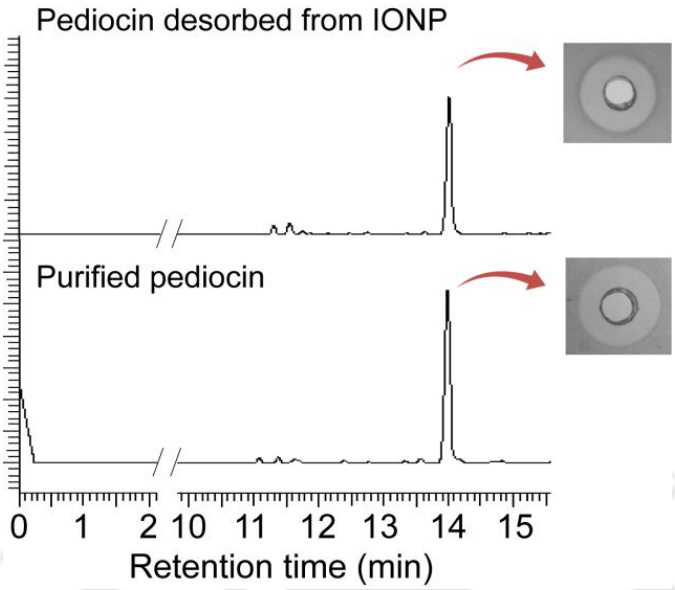

Figure 6.12. HPLC profile for pediocin desorbed from IONP and pediocin purified by cell-adsorption method and respective anti-listerial activity of eluted fractions.

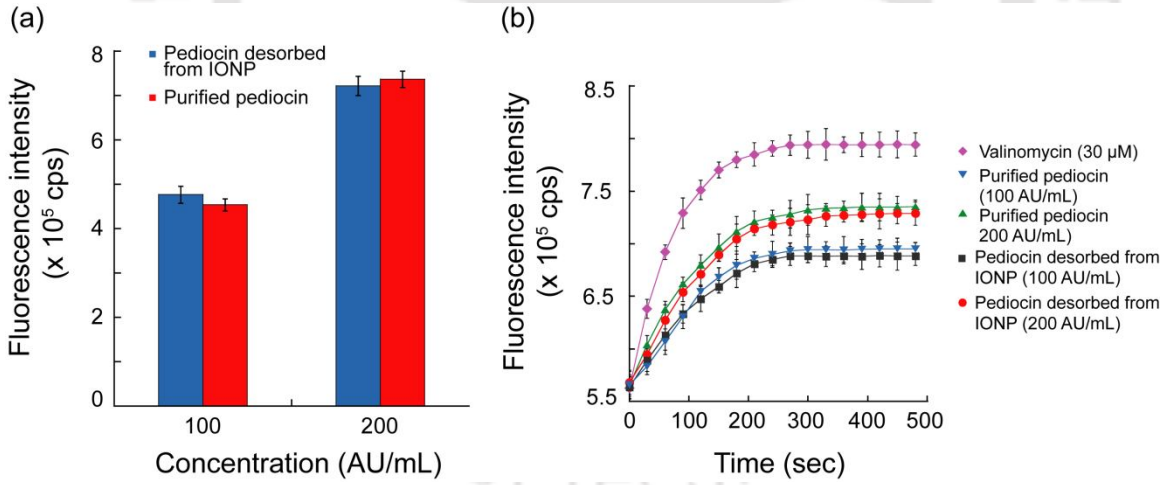

Figure 6.13. (a) cFDA-SE leakage assay with HPLC-eluted fraction of purified pediocin and pediocin desorbed from IONPs. **(b)** Membrane depolarization assay of *L. monocytogenes* Scott A cells treated with HPLC-eluted fractions of pediocin desorbed from IONP-pediocin composite and purified pediocin.

6.3.6. Storage studies

Storage studies indicated that pediocin desorbed from IONP and all three NP-P composites were stable with substantial retention of bactericidal activity (~85-90%) for 7 days at 4°C (Figure 6.14a). The degree of the antibacterial activity was comparable with that of purified pediocin stored under similar conditions (Figure 6.14a). The stability of the tested desorbed pediocin from IONPs and the NP-P was marginally reduced upon storage at room temperature (25°C) as evident from the reduction in the bactericidal activity to around 65-80% (Figure 6.13b). Overall the storage studies indicated that the NP-P composites were quite stable with considerable retention of activity.

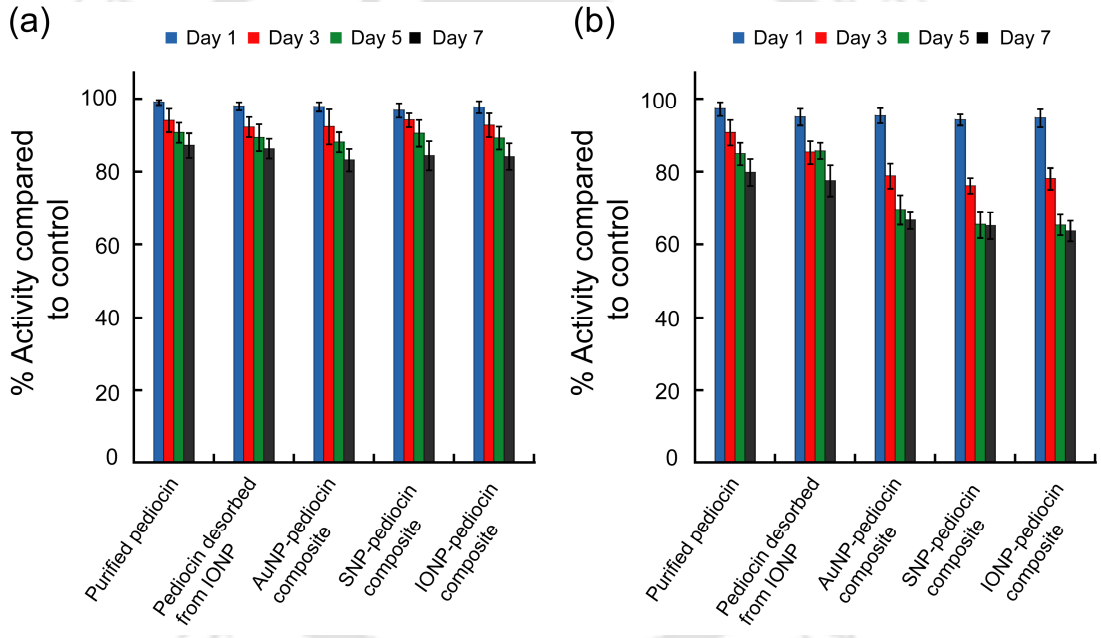

Figure 6.14. Antimicrobial activity of purified pediocin, pediocin desorbed from IONP, AuNP-pediocin composite, SNP-pediocin composite and IONP-pediocin composite stored at **(a)** 4°C and **(b)** room temperature (25°C).

6.3.7. Cytotoxic effect

In order to ascertain the cytotoxic implications of the developed nanocomposites on cultured HT-29 cells, an MTT assay was conducted. Interestingly, the NPs alone (Figure A6.6 in Appendix) as well as purified pediocin and all the pediocin-nanocomposites were non-cytotoxic to human HT-29 cells (Figure 6.15). Further it is significant to mention that

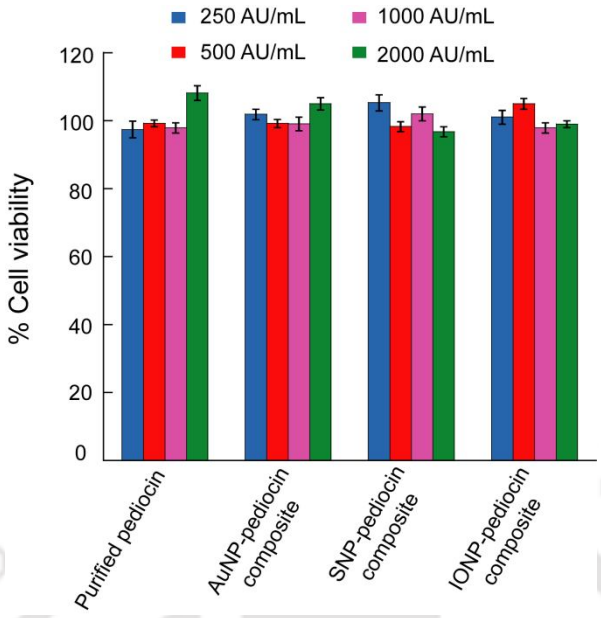

Figure 6.15. MTT assay to determine % viability of HT-29 cells following treatment with varying concentrations of nanoparticle-pediocin composites. Each data point represents mean ± standard deviation from six samples.

purified pediocin as well as all the nanocomposites were observed to be non-toxic to the model human cell line even at concentrations in excess of the minimal inhibitory concentration (MIC) against model pathogens (Table A6.3 in Appendix). MIC is largely regarded as one of the major parameters to quantify the efficacy of an antibacterial agent. However, it is important to understand that MIC essentially measures the *in vitro* susceptibility of a microorganism to a given drug and thus cannot be regarded as an absolute measure for efficient *in vivo* therapy of bacterial infection. The *in vivo* efficiency of an antibacterial agent is likely to be influenced by various parameters such as serum concentration, binding to plasma protein and tissue distribution (Craig, 1998; Mueller et al., 2004). Thus bactericidal agents are generally used at concentrations in excess of their MIC in order to achieve effective killing concentrations *in vivo* against target pathogens (Wispelwey, 2005; Craig, 1998; Craig, 2003). However, it is also pertinent to determine whether usage of a bactericidal agent at concentrations higher than MIC leads to manifestation of any undesirable cytotoxicity. In the present study, the results of the cytotoxicity assay were encouraging as they suggested that even at concentrations

exceeding the MIC, the NP-P composites could perhaps be explored to eliminate the target pathogens without the added risk of any adverse effect on human cells. However, the true therapeutic potential of the NP-P composites need to be determined in *in vivo* models.

6.4. Significant Findings

The present study essentially demonstrates a facile method to selectively capture a potent bacteriocin from the cell-free culture filtrate of food-grade lactic acid bacteria with concurrent generation of a bactericidal nanocomposite. The prominent findings of the study are as follows:

1. The present work unveils the utility of anionic nanoparticles in a facile one-step process of selective capture of a bacteriocin secreted by a food-grade LAB leading to simultaneous generation of a robust bactericidal nanocomposite. Retention of archetypal pediocin activity in all the nanoparticle-pediocin composites vindicated the merit of the NP-based capture of pediocin to generate bactericidal composites.
2. The general principle of charge-based adsorption-desorption, magnetic separation and re-usability of IONPs demonstrated in the present study can perhaps be also exploited to generate potent bactericidal nanocomposites with other cationic antimicrobial peptides.
3. A bacteriocin such as pediocin is known to have a restricted antimicrobial spectrum. In the age of rampant antibiotic-resistance, it is thus envisaged that the bacteriocin-based nanocomposites may assume the role of designer therapeutics to specifically combat pathogenic bacteria with minimal impact on natural commensal microbiota.
4. Given the high bactericidal activity and lack of cytotoxicity on human cells, it would be stimulating in future to ascertain or validate the *in vivo* efficacy of the developed nanocomposites against clinically relevant drug-resistant pathogens.

SUMMARY AND FUTURE SCOPE

SUMMARY AND FUTURE SCOPE

A representative figure indicating the prominent findings of the Ph.D. thesis work is indicated in the cartoon shown in Scheme 1.

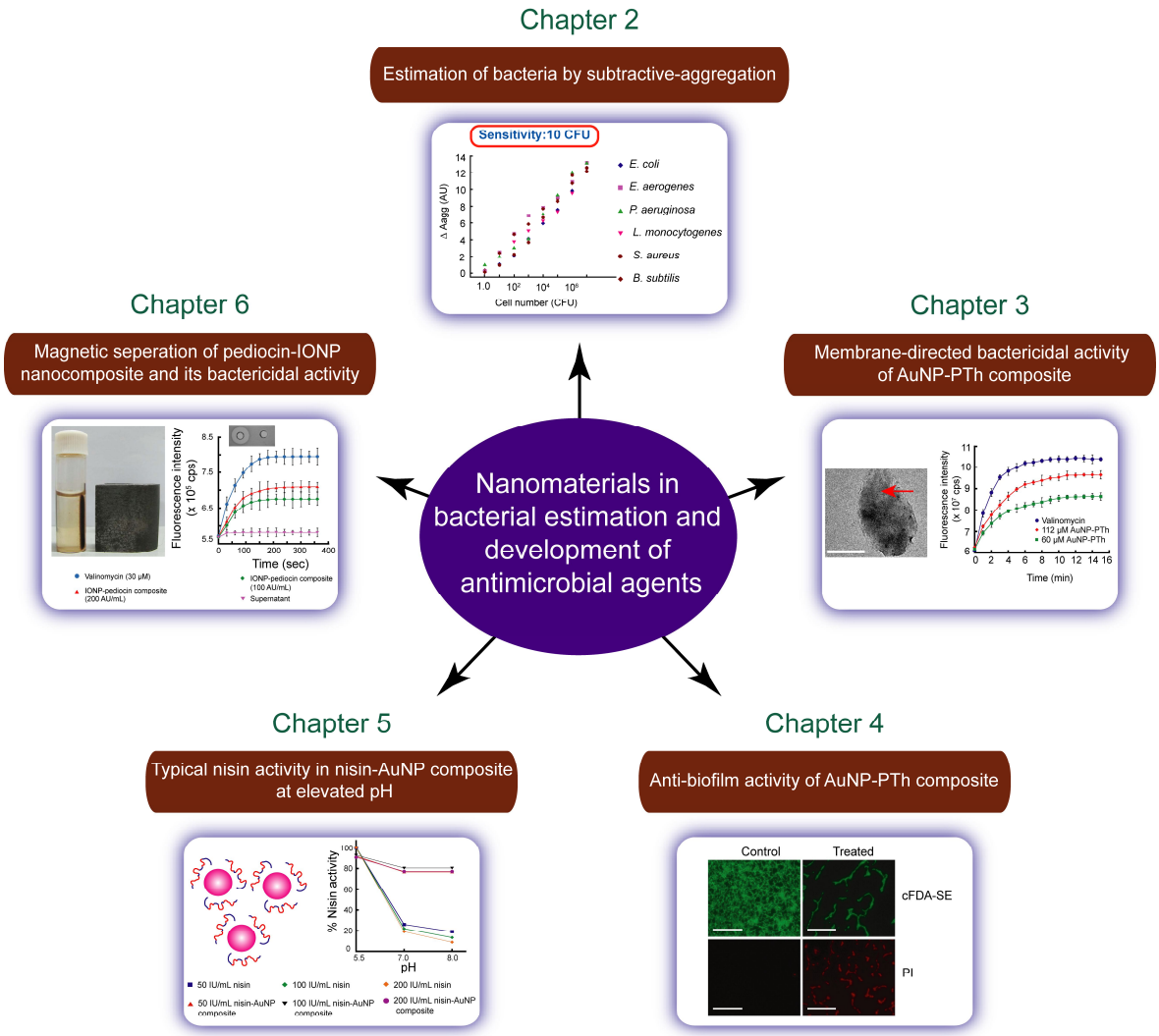

Scheme 1. Schematic representation of prominent findings of Ph. D research work.

A facile method of estimation of bacterial cell numbers in solution was developed based on the aggregation of citrate-stabilized nanoparticles. The developed method was based on the principle of subtractive-aggregation, a phenomenon which was driven by the

presence of bacterial cells in solution and which provided a quantitative measure of the cell numbers. The method was generic and was able to estimate a wide variety of bacterial cells with a sensitivity of 10 CFU. Interestingly the method was non-destructive and specific for estimation of viable cell numbers. It is envisaged that the developed method can be extended in future for analysis of complex samples and development of miniaturized detection devices and would find niche applications in the area of pathogen detection and microbiological quality control.

A potent bactericidal agent was developed with gold nanoparticle-polythiophene composite. The nanocomposite displayed prominent membrane-directed activity and thus holds considerable promise in combating the menace of drug-resistant pathogens. Interestingly, the nanocomposite was non-toxic to cultured human cells in an *in vitro* assay. The membrane-directed bactericidal activity of the composite could be exploited in combination therapy with prototype antibiotics. A significant finding was the potent anti-biofilm activity of the nanocomposite. Given the potential therapeutic implications of the composite it would be worthwhile in future to probe the activity of the developed composite against drug-resistant pathogens such as MRSA, nosocomial infections caused by biofilms and in other *in vivo* infection models.

In the context of generating safe antibacterial nanocomposite, a significant contribution of the present work was to develop a soft tailoring strategy for retaining the activity of the FDA approved peptide nisin at physiologically relevant pH in a nisin-gold nanoparticle composite. Further, a judicious choice of magnetic anionic nanoparticles enabled a one-step selective capture of the bacteriocin pediocin produced by a food-grade lactic acid bacterium with concurrent generation of a potent bactericidal nanocomposite. Given the favorable antimicrobial spectrum of pediocin and non-toxic nature of the nanoparticle-pediocin composite, there is enormous potential in exploring the nanocomposite as a designer therapeutic against specific pathogenic bacteria with minimal collateral damage on commensal gut bacteria. In future it would be interesting to exploit the antimicrobial peptide-based nanocomposites for elimination of infections caused by vancomycin-resistant enterococci (VRE), anti-listerial therapy and combination therapy with probiotic lactic acid bacteria.

BIBLIOGRAPHY

Abdel-Hamid, I.; Ivnitski, D.; Atanasov, P.; Wilkins, E. Highly sensitive flow-injection immunoassay system for rapid detection of bacteria. *Anal Chim Acta* **1999b**, *399*, 99-108.

Afonso, A. S.; Pérez-Lépez, B.; Faria, R. C.; Mattoso, L. H. C.; Hernández-Herrero, M.; Roig-Sagués, A. X.; Costa, M. M.; Merkoçi, A. Electrochemical detection of *Salmonella* using gold nanoparticles. *Biosensors and Bioelectronics* **2013**, *40*, 121-126.

Agasti, S. S.; Rana, S.; Park, M.; Kim, C. K.; You, C.; Rotello, V. M. Nanoparticles for detection and diagnosis. *Adv. Drug Del. Rev.* **2010**, *62*, 316-328.

Agrawal, A.; Tripp, R. A.; Anderson, L. J.; Nie, S. Real-time detection of virus particles and viral protein expression with two-color nanoparticle probes. *J Virol* **2005**, *79*, 8625-8628.

Ahamed, M.; AlSalhi, M. S.; Siddiqui, M. K. J. Silver nanoparticle applications and human health. *Clinica Chimica Acta* **2010**, *411*, 1841-1848.

Akerman, M. E.; Chan, W. C.; Laakkonen, P.; Bhatia, S. N.; Ruoslahti, E. Nanocrystal targeting in vivo. *Proc Natl Acad Sci* USA **2002**, *99*, 12617-12621.

Alakomi, H. L.; Paananen, A.; Suihko, M. L.; Helander, I. M.; Saarela, M. Weakening effect of cell permeabilizers on gram-negative bacteria causing biodeterioration. *Appl. Environ. Microbiol.* **2006**, *72*, 4695-4703.

Aldus, C. F.; van Amerongen, A.; Ariens, R. M. C.; Peck, M. W.; Wichers, J. H.; Wyatt, G. M. Principles of some novel rapid dipstick methods for detection and characterization of verotoxigenic *Escherichia coli*. *J Appl Microbiol* **2003**, *95*, 380-389.

Alivisatos, P. The use of nanocrystals in biological detection. *Nat. Biotechnol.* **2004**, *22*, 47-52.

Allahverdiyev, A. M.; Kon, K. V.; Abamor, E. S.; Bagirova, M.; Rafailovich, M. Coping with antibiotic resistance: Combining nanoparticles with antibiotics and other antimicrobial agents. *Expert Rev. Anti Infect. Ther.* **2011**, *9*, 1035-1052.

Allen, H. K.; Donato, J.; Wang, H. H.; Cloud-Hansen, K. A.; Davies, J.; Handelsman, J. Call of the wild: antibiotic resistance genes in natural environments. *Nat. Rev. Microbiol.* **2010**, *8*, 251-259.

Alonso, A.; Muñoz-Berbel, X.; Vigues, N.; Macanas, J.; Munoz, M.; Mas, J.; Muraviev, D. N. Characterization of fibrous polymer silver/cobalt nanocomposite with enhanced bactericide activity. *Langmuir* **2012**, *28*, 783-790.

Alphandary, H. P.; Andremont, A.; Couvreur, P. Targeted delivery of antibiotics using liposomes and nanoparticles: research and applications. *Int. J. Antimicrob. Agents* **2000**, *13*, 155-168.

Amieva, M. R.; El-Omar, E. M. Host-bacterial interactions in *Helicobacter pylori* infection. *Gastroenterology* **2008**, *134*, 306-323.

Amini, S.; Hottes, A. K.; Smith, L. E.; Tavazoie, S. Fitness landscape of antibiotic tolerance in *Pseudomonas aeruginosa* biofilms. *PLoS Pathogens*, **2011**, *7*, 1-15.

Amor, K. B.; Breeuwer, P.; Verbaarschot, P.; Rombouts, F. M.; Akkermans, A. D. L.; De Vos, W. M.; Abee, T. Multiparametric flow cytometry and cell sorting for the assessment of viable, injured, and dead bifidobacterium cells during bile salt stress. *Appl. Environ. Microbiol*. **2002**, *68*, 5209-5216.

Ansari, M. A.; Khan, H. M.; Khan, A. A.; Sultan, A.; Azam, A. Synthesis and characterization of the antibacterial potential of ZnO nanoparticles against extended-spectrum β-lactamases-producing *Escherichia coli* and *Klebsiella pneumoniae* isolated from a tertiary care hospital of North India. *Appl Microbiol Biotechnol* **2012**, *94*, 467-477.

Applerot, G.; Lellouche, J.; Perkas, N.; Nitzan, Y.; Gedanken, A.; Banin, E. ZnO nanoparticle-coated surfaces inhibit bacterial biofilm formation and increase antibiotic susceptibility. *RSC Advances* **2012**, *2*, 2314-2321.

Artault, S.; Blind, J. L.; Delaval, J.; Dureuil, Y.; Gaillard, N. Detecting *Listeria monocytogenes* in food. *Int Food Hyg* **2001**, *12*, 23.

Avery, S. V.; Howlett, N. G.; Radice, S. A. Copper toxicity towards *Saccharomyces cerevisiae*: Dependence on plasma membrane fatty acid composition. *Appl. Environ. Microbiol.* **1996**, *62*, 3960-3966.

Ayçiçek, H.; Aydogan, H.; Küçükkaraaslan, A.; Baysallar, M.; Basustaoglu, A. C. Assessment of the bacterial contamination on hands of hospital food handlers. *Food Control* **2004**, *15*, 253-259.

Azam, A.; Ahmed, A.S.; Oves, M.; Khan, M. S.; Memic, A. Size-dependent antimicrobial properties of CuO nanoparticles against Gram-positive and -negative bacterial strains. *International Journal of Nanomedicine* **2012**, *7*, 3527-3535.

Bae, S. W.; Tan, W.; Hong, J. Fluorescent dye-doped silica nanoparticles: new tools for bioapplications. *Chem. Commun.* **2012**, *48*, 2270-2282.

Bambeke, F. V.; Mingeot-Leclercq, M. P.; Struelens, M. J.; Tulkens, P. M. The bacterial envelope as a target for novel anti-MRSA antibiotics. *Trends Pharmacol. Sci.* **2008**, *29*, 124-134.

Bao, J.; Chen, W.; Liu, T.; Zhu, Y.; Jin, P.; Wang, L.; Liu, J.; Wei, Y.; Li, Y. Bifunctional Au-Fe_3O_4 nanoparticles for protein separation. *ACS Nano* **2007**, *1*, 293-298.

Bao, Y. P.; Wei, T. F.; Lefebvre, P. A.; An, H.; He, L.; Kunkel, G. T.; Muller, U. R. Detection of protein analytes via nanoparticle-based bio bar code technology. *Anal Chem* **2006**, *78*, 2055-2059.

Barone, P.W.; Baik, S.; Heller, D. A.; Strano, M. S. Near-infrared optical sensors based on single-walled carbon nanotubes. *Nat Mater* **2005**, *4*, 86-92.

Bavaro, M. F. *Escherichia coli* O157: what every internist and gastroenterologist should know. *Curr. Gastroenterol. Rep.* **2009**, *11*, 301-306.

Beaulieu, L.; Aomari, H.; Groleau, D.; Subirade, M. An improved and simplified method for the large-scale purification of pediocin PA-1 produced by *Pediococcus acidilactici*. *Biotechnol. Appl. Biochem.* **2006**, *43*, 77-84.

Bernbom, N.; Jelle, B.; Brogren, C. H.; Vogensen, F. K.; Norrung, B.; Licht, T. R. Pediocin PA-1 and a pediocin producing *Lactobacillus plantarum* strain do not change the HMA rat microbiota. *Int. J. Food Microbiol.* **2009**, *130*, 251-257.

Berry, V.; Gole, A.; Kundu, S.; Murphy, C. J.; Saraf, R. F. Deposition of CTAB-terminated nanorods on bacteria to form highly conducting hybrid systems. *J. Am. Chem. Soc.* **2005**, *127*, 17600-17601.

Blaser, M. Antibiotic overuse: Stop the killing of beneficial bacteria. *Nature*, **2011**, *476*, 393-394.

Boisselier, E.; Astruc, D. Gold nanoparticles in nanomedicine: preparations, imaging, diagnostics, therapies and toxicity. *Chem. Soc. Rev.* **2009**, *38*, 1759-1782.

Bolla, J.; Alibert-Franco, S.; Handzlik, J.; Chevalier, J.; Mahamoud, A.; Boyer, G.; Kiec-Kononowicz, K.; Pages, J. Strategies for bypassing the membrane barrier in multidrug resistant Gram-negative bacteria. *FEBS Lett.* **2011**, *585*, 1682-1690.

Bonelli, R. R.; Schneider, T.; Sahl, H. G.; Wiedemann. I. Insights into in vivo activities of lantibiotics from gallidermin and epidermin modeof- action studies. *Antimicrob. Agents Chemother.* **2006**, *50*, 1449-1457.

Bonoiu, A. C.; Mahajan, S. D.; Ding, H.; Roy, I.; Yong, K. T.; Kumar, R.; Hu, R.; Bergey, E. J.; Schwartz, S. A.; Prasad, P. N. Nanotechnology approach for drug addiction therapy: gene silencing using delivery of gold nanorod-siRNA nanoplex in dopaminergic neurons. *Proc Natl Acad Sci* USA **2009**,*106*, 5546-5550.

Brayner, R. The toxicological impact of nanoparticles. *NanoToday* **2008**, *3*, 48-55.

Breukink, E.; de Kruijff, B. The lantibiotic nisin, a special case or not?. *Biochim. Biophys. Acta* **1999**, *1462*, 223-234.

Breukink, E.; Wiedemann, I.; van Kraaij, C.; Kuipers, O. P.; Sahl, H.; de Kruijff, B. Use of the cell wall precursor lipid II by a pore-forming peptide antibiotic. *Science* **1999**, *286*, 2361-2364.

Brogden, K. A. Antimicrobial peptides: pore formers or metabolic inhibitors in bacteria?. *Nat. Rev. Microbiol.* **2005**, *3*, 238-250.

Brown, S. D.; Nativo, P.; Smith, J. A.; Stirling, D.; Edwards, P. R.; Venugopal, B.; Flint, D. J.; Plumb, J. A.; Graham, D.; Wheate, N. J. Gold nanoparticles for the improved anticancer drug delivery of the active component of oxaliplatin. *J. Am. Chem. Soc.* **2010**, *132*, 4678-4684.

Brumfitt, W.; Salton, M. R. J.; Hamilton-Miller, J. M. T. Nisin, alone and combined with peptidoglycan-modulating antibiotics: activity against methicillin-resistant *Staphylococcus aureus* and vancomycin-resistant *enterococci*. *J. Antimicrob. Chemother.* **2002**, *50*, 731-734.

Bruno, J. G.; Phillips, T.; Carrillo, M. P.; Crowell, R. Plastic-adherent DNA aptamer magnetic bead and quantum dot sandwich assay for *Campylobacter* detection. *J Fluoresc* **2009**, *3*, 427-435.

Brust, M.; Walker, M.; Bethell, D.; Schiffrin, D. J.; Whyman, R. Synthesis of thiol derivatized gold nanoparticles in a 2-phase liquid-liquid system. *J. Chem. Soc., Chem. Commun.* **1994**, 801-802.

Bu, T.; Zako, T.; Fujita, M.; Maeda, M. Detection of DNA induced gold nanoparticle aggregation with dark field imaging. *Chem. Commun.* **2013**, *49*, 7531-7533.

Bulte, J. W. M.; Douglas, T.; Witwer, B.; Zhang, S.; Strable, E.; Lewis, B. K.; Zywicke, H.; Miller, B.; van Gelderen, P.; Moskowitz, B. M., Duncan, I. D.; Frank, J. A. Magnetodendrimers allow endosomal magnetic labeling and in vivo tracking of stem cells. *Nat. Biotechnol.* **2001**, *19*, 1141-1147.

Bunthof, C. J.; Bloemen, K.; Breeuwer, P.; Rombouts, F. M.; Abee, T. Flow cytometric assessment of viability of lactic acid bacteria. *Appl. Environ. Microbiol*. **2001**, *67*, 2326-2335.

Carolissen-MacKay, V.; Arendse, G.; Hastings, J. W. Purification of bacteriocins of lactic acid bacteria: problems and pointers. *Int. J. Food Microbiol.* **1997**, *34*, 1-16.

Chadeau, E.; Brunon, C.; Degraeve, P.; Leonard, D.; Grossiord, C.; Bessueille, F.; Cottaz, A.; Renaud, F.; Ferreira, I.; Darroux, C.; Simon, F.; Rimbault, F.; Oulahal, N. Evaluation of antimicrobial activity of a polyhexamethylene biguanidecoated textile by monitoring both bacterial growth (ISO 20743/2005 standard) and viability (live/dead baclight kit). *J. Food Safety* **2012**, *32*, 141-151.

Chan, P.; Yuen, T.; Ruf, F.; Gonzalez-Maeso. J.; Sealfon, S. C. Method for multiplex cellular detection of mRNAs using quantum dot fluorescent in situ hybridization. *Nucleic Acids Res* **2005**, *33*, e161. doi:10.1093/nar/gni162.

Chan, W. C.; Nie, S. Quantum dot bioconjugates for ultrasensitive nonisotopic detection. *Science* **1998**, *281*, 2016- 2018.

Chang, Y.; Yang, C.; Sun, R.; Cheng, Y.; Koa, W.; Yang, P. Rapid single cell detection of *Staphylococcus aureus* by aptamer-conjugated gold nanoparticles. *Scientific Reports* **2013**, *3*, 1-7.

Charteris, W. P.; Kelly, P. M.; Morelli, L.; Collins, J. K. Development and application of an in vitro methodology to determine the transit tolerance of potentially probiotic *Lactobacillus* and *Bifidobacterium* species in the upper human gastrointestinal tract. *J. Appl. Microbiol.* **1998**, *84*, 759-768.

Chatterjee, A. K.; Sarkar, R. K.; Chattopadhyay, A. K.; Aich, P.; Chakraborty, R.; Basu, T. A simple robust method for synthesis of metallic copper nanoparticles of high antibacterial potency against *E. coli*. *Nanotechnology* **2012**, *23*, 085103.

Chatterjee, C.; Paul, M.; Xie, L.; van der Donk, W A. Biosynthesis and mode of action of lantibiotics. *Chem. Rev.* **2005**, *105*, 633-683.

Chatterjee, S. S.; Otto, M. Improved understanding of factors driving methicillin-resistant *Staphylococcus aureus* epidemic waves. *Clin Epidemiol.* **2013**, *5*, 205-217.

Chen, C. S.; Durst, R. A. Simultaneous detection of *Escherichia coli* O157: H7, *Salmonella* spp. and *Listeria monocytogenes* with an array-based immunosorbent assay using universal protein G-liposomal nanovesicles. *Talanta* **2006**, *69*, 232-238.

Chen, H.; Hoover, D. G. Bacteriocins and their food applications. *Comp. Rev. Food. Sci. Food Safety* **2003**, *2*, 81-100.

Chen, J.; McLellan, J. M.; Siekkinen, A.; Xiong, Y.; Li, Z.-Y.; Xia, Y. Facile synthesis of gold-silver nanocages with controllable pores on the surface. *J. Am. Chem. Soc.* **2006**, *128*, 14776-14777.

Chen, J.; Wang, D.; Xi, J.; Au, L.; Siekkinen, A.;Warsen, A.; Li, Z.-Y.; Zhang, H.; Xia, Y.; Li, X. Immuno gold nanocages with tailored optical properties for targeted photothermal destruction of cancer cells. *Nano Lett.* **2007**, *7*, 1318-1322.

Chen, W. J.; Tsai, P. J.; Chen, Y. C. Functional nanoparticle-based proteomic strategies for characterization of pathogenic bacteria. *Anal. Chem.* **2008**, *80*, 9612-9621.

Chen, Y.; Chen, H.; Zeng, D.; Tian, Y.; Chen, F.; Feng, J.; Shi, J. Core/Shell structured hollo mesoporous nanocapsules: A potential platform for simultaneous cell imaging and anticancer drug delivery. *ACS Nano* **2010**, *4*, 6001-6013.

Cheng, Y.; Liu, Y.; Huang, J.; Li, K.; Zhang, W.; Xian, Y.; Jin, L. Combining biofunctional magnetic nanoparticles and ATP bioluminescence for rapid detection of *Escherichia coli*. *Talanta* **2009**, *77*, 1332-1336.

Cheow, W. S.; Chang, M. W.; Hadinoto, K. Antibacterial efficacy of inhalable levofloxacin-loaded polymeric nanoparticles against *E. coli* biofilm cells: The effect of antibiotic release profile. *Pharm Res.* **2010**, *27*, 1597-1609.

Chunglok, W.; Wuragila, D. K.; Oaew, S.; Somasundrum, M.; Surareungchai, W. Immunoassay based on carbon nanotubes-enhanced ELISA for *Salmonella enterica* serovar *Typhimurium*. *Biosensors and Bioelectronics* **2011**, *26*, 3584-3589.

Churchill, R. L. T.; Lee, H.; Hall, J. C. Detection of *Listeria monocytogenes* and the toxin listeriolysin O in food. *J Microbiol Methods* **2006**, 64,141-170.

Cioffi, N.; Ditaranto, N.; Torsi, L.; Picca, R. A.; De Giglio, E.; Sabbatini, L.; Novello, L.; Tantillo, G.; Bleve-Zacheo, T.; Zambonin, P. G. Synthesis, analytical characterization and bioactivity of Ag and Cu nanoparticles embedded in poly-vinyl-methyl-ketone films. *Anal. Bioanal. Chem.* **2005**, *382*, 1912-1918.

Cioffi, N.; Torsi, L.; Ditaranto, N.; Sabbatini, L.; Zambonin, P. G.; Tantillo, G.; Ghibelli, L.; D'Alessio, M.; Bleve-Zacheo, T.; Traversa, E. Antifungal activity of polymer-based copper nanocomposite coatings. *Appl. Phys. Lett.* **2004**, *85*, 2417-2419.

Cioffi, N.; Torsi, L.; Ditaranto, N.; Tantillo, G.; Ghibelli, L.; Sabbatini, L.; Bleve-Zacheo, T.; D'Alessio, M.; Zambonin, P. G.; Traversa, E. Copper nanoparticle/polymer composites with antifungal and bacteriostatic properties. *Chem. Mater.* **2005b**, *17*, 5255-5262.

Cleveland, J.; Montville, T. J.; Nes, I. F.; Chikindas, M. L. Bacteriocins: safe, natural antimicrobials for food preservation. *Int. J. Food Microbiol.* **2001**, *71*, 1-20.

Coates, A.; Hu, Y.; Bax, R.; Page, C. The future challenges facing the development of new antimicrobial drugs. *Nature Reviews Drug Discovery* **2002**, *1*, 895-910.

Cobley, C. M.; Chen, J.; Cho, E. C.; Wang, L. V.; Xia, Y. Gold nanostructures: a class of multifunctional materials for biomedical applications. *Chem. Soc. Rev.* **2011**, *40*, 44-56.

Conde, J.; de la Fuente, J. M.; Baptista, P. V. RNA quantification using gold nanoprobes - application to cancer diagnostics. *J. Nanobiotechnol.* **2010**, *8*, 1-8.

Conte, M.; Aliberti, F.; Fucci, L.; Piscopo, M. Antimicrobial activity of various cationic molecules on foodborne pathogens. *World J. Microbiol. Biotechnol*. **2007**, *23*, 1679-1683.

Costerton, J. W.; Stewart, P. S.; Greenberg, E. P. Bacterial biofilms: A common cause of persistent infections. *Science* **1999**, *284*, 1318-1322.

Cotter, P. D.; Gahan, C. G. M.; Hill, C. Analysis of the role of the *Listeria monocytogenes* F_0 F_1 -ATPase operon in the acid tolerance response. *Int. J. Food. Microbiol*. **2000**, *60*, 137-146.

Cotter, P. D.; Hill, C.; Ross, R. P. Bacteriocins: developing innate immunity for food. *Nat. Rev. Microbiol.* **2005**, *3*, 777-788.

Cotter, P. D.; Ross, R. P.; Hill, C. Bacteriocins - a viable alternative to antibiotics?. *Nat. Rev. Microbiol.* **2013**, *11*, 95-105.

Craig, W. A. Basic pharmacodynamics of antibacterials with clinical applications to the use of beta-lactams, glycopeptides, and linezolid. *Infect. Dis. Clin.* **2003**, *17*, 479-501.

Craig, W. A. Pharmacokinetic/pharmacodynamic parameters: rationale for antibacterial dosing of mice and men. *Clin. Infect. Dis.* **1998**, *26*, 1-12.

Cui, Y.; Zhao, Y.; Tian, Y.; Zhang, W.; Lu, X.; Jiang, X. The molecular mechanism of action of bactericidal gold nanoparticles on *Escherichia coli*. *Biomaterials* **2012**, *33*, 2327-2333.

Daniel, M. C.; Astruc, D. Gold nanoparticles: assembly, supramolecular chemistry, quantum-size-related properties, and applications toward biology, catalysis, and nanotechnology. *Chem. Rev.* **2004**, *104*, 293-346.

Das, S.; Das, M. P.; Das, J. Fabrication of porous chitosan/silver nanocomposite film and its bactericidal efficacy against multi-drug resistant (MDR) clinical isolates. *Journal of Pharmacy Research* **2013**, *6*, 11-15.

Davies, D. Understanding biofilm resistance to antibacterial agents. *Nat. Rev. Drug Discov.* **2003**, *2*, 114-122.

De la Rica, R.; Baldi, A.; Fernandex-Sanchez, C.; Matsui, H. Single-cell pathogen detection with a reverse-phase immunoassay on impedimetric transducers. *Anal. Chem.* **2009**, *81*, 7732-7736.

De Liu, Z.; Chen, S. F.; Huang, C. Z.; Zhen, S. J.; Liao, Q. G. Light scattering sensing detection of pathogens based on the molecular recognition of immunoglobulin with cell wall-associated protein A. *Anal Chim Acta* **2007**, *2*, 279-286.

de Steenwinkel, J. E.; van Vianen, W.; Ten Kate, M. T.; Verbrugh, H. A.; van Agtmael, M. A.; Schiffelers, R. M.; Bakker-Woudenberg, I. A. Targeted drug delivery to enhance efficacy and shorten treatment duration in disseminated Mycobacterium avium infection in mice. *J Antimicrob Chemother* **2007**, *60*, 1064-1073.

De, M.; Ghosh, P. S.; Rotello, V. M. Applications of nanoparticles in biology. *Adv. Mater.* **2008**, *20*, 4225-4241.

DeBoer, E.; Beumer, R. R. Methodology for detection and typing of foodborne microorganisms. *Int. J. Food Microbiol.* **1999**, *50*, 119-130.

Deegan, L. H.; Cotter, P. D.; Hill, C.; Ross, P. Bacteriocins: Biological tools for bio-preservation and shelf-life extension. *Int. Dairy J.* **2006**, *16*, 1058-1071.

Deka, J.; Paul, A.; Chattopadhyay, A. Estimating conformation content of a protein using citrate-stabilized Au nanoparticles. *Nanoscale* **2010**, *2*, 1405-1412.

Deka, J.; Paul, A.; Chattopadhyay, A. Sensitive protein assay with distinction of conformations based on visible absorption changes of citrate-stabilized gold nanoparticles. *J. Phys. Chem. C.* **2009**, *113*, 6936-6947.

Deka, J.; Paul, A.; Ramesh. A.; Chattopadhyay, A. Probing Au nanoparticle uptake by enzyme following the digestion of a starch-Au-nanoparticle composite. *Langmuir*, **2008**, *24*, 9945-9951.

Delcour, A. H. Outer membrane permeability and antibiotic resistance. *Biochimica et Biophysica Acta* **2009**, *1794*, 808-816.

Dillen, K.; Vandervoort, J. Van den Mooter, G.; Ludwig, A. Evaluation of ciprofloxacin-loaded Eudragit RS100 or RL100/PLGA nanoparticles. *Int J Pharm* **2006**, *314*, 72-82.

Donlan, R. M.; Costerton, J. W. Biofilms: survival mechanisms of clinically relevant microorganisms. *Clin. Microbiol. Rev.* **2002**, *15*, 167-193.

Drbohlavova, J.; Chomoucka, J.; Adam, V.; Ryvolova, M.; Eckschlager, T.; Hubalek, J.; Kizek, R. Nanocarriers for anticancer drugs-new trends in nanomedicine. *Current Drug Metabolism* **2013**, *14*, 547-564.

Dreaden, E. C.; Alkilany, A. M.; Huang, X.; Murphy, C. J.; El-Sayed, M. A. The golden age: gold nanoparticles for biomedicine. *Chem. Soc. Rev.* **2012**, *41*, 2740-2779.

Dreaden, E. C.; Mwakwari, S. C.; Sodji, Q. H.; Oyelere, A. K.; El-Sayed, M. A. Tamoxifen-poly(ethylene glycol)-thiol gold nanoparticle conjugates: enhanced potency and selective delivery for breast cancer treatment. *Bioconjugate Chem.* **2009**, *20*, 2247-2253.

Drenkard, E.. Antimicrobial resistance of *Pseudomonas aeruginosa* biofilms. *Microbes Infect.* **2003**, *5*, 1213-1219.

Drider, D.; Fimland, G.; Hechard, Y.; McMullen, L. M.; Prevost, H. The continuing story of class IIa bacteriocins. *Microbiol. Mol. Biol. Rev.* **2006**, *70*, 564-582.

Du, W. L.; Niu, S. S.; Xu, Y. L.; Xu, Z. R.; Fan, C. L. Antibacterial activity of chitosan tripolyphosphate nanoparticles loaded with various metal ions. *Carbohydrate Polymers* **2009**, *75*, 385-389.

Dudak, F.C.; Boyaci, I. H. Multiplex detection of *E. coli* and *S. enteritidis* by using quantum dot-labelled antibodies. *J Rapid Methods Autom Microbiol* **2009**, *17*, 315-327.

Dutreux, N.; Notermans, S.; Gongora-Nieto, M. M.; Barbosa-Canovas, G. V.; Swanson, B. G. Effects of combined exposure of *Micrococcus luteus* to nisin and pulsed electric fields. *Int. J. Food Microbiol.* **2000**, *60*, 147-152.

Dutta, R. K.; Nenavathu, B. P.; Gangishetty, M. K.; Reddy, A.V.R. Studies on antibacterial activity of ZnO nanoparticles by ROS induced lipid Peroxidation. *Colloids and Surfaces B: Biointerfaces* **2012**, *94*, 143-150.

Dykman, L.; Khlebtsov, N. Gold nanoparticles in biomedical applications: recent advances and perspectives. *Chem. Soc. Rev*. **2012**, *41*, 2256-2282.

El-Boubbou, K.; Gruden, C.; Huang, X. Magnetic Glyco-nanoparticles: A unique tool for rapid pathogen detection, decontamination, and strain differentiation. *J. Am. Chem. Soc.* **2007**, *129*, 13392-13393.

Elghanian, R.; Storhoff, J. J.; Mucic, R. C.; Letsinger, R. L.; Mirkin, C. A. Selective colorimetric detection of polynucleotides based on the distance-dependent optical properties of gold nanoparticles. *Science* **1997**, *277*, 1078-1081.

Elkin, T.; Jiang, X.; Taylor, S.; Lin, Y.; Gu, L.; Yang, H.; Brown, J.; Collins, S.; Sun,Y. Immuno-carbon nanotubes and recognition of pathogens. *Chem BioChem* **2005**, *6*, 640-643.

El-Sayed, I. H.; Huang, X.; El-Sayed, M. A. Surface plasmon resonance scattering and absorption of Anti-EGFR antibody conjugated gold nanoparticles in cancer diagnostics: Applications in oral cancer. *Nano Lett.* **2005**, *5*, 829-834.

El-Sayed, M. A. Some interesting properties of metals confined in time and nanometer space of different shapes. *Acc. Chem. Res.* **2001**, *34*, 257-264.

Epand, R. F.; Pollard, J. E.; Wright, J. O.;. Savage, P. B.; Epand, R. M. Depolarization, bacterial membrane composition, and the antimicrobial action of ceragenins. *Antimicrobial Agents and Chemotherapy* **2010**, *54*, 3708-3713.

Faraday, M. The Bakerian lecture: Experimental relations of gold (and other metals) to light. *Phil. Trans. R. Soc.* **1857**, *147*, 145-181.

Fayaz A. M.; Balaji, K.; Girilal, M.; Yadav, R.; Kalaichelvan, P.T.; Venketesan, R. Biogenic synthesis of silver nanoparticles and their synergistic effect with antibiotics: a study against gram-positive and gram-negative bacteria. *Nanomedicine* **2010**, *6*, 103-109.

Feng, Q. L.; Wu, J.; Chen, G. Q.; Cui, F. Z.; Kim, T. N.; Kim, J. O. A mechanistic study of the antibacterial effect of silver ions on *Escherichia coli* and *Staphylococcus aureus*. *J. Biomed. Mater. Res.* **2000**, *52*, 662-668.

Fernández-Olmos, A.; García-Castillo, M.; Maiz, L.; Lamas, A.; Baquero, F.; Cantón, R. In vitro prevention of *Pseudomonas aeruginosa* early biofilm formation with antibiotics used in cystic fibrosis patients. *International Journal of Antimicrobial Agents* **2012**, *40*, 173-176.

Field, D.; Begley, M.; O'Connor, P. M.; Daly, K. M.; Hugenholtz, F.; Cotter, P. D.; Hill, C.; Ross, R. P. Bioengineered nisin A derivatives with enhanced activity against both gram-positive and gram-negative pathogens. *PLoS ONE* **2012**, *7*, 1-12.

Field, D.; Hill, C.; Cotter, P. D.; Ross, R. P. The dawning of a 'Golden era' in lantibiotic bioengineering. *Mol. Microbiol.* **2010**, *78*, 1077-1087.

Fischbach, M. A.; Walsh, C. T. Antibiotics for emerging pathogens. *Science* **2009**, *325*, 1089-1093.

Flemming, H. C.; Wingender, J. The biofilm matrix. *Nat. Rev. Microbiol.* **2010**, 8, 623-633.

Flynn, N. T.; Tran, T. N. T.; Cima, M. J.; Langer, R. Long-term stability of self-assembled monolayers in biological media. *Langmuir* **2003**, *19*, 10909-10915.

Foster, J. W. When protons attack: microbial strategies of acid adaptation. *Curr. Opin. Microbiol.* **1999**, *2*, 170-174.

Foster, J. W. *Escherichia coli* acid resistance: tales of an amateur acidophile. *Nat. Rev. Microbiol.* **2004**, *2*, 898-907.

Fournier-Wirth, C.; Coste, J. Nanotechnologies for pathogen detection: Future alternatives?. *Biologicals* **2010**, *38*, 9-13.

Fu, J.; Mao, P.; Han, J. Artificial molecular sieves and filters: a new paradigm for biomolecule separation. *Trends Biotechnol* **2008**, *26*, 311-320.

Furno, F.; Morley, K. S.; Wong, B.; Sharp, B. L.; Arnold, P. L.; Howdle, S. M.; Bayston, R.; Brown, P. D.; Winship, P. D.; Reid, H. J. Silver nanoparticles and polymeric medical devices: a new approach to prevention of infection?. *J. Antimicrob. Chemother.* **2004**, *54*, 1019-1024.

Fux, C. A.; Costerton, J. W.; Stewart, P. S.; Stoodley, P. Survival strategies of infectious biofilms. *Trends Microbiol.* **2005**, *13*, 34-40.

Gan, Q.; Wang, T. Chitosan nanoparticle as protein delivery carrier-systematic examination of fabrication conditions for efficient loading and release. *Colloids and Surfaces B: Biointerfaces* **2007**, *59*, 24-34.

García-Lara, J.; Masalha, M.; Foster, S. J. *Staphylococcus aureus*: the search for novel targets. *Drug Discovery Today* **2005**, *10*, 643-651.

Gelperina, S.; Kisich, K.; Iseman, M. D.; Heifets, L. The potential advantages of nanoparticle drug delivery systems in chemotherapy of tuberculosis. *Am J Respir Crit Care Med* **2005**, *172*, 1487-1490.

Geng, T.; Morgan, M. T.; Bhunia, A. K. Detection of low levels of *Listeria monocytogenes* cells by using a fiber-optic immunosensor. *Appl. Environ. Microbiol.* **2004**, *70*, 6138-6146.

Georganopoulou, D. G.; Chang, L.; Nam, J. M.; Thaxton, C. S.; Mufson, E. J.; Klein, W. L.; Markin, C. A. Nanoparticle based detection in cerebral spinal fluid of a soluble pathogenic biomarker for Alzheimer's disease. *PNAS* **2005**, *102*, 2273-2276.

George, M.; Abraham, T. M. Polyionic hydrocolloids for the intestinal delivery of protein drugs: alginate and chitosan - A review. *J. Control Release* **2006**, *114*, 1-14.

Giacomettia, A.; Cirioni, O.; Del Prete, M. S.; Paggi, A. M.; D'Errico, M. M.; Scalise, G. Combination studies between polycationic peptides and clinically used antibiotics against gram-positive and gram-negative bacteria. *Peptides* **2000**, *21*, 1155-1160.

Gogoi, S. K.; Gopinath, P.; Paul, A.; Ramesh, A.; Ghosh, S. S.; Chattopadhyay, A. Green fluorescent protein-expressing *Escherichia coli* as a model system for investigating the antimicrobial activities of silver nanoparticles. *Langmuir* **2006**, *22*, 9322-9328.

Goodman, C. M.; McCusker, C. D.; Yilmaz, T.; Rotello, V. M. Toxicity of gold nanoparticles functionalized with cationic and anionic side chains. *Bioconjugate Chem.* **2004**, *15*, 897-900.

Gootz, T. D. The global problem of antibiotic resistance. *Crit. Rev. Immun.* **2010**, *30*, 79-93.

Gordon, J.; Small, P. L. Acid resistance in enteric bacteria. *Infect. Immun.* **1993**, *61*, 364-367.

Green, G. C.; Chan, A. D. C.; Luo, B. S.; Dan, H.; Lin, M. Identification of *Listeria* species using a low-cost surface-enhanced raman scattering system with wavelet-based signal processing. *IEEE Trans Instrum Meas* **2009**, *58*, 3713-3722.

Gu, H.; Ho, P. L.; Tong, E.; Wang, L.; Xu, B. Presenting vancomycin on nanoparticles to enhance antimicrobial activities. *Nano Lett.* **2003**, *3*, 1261-1263.

Guo, R.; Zhang, L.; Qian, H.; Li, R.; Jiang, X.; Liu, B. Multifunctional nanocarriers for cell imaging, drug delivery, and near-IR photothermal therapy. *Langmuir* **2010**, *26*, 5428-5434.

Guo, S.; Huang, Y.; Jiang, Q.; Sun, Y.; Deng, L.; Liang, Z.; Du, Q.; Xing, J.; Zhao, Y.; Wang, P. C.; Dong, A.; Liang, X. J. Enhanced gene delivery and siRNA silencing by gold nanoparticles coated with charge-reversal polyelectrolyte. *ACS Nano* **2010b**, *4*, 5505-5511.

Gutsmannn, T.; Seydel, U. Impact of the glycostructure of amphiphilic membrane components on the function of the outer membrane of gram-negative bacteria as a matrix for incorporated channels and a target for antimicrobial peptides or proteins. *Eur. J. Cell Biol.* **2010**, *89*, 11-23.

Guven, B.; Basaran-Akgul, N.; Temur, E.; Tamer, U.; Boyaci, I. H. SERS-based sandwich immunoassay using antibody coated magnetic nanoparticles for *Escherichia coli* enumeration. *Analyst* **2011**,*136*, 740-748.

Gwynn, M. N.; Portnoy, A.; Rittenhouse, S. F.; Payne, D. J. Challenges of antibacterial discovery revisited. *Ann. N.Y. Acad. Sci.* **2010**, *1213*, 5-19.

Hahn, M.; Tabb, J.; Krauss, T. Detection of single bacterial pathogens with semiconductor quantum dots. *Anal Chem* **2005**, *15*, 4861-4869.

Halami, P. M.; Ramesh, A.; Chandrashekar, A. Fermenting cucumber, a potential source for the isolation of pediocin-like bacteriocin producers. *World J. Microbiol. Biotechnol.* **2005**, *21*, 1351-1358.

Hamm, S. C.; Shankaran, R.; Korampally, V.; Bok, S.; Praharaj, S.; Baker, G. A.; Robertson, J. D.; Lee, B. D.; Sengupta, S.; Gangopadhyay, K.; Gangopadhyay, S. Sputter-deposition of silver nanoparticles into ionic liquid as a sacrificial reservoir in antimicrobial organosilicate nanocomposite coatings. *Appl. Mater. Interfaces* **2012**, *4*, 178-184.

Hancock, R. E. W. The bacterial outer membrane as a drug barrier. *Trends Microbiol.* **1997**, *5*, 37-42.

Hancock, R. E.; Chapple, D. S. Peptide antibiotics. *Antimicrob. Agents Chemother*. **1999**, *43*, 1317-1323.

Hasper, H. E.; Kramer, N. E.; Smith, J. L.; Hillman, J. D.; Zachariah, C.; Kuipers, O. P.; de Kruijff, B.; Breukink, E. An alternative bactericidal mechanism of action for lantibiotic peptides that target lipid II. *Science* **2006**, *313*, 1636-1637.

Hassan, M. S.; Amna, T.; Yang, O. B.; El-Newehy, M. H.; Al-Deyab, S. S.; Khil, M. S. Smart copper oxide nanocrystals: Synthesis, characterization, electrochemical and potent antibacterial activity. *Colloids and Surfaces B: Biointerfaces* **2012**, *97*, 201-206.

Helander, I. M.; Latva-Kala, K.; Lounatmaa, K. Permeabilizing action of polyethyleneimine on *Salmonella typhimurium* involves disruption of the outer membrane and interactions with lipopolysaccharide. *Microbiology* **1998**, *144*, 385-390.

Helander, I. M.; Mattila-Sandholm, T. Fluorometric assessment of gram-negative bacterial permeabilization. *J. Appl. Microbiol.* **2000**, *88*, 213-219.

Heng, B. C.; Zhao, X.; Xiong, S.; Ng, K. W.; Boey, F. Y.-C.; Loo, J. S.-C. Toxicity of zinc oxide (ZnO) nanoparticles on human bronchial epithelial cells (BEAS-2B) is accentuated by oxidative stress. *Food and Chemical Toxicology* **2010**, *48*, 1762-1766.

Hetrick, E. M.; Shin, J. H.; Stasko, N. A.; Johnson, C. B.; Wespe, D. A.; Holmuhamedov, E.; Schoenfisch, M. H. Bactericidal efficacy of nitric oxide-releasing silica nanoparticles. *ACS Nano* **2008**, *2*, 235-246.

Hibi, K.; Abe, A.; Ohashi, E.; Mitsubayashi, K.; Ushio, H.; Hayashi, T.; Rena, H.; Endo, H. Combination of immunomagnetic separation with flow cytometry for detection of *Listeria monocytogenes*. *Anal Chim Acta* **2006**, *573*, 158-163.

Hochel, I.; Slavickova, D.; Viochna, D.; Skvor, J.; Steinhauserova, I. Detection of *Campylobacter* species in foods by indirect competitive ELISA using hen and rabbit antibodies. *Food Agric Immunol* **2007**, *18*, 151-167.

Hoefel, D.; Groobya, W. L.; Monisa, P. T.; Andrews, S.; Saint, C. P. A comparative study of carboxyfluorescein diacetate and carboxyfluorescein diacetate succinimidyl ester as indicators of bacterial activity. *J. Microbiol. Methods* **2003**, *52*, 379-388.

Hong, W.; Wu, Y. E.; Fu, X.; Chang, Z. Chaperone-dependent mechanisms for acid resistance in enteric bacteria. *Trends Microbiol.* **2012**, *20*, 328-335.

Hsu, S. T.; Breukink, E.; Tischenko, E.; Lutters, M. A.; de Kruijff, B.; Kaptein, R.; Bonvin, A.M.; van Nuland. N. A. The nisin-lipid II complex reveals a pyrophosphate cage that provides a blueprint for novel antibiotics. *Nat. Struct. Mol. Biol.* **2004**, *11*, 963-967.

Huang, X.; Jain, P. K.; El-Sayed, I. H.; El-Sayed, M. A. Gold nanoparticles: interesting optical properties and application in cancer diagnostic and therapy. *Nanomedicine* **2007**, *2*, 681-693.

Huang, X.; Kang, B.; Qian, W.; Mackey, M. A.; Chen, P. C.; Oyelere, A. K.; El-Sayed, I. H.; El-Sayed, M. A. Comparative study of photothermolysis of cancer cells with nuclear-targeted or cytoplasmtargeted gold nanospheres: continuous wave or pulsed lasers. *J. Biomed. Opt.* **2010**, *15*, 058002.

Huang, Z.; Zheng, X.; Yan, D.; Yin, G.; Liao, X.; Kang, Y.; Yao, Y.; Huang, D.; Hao, B. Toxicological effect of ZnO nanoparticles based on bacteria. *Langmuir* **2008**, *24*, 4140-4144.

Huh, A. J.; Kwon, Y. J. "Nanoantibiotics": A new paradigm for treating infectious diseases using nanomaterials in the antibiotics resistant era. *J. Control. Release* **2011**, *156*, 128-145.

Hurdle, J. G.; O'Neill, A. J.; Chopra, I.; Lee, R. E. Targeting bacterial membrane function: an underexploited mechanism for treating persistent infections. *Nat. Rev. Microbiol.* **2011**, *9*, 62-75.

Ip, M.; Lui, S. L.; Poon, V. K.; Lung, I.; Burd, A. Antimicrobial activities of silver dressings: an in vitro comparison. *J. Med. Microbiol.* **2006**, *55*, 59-63.

Iqbal, S. S.; Mayo, M. W.; Bruno, J. G.; Bronk, B. V.; Batt, C. A.; Chambers, J. P. A review of molecular recognition technologies for detection of biological threat agents. *Biosens Bioelectron* **2000**, *15*, 549-578.

Izano, E. A.; Sadovskaya, I.; Wang, H.; Vinogradov, E.; Ragunath, C.; Ramasubbu, N.;Jabbouri, S.; Perry, M. B.; Kaplan, J. B. Poly-N-acetylglucosamine mediates biofilm formation and detergent resistance in *Aggregatibacter actinomycetemcomitans*. *Microbial Pathogenesis* **2008**, *44*, 52-60.

Jacqueline, C.; Caillon, J.; Boutoille, D. Management of MRSA/GISA, VISA endocarditis. *Curr Infect Dis Rep.* **2013**, *15*, 329-334.

Jain, J.; Arora, S.; Rajwade, J. M.; Omray, P.; Khandelwal, S.; Paknikar, K. M. Silver nanoparticles in therapeutics: Development of an antimicrobial gel formulation for topical use. *Mol. Pharm.* **2009**, *6*, 1388-1401.

Jain, P. K.; El-Sayed, I. H.; El-Sayed, M. A. Au nanoparticles target cancer. *Nanotoday* **2007**, *2*, 18-29.

Jain, P. K.; Huang, X. H.; El-Sayed, I. H.; El-Sayed, M. A. Noble metals on the nanoscale: optical and photothermal properties and some applications in imaging, sensing, biology, and medicine. *Acc. Chem. Res.* **2008**, *41*, 1578-1586.

Jana, N. R.; Gearheart, L.; Murphy, C. J. Seed-mediated growth approach for shape-controlled synthesis of spheroidal and rod-like gold nanoparticles using a surfactant template. *Adv. Mater.* **2001**, *13*, 1389-1393.

Jeng, K.; Gaydos, C. A.; Blyn, L. B.; Yang, S.; Won, H.; Matthews, H.; Toleno, D.; Hsieh, Y.-H.; Carroll, K. C.; Hardick, J.; Masek, B.; Kecojevic, A.; Sampath, R.; Peterson, S.; Rothman, R. E. Comparative analysis of two broad-range PCR assays for pathogen detection in positive-blood-culture bottles: PCR-high-resolution melting analysis versus PCR-mass spectrometry. *J. Clin. Microbiol.* **2012**, *50*, 3287-3292.

Jo, S. C.; Rim, A. R.; Park, H. J.; Yuk, H. G.; Lee, S. C. Combined treatment with silver ions and organic acid enhances growth-inhibition of *Escherichia coli* O157:H7. *Food Control* **2007**, *18*, 1235-1240.

Joo, J.; Yim, C.; Kwon, D.; Lee, J.; Shin, H. H.; Cha H. J.; Jeon, S. A facile and sensitive detection of pathogenic bacteria using magnetic nanoparticles and optical nanocrystal probes. *Analyst* **2012**, *137*, 3609-3612.

Joshi, P.; Chakraborti, S.; Ramirez-Vick, J. E.; Ansari, Z. A.; Shanker, V.; Chakrabarti, P.; Singh, S. P. The anticancer activity of chloroquine-gold nanoparticles against MCF-7 breast cancer cells. *Colloids and Surfaces B: Biointerfaces* **2012**, *95*, 195-200.

Kaittanis, C.; Naser, S. A.; Perez, J. M. One-Step, Nanoparticle-mediated bacterial detection with magnetic relaxation. *Nano Lett.***2007**, *7*, 380-383.

Kaplan, C. W.; Sim, J. H.; Shah, K. R.; Kolesnikova-Kaplan, A.; Shi, W.; Eckert, R. Selective membrane disruption: Mode of action of C16G2, a specifically targeted antimicrobial peptide. *Antimicrobial Agents and Chemotherapy* **2011**, *55*, 3446-3452.

Karlsson, H. L.; Cronholm, P.; Gustafsson, J.; Möller, L. Copper oxide nanoparticles are highly toxic: A comparison between metal oxide nanoparticles and carbon nanotubes. *Chem. Res. Toxicol.* **2008**, *21*, 1726-1732.

Kaye, K. S.; Kaye, D. Multidrug-resistant pathogens: mechanisms of resistance and epidemiology. *Curr. Infect. Dis. Rep.* **2000**, *2*, 391-398.

Kell, A. J.; Stewart, G.; Ryan, S.; Peytavi, R.; Boissinot, M.; Huletsky, A.; Bergeron, M. G.; Simard, B. Vancomycin-modified nanoparticles for efficient targeting and preconcentration of gram-sositive and gram-negative bacteria. *ACS Nano* **2008**, *2*, 1777-1788.

Kelly, K.; Coronado, E.; Zhao, L.; Schatz, G. C. The optical properties of metal nanoparticles: the influence of size, shape, and dielectric environment. *J. Phys. Chem. B* **2003**, *107*, 668-677.

Keren, I.; Kaldalu, N.; Spoering, A.; Wang, Y.; Lewis, K. Persister cells and tolerance to antimicrobials. *FEMS Microbiol. Lett.* **2004**, *230*,13-18.

Khan, S. A.; Singh, A. K.; Senapati, D.; Fan, Z.; Ray, P. C. Targeted highly sensitive detection of multi-drug resistant *Salmonella* DT104 using AuNPs. *Chem Commun* **2011**, *33*, 9444-9446.

Kim, C. K.; Ghosh, P.; Pagliuca, C.; Zhu, Z. J.; Menichetti, S.; Rotello, V. M. Entrapment of hydrophobic drugs in nanoparticle monolayers with efficient release into cancer cells. *J. Am. Chem. Soc.* **2009**, *131*, 1360-1361.

Kim, H. J.; Jones, M. N. The delivery of benzyl penicillin to Staphylococcus aureus biofilms by use of liposomes. *J. Liposome Res.* **2004**, *14*, 123-139.

Kim, J.; Pitts, B.; Stewart, P. S.; Camper, A.; Yoon, J. Comparison of the antimicrobial effects of chlorine, silver ion, and tobramycin on biofilm. *Antimicrob. Agents Chemother.* **2008**, *52*, 1446-1453.

Kuo, W. S.; Chang, Y. T.; Cho, K. C.; Chiu, K. C.; Lien, C. H.; Yeh, C. S.; Chen, S. J. Gold nanomaterials conjugated with indocyanine green for dual-modality photodynamic and photothermal therapy. *Biomaterials* **2012**, *33*, 3270-3278.

Lal, S.; Clare, S. E.; Halas, N. J. Nanoshell-enabled photothermal cancer therapy: Impending clinical impact. *Acc. Chem. Res.* **2008**, *41*, 1842-1851.

Lam, C. W.; James, J. T.; McCluskey, R.; Hunter, R. L. Pulmonary toxicity of single-wall carbon nanotubes in mice 7 and 90 days after intratracheal instillation. *Toxicological Sciences* **2004**, *77*, 126-134.

Lamp, K.C.; Rybak, M. J.; Bailey, E. M.; Kaatz, G. W. In vitro pharmacodynamic effects of concentration, pH, and growth phase on serum bactericidal activities of daptomycin and vancomycin. *Antimicrob. Agents Chemother*. **1992**, *36*, 2709-2714.

Lara, H. H.; Nilda, V. A.; Turrent, L. C. I.; Padilla, C. R. Bactericidal effect of silver nanoparticles against multidrug-resistant bacteria. *World J Microbiol Biotechnol.* **2010**, *26*, 615-621.

Laurent, S.; Forge, D.; Port, M.; Roch, A.; Robic, C.; Elst, L. V.; Muller, R. N. Magnetic iron oxide nanoparticles: synthesis, stabilization, vectorization, physicochemical characterizations, and biological applications. *Chem. Rev.* **2008**, *108*, 2064-2110.

Lauri, A.; Mariani, P. O. Potentials and limitations of molecular diagnostic methods in food safety. *Genes Nutr.* **2009**, *4*, 1-12.

Laurino, P.; Kikkeri, R.; Azzouz, N.; Seeberger, P. H. Detection of bacteria using glyco-dendronized polylysine prepared by continuous flow photofunctionalization. *Nano Lett.* **2011**, *11*, 73-78.

le Blay, G.; Lacroix, C.; Zihler, A.; Fliss, I. In vitro inhibition activity of nisin A, nisin Z, pediocin PA-1 and antibiotics against common intestinal bacteria. *Lett. Appl. Microbiol.* **2007**, *45*, 252-257.

Lee, J.; Hasan, W.; Stender, C. L.; Odom, T. W. Pyramids: a platform for designing multifunctional plasmonic particles. *Acc. Chem. Res.* **2008**, *41*, 1762-1771.

Lee, S. Y.; Ahn, C. Y.; Lee, J.; Chang, J, H. Amino acid side chain-like surface modification on magnetic nanoparticles for highly efficient separation of mixed proteins. *Talanta* **2012b**, *93*, 160-165.

Lee, S. Y.; Ahn, C. Y.; Lee, J.; Lee, J. H.; Chang, J. H. Rapid and selective separation for mixed proteins with thiol functionalized magnetic nanoparticles. Nanoscale Research Letters **2012**, *7*, 279.

Lee, Y.K.; Ho, P.S.; Low, C.S.; Arvilommi, H.; Salminen, S. Permanent colonization by *Lactobacillus casei* is hindered by the low rate of cell division in mouse gut. *Applied and Environmental Microbiology* **2004**, *70*, 670-674.

Lellouche, J.; Friedman, A.; Lellouche, J. P.; Gedanken, A.; Banin, E. Improved antibacterial and antibiofilm activity of magnesium fluoride nanoparticles obtained by water-based ultrasound chemistry. *Nanomedicine: Nanotechnology, Biology, and Medicine* **2012**, *8*, 702-711.

Lellouche, J.; Kahana, E.; Elias, S.; Gedanken, A.; Banin, E. Antibiofilm activity of nanosized magnesium fluoride. *Biomaterials* **2009**, *30*, 5969-5978.

Lewin, M.; Carlesso, N.; Tung, C.; Tang, X.; Cory, D.; Scadden, D. T.; Weissleder, R. Tat peptide-derivatized magnetic nanoparticles allow in vivo tracking and recovery of progenitor cells. *Nat. Biotechnol.* **2000**, *18*, 410-414.

Li, J. J.; Hartono, D.; Ong, C. N.; Bay, B. H.; Yung, L. Y. L. Autophagy and oxidative stress associated with gold nanoparticles. *Biomaterials* **2010**, *31*, 5996-6003.

Li, M.; Zhu, L.; Lin, D. Toxicity of ZnO nanoparticles to *Escherichia coli*: Mechanism and the influence of medium components. *Environ. Sci. Technol.* **2011**, *45*, 1977-1983.

Li, Y.; Sun, L.; Jin, M.; Du, Z.; Liu, X.; Guo, C.; Li, Y.; Huang, P.; Sun, Z. Size-dependent cytotoxicity of amorphous silica nanoparticles in human hepatoma HepG2 cells. *Toxicology in Vitro* **2011**, *25*, 1343-1352.

Liandris, E.; Gazouli, M.; Andreadou, M.; Sechi, L. A.; Rosu, V.; Ikonomopoulos, J. Detection of pathogenic *Mycobacteria* based on functionalized quantum dots coupled with immunomagnetic separation. *PLoS ONE*, **2011**, *6*, 1-6.

Liau, S. Y.; Read, D. C.; Pugh, W. J.; Furr, J. R.; Russell, A. D. Interaction of silver nitrate with readily identifiable groups: relationship to the antibacterial action of silver ions. *Lett. Appl. Microbiol.* **1997**, *25*, 279-283.

Lin, Y.; Jiang, X.; Elkin, T.; Fernando, K.A.; Gu, L.; Taylor, S.; Yang, H.; Jones, E.; Wang, W.; Sun, Y.P. Carbon nanotubes for immunomagnetic separation of *Escherichia coli* O157: H7. *J. Nanosci. Nanotechnol.* **2006**, *6*, 868-871.

Lin, Y.-H.; Chen, S.-H.; Chuang, Y.-C.; Lu, Y.-C.; Shen, T. Y.; Chang, C. A.; Lin, C.-S. Disposable amperometric immunosensing strips fabricated by Au nanoparticles-modified screen-printed carbon electrodes for the detection of foodborne pathogen *Escherichia coli* O157:H7. *Biosensors and Bioelectronics* **2008**, *23*, 1832-1837.

Liong, M.; Lu, J.; Kovochich, M.; Xia, T.; Ruehm, S. G.; Nel, A.E.; Tamanoi, F.; Zink, J. I. Multifunctional inorganic nanoparticles for imaging, targeting, and drug delivery. *ACS Nano* **2008**, *2*, 889-896.

Liu, J. L.; Luo, Z., Bashir, S.; A progressive approach on inactivation of bacteria using silver-titania nanoparticles. *Biomater. Sci.* **2013**, *1*, 194-201.

Liu, J.; Liu, F.; Gao, K.; Wu. J.; Xue, D. Recent developments in the chemical synthesis of inorganic porous capsules. *J Mater Chem* **2009**, *19*, 6073-6084.

Liu, J.; Xia, H.; Xue, D.; Lu, L. Double-shelled nanocapsules of V_2O_5-based composite as high-performance anode and cathode materials for Li ion batteries. *J Am Chem Soc* **2009b**, *131*, 12086-12087.

Liu, W.; Hansen, J. N. Some chemical and physical properties of nisin, a small-protein antibiotic produced by *Lactococcus lactis*. *Appl. Environ. Microbiol.* **1990**, *56*, 2551-2558.

Liu, X.; Dai, Q.; Austin, L.; Coutts, J.; Knowles, G.; Zou, J.; Chen, H.; Huo, Q. A One-step homogeneous immunoassay for cancer biomarker detection using gold nanoparticle probes coupled with dynamic sight Scattering. *J. Am. Chem. Soc*. **2008**, *130*, 2780-2782.

Livermore, D. M. Discovery research: the scientific challenge of finding new antibiotics. *J. Antimicrob. Chemother.* **2011**, *66*, 1941-1944.

Livermore, D. M. The need for new antibiotics. *Clinical Microbiology and Infection* **2004**, *10*, 1-9.

Lofmark, S.; Jernberg, C.; Jansson, J. K.; Edlund, C. Clindamycin-induced enrichment and long-term persistence of resistant Bacteroides spp. and resistance genes. *J. Antimicrob. Chemother.* **2006**, *58*, 1160-1167.

Love, S. A.; Maurer-Jones, M. A.; Thompson, J. W.; Lin, Y.; Haynes, C. L. Assessing nanoparticle toxicity. *Annu. Rev. Anal. Chem.* **2012**, 5,181-205.

Lowery, C. A.; Park, J.; Gloeckner, C.; Meijler, M. M.;. Mueller, R. S.; Boshoff, H. I.; Ulrich, R. L.; Barry, C. E.; Bartlett, D. H.; Kravchenko, V. V.; Kaufmann, G. F.; Janda, K. D. Defining the mode of action of tetramic acid antibacterials derived from *Pseudomonas aeruginosa* quorum sensing signals. *J. Am. Chem. Soc.* **2009**, *131*, 14473-14479.

Lu, Q.; Lin, H.; Ge, S.; Luo, S.; Cai, Q.; Grimes, C. A. Wireless, remote-query, and high sensitivity *Escherichia coli* O157:H7 biosensor based on the recognition action of concanavalin A. *Anal. Chem.* **2009**, *81*, 5846-5850.

Lu, Z.; Li, C. M.; Bao, H.; Qiao, Y.; Toh, Y.; Yang, X. Mechanism of antimicrobial activity of CdTe quantum dots. *Langmuir* **2008**, *24*, 5445-5452.

Lubelski, J.; Rink, R.; Khusainov, R.; Moll, G. N.; Kuipers, O. P. Biosynthesis, immunity, regulation, mode of action and engineering of the model lantibiotic nisin. *Cell. Mol. Life Sci.* **2008**, *65*, 455-476.

Luo, Z.; Wua, Q.; Zhang, M.; Li, P.; Ding, Y. Cooperative antimicrobial activity of CdTe quantum dots with rocephin and fluorescence monitoring for *Escherichia coli*. *J. Colloid Interface Sci.* **2011**, *362*, 100-106.

Maalouf, R.; Fournier-Wirth, C.; Coste, J.; Chebib, H.; Sailkali, Y.; Vittori, O.; Errachid, A.; Jean-Pierre, C.; Claude, M.; Jaffrezic-Renault, N. Label-free detection of bacteria by electrochemical impedance spectroscopy: comparison to surface plasmon resonance. *Anal. Chem.* **2007**, *79*, 4879-4886.

Madhumathi, K.; Kumar, P. T. S.; Abilash, S.; Sreeja, V.; Tamura, H.; Manzoor, K.; Nair, S. V.; Jayakumar, R. Development of novel chitin/nanosilver composite scaffolds for wound dressing applications. *J Mater Sci Mater Med.* **2010,** *21*, 807-813.

Magliulo, M.; Simoni, P.; Guardigli, M.; Michelini, E.; Luciani, M.; Lelli, R.; Roda, A. A rapid multiplexed chemiluminescent immunoassay for the detection of *Escherichia coli* O157: H7, *Yersinia enterocolitica*, *Salmonella typhimurium*, and *Listeria monocytogenes* pathogen bacteria. *J Agric Food Chem* **2007**, *55*, 4933-4939.

Mah, T. F.; O'Toole, G. A,; Mechanisms of biofilm resistance to antimicrobial agents. *Trends Microbiol.* **2001**, *9*, 34-39.

Mahmoudi, M.; Serpooshan, V. Silver-coated engineered magnetic nanoparticles are promising for the success in the fight against antibacterial resistance threat. *ACS Nano* **2012**, *6*, 2656-2664.

Majumdar, S. S.; Padiglione, A. A. Nosocomial infections in the intensive care unit. *Anaesthesia & Intensive Care Medicine* **2012**, *13*, 204-208.

Mancini, N.; Carletti, S.; Ghidoli, N.; Cicehro, P.; Burioni, R.; Clementi, M. The era of molecular and other non-culture-based methods in diagnosis of sepsis. *Clin. Microbiol. Rev.* **2010**, *23*, 235-251.

Mangoni, M. L.; Papo, N.; Mignogna, G.; Andreu, D.; Shai, Y.; Barra, D.; Simmaco, M. Ranacyclins, a new family of short cyclic antimicrobial peptides: biological function, mode of action, and parameters involved in target specificity. *Biochemistry* **2003**, *42*, 14023-14035.

Mani-Lopez, E.; García, H. S.; Lopez-Malo, A. Organic acids as antimicrobials to control *Salmonella* in meat and poultry products. *Food Res. Int.* **2012**, *45*, 713-721.

Max, J.; Chapados, C. Infrared spectroscopy of aqueous carboxylic acids: comparison between different acids and their salts. *J. Phys. Chem. A* **2004**, *108*, 3324-3337.

Maxwell, D.; Taylor, M. J.; Nie, S. Self-assembled nanoparticle probes for recognition and detection of biomolecules. *J Am Chem Soc* **2002**, *124*, 9606-9612.

McAuliffe, O.; Ross, R. P.; Hill, C. Lantibiotics: structure, biosynthesis and mode of action. *FEMS Microbiol. Rev.* **2001**, *25*, 285-308.

Medintz, I. L.; Uyeda, H. T.; Goldman, E. R.; Matoussi, H. Quantum dot bioconjugates for imaging, labelling and sensing. *Nat Mater* **2005**, *4*, 435-446.

Meng, J. H.; Doyle, M. P. Introduction. Microbiological food safety. *Microb Infect* **2002**, *4*, 395-397.

Mercier, R.; Stumpo, C.; Rybak, M. J. Effect of growth phase and pH on the in vitro activity of a new glycopeptide, oritavancin (LY333328), against *Staphylococcus aureus* and *Enterococcus faecium*. *J. Antimicrob. Chemother.* **2002**, *50*, 19-22.

Merrell, D. S.; Camilli, A. Acid tolerance of gastrointestinal pathogens. *Curr. Opin. Microbiol.* **2002**, *5*, 51-55.

Michalet, X.; Pinaud, F. F.; Bentolila, L. A.; Tsay, J. M.; Doose, S.; Li, J. J. Quantum dots for live cells, in vivo imaging, and diagnostics. *Science* **2005**, *307*, 538-544.

Mie, G. Beitrage zer Optik truber Meiden speziell kolloidaler Metallosungen. Ann. Phys. **1908**, 25, 377-445.

Miranda, O. R.; Li, X.; Garcia-Gonzalez, L.; Zhu, Z. J.; Yan, B.; Bunz, U. H. F. Rotello, V. M. Colorimetric bacteria sensing using a supramolecular enzyme-nanoparticle biosensor. *J. Am. Chem. Soc.* **2011**, *133*, 9650-9653.

Moghimi, S. M.; Hunter, A. C.; Murray, J. C. Nanomedicine: current status and future prospects. *FASEB J.* **2005**, *19*, 311-330.

Morar, M.; Wright, G. D. The genomic enzymology of antibiotic resistance. *Ann. Rev. Genet*. **2010**, *44*, 25-51.

Mota-Meira, M.; Lapointe, G.; Lacroix, C.; Lavoie, M. C. MICs of mutacin B-Ny266, nisin A, vancomycin, and oxacillin against bacterial pathogens. *Antimicrob. Agents Chemother.* **2000**, *44*, 24-29.

Mothershed, E. A.; Whitney, A. M. Nucleic acid-based methods for the detection of bacterial pathogens: present and future considerations for the clinical laboratory. *Clinica. Chimica. Acta*. **2006**, *363*, 206-220.

Mueller, M.; de la Pena, A.; Derendorf, H. Issues in pharmacokinetics and pharmacodynamics of anti-infective agents: Kill curves versus MIC. *Antimicrob. Agents Chemother.* **2004**, *48*, 369-377.

Mukhopadhyay, B.; Martins, M. B.; Karamanska, R.; Russell, D. A.; Field, R. A. Bacterial detection using carbohydrate-functionalised CdS quantum dots: a model study exploiting *E. coli* recognition of mannosides. *Tetrahedron Lett.* **2009,** *50*, 886-889.

Murphy, C. J.; Gole, A. M.; Stone, J. W.; Sisco, P. N.; Alkilany, A. M.; Goldsmith, E. C.; Baxter, S. C. Gold nanoparticles in biology: beyond toxicity to cellular imaging. *Acc. Chem. Res.* **2008**, *41*, 1721-1730.

Musken, M.; Fiore, S. D.; Romling, U.; Haussler, S. A 96-well-plate–based optical method for the quantitative and qualitative evaluation of *Pseudomonas aeruginosa* biofilm formation and its application to susceptibility testing. *Nat. Protocols* **2010**, *5*, 1460-1469.

Nakamoto, K. Infrared and Raman spectra of inorganic and coordination compounds, 5th ed., John Wiley & Sons Inc., New York, 1997.

Nam, J. M.; Thaxton, C. S.; Mirkin, C. A. Nanoparticle-based Bio-Bar codes for the ultrasensitive detection of proteins. *Science* **2003**, *301*, 1884-1886.

Niemeyer, C. M. Nanoparticles, proteins, and nucleic acids: biotechnology meets materials science. *Angew. Chem., Int. Ed.* **2001**, *40*, 4128-4158.

Nikaido, H. Molecular basis of bacterial outer membrane permeability revisited. *Microbiol. Mol. Biol. Rev.* **2003**, *67*, 593-656.

Nikaido, H. Multidrug resistance in bacteria. *Annu. Rev. Biochem*. **2009**, *78*, 119-146.

Nikoobakht, B.; El-Sayed, M. A. Preparation and growth mechanism of gold nanorods (NRs) using seed-mediated growth method. *Chem. Mater*. **2003**, *15*, 1957-1962.

Norman, R. S.; Stone, J. W.; Gole, A.; Murphy, C. J.; Sabo-Attwood, T. L. Targeted photothermal lysis of the pathogenic bacteria, *Pseudomonas aeruginosa*, with gold nanorods. *Nano Lett.* **2008**, *8*, 302-306.

Nykanen, A.; Vesanen, S.; Kallio, H. Synergistic antimicrobial effect of nisin whey permeate and lactic acid on microbes isolated from fish. *Lett. Appl. Microbiol.* **1998**, *27*, 345-348.

Oldenburg, S. J.; Averitt, R. D.; Westcott, S. L.; Halas, N. J. Nanoengineering of optical resonances. *Chem. Phys. Lett.* **1998**, *288*, 243-247.

Paciotti, G. F.; Myer, L.; Weinreich, D.; Goia, D.; Pavel, N.; McLaughlin, R. E.; Tamarkin, L. Colloidal gold: a novel nanoparticle vector for tumor directed drug delivery. *Drug Deliv*. **2004**, *11*, 169-183.

Padil, V. V. T.; Černík, M. Green synthesis of copper oxide nanoparticles using gum karaya as a biotemplate and their antibacterial application. *International Journal of Nanomedicine* **2013**, *8*, 889-898.

Pal, S.; Tak, Y. K.; Song, J. M. Does the antibacterial activity of silver nanoparticles depend on the shape of the nanoparticle? A study of the gram-negative bacterium *Escherichia coli*. *Appl. Environ. Microbiol.* **2007**, *27*, 1712-1720.

Panacek, A.; Kvıtek, L.; Prucek, R.; Kolar, M.; Vecerova, R.; Pizurova, N.; Sharma, V. K.; Nevecna, T.; Zboril, R. Silver colloid nanoparticles: Synthesis, characterization, and their antibacterial activity. *J. Phys. Chem. B* **2006**, *110*, 16248-16253.

Panda, B. R.; Chattopadhyay, A. A water-soluble polythiophene–Au nanoparticle composite for pH sensing. *J. Colloid Interface Sci.* **2007**, *316*, 962-967;

Panda, B. R.; Singh, A. K.; Ramesh, A.; Chattopadhyay, A. Rapid estimation of bacteria by a fluorescent gold nanoparticle-polythiophene composite. *Langmuir* **2008**, *24*, 11995-12000.

Papadimitriou, K.; Pratsinis, H.; Nebe-von-Caron, G.; Kletsas, D.; Tsakalidou, E. Rapid assessment of the physiological status of *Streptococcus macedonicus* by flow cytometry and fluorescence probes. *Int. J. Food Mmicrobiol*. **2006**, *111*, 197-205.

Papagianni, M.; Anastasiadou, S. Pediocins: The bacteriocins of *Pediococci*. Sources, production, properties and applications. *Microbial Cell Factories* **2009**, *8*, 3.

Park, S.; Chibli, H.; Wong J.; Nadeau, J. L. Antimicrobial activity and cellular toxicity of nanoparticle-polymyxin B conjugates. *Nanotechnology* **2011**, *22*, 1-10.

Parsek, M. R.; Singh, P. K. Bacterial biofilms: an emerging link to disease pathogenesis. *Ann. Rev. Microbiol.* **2003**, *57*, 677-701.

Pera, N. P.; Kouki, A.; Haataja, S.; Branderhorst, H. M.; Liskamp, R. M. J.; Visser, G. M.; Finne, J.; Pieters, R. J. Detection of pathogenic *Streptococcus suis* bacteria using magnetic glycoparticles. *Org. Biomol. Chem.* **2010**, *8*, 2425-2429.

Phillips, R. L.; Miranda, O. R.; You, C. C.; Rotello, V. M.; Bunz, U. H. F. Rapid and efficient identification of bacteria using gold-nanoparticle-poly(para-phenyleneethynylene) constructs. *Angew. Chem. Int. Ed.* **2008**, *47*, 2590-2594.

Pinto, R. J. B.; Fernandes, S. C. M.; Freire, C. S. R.; Sadocco, P.; Causio, J.; Neto, C. P.; Trindade, T. Antibacterial activity of optically transparent nanocomposite films based on chitosan or its derivatives and silver nanoparticles. *Carbohydrate Research* **2012**, *348*, 77-83.

Piper, C.; Draper, L. A.; Cotter, P. D.; Ross, R. P.; Hill, C. A comparison of the activities of lacticin 3147 and nisin against drug-resistant *Staphylococcus aureus* and *Enterococcus* species. *J. Antimicrob. Chemother.* **2009**, *64*, 546-551.

Pissuwan, D.; Cortie, C. H.; Valenzuela, S. M.; Cortie, M. B. Functionalised gold nanoparticles for controlling pathogenic bacteria. *Trends Biotechnol.* **2009**, *28*, 207-213.

Pramanik, A.; Laha, D.; Bhattacharya, D.; Pramanik, P.; Karmakar, P. A novel study of antibacterial activity of copper iodide nanoparticle mediated by DNA and membrane damage. *Colloids and Surfaces B: Biointerfaces* **2012**, *96*, 50-55.

Preidis, G. A.; Hill, C.; Guerrant, R. L.; Ramakrishna, B.S.; Tannock, G. W.; Versalovic, J. Probiotics, enteric and diarrheal diseases, and global health. *Gastroenterology* **2011**, *140*, 8-14.

Premanathan, M.; Karthikeyan, K.; Jeyasubramanian, K.; Manivannan, G. Selective toxicity of ZnO nanoparticles toward Gram-positive bacteria and cancer cells by apoptosis through lipid peroxidation. *Nanomedicine: Nanotechnology, Biology, and Medicine* **2011**, *7*, 184-192.

Qi, L.; Xu, Z.; Jiang, X.; Hu, C.; Zou, X. Preparation and antibacterial activity of chitosan nanoparticles. *Carbohydr Res.* **2004**, *339*, 2693-2700.

Qiu, Y.; Liu, Y.; Wang, L.; Xu, L.; Bai, R.; Ji, Y.; Wu, X.; Zhao, Y.; Li, Y.; Chen, C. Surface chemistry and aspect ratio mediated cellular uptake of Au nanorods. *Biomaterials* **2010**, *31*, 7606-7619.

Rabea, E. I.; Badawy, M. E. T.; Stevens, C. V.; Smagghe, G.; Steurbaut, W. Chitosan as antimicrobial agent: applications and mode of action. *Biomacromolecules* **2003**, *4*, 1457-1465.

Raffi, M.; Mehrwan, S.; Bhatti, T. M.; Akhter, J. I.; Hameed, A.; Yawar, W.; Hasan, M. M. Investigations into the antibacterial behavior of copper nanoparticles against *Escherichia coli*. *Ann Microbiol* **2010**, *60*, 75-80.

Raghupathi, K. R.; Koodali, R. T.; Manna, A. C. Size-dependent bacterial growth inhibition and mechanism of antibacterial activity of zinc oxide nanoparticles. *Langmuir* **2011**, *27*, 4020-4028.

Ramos, J.; Rege, K. Transgene delivery using poly(amino ether)-gold nanorod assemblies. *Biotechnol. Bioeng.* **2012**, *109*, 1336-1346.

Ramstedt, M.; Cheng, N.; Azzaroni, O.; Mossialos, D.; Mathieu, H. J.; Huck, W. T. S. Synthesis and characterization of poly(3-sulfopropylmethacrylate) brushes for potential antibacterial applications. *Langmuir* **2007**, *23*, 3314-3321.

Rangnekar, A.; Sarma, T. K.; Singh, A. K.; Deka, J.; Ramesh, A.; Chattopadhyay, A. Retention of enzymatic activity of α-amylase in the reductive synthesis of gold nanoparticles. *Langmuir* **2007**, *23*, 5700-5706.

Rastogi, L.; Arunachalam, J. Synthesis and characterization of bovine serum albumin-copper nanocomposites for antibacterial applications. *Colloids and Surfaces B: Biointerfaces* **2013**,*108*, 134-141.

Ravindranath, S.P.; Mauer, L. J.; Deb-Roy, C.; Irudayaraj, J. Biofunctionalized magnetic nanoparticle integrated mid-infrared pathogen sensor for food matrixes. *Anal. Chem.* **2009**, *81*, 2840-2846.

Regmi, U.; Palma, M.; Barroso, C. G. Direct determination of organic acids in wine and wine-derived products by Fourier transform infrared (FT-IR) spectroscopy and chemometric techniques. *Anal. Chim. Acta*. **2012**, *732*, 137-144.

Rhim, J. W.; Hong, S.; Park, H. M.; Perry, K. W. N. Preparation and characterization of chitosan-based nanocomposite films with antimicrobial activity. *J. Agric. Food Chem.* **2006**, *54*, 5814-5822.

Richard, H.; Foster, J. W. *Escherichia coli* glutamate- and arginine- dependent acid resistance systems increase internal pH and reverse transmembrane potential. *J. Bacteriol.* 2004, 186, 6032-6041.

Risbud, M. V.; Hardikar, A. A.; Bhat, S. V.; Bhonde, R. R. pH-sensitive freeze-dried chitosan–polyvinyl pyrrolidone hydrogels as controlled release system for antibiotic delivery. *J. Control. Release* **2000**, *68*, 23-30.

Rodríguez, J. M.; Martínez, M. I.; Kok, J. Pediocin PA-1, a wide-spectrum bacteriocin from lactic acid bacteria. *Crit. Rev. Food Sci. Nutrition* **2002**, *42*, 91-121.

Roe, D.; Karandikar, B.; Bonn-Savage, N.; Gibbins, B.; Roullet, J. B. Antimicrobial surface functionalization of plastic catheters by silver nanoparticles. *Journal of Antimicrobial Chemotherapy* **2008**, *61*, 869-876.

Rogueda, P.G.A.; Traini, D. The nanoscale in pulmonary delivery. Part 1: deposition, fate, toxicology and effects. *Expert Opinion on Drug Delivery* **2007**, *4*, 595-606.

Rollema, H. S.; Kuipers, O. P.; Both, P.; de Vos, W. M.; Siezen, R. J. Improvement of solubility and stability of the antimicrobial peptide nisin by protein engineering. *Appl. Environ. Microbiol.* **1995**, *61*, 2873-2878.

Rosemary, M. J.; MacLaren, I.; Pradeep, T. Investigations of the antibacterial properties of Ciprofloxacin@SiO_2. *Langmuir* **2006**, *22*, 10125-10129.

Rosi, N. L.; Mirkin, C. A. Nanostructures in biodiagnostics. *Chem. Rev.* **2005**, *105*, 1547-1562.

Ruden, S.; Hilpert, K.; Berditsch, M.; Wadhwani, P.; Ulrich, A. S. Synergistic interaction between silver nanoparticles and membrane-permeabilizing antimicrobial peptides. *Antimicrob Agents Chemother.* **2009**, *53*, 3538-3540.

Russell, A. D.; Hugo, W. B. Antimicrobial activity and action of silver. *Prog. Med. Chem.* **1994**, *31*, 351-370.

Ryder, M. P.; Schilke, K. F.; Auxier, J. A.; McGuire, J.; Neff, J. A. Nisin adsorption to polyethylene oxide layers and its resistance to elution in the presence of fibrinogen. *J Colloid Interface Sci.* **2010**, *350*, 194-199.

Saha, B.; Das, S.; Saikia, J.; Das, G. Preferential and enhanced adsorption of different dyes on iron oxide nanoparticles: A comparative study. *J. Phys. Chem. C* **2011**, *115*, 8024-8033.

Saha, K.; Agasti, S. S.; Kim, C.; Li, X.; Rotello, V. M. Gold nanoparticles in chemical and biological sensing. *Chem. Rev.* **2012**, *112*, 2739-2779.

Saha, S.; Savage, P. B.; Bal, M. Enhancement of the efficacy of erythromycin in multiple antibiotic-resistant gram-negative bacterial pathogens. *J. Appl. Microbiol.* **2008**, *105*, 822-828.

Sanhai, W. R.; Sakamoto, J. H.; Canady, R.; Ferrari, M. Seven challenges for nanomedicine. *Nat. Nanotechnol.* **2008**, *3*, 242-244.

Sanpui, P.; Murugadoss, A.; Durga Prasad, P.V.; Ghosh, S. S; Chattopadhyay, A. The antibacterial properties of a novel chitosan-Ag-nanoparticle composite. *International Journal of Food Microbiology* **2008,** *124*, 142-146.

Sanvicens, N.; Pascual, N.; Fernández-Argüelles, M. T.; Adrián, J.; Costa-Fernández, J. M.; Sánchez-Baeza, F.; Sanz-Medel, A.; Marco, M. Quantum dot-based array for sensitive detection of *Escherichia coli*. *Anal Bioanal Chem* **2011**, *399*, 2755-2762.

Sarkar, S.; Jana, A. D.; Samanta, S. K.; Mostafa, G. Facile synthesis of silver nanoparticles with highly efficient anti-microbial property. *Polyhedron* **2007**, *26*, 4419-4426.

Schneid, A. D.; Ludtke, C. B.; Diel, C.; Aleixo. J. A. G. Production and characterization of monoclonal antibodies for the detection of *Salmonella enterica* in chicken meat. *Braz J Microbiol* **2005**, *36*, 163-169.

Schurek, K. N.; Sampaio, J. L. M.; Kiffer, C. R. V.; Sinto, S.; Mendes, C. M. F.; Hancock, R. E. W. Involvement of *pmrAB* and *phoPQ* in polymyxin B adaptation and inducible resistance in non-cystic fibrosis clinical isolates of *Pseudomonas aeruginosa*. *Antimicrob. Agents Chemother.* **2009**, *53*, 4345-4351.

Sebti, I.; Delves-Broughton, J.; Coma, V. Physicochemical properties and bioactivity of nisin-containing cross-linked hydroxypropylmethylcellulose films. *J. Agric. Food Chem.* **2003**, *51*, 6468-6474.

Seil, J. T.; Webster, T. J. Antibacterial effect of zinc oxide nanoparticles combined with ultrasound. *Nanotechnology* **2012**, *23*, 495101.

Sekirov, I.; Russell, S. L.; Antunes, L. C. M.; Finlay, B. B. Gut microbiota in health and disease. *Physiol. Rev.* **2010**, *90*, 859-904.

Severina, E.; Severin, A.; Tomasz, A. Antibacterial efficacy of nisin against multidrug-resistant gram-positive pathogens. *J. Antimicrob. Chemother.* **1998**, *41*, 341-347.

Shahverdi, A. R.; Fakhimi, A.; Shahverdi, H. R.; Minaian, S. Synthesis and effect of silver nanoparticles on the antibacterial activity of different antibiotics against *Staphylococcus aureus* and *Escherichia coli*. *Nanomed: Nanotechnol. Biol Med* **2007**, *3*,168-171.

Shen, Z.; Huang, M.; Xiao, C.; Zhang, Y.; Zeng, X.; Wang, P. G. Non-labeled QCM biosensor for bacterial detection using carbohydrate and lectin recognitions. *Anal. Chem.* **2007**, *79*, 2312-2319.

Shrivastava, S.; Bera, T.; Roy, A.; Singh, G.; Ramachandrarao, P.; Dash, D. Characterization of enhanced antibacterial effects of novel silver nanoparticles. *Nanotechnology* **2007**, *18*,1-9.

Sibley, C. D.; Peirano, G.; Church, D. L. Molecular methods for pathogen and microbial community detection and characterization: Current and potential application in diagnostic microbiology. *Infect. Genet. Evol.* **2012**, *12*, 505-521.

Silver, L. L. Challenges of antibacterial discovery. *Clin. Microbiol. Rev.* **2011**, *24*, 71-109.

Singh, A. K.; Mukherjee, S.; Adhikari, M. D.; Ramesh, A. Fluorescence-based comparative evaluation of bactericidal potency and food application potential of anti-listerial bacteriocin produced by lactic acid bacteria isolated from indigenous samples. *Prob. Antimicrob. Proteins* **2012**, *4*, 122-132.

Singh, A. K.; Senapati, D.; Wang, S.; Griffin, J.; Neely, A.; Candice, P.; Naylor, K. M.; Varisli, B.; Kalluri, J. R.; Ray, P. C. Gold nanorod based selective identification of *Escherichia coli* bacteria using Two-Photon Rayleigh Scattering spectroscopy. *ACS nano*, **2009**, *3*, 1906-1912.

Skrabalak, S. E.; Chen, J.; Sun, Y.; Lu, X.; Au, L.; Cobley C. M.; Xia, Y. Gold nanocages: synthesis, properties, and applications. *Acc. Chem. Res.* **2008**, *41*, 1587-1595.

Smetana, A. B.; Klabunde, K. J.; Marchin, G. R.; Sorensen, C. M. Biocidal activity of nanocrystalline silver powders and particles. *Langmuir* **2008**, *24*, 7457-7464.

Sobrino-Lopez, A.; Martin-Belloso, O. Use of nisin and other bacteriocins for preservation of dairy products. *Int. Dairy Journal* **2008**, *18*, 329-343.

Soenen, S. J.; Rivera-Gil, P.; Montenegro, J. M.; Parak, W. J.; Smedt, S. C. D.; Braeckmans, K. Cellular toxicity of inorganic nanoparticles: Common aspects and guidelines for improved nanotoxicity evaluation. *Nano Today* **2011**, *6*, 446-465.

Solve, M.; Boel, J.; Norrung, B. Evaluation of a monoclonal antibody able to detect live *Listeria monocytogenes* and *Listeria innocua*. *Int J Food Microbiol* **2000**, *57*, 219-24.

Sondi, I.; Salopek-Sondi, B. Silver nanoparticles as antimicrobial agent: a case study on *E. coli* as a model for Gram-negative bacteria. *J Colloid Interface Sci*. **2004**, *275*, 177-182.

Song, J. What's new on the antimicrobial horizon?. *Int. J. Antimicrob. Agents* **2008**, *32*, S207-S213.

Song, J.; Kang, H.; Lee, C.; Hwang, S. H.; Jang, J. Aqueous synthesis of silver nanoparticle embedded cationic polymer nanofibers and their antibacterial activity. *ACS Appl. Mater. Interfaces* **2012**, *4*, 460-465.

Song, J.; Kong, H.; Jang, J. Enhanced antibacterial performance of cationic polymer modified silica nanoparticles. *Chem. Commun.* **2009**, 5418-5420.

Sperling, R. A.; Gil, P. R.; Zhang, F.; Zanella, M.; Parak, W. J. Biological applications of gold nanoparticles. *Chem. Soc. Rev.* **2008**, *37*, 1896-1908.

Stephan, R.; Schumacher, S.; Zychowska, M. A. The VITR technology for rapid detection of *Listeria monocytogenes* and other *Listeria* spp. *Int. J. Food Microbiol.* **2003**, *89*, 287-290.

Stewart, P. S. Multicellular resistance: biofilms. *Trends Microbiol*. **2001**, *9*, 204.

Stewart, P. S.; McFeters, G. A.; Huang, C.T. Biofilm control by antimicrobial agents, **2000**, 373-405. In J. D. Bryers (ed.), Biofilms II: process analysis and applications. Wiley-Liss, Inc., New York, NY.

Stoimenov, P. K.; Klinger, R. L.; Marchin, G. L.; Klabunde, K. J. Metal oxide nanoparticles as bactericidal agents. *Langmuir* **2002**, *18*, 6679-6686.

Su, X. L.; Li, Y. Quantum dot biolabeling coupled with immunomagnetic separation for detection of *Escherichia coli* O157: H7. *Anal. Chem.* **2004**, *76*, 4806-4810.

Suginta, W.; Khunkaewla, P.; Schulte, A. Electrochemical biosensor applications of polysaccharides chitin and chitosan. *Chem. Rev.* **2013**, *113*, 5458-5479.

Sundaram, J.; Park, B.; Kwon, Y.; Lawrwnce, K. C. Surface enhanced Raman scattering (SERS) with biopolymer encapsulated silver nano substrates for rapid detection of foodborne pathogens. *Int. J. Food Microbiol.* 2013, doi: 10.1016/j.ijoodmicro.2013.05.013.

Sunwoo, H. H.; Wang, W. W.; Sim, J. S. Detection of *Escherichia coli* O157:H7 using chicken immunoglobulin Y. *Immunol Lett* **2006**, *106*, 191-193.

Swenson, C. E.; Stewart, K. A.; Hammett, J. L.; Fitzsimmons, W. E.; Ginsberg, R. S. Pharmacokinetics and in vivo activity of liposome-encapsulated gentamicin. *Antimicrob Agents Chemother* **1990**, *34*, 235-240.

Taglietti, A.; Fernandez,Y. A. D.; Amato, E.; Cucca, L.; Dacarro, G.; Grisoli, P.; Necchi, V.; Pallavicini, P.; Pasotti, L.; Patrini, M. Antibacterial activity of glutathione-coated silver nanoparticles against gram-positive and gram-negative bacteria. *Langmuir* **2012**, *28*, 8140-8148.

Tamplin, M. L. Inactivation of *Escherichia coli* O157:H7 in simulated human gastric fluid. *Appl. Environ. Microbiol.* **2005**, *71*, 320-325.

Templeton, A. C.; Wuelfing, W. P.; Murray, R. W. Monolayer-protected cluster molecules. *Acc. Chem. Res.* **2000**, *33*, 27-36.

Thill, A.; Liezeyons, O.; Spalla, O.; Chauvat, F.; Rose, J.; Auffan, M.; Flank, A. M Cytotoxicity of CeO_2 nanoparticles for *Escherichia coli*. Physico-chemical insight of the cytotoxicity mechanism. *Environ. Sci. Technol.* **2006**, *40*, 6151-6156.

Thomsen, J.; Friis, B. High dosage tobramycin treatment of children with cystic fibrosis. *Bacteriological effect and clinical ototoxicity* **1979**, *1*, 33-40.

Thomson, J. M.; Bonomo, R. A. The threat of antibiotic resistance in gram-negative pathogenic bacteria: β-lactams in peril!. *Curr. Opinion Microbiol*. **2005**, *8*, 518-524.

Tokarskyy, O.; Marshall, D. L. Immunosensors for rapid detection of *Escherichia coli* O157:H7 -Perspectives for use in the meat processing industry. *Food Microbiol.* **2008**, *25*, 1-12.

Tom, R. T.; Suryanarayanan, V.; Reddy,P. G.; Baskaran, S.; Pradeep, T. Ciprofloxacin-protected gold nanoparticles. *Langmuir* **2004**, *20*, 1909-1914.

Tong, S.; Ren, B.; Zheng, Z.; Shen, H.; Bao, G. Tiny grains give huge gains: nanocrystal-based signal amplification for biomolecule detection. *ACS Nano* **2013**, *7*, 5142-5150.

Torrent, M.; Navarro, S.; Moussaoui, M.; Nogues, M. V.; Boix, E. Eosinophil cationic protein high-affinity binding to bacteria-wall lipopolysaccharides and peptidoglycans. *Biochemistry* **2008**, *47*, 3544-3555.

Toze, S. PCR and the detection of microbial pathogens in water and wastewater. *Water Res* **1999**, *33*, 3545-3556.

Tré-Hardy, M.; Traore, H.; Manssouri, N. E.; Vanderbist, F.; Vaneechoutte, M.; Devleeschouwer, M. J. Evaluation of long-term co-administration of tobramycin and clarithromycin in a mature biofilm model of cystic fibrosis clinical isolates of *Pseudomonas aeruginosa*. *Int. J. Antimicrob. Agents* **2009**, *34*, 370-374.

Tsena, Y.; Chang, H.; Chen, C.; Chen, C.; Huang, C. Preparation of highly luminescent mannose-gold nanodots for detection and inhibition of growth of *Escherichia coli*. *Biosensors and Bioelectronics* **2011**, *27*, 95-100.

Tully, E.; Hearty, S.; Leonard, P.; O'Kennedy, R. The development of rapid fluorescence-based immunoassays, using quantum dot-labelled antibodies for the detection of *L. monocytogenes* cell surface proteins. *Int J Biol Macromol*. **2006**, *39*,127-134.

Tun, T. N.; Cameron, P. J.; Jenkins, A. T. A. Sensing of pathogenic bacteria based on their interaction with supported bilayer membranes studied by impedance spectroscopy and surface plasmon resonance. *Biosensors and Bioelectronics* **2011**, *28*, 227-231.

Turkevich, J.; Stevenson, P. C.; Hillier, J. A study of the nucleation and growth processes in the synthesis of colloidal gold. *Discussions of the Faraday Society* **1951**, *11*, 55-75.

Valdivieso-Garcia, A.; Desruisseau, A.; Riche, E.; Fukuda, S.; Tatsumi, H. Evaluation of a 24- hour bioluminescent enzyme immunoassay for the rapid detection of *Salmonella* in chicken carcass rinses. *J Food Prot* **2003**, *66*, 1996-2004.

Valodkar, M.; Rathore, P. S.; Jadeja, R. N.; Thounaojam, M.; Devkar, R. V.; Thakore, S. Cytotoxicity evaluation and antimicrobial studies of starch capped water soluble copper nanoparticles. *Journal of Hazardous Materials* **2012**, *201-202*, 244-249.

van Heusden, H. E.; de Kruijff, B.; Breukink, E. Lipid II Induces a transmembrane orientation of the pore-forming peptide lantibiotic nisin. *Biochemistry* **2002**, *41*, 12171-12178.

van Kraaij, C.; Breukink, E.; Noordermeer, M. A.; Demel, R. A.; Siezen, R. J.; Kuipers, O. P.; de Kruijff, B. Pore formation by nisin involves translocation of its C-terminal part across the membrane. *Biochemistry* **1998**, *37*, 16033-16040.

van Kraaij, C.; de Vos, W. M.; Siezen, R. J.; Kuipers, O.P. Lantibiotics: biosynthesis, mode of action and applications. *Nat. Prod. Rep.* **1999**, *16*, 575-587.

Varshney, M.; Yang, L. J.; Su, X. L.; Li, Y. B. Magnetic nanoparticle-antibody conjugates for the separation of *Escherichia coli* 0157: H7 in ground beef. *J. Food Prot.* **2005**, *68*, 1804-1811.

Velusamy, V.; Arshak, K.; Korostynska, O.; Oliwa, K.; Adley, C. An overview of foodborne pathogen detection: In the perspective of biosensors. *Biotechnol. Adv.* **2010**, *28*, 232-254.

Vidotti, M.; Carvalhal, R. F.; Mendes, R. K.; Ferreira, D. C. M.; Kubota, L. T. Biosensors based on gold nanostructures. *J Brazilian Chem Soc* **2011**, *1*, 3-20.

Vigderman, L., Zubarev, E. R. Therapeutic platforms based on gold nanoparticles and their covalent conjugates with drug molecules. *Adv. Drug Deliv. Rev.* **2013**, *65*, 663-667.

Vinayaka, A. C.; Thakur, M. S. Focus on quantum dots as potential fluorescent probes for monitoring food toxicants and food-borne pathogens. *Anal Bioanal Chem* **2010**, *4*, 1445-1455.

Virto, R.; Manas, P.; Alvarez, I.; Condon, S.; Raso, J. Membrane damage and microbial inactivation by chlorine in the absence and presence of a chlorine-demanding substrate. *Appl. Environ. Microbiol.* **2005**, *71*, 5022-5028.

Vooturi, S. K.; Cheung, C. M.; Rybak, M. J.; Firestine, S. M. Design, synthesis, and structure-activity relationships of benzophenone- based tetraamides as novel antibacterial agents. *J Med Chem.* **2009**, *52*, 5020-5031.

Vudumula, U.; Adhikari, M. D.; Ojha, B.; Goswami, S.; Das, G.; Ramesh, A. Tuning the bactericidal repertoire and potency of quinoline-based amphiphiles for enhanced killing of pathogenic bacteria. *RSC Advances* **2012**, *2*, 3864-3871.

Wan, Y.; Zhang, D.; Wang, Y.; Qi, P.; Wu, J.; Hou, B. Vancomycin-functionalised Ag@TiO2 phototoxicity for bacteria. *Journal of Hazardous Materials* **2011**, *186*, 306-312.

Wang, C.; Irudayaraj, J. Gold nanorod probes for the detection of multiple pathogens. *Small* **2008**, *4*, 2204-2208.

Wang, F.; Gao, F.; Lan, M.; Yuan, H.; Huang, Y.; Liu, J. Oxidative stress contributes to silica nanoparticle-induced cytotoxicity in human embryonic kidney cells. *Toxicology in Vitro* **2009**, *23*, 808-815.

Wang, J.; Gao, J.; Liu, D.; Han, D.; Wang, Z. Phenylboronic acid functionalized gold nanoparticles for highly sensitive detection of Staphylococcus aureus. *Nanoscale* **2012**, *4*, 451-454.

Wang, S.; Singh, A. K.; Senapati, D.; Neely, A.; Yu, H.; Ray, P. C. Rapid colorimetric identification and targeted photothermal lysis of *Salmonella* bacteria by using bioconjugated oval-shaped Au NPs. *Chem Eur J* **2010**, *19*, 5600-5606.

Wang, Z.; Miu, T.; Xu, H.; Duan, N.; Ding, X.; Li, S. Sensitive immunoassay of *Listeria monocytogenes* with highly fluorescent bioconjugated silica nanoparticles probe. *J Microbiol Methods* **2010**, *83*, 179-184.

Warheit, D. B.; Laurence, B. R.; Reed, K. L.; Roach, D. H.; Reynolds, G. A. M.; Webb, T. R. Comparative pulmonary toxicity assessment of single-wall carbon nanotubes in rats. *Toxicological Sciences* **2004**, *77*, 117-125.

Warren, B. R.; Parish, M. E.; Schneider, K. R. *Shigella* as a foodborne pathogen and current methods for detection in food. *Crit Rev Food Sci Nutr* **2006**, *46*, 551-567.

Weagant, S. D. A new chromogenic agar medium for detection of potentially virulent Yersinia enterocolitica. *J Microbiol Methods* **2008**, 72, 185-190.

Weidenmaier, C.; Peschel, A. Teichoic acids and related cell-wall glycopolymers in Gram-positive physiology and host interactions. *Nat. Rev. Microbiol.* **2008**, *6*, 276-287.

Wiedemann, I.; Breukink, E.; van Kraaij, C.; Kuipers, O. P.; Bierbaum, G.; de Kruijff, B.; Sahl. H. G. Specific binding of nisin to the peptidoglycan precursor lipid II combines pore formation and inhibition of cell wall biosynthesis for potent antibiotic activity. *J. Biol. Chem.* **2001**, *276*, 1772-1779.

Wiley, B. J.; Im, S. H.; Li, Z. Y.; McLellan, J.; Siekkinen, A. R.; Xia, Y. Maneuvering the surface plasmon resonance of silver nanostructures through shape-controlled synthesis. *J. Phys. Chem. B* **2006**, *110*, 15666-15675.

Willey, J. M.; van der Donk, W. A. Lantibiotics: peptides of diverse structure and function. *Annu. Rev. Microbiol.* **2007**, *61*, 477-501.

Willing, B. P.; Russell, S. L.; Finlay, B. B. Shifting the balance: antibiotic effects on host–microbiota mutualism. *Nature Rev. Microbiol.* **2011**, *9*, 233-243.

Wilson, R. The use of gold nanoparticles in diagnostics and detection. *Chem. Soc. Rev.* **2008**, *37*, 2028-2045.

Wilson, W. W.; Wade, M. M.; Holman, S. C.; Champlin, F. R. Status of methods for assessing bacterial cell surface charge properties based on zeta potential measurements. *J. Microbiol. Methods*. **2001**, *43*, 153-164.

Wise, R.; Piddock, L. The need for new antibiotics. *Lancet* **2010**, *375*, 638.

Wispelwey, B. Clinical implications of pharmacokinetics and pharmacodynamics of fluoroquinolones. *Clin. Infect. Dis.* **2005**, *41*, S127-S135.

Wright, G. D. Molecular mechanisms of antibiotic resistance. *Chem. Commun.* **2011**, *47*, 4055-4061.

Xia, F.; Zuo, X.; Yang, R.; Xiao, Y.; Kang, D.; Vallee-Belisle, A.; Gong, X.; Yuen, J. D.; Hsu, B. B. Y.; Heeger, A. J.; Plaxco, K. W. Colorimetric detection of DNA, small molecules, proteins, and ions using unmodified gold nanoparticles and conjugated polyelectrolytes. *Proc. Nat. Acad. Sci.* **2010**, *107*, 10837-10841.

Xia, T.; Kovochich, M.; Liong, M.; Mädler, L.; Gilbert, B.; Shi, H.; Yeh, J. I.; Zink, J. I.; Nel, A. E. Comparison of the mechanism of toxicity of zinc oxide and cerium oxide nanoparticles based on dissolution and oxidative stress properties. *ACS Nano* **2008**, *2*, 2121-2134.

Xia, Y.; Li, W.; Cobley, C. M.; Chen, J.; Xia, X.; Zhang, Q.; Yang, M.; Cho, E. C.; Brown, P. K. Gold nanocages: from synthesis to theranostic applications. *Acc. Chem. Res.* **2011**, *44*, 914-924.

Xie, Y.; He, Y.; Irwin, P. L.; Jin, T.; Shi, X. Antibacterial activity and mechanism of action of zinc oxide nanoparticles against *Campylobacter jejuni*. *Appl Environ Microbiol.* **2011**, *77*, 2325-2331.

Xing, K.; Chen, X. G.; Li, Y. Y.; Liu, C. S.; Liu, C. G.; Cha, D. S.; Park, H. J. Antibacterial activity of oleoyl-chitosan nanoparticles: A novel antibacterial dispersion system. *Carbohydrate Polymers* **2008**, *74*, 114-120.

Xing, K.; Chen, X. G.; Liu, C.S.; Cha, D.S.; Park, H. J. Oleoyl-chitosan nanoparticles inhibits *Escherichia coli* and *Staphylococcus aureus* by damaging the cell membrane and putative binding to extracellular or intracellular targets. *Int. J. Food Microbiol.* **2009**, *132*,127-133.

Xu, F.; Piett, C.; Farkas, S.; Qazzaz, M.; Syed, N. I. Silver nanoparticles (AgNPs) cause degeneration of cytoskeleton and disrupt synaptic machinery of cultured cortical neurons. *Molecular Brain* **2013**, *6*, 1-15.

Xu, X.; Chen, Y.; Wei, H.; Xia, B.; Liu, F.; Li, N. Counting bacteria using functionalized gold nanoparticles as the light-scattering reporter. *Anal. Chem.* **2012**, *84*, 9721-9728.

Xue, X.; Pan, J.; Xie, H.; Wang, J.; Zhang, S. Fluorescence detection of total count of *Escherichia coli* and *Staphylococcus aureus* on water-soluble CdSe quantum dots coupled with bacteria. *Talanta* **2009**, *77*, 1808-1813.

Yamanaka, M.; Hara, K.; Kudo, J. Bactericidal actions of a silver ion solution on *Escherichia coli*, studied by energy-filtering transmission electron microscopy and proteomic analysis. *Appl Environ Microbiol.* **2005**, *71*, 7589-7593.

Yang, G. J.; Huang, J. L.; Meng, W. J.; Shen, M.; Jiao, X. A. A reusable capacitive immunosensor for detection of *Salmonella* spp. based on grafted ethylene diamine and self-assembled gold nanoparticle monolayers. *Analytica Chimica Acta* **2009**, *647*,159-166.

Yang, H.; Liu, C.; Yang, D.; Zhang, H.; Xi, Z. Comparative study of cytotoxicity, oxidative stress and genotoxicity induced by four typical nanomaterials: the role of particle size, shape and composition. *J. Appl. Toxicol.* **2009**, *29*, 69-78.

Yang, H.; Qu, L.; Wimbrow, A. N.; Jiang, X.; Sun, Y. Rapid detection of *Listeria monocytogenes* by nanoparticle-based immunomagnetic separation and real-time PCR. *Int. J. Food Microbiol.* **2007**, *118*, 132-138.

Yang, L.; Li, Y. Simultaneous detection of *E. coli* O157:H7 and *S. Typhimurium* using quantum dots as fluorescence labels. *Analyst* **2006**, *3*, 394-401.

Yang, R.; Johnson, M. C.; Ray, B. Novel method to extract large amounts of bacteriocins from lactic acid bacteria. *Appl. Environ. Microbiol.* **1992**, *58*, 3355-3359.

Yeaman, M. R.; Yount, N. Y. Mechanisms of antimicrobial peptide action and resistance. *Pharmacol. Rev.* **2003**, *55*, 27-55.

Yoshida, T.; Nagasawa, T. ε-Poly-L-lysine: microbial production, biodegradation and application potential. *Appl. Microbiol. Biotechnol.* **2003**, *62*, 21-26.

Yu, K. Y.; Noh, Y.; Chung, M. S.; Park, H. J.; Lee, N.; Youn, M.; Jung, B. Y.; Youn, B. Use of monoclonal antibodies that recognize p60 for identification of *Listeria monocytogenes. Clin Diagn Lab Immunol* **2004b**, *11*, 446-451.

Yu, Y. Y.; Chang, S. S.; Lee, C. L.; Wang, C. R. C. Gold nanorods: Electrochemical synthesis and optical properties. *J. Phys. Chem. B* **1997**, *101*, 6661-6664.

Zasloff, M. Antimicrobial peptides of multicellular organisms. *Nature* **2002**, *415*, 389-395.

Zavascki, A. P.; Goldani, L. Z.; Li, J.; Nation, R. L. Polymyxin B for the treatment of multidrug-resistant pathogens: a critical review. *J. Antimicrob. Chemother.* **2007**, *60*, 1206-1215.

Zelada-Guillén, G. A.; Riu, J.; Düzgün, A.; Rius, F. X. Immediate detection of living bacteria at ultralow concentrations using a carbon nanotube based potentiometric aptasensor. *Angew. Chem. Int. Ed.* **2009**, *48*, 7334 -7337.

Zelada-Guillén, G. A.; Sebastián-Avila, J. L.; Blondeau, P.; Riu, J.; Rius, F. X. Label-free detection of *Staphylococcus aureus* in skin using real-time potentiometric biosensors based on carbon nanotubes and aptamers. *Biosensors and Bioelectronics* **2012**, *31*, 226-232.

Zendo, T.; Yoneyama, F.; Sonomoto, K. Lactococcal membrane-permeabilizing antimicrobial peptides. *Appl. Microbiol. Biotechnol*. **2010**, *88*, 1-9.

Zhang, J.; Langille, M. R.; Personick, M. L.; Zhang, K.; Li, S.; and Mirkin C. A. Concave cubic gold nanocrystals with high-index facets. *J. Am. Chem. Soc.* **2010**, *132*, 14012-14014.

Zhang, J.; Sun, J.; Liu, Y.; Li, J.; Su, Y.; Xia, W.; Yang, Y. Separation and purification of phosvitin phosphopeptides using immobilized metal affinity nanoparticles. *Journal of Chromatography B* **2012**, *893-894*, 121-126.

Zhang, L.; Dhillon, P.; Yan, H.; Farmer, S.; Hancock, R. E. W. Interactions of bacterial cationic peptide antibiotics with outer and cytoplasmic membranes of *Pseudomonas aeruginosa*. *Antimicrob. Agents Chemother.* **2000**, *44*, 3317-3321.

Zhang, L.; Gu, F. X.; Chan, J. M.; Wang, A. S.; Langer, R. S.; Farokhzad, O. C. Nanoparticles in medicine: Therapeutic applications and developments. *Clin Pharmacol Ther.* **2008**, *83*, 761-769.

Zhang, L.; Pornpattananangkul, D.; Hu, C. M.; Huang, C. M. Development of nanoparticles for antimicrobial drug delivery. *Curr. Med. Chem.* **2010**, *17*, 585-584.

Zhang, N.; Liu, Y.; Tong, L. L.; Xu, K.; Zhuo, L.; Tang, B. A novel assembly of AuNPs-β-CDs-FL for the fluorescent probing of cholesterol and its application in blood serum. *Analyst* **2008**,*133*, 1176-1181.

Zhang, W.; Li, Y.; Niu, J.; Chen, Y. Photogeneration of reactive oxygen species on uncoated silver, gold, nickel, and silicon nanoparticles and their antibacterial effects. *Langmuir* **2013**, *29*, 4647-4651.

Zhang, X.; Chibli, H.; Mielke, R.; Nadeau, J. Ultrasmall gold-doxorubicin conjugates rapidly kill apoptosis-resistant cancer cells. *Bioconjugate Chem.* **2011**, *22*, 235-243.

Zhang, Y. S.; Wang, Y.; Wang, L.; Wang, Y.; Cai, X.; Zhang, C.; Wang, L. V.; Xia, Y. Labeling human mesenchymal stem cells with gold nanocages for in vitro and in vivo tracking by two-photon microscopy and photoacoustic microscopy. *Theranostics* **2013**, *3*, 532-543.

Zhao, W.; Brook, M. A.; Li, Y. Design of gold nanoparticle-based colorimetric biosensing assays. *ChemBioChem* **2008**, *9*, 2363-2371.

Zhao, Y.; Ye, M.; Chao, Q.; Jia, N.; Ge, Y.; Shen, H. Simultaneous detection of multi food-borne pathogenic bacteria based on functionalized quantum dots coupled with immunomagnetic separation in food samples. *J Agric Food Chem* **2009**, *2*, 517-524.

Zhao, Z. J.; Liu, X. M. Preparation of monoclonal antibody and development of enzyme linked immunosorbent assay specific for *Escherichia coli* O157 in foods. *Biomed Environ Sci.* **2005**, *18*, 254-259.

APPENDIX

APPENDIX

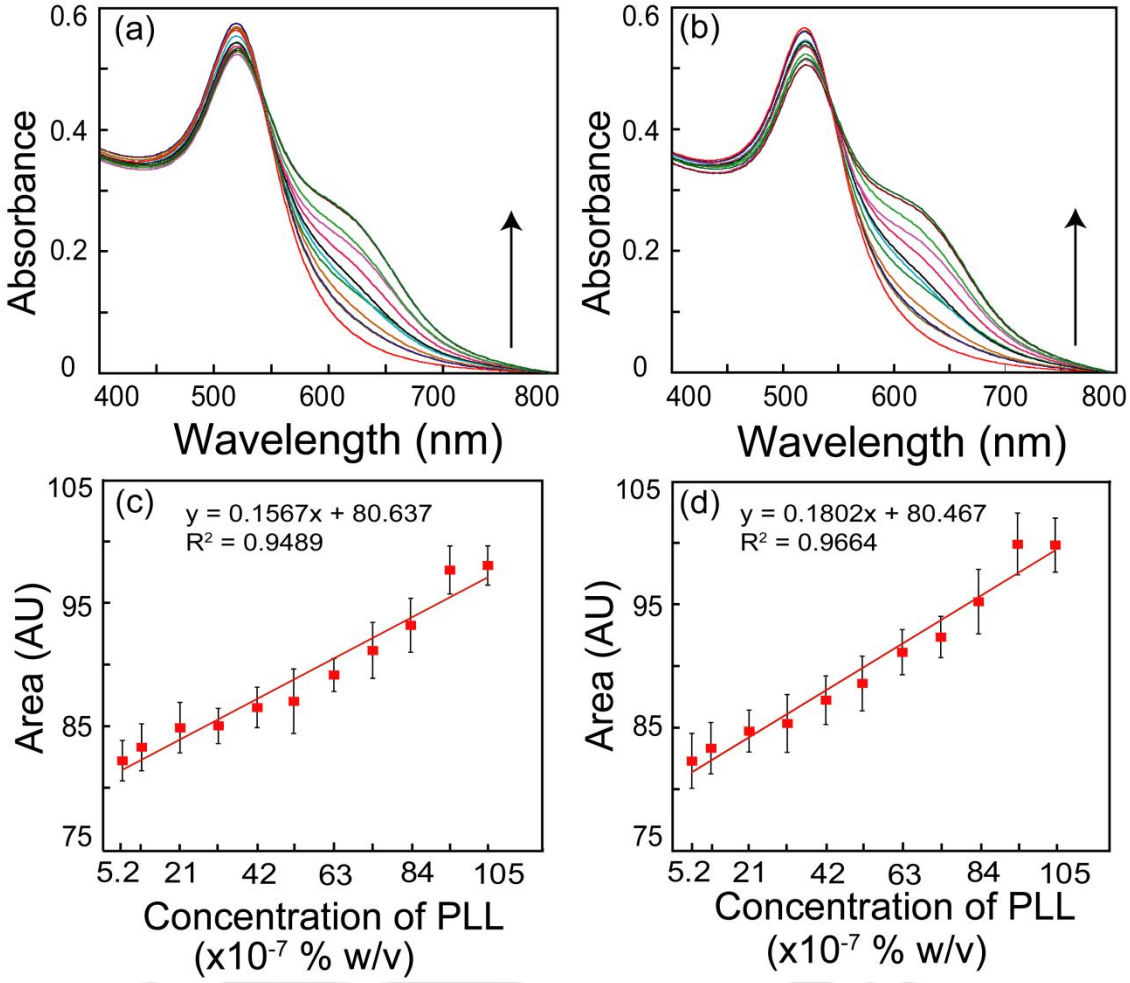

Figure A2.1. UV-visible extinction spectrum of citrate-stabilized AuNPs with increasing concentrations of PLL (5.2 x 10^{-7}, 10.5 x 10^{-7}, 21 x 10^{-7}, 31.5 x 10^{-7}, 42 x 10^{-7}, 52 x 10^{-7}, 63 x 10^{-7}, 73.6 x 10^{-7}, 84 x 10^{-7}, 95 x 10^{-7} and 105 x 10^{-7} % w/v). Measurements were taken after **(a)** 15 min and **(b)** 60 min of addition of PLL, respectively. The lowest trace is the control sample consisting of AuNP alone (volume adjusted). The subsequent traces were obtained with increasing concentration of PLL as indicated by arrow. The corresponding areas under the curve versus PLL concentrations are indicated in **(c)** and **(d)**, respectively.

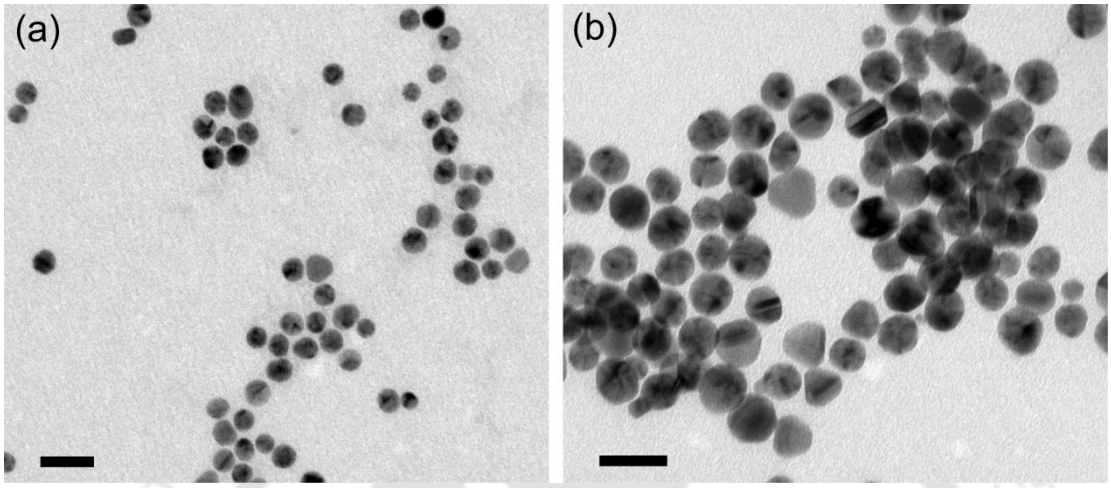

Figure A2.2. TEM images of AuNPs in the presence of **(a)** 21 x 10^{-7} % w/v PLL and **(b)** 42 x 10^{-7} % w/v of PLL. Scale bar for the samples is 20 nm.

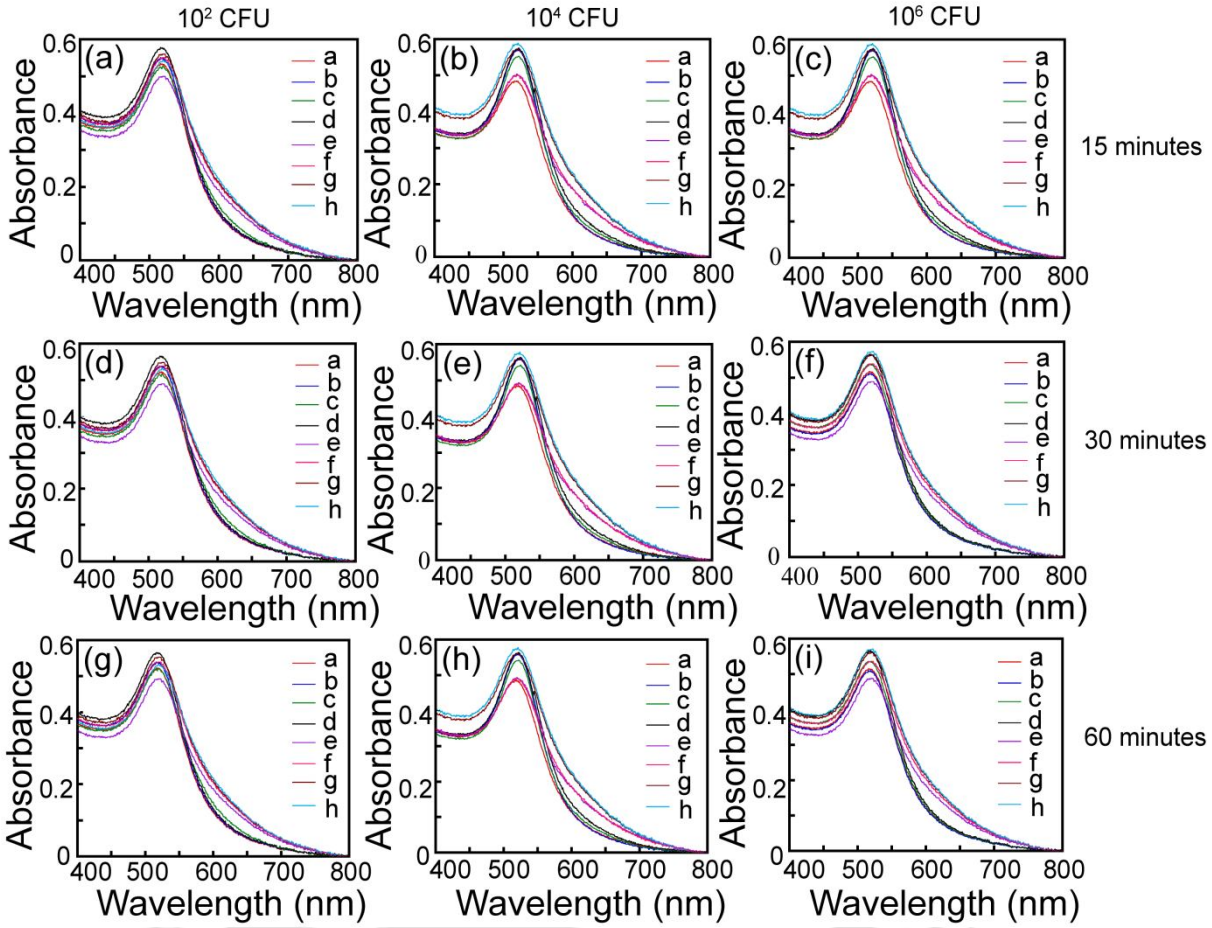

Figure A2.3. UV-visible extinction spectrum of AuNP obtained after interaction with unbound PLL. Initially varying cell numbers of *E. coli* MTCC 433 were interacted for 15, 30 and 60 minutes with various concentrations of PLL (traces b-h correspond to 0.25 x 10^{-5}, 0.5 x 10^{-5}, 1.0 x 10^{-5}, 3.0 x 10^{-5}, 3.5 x 10^{-5}, 4.0 x 10^{-5} and 5.0 x 10^{-5} % w/v PLL). The control sample is represented by trace a (Au NP alone).

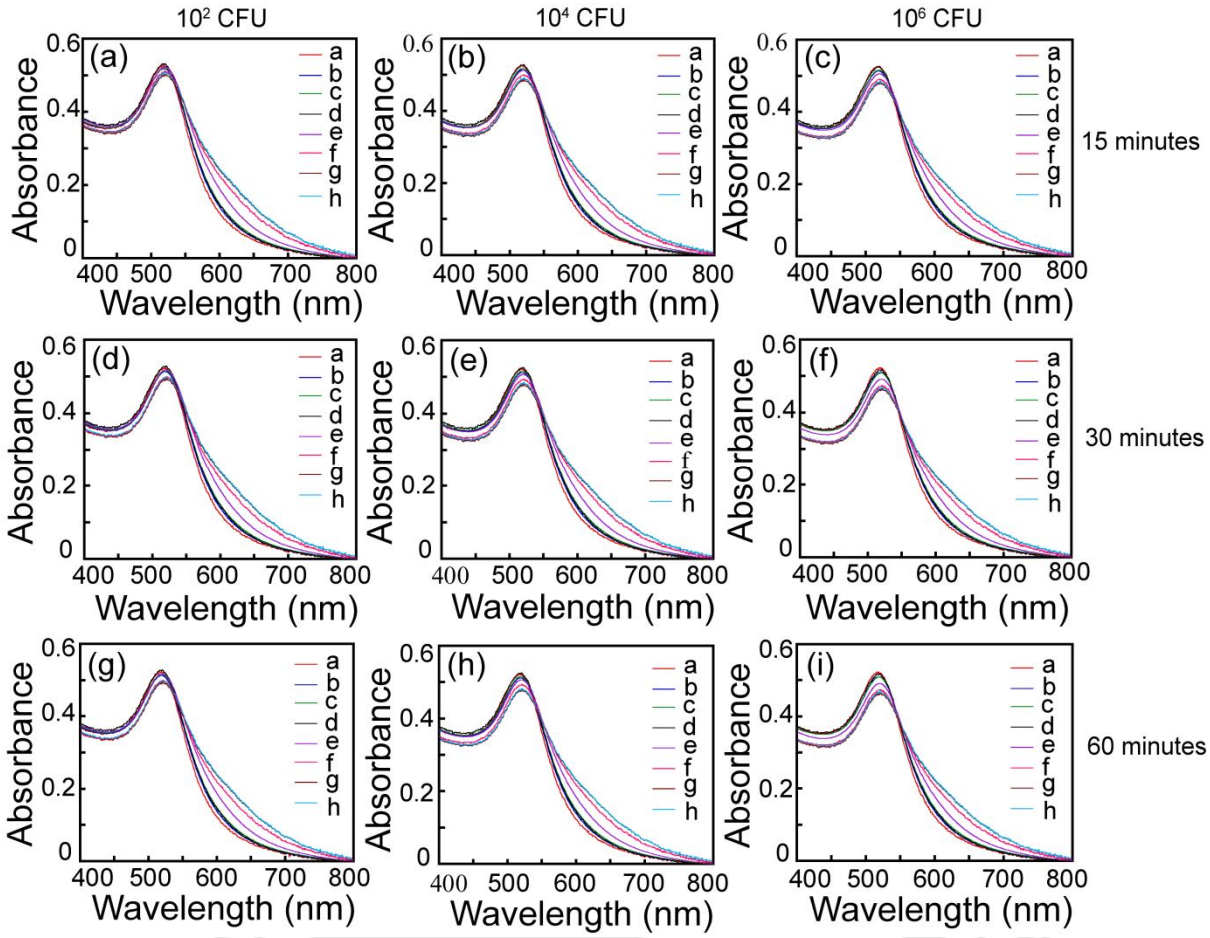

Figure A2.4. UV-visible extinction spectrum of AuNP obtained after interaction with unbound PLL. Initially varying cell numbers of *L. monocytogenes* Scott A were interacted for 15, 30 and 60 minutes with various concentrations of PLL (traces b-h correspond to 0.25 x 10^{-5}, 0.5 x 10^{-5}, 1.0 x 10^{-5}, 3.0 x 10^{-5}, 3.5 x 10^{-5}, 4.0 x 10^{-5} and 5.0 x 10^{-5} % w/v PLL). The control sample is represented by trace a (Au NP alone).

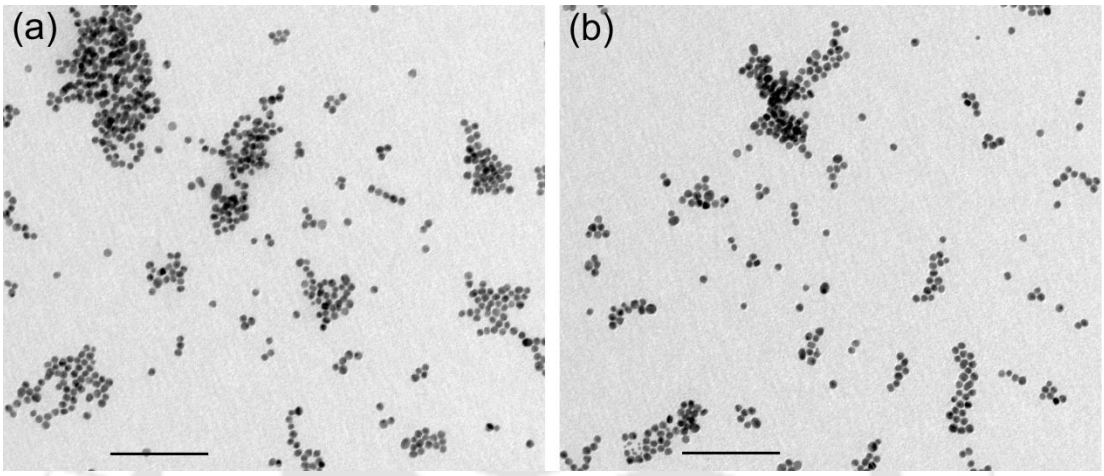

Figure A2.5. TEM images of aggregates of AuNP obtained with unbound PLL following interaction of 3.5 x 10^{-5} % w/v PLL with **(a)** 10^2 CFU and **(b)** 10^4 CFU of *E. coli* MTCC 433. Scale bar is 50 nm for the samples.

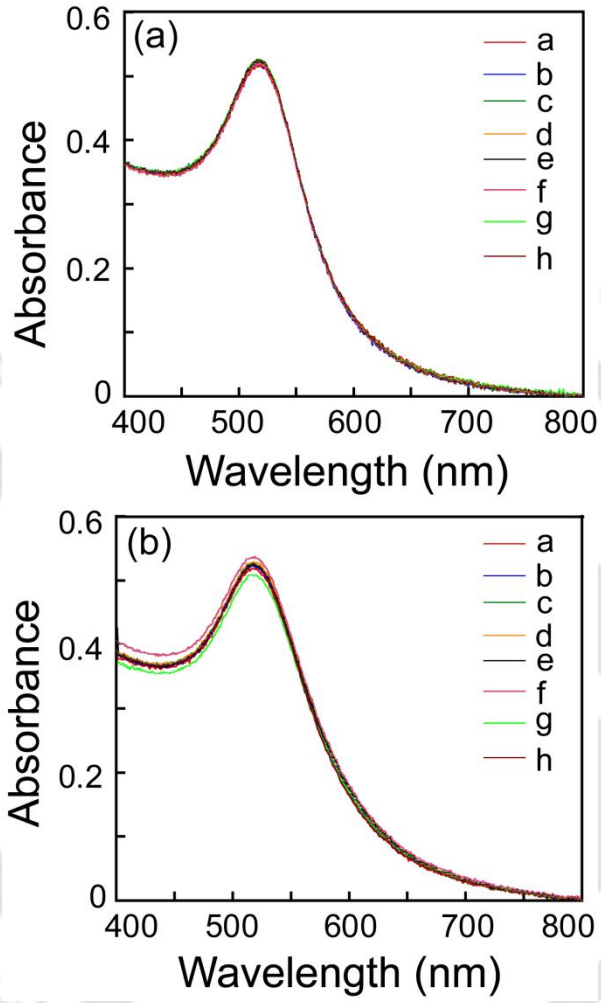

Figure A2.6. UV-visible extinction spectrum of AuNP interacted with cell bound PLL. **(a)** *E. coli* MTCC 433, **(b)** *L. monocytogenes* Scott A. Traces a-g correspond to 0.25 x 10^{-5}, 0.5 x 10^{-5}, 1.0 x 10^{-5}, 3.0 x 10^{-5}, 3.5 x 10^{-5}, 4.0 x 10^{-5} and 5.0 x 10^{-5} % w/v PLL, Trace h: Au NP alone (volume adjusted).

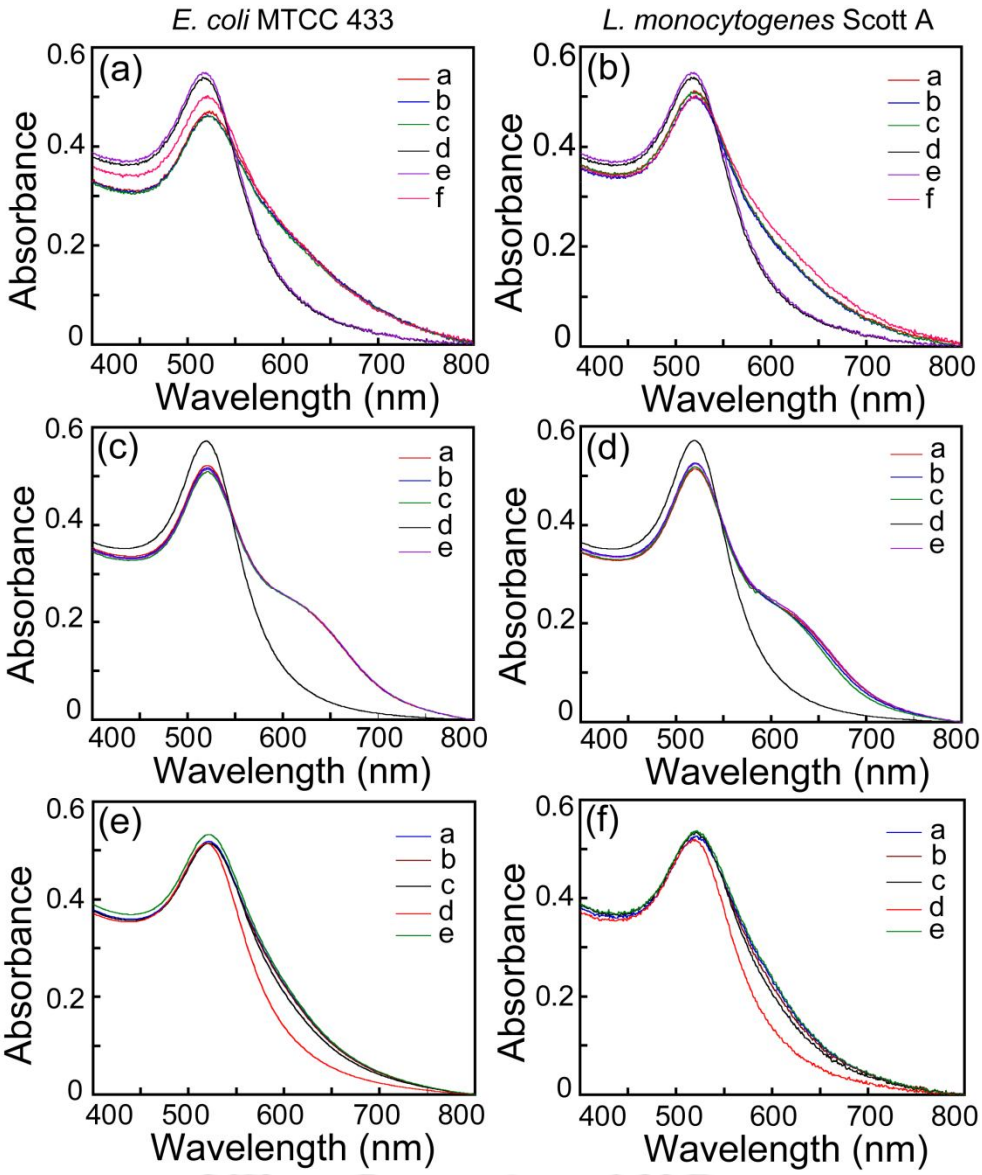

Figure A2.7. UV-visible extinction spectrum for control experiments. **(a-b)** Experiment I, **(c-d)** Experiment II and **(e-f)** Experiment III. For experiment I: traces a-c correspond to 10^2, 10^4 and 10^6 CFU, respectively; trace d: AuNP alone (volume adjusted), trace e: 10^6 CFU bacteria interacted with Au NP alone, trace f: AuNP interacted with 3.5 x 10^{-5} % w/v PLL. For experiment II and III: traces a-c correspond to 10^2, 10^4 and 10^6 CFU, respectively; trace d: Au NP alone (volume adjusted) and trace e: AuNP interacted with 3.5 x 10^{-5} % w/v PLL.

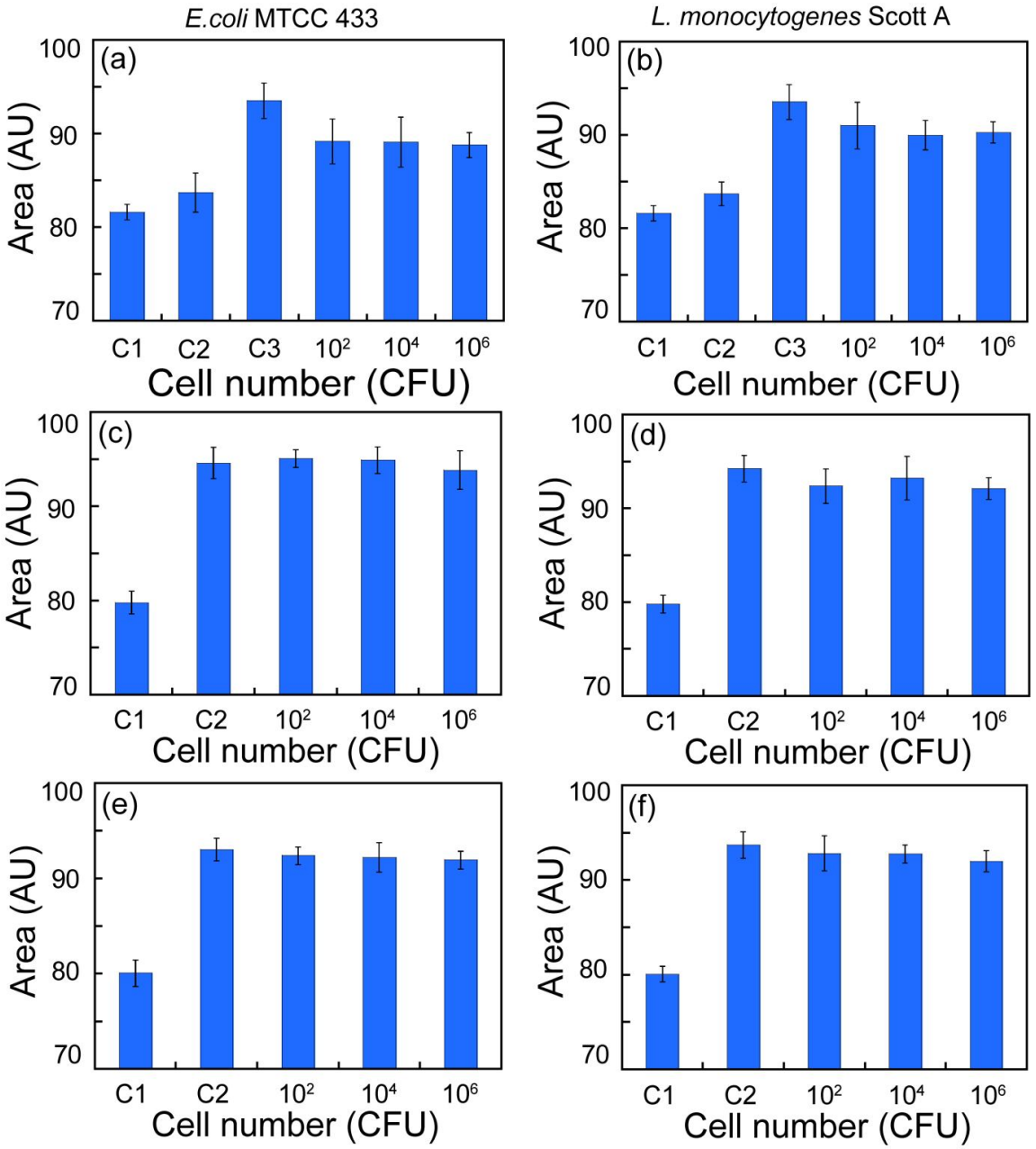

Figure A2.8. Area under UV-visible extinction spectrum obtained for various control experiments. **(a-b)** Experiment I, **(c-d)** Experiment II and **(e-f)** Experiment III. For **(a-b)**, C1: Au NP alone (volume adjusted) C2: 10^6 CFU bacteria (in 0.4 mL) interacted with 1.5 mL AuNP and C3: AuNP interacted with 3.5 x 10^{-5} % w/v PLL. For **(c-f)**, C1: AuNP alone (volume adjusted) and C2: AuNP interacted with 3.5 x 10^{-5} % w/v PLL.

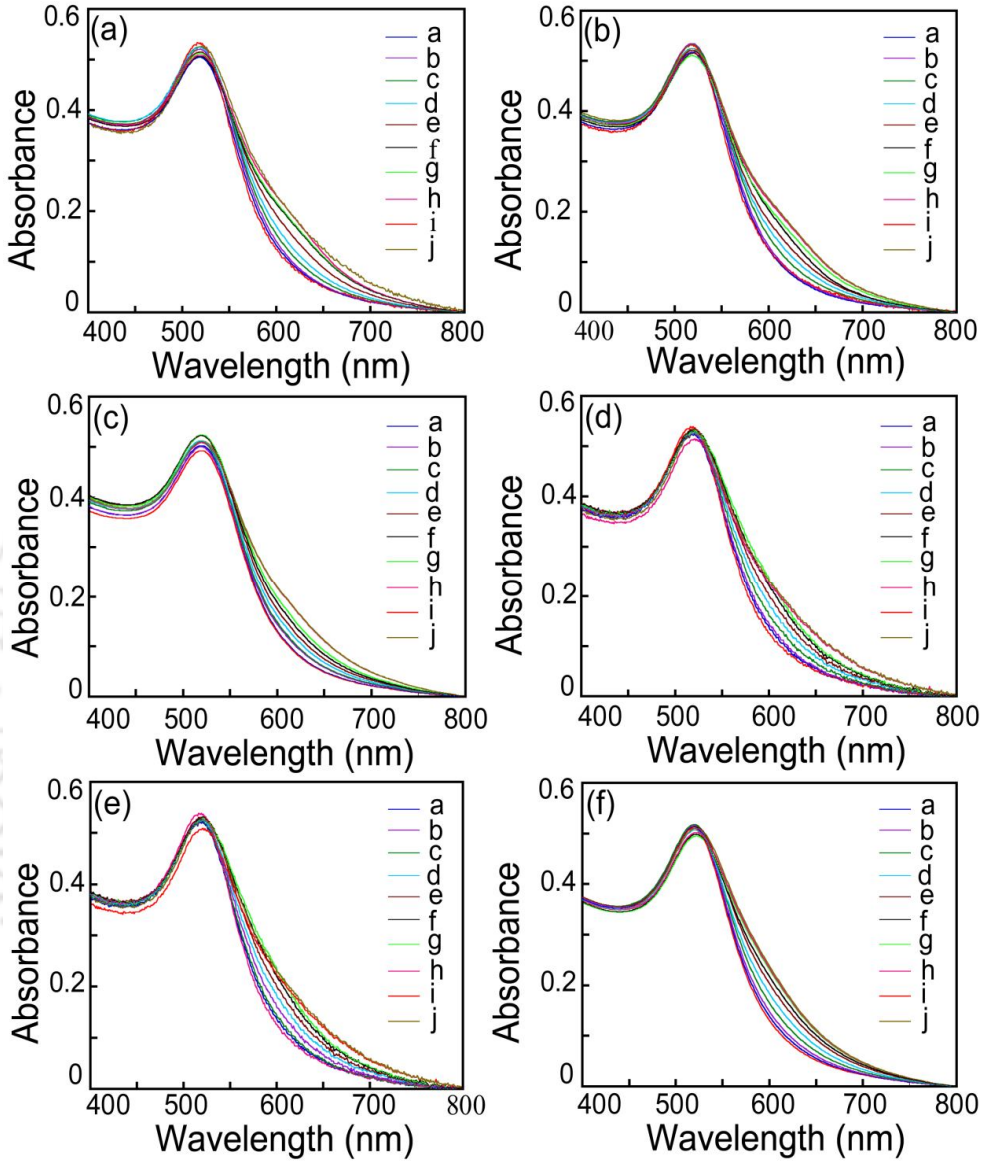

Figure A2.9. UV-visible extinction spectrum for estimation of bacterial cell numbers by AuNP aggregation. **(a)** *Escherichia coli* MTCC 433, **(b)** *Listeria monocytogenes* Scott A, **(c)** *Bacillus subtilis* MTCC 1305, **(d)** *Pseudomonas aeruginosa* MTCC 2488, **(e)** *Staphylococcus aureus* MTCC 740 and **(f)** *Enterobacter aerogenes* MTCC 2822. Traces a-h correspond to decreasing cell numbers (10^7 – 1.0 CFU), trace i: AuNP alone (volume adjusted) and trace j: Au NP interacted with 3.5 x 10^{-5} % w/v PLL.

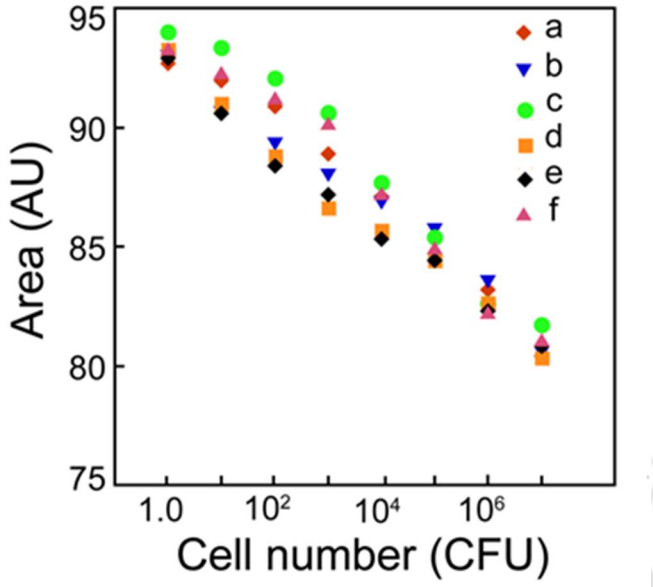

Figure A2.10. Area under UV-visible extinction spectrum as a function of bacterial cell numbers. (a) *Escherichia coli* MTCC 433, (b) *Listeria monocytogenes* Scott A, (c) *Staphylococcus aureus* MTCC 740, (d) *Enterobacter aerogenes* MTCC 2822, (e) *Bacillus subtilis* MTCC 1305 and (f) *Pseudomonas aeruginosa* MTCC 2488. The area represents mean value of three independent measurements.

Table A2.1 Measurement of area under UV-visible extinction spectrum as a function of bacterial cell numbers

Bacterial strains	**[$] Equation for area under UV-vis extinction spectrum (AU) versus cell number (CFU)**
Escherichia coli MTCC 433	$y = -1.762x + 95.50$ ($R^2 = 0.976$)
Pseudomonas aeruginosa MTCC 2488	$y = -1.873x + 96.24$ ($R^2 = 0.970$)
Enterobacter aerogenes MTCC 2822	$y = -1.746x + 94.46$ ($R^2 = 0.987$)
Listeria monocytogenes Scott A	$y = -1.598x + 94.38$ ($R^2 = 0.976$)
Bacillus subtilis MTCC 1305	$y = -1.665x + 93.98$ ($R^2 = 0.990$)
Staphylococcus aureus MTCC 740	$y = -1.936x + 97.14$ ($R^2 = 0.972$)

[$] Equations are for the plots indicated in **Figure A2.10**.

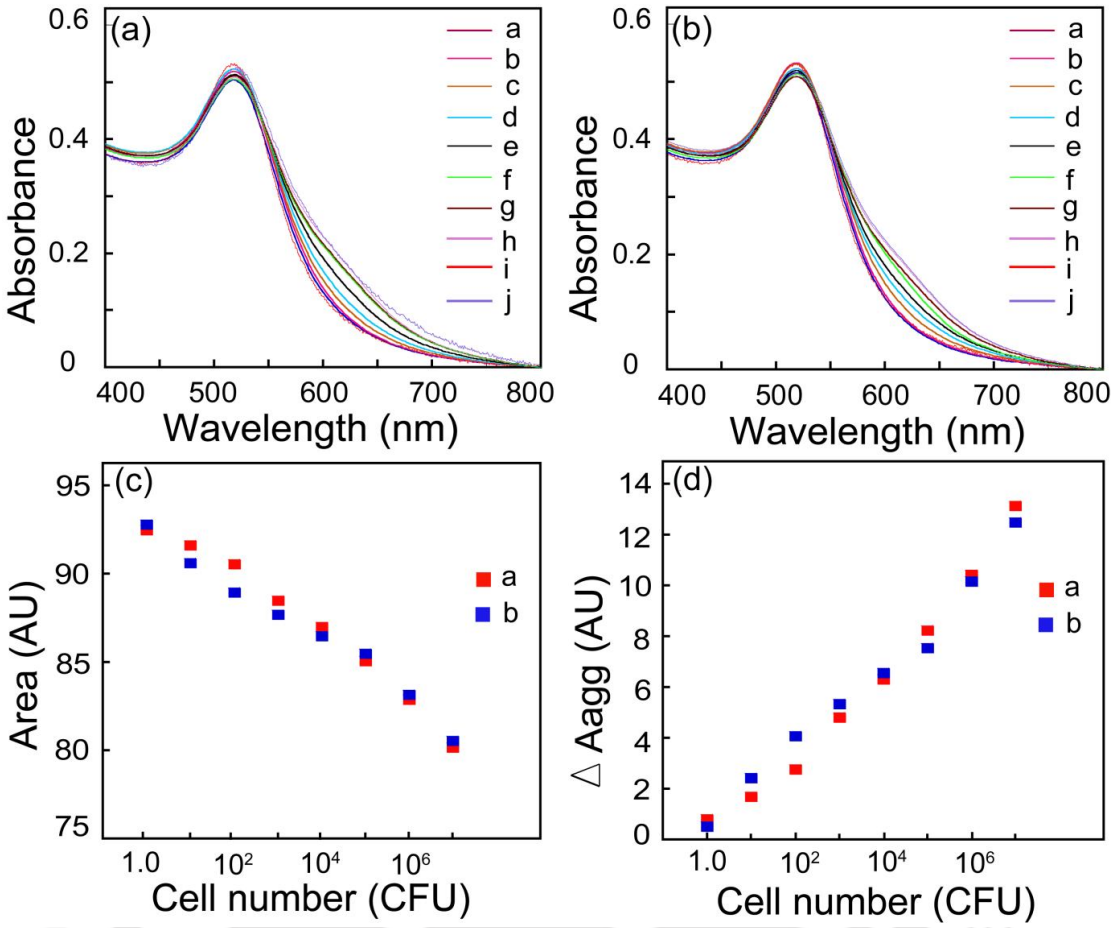

Figure A2.11. UV-visible extinction spectrum for AuNP incubated with unbound PLL following separation of bacterial cells by centrifugal filter device (Costar Spin-X centrifuge tube filter). Varying cell numbers of **(a)** *Escherichia coli* MTCC 433 and **(b)** *Listeria monocytogenes* Scott A were taken for the experiments. Traces a-h correspond to decreasing cell numbers (10^7–1.0 CFU), trace i: AuNP alone (volume adjusted) and trace j: Au NP interacted with 3.5 x 10^{-5} % w/v PLL. **(c)** Area under UV-vis extinction spectrum as a function of bacterial cell numbers for a: *Escherichia coli* MTCC 433, b: *Listeria monocytogenes* Scott A. The area represents mean value of three independent measurements. **(d)** Plot for subtractive-aggregation (ΔAagg) versus bacterial cell numbers for a: *Escherichia coli* MTCC 433 and b: *Listeria monocytogenes* Scott A.

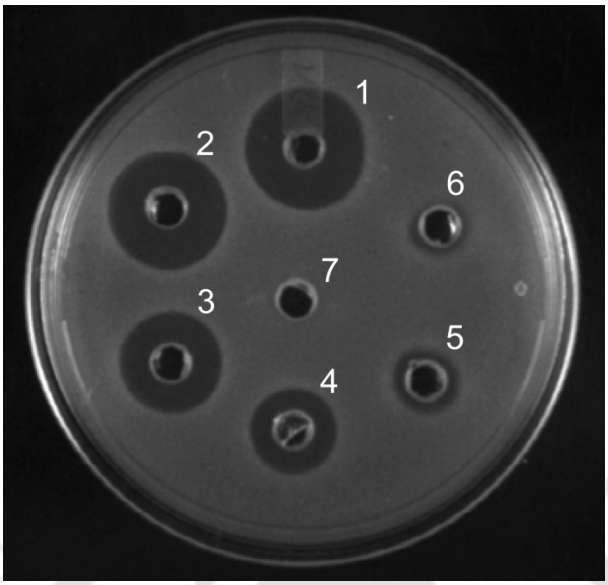

Figure A2.12. Agar well diffusion assay to test antimicrobial activity of nisin against *Leuconostoc mesenteroides* NRRL B640. Well nos. 1-6: 1000 IU/mL, 800 IU/mL, 400 IU/mL, 200 IU/mL, 100 IU/mL, and 50 IU/mL nisin; 7: 0.75% NaCl (pH 5.3). Nisin stock solution (10000 IU/mL) was made in 0.75% NaCl (pH 5.3).

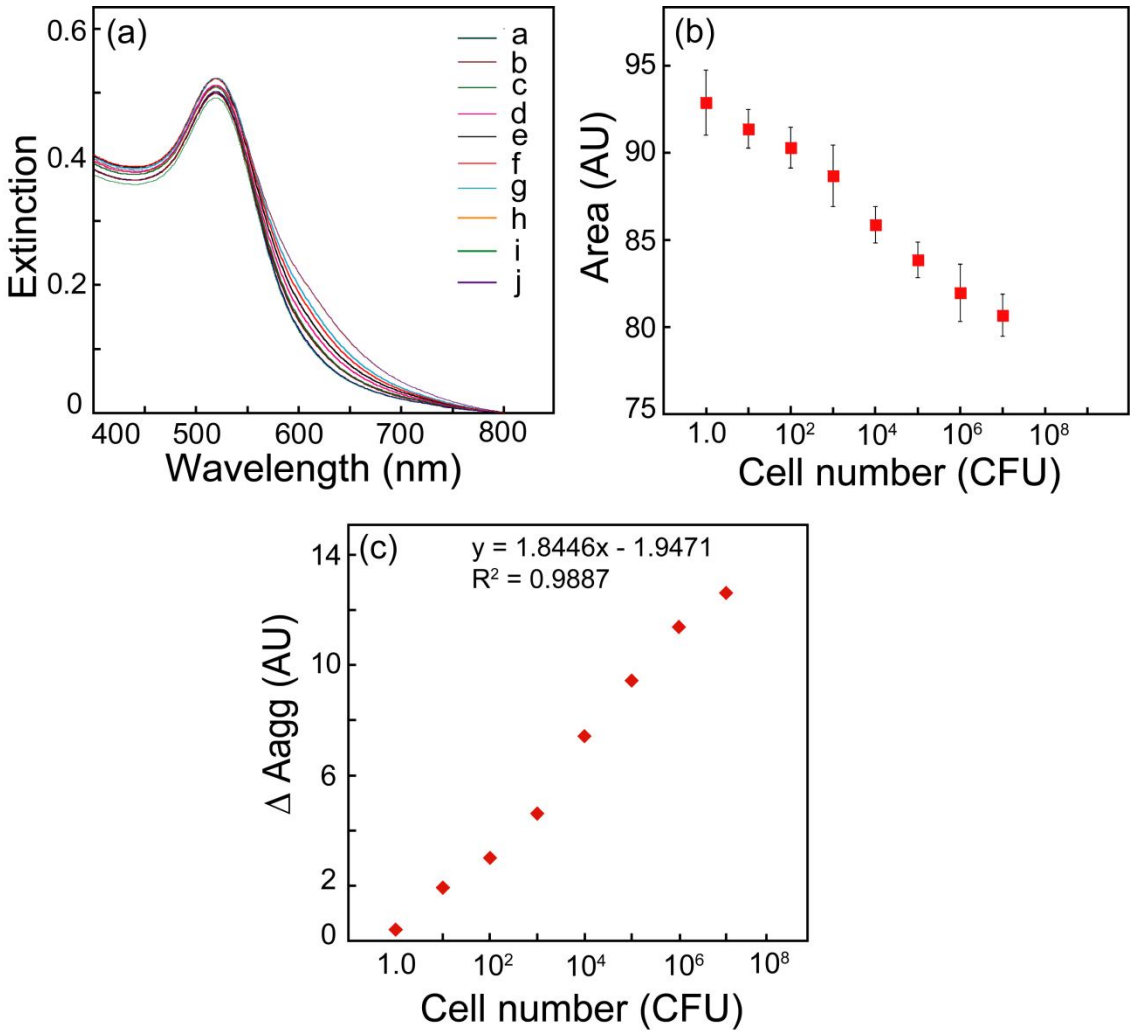

Figure A2.13. (a) UV-visible extinction spectrum for estimation of cell numbers for *Leuconostoc mesenteroides* NRRL B640 by AuNP aggregation. Traces a-h correspond to decreasing cell numbers (10^7 – 1.0 CFU), trace i: AuNP alone (volume adjusted) and trace j: AuNP interacted with 3.5 x 10^{-5} % w/v PLL. **(b)** Area under UV-visible extinction spectrum as a function of bacterial cell numbers. **(c)** Plot for subtractive-aggregation (ΔAagg) versus bacterial cell numbers.

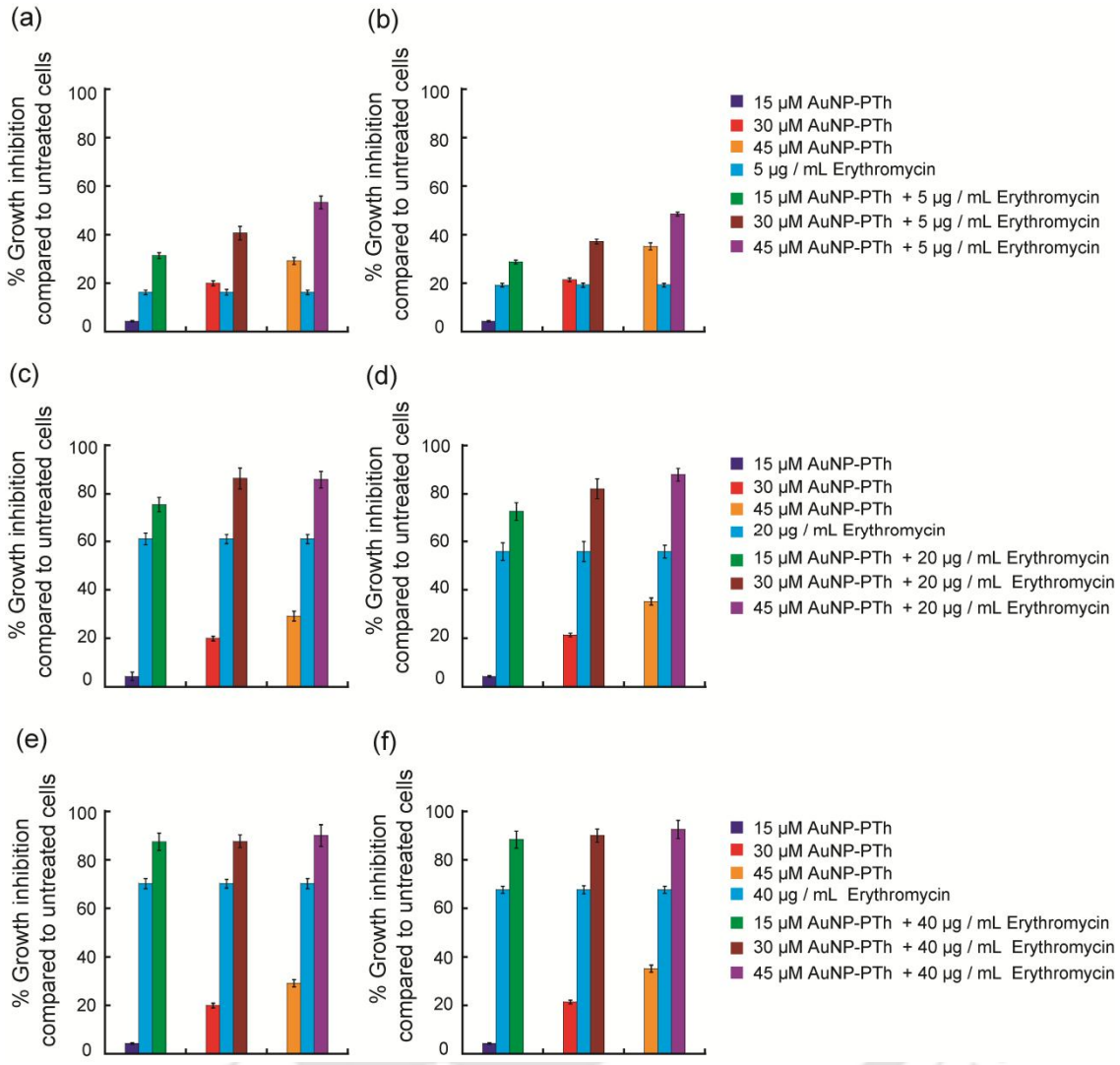

Figure A4.1. Effect of combined treatment of AuNP-PTh nanocomposite and erythromycin on the growth of **(a, c and e)** *E. coli* MTCC 433 and **(b, d and f)** *Y. enterocolitica* MTCC 859.

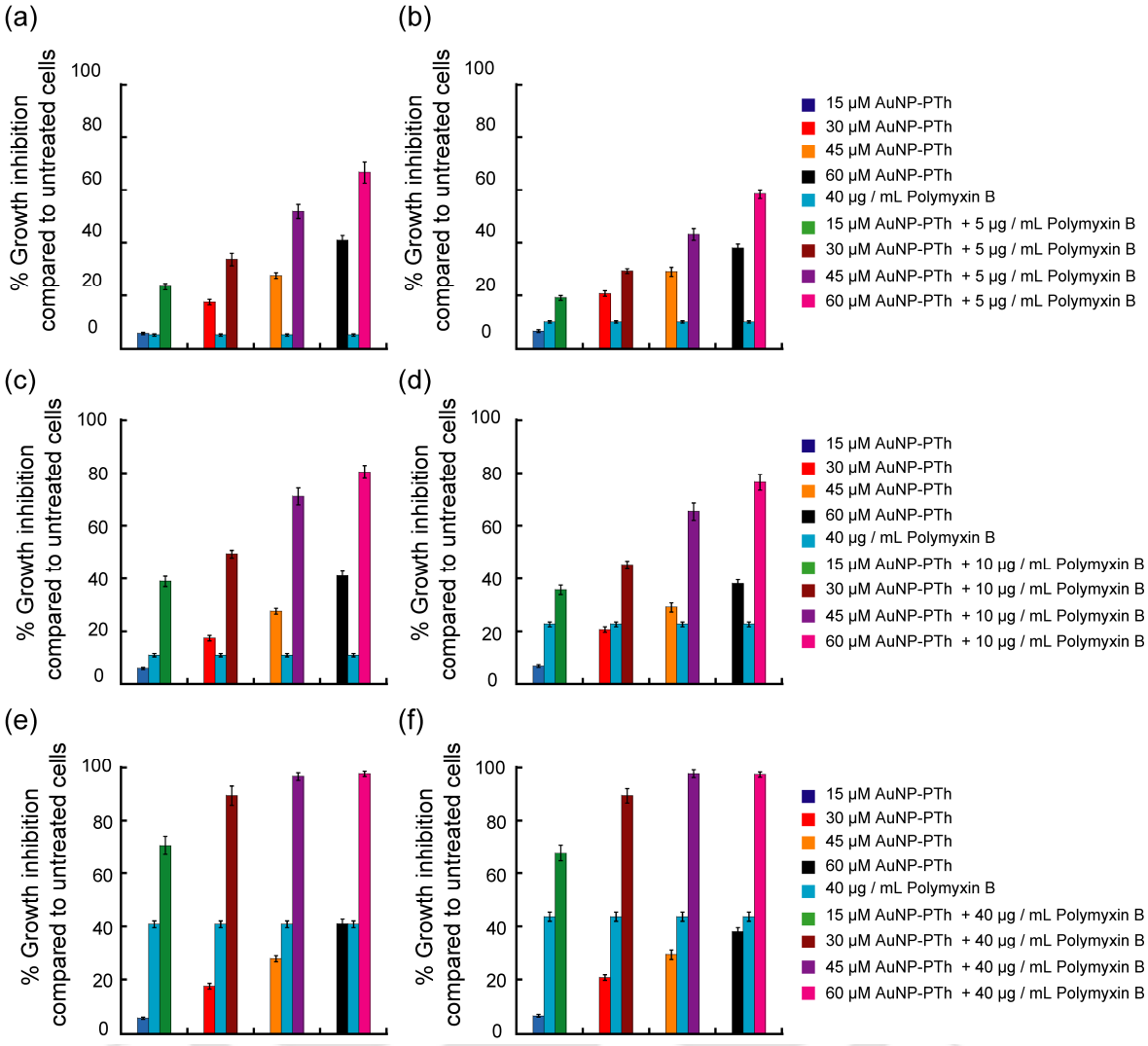

Figure A4.2. Effect of combined treatment of AuNP-PTh and polymyxin B on the growth of **(a, c and e)** *S. aureus* MTCC 96 and **(b, d and f)** *E. faecalis* MTCC 439.

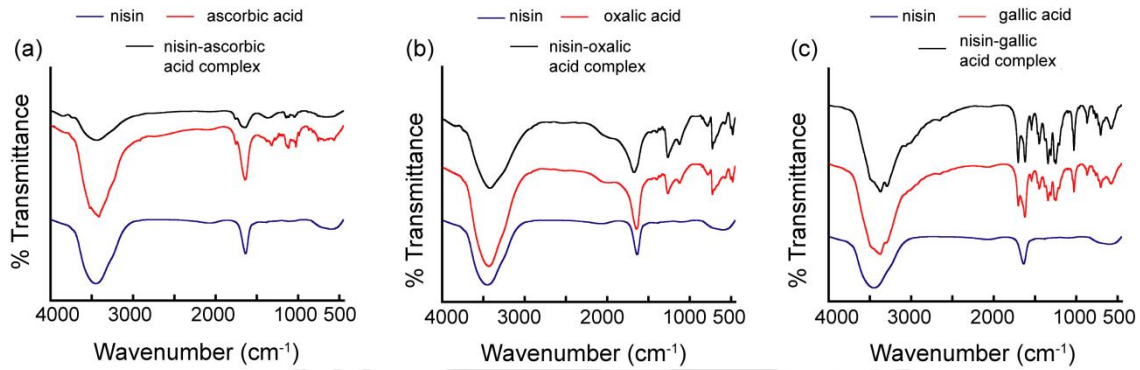

Figure A5.1. FTIR analysis of nisin-organic acid complex.

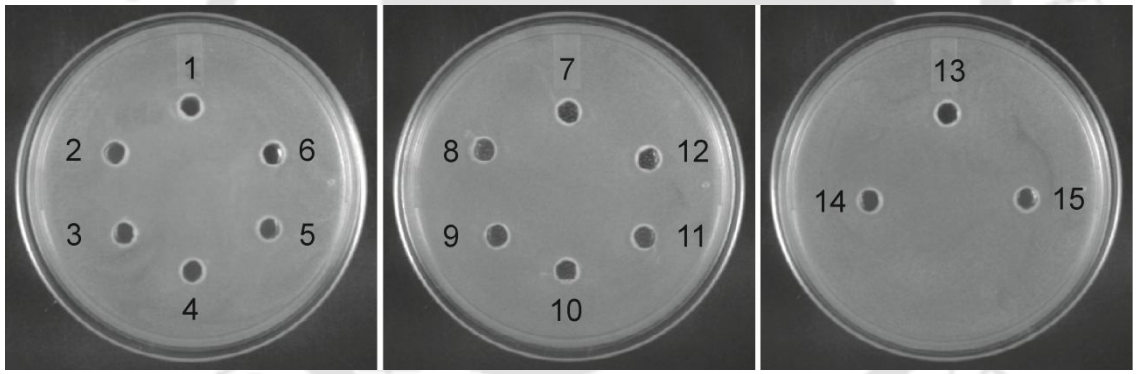

Figure A5.2. Agar well diffusion assay to test the antimicrobial activity of different organic acids against *M. luteus* ATCC 9341. The samples tested were: 1. Citric acid (pH 5.5), 2. Citric acid (pH 7.0), 3. Citric acid (pH 8.0), 4. Ascorbic acid (pH 5.5), 5. Ascorbic acid (pH 7.0), 6. Ascorbic acid (pH 8.0), 7. Oxalic acid (pH 5.5), 8. Oxalic acid (pH 7.0), 9. Oxalic acid (pH 8.0), 10. Lactic acid (pH 5.5), 11. Lactic acid (pH 7.0), 12. Lactic acid (pH 8.0), 13. Gallic acid (pH 5.5), 14. Gallic acid (pH 7.0), 15. Gallic acid (pH 8.0).

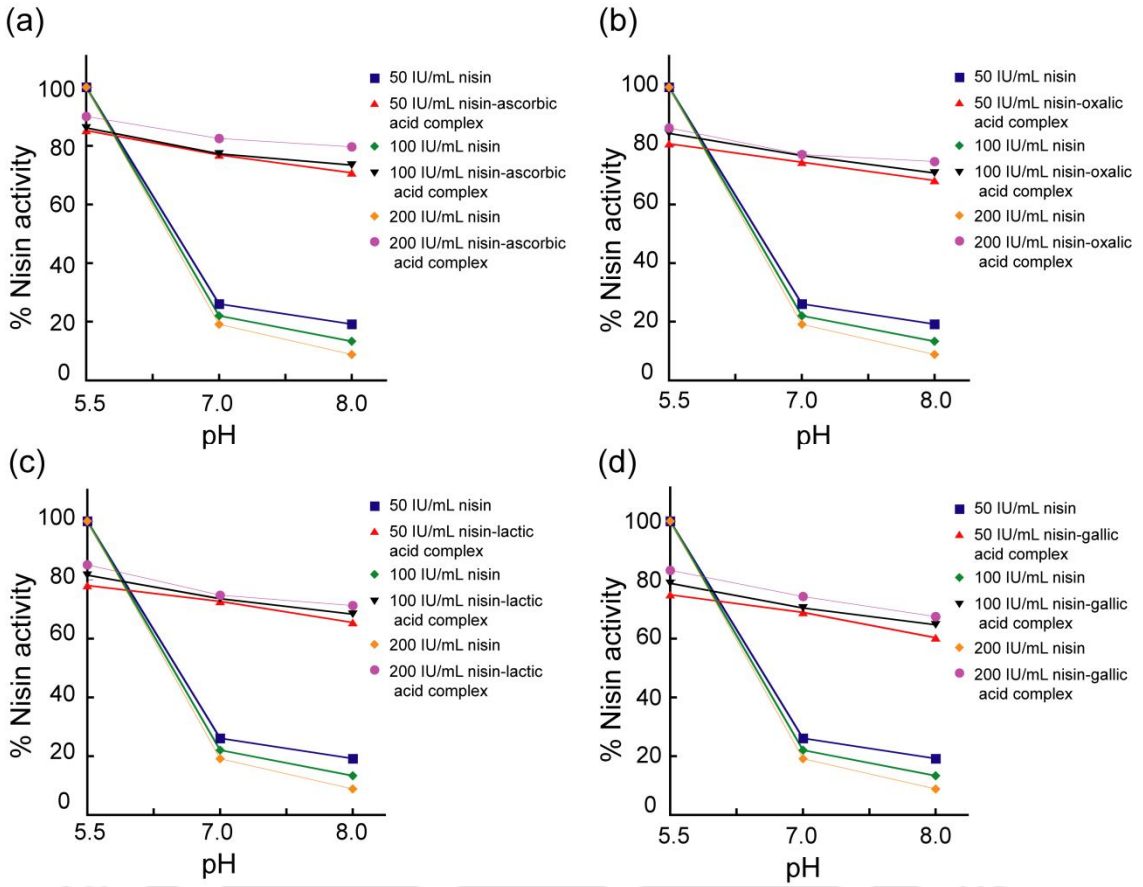

Figure A5.3. cFDA-SE dye leakage assay with *M. luteus* ATCC 9341 cells treated with various nisin-organic acid complex at different pH.

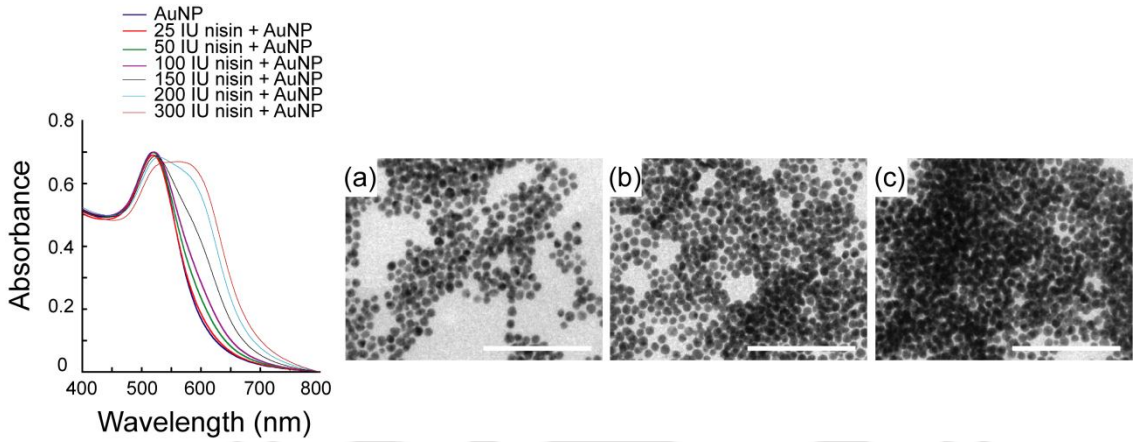

Figure A5.4. UV-visible extinction spectrum of citrate-stabilized AuNPs incubated with increasing concentration of nisin is indicated in the left panel. TEM images of AuNPs in the presence of (a) 50 IU, (b) 100 IU and (c) 200 IU of nisin is shown in the right panel. Scale bar is 200 nm for the images.

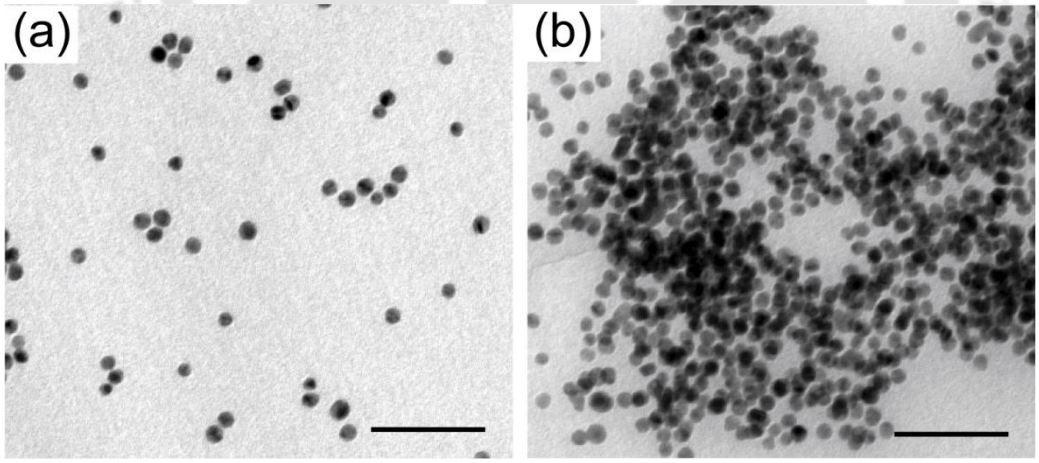

Figure A5.5. TEM image of **(a)** as synthesized citrate-stabilized AuNPs and **(b)** nisin-AuNP composite (200 IU/mL nisin concentration). Scale bar for the images is 50 nm.

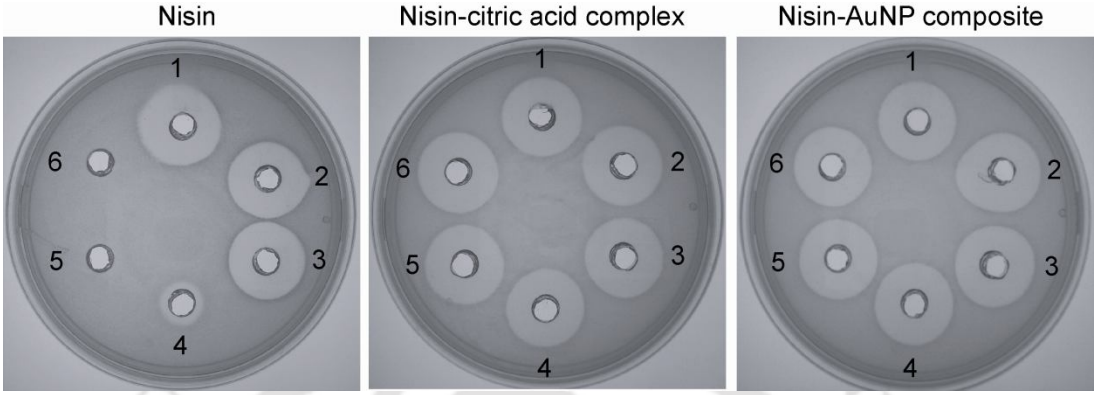

Figure A5.6. Agar well diffusion assay to determine the activity of nisin, nisin-citric acid complex and nisin-AuNP composite at different pH against *M. luteus* ATCC 9341. 1. pH 3.0, 2. pH 4.0, 3. pH 5.0, 4. pH 6.0, 5. pH 7.0, 6. pH 8.0. Nisin concentration in the samples was 200 IU/mL.

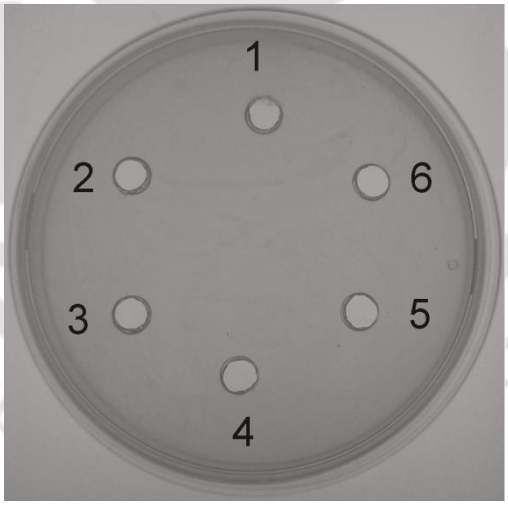

Figure A5.7. Agar well diffusion assay to determine antimicrobial activity of citrate-stabilized AuNP solution of varying pH against *M. luteus* ATCC 9341. 1. pH 3.0, 2. pH 4.0, 3. pH 5.0, 4. pH 6.0, 5. pH 7.0, 6. pH 8.0.

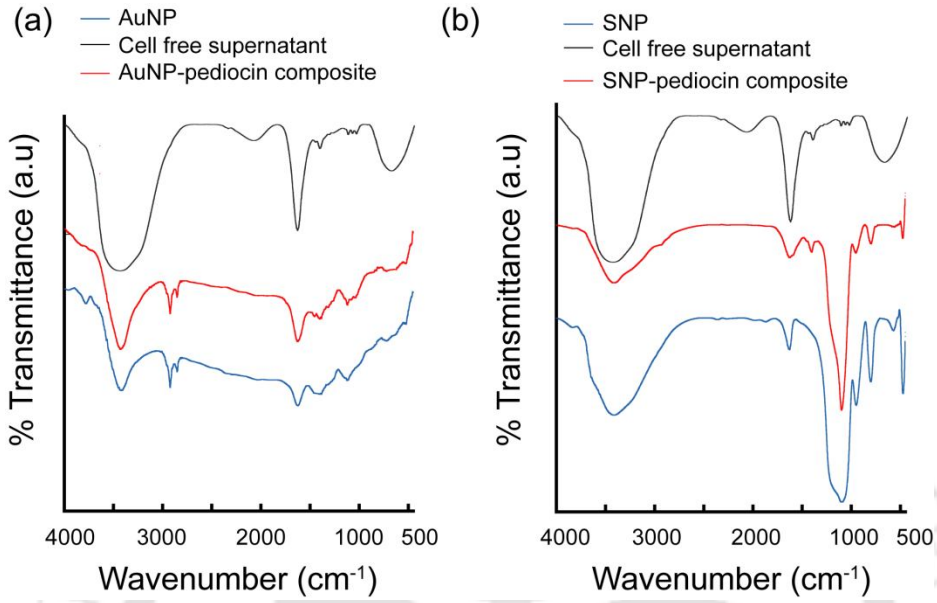

Figure A6.1. FTIR analysis of **(a)** AuNP-pediocin composite and **(b)** SNP-pediocin composite.

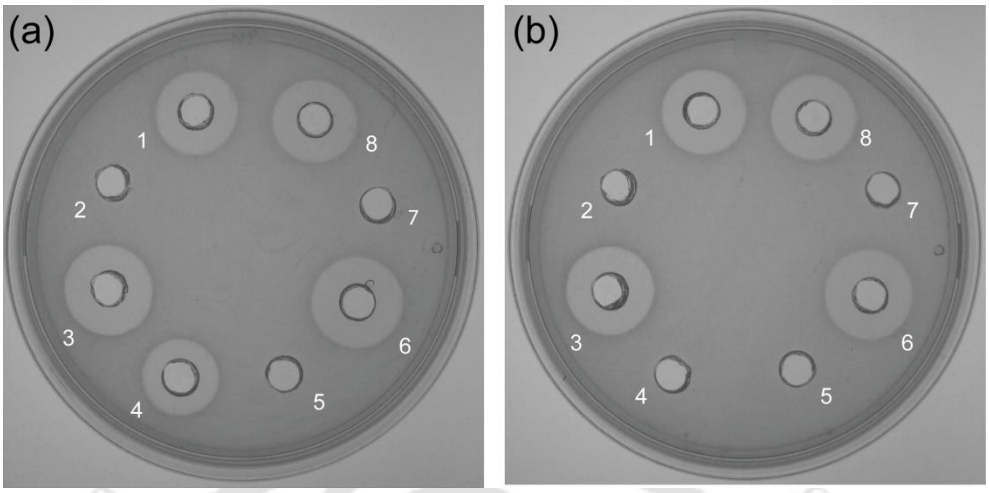

Figure A6.2. Antimicrobial activity of AuNP-pediocin composite and recovered supernatant following separation of AuNP-pediocin composite. **(a)** Well nos. 1-4 corresponds to interaction of 10 mL cell-free culture supernatant with 10 mL of 0.32 nM AuNP solution. Well nos. 5-8 corresponds to interaction of 10 mL cell-free culture supernatant with 20 mL of 0.32 nM AuNP solution. Well nos. 1 and 8: cell-free culture filtrate, 2 and 7: AuNP alone, 3 and 6: AuNP-pediocin composite, 4 and 5: supernatant obtained after separation of composite by centrifugation, **(b)** Well nos. 1-4 corresponds to interaction of 10 mL cell-free culture supernatant with 20 mL of 0.32 nM AuNP solution for 30 min. Well nos. 5-8 corresponds to interaction of 10 mL cell-free culture supernatant with 20 mL of 0.32 nM AuNP solution for 60 min. Well nos. 1 and 8: cell-free culture filtrate, 2 and 7: AuNP alone, 3 and 6: AuNP-pediocin composite, 4 and 5: supernatant obtained after separation of composite by centrifugation.

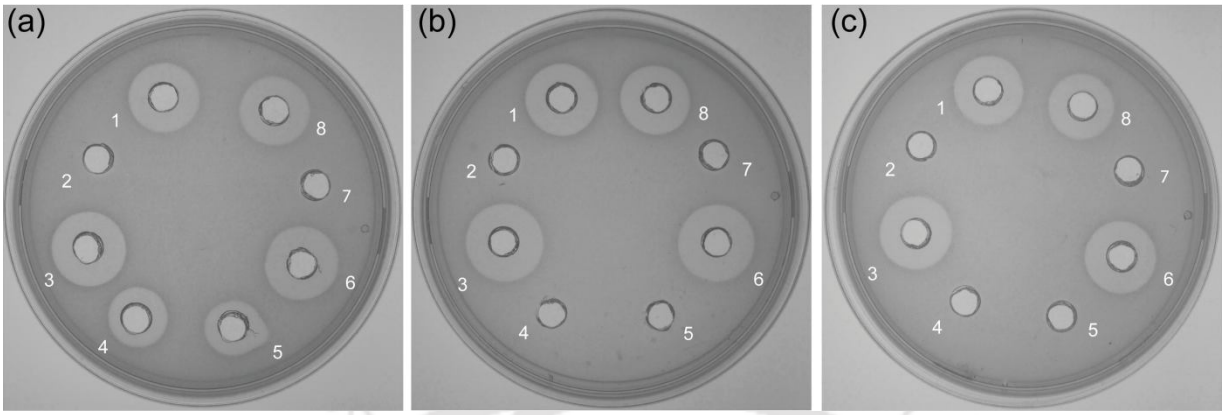

Figure A6.3. Antimicrobial activity of SNP-pediocin composite and recovered supernatant following separation of SNP-pediocin composite. **(a)** Well nos. 1-4 corresponds to interaction of 10 mL cell-free culture supernatant with 0.1 mg/mL SNP solution. Well nos. 5-8 corresponds to interaction of 10 mL cell-free culture supernatant with 0.25 mg/mL SNP solution. Well nos. 1 and 8: cell-free culture filtrate, 2 and 7: SNP alone, 3 and 6: SNP-pediocin composite, 4 and 5: supernatant after separation of composite by centrifugation, **(b)** Well nos. 1-4 corresponds to interaction of 10 mL cell-free culture supernatant with 0.5 mg/mL SNP solution. Well nos. 5-8 corresponds to interaction of 10 mL cell-free culture supernatant with 1.0 mg/mL SNP solution. Well nos. 1 and 8: cell-free culture filtrate, 2 and 7: SNP alone, 3 and 6: SNP-pediocin composite, 4 and 5: supernatant after separation of composite by centrifugation, **(c**) Well nos. 1-4 corresponds to interaction of 10 mL cell-free culture supernatant with 0.5 mg/mL SNP solution for 30 min. Well nos. 5-8 corresponds to interaction of 10 mL cell-free culture supernatant with 0.5 mg/mL SNP solution for 60 min. Well nos. 1 and 8: cell-free culture filtrate, 2 and 7: SNP alone, 3 and 6: SNP-pediocin composite, 4 and 5: supernatant after separation of composite by centrifugation.

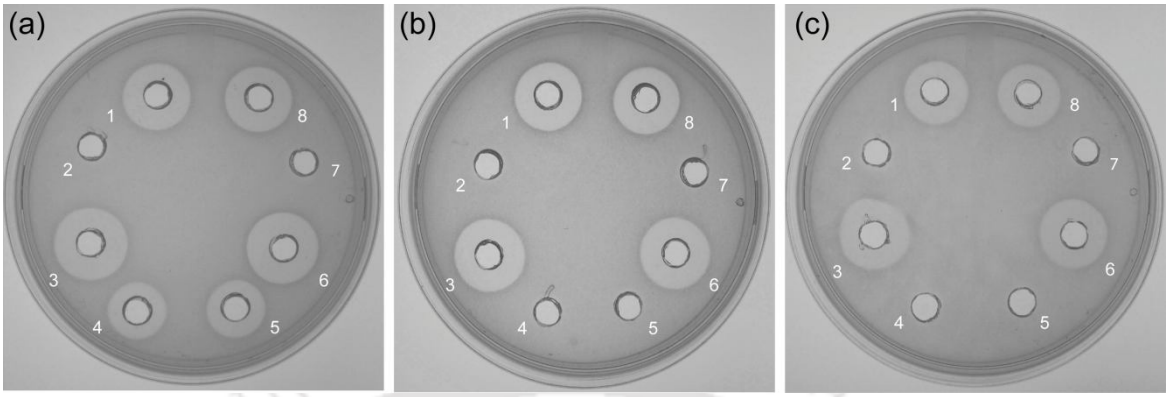

Figure A6.4. Antimicrobial activity of IONP-pediocin composite and recovered supernatant following separation of IONP-pediocin composite. **(a)** Well nos. 1-4 corresponds to interaction of 10 mL cell-free culture supernatant with 0.1 mg/mL IONP solution. Well nos. 5-8 corresponds to interaction of 10 mL cell-free culture supernatant with 0.25 mg/mL IONP solution. Well nos. 1 and 8: cell-free culture filtrate, 2 and 7: IONP alone, 3 and 6: IONP-pediocin composite, 4 and 5: supernatant after separation of composite by centrifugation, **(b)** Well nos. 1-4 corresponds to interaction of 10 mL cell-free culture supernatant with 0.5 mg/mL IONP solution. Well nos. 5-8 corresponds to interaction of 10 mL cell-free culture supernatant with 1.0 mg/mL IONP solution. Well nos. 1 and 8: cell-free culture filtrate, 2 and 7: IONP alone, 3 and 6: IONP-pediocin composite, 4 and 5: supernatant after separation of composite by centrifugation, **(c)** Well nos. 1-4 corresponds to interaction of 10 mL cell-free culture supernatant with 0.5 mg/mL IONP solution for 30 min. Well nos. 5-8 corresponds to interaction of 10 mL cell-free culture supernatant with 0.5 mg/mL IONP solution for 60 min. Well nos. 1 and 8: cell-free culture filtrate, 2 and 7: IONP alone, 3 and 6: IONP-pediocin composite, 4 and 5: supernatant after separation of composite by centrifugation.

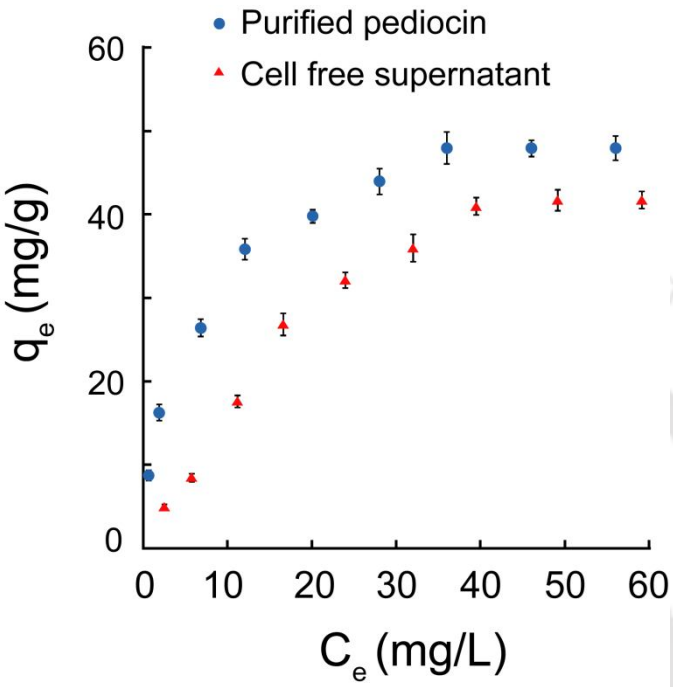

Figure A6.5. Adsorption isotherm of purified pediocin and cell-free culture filtrate on iron oxide nanoparticles.

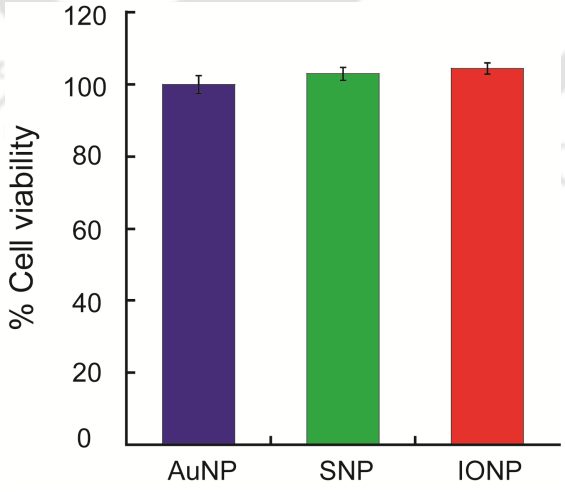

Figure A6.5. MTT assay to ascertained cytotoxic effect of AuNPs, SNP, and IONPs on HT-29 cells. Each data point represents mean ± standard deviation from six samples.

Table A6.1. Langmuir adsorption isotherm parameters of cell-free culture supernatant and purified pediocin on iron oxide nanoparticles

Sample	Langmuir Adsorption Isotherm Parameters*			
	Q_m (mg /g)	b (L/g)	R^2	R_L
Cell-free culture supernatant	68.97	149.9	0.94	4×10^{-4}
Purified pediocin	52.35	559.36	0.99	9.3×10^{-5}

*Langmuir adsorption isotherm parameters were calculated according to a standard method described previously (Saha et al. *J. Phys. Chem. C* **2011**, *115*, 8024-8033).

Table A6.2. Summary of pediocin purification from *Pediococcus pentosaceus* CRA51 using iron oxide nanoparticles

Source	Volume (mL)	Protein (mg/mL)	Activity (AU/mL)	Total Activity (AU)	Specific Activity (AU/mg)	Yield (%)	Purification Fold
Cell-free culture filtrate	10.0	0.16	800	8000	10000	100	1.0
Desorbed pediocin from IONP	5.0	0.02	3200	16000	160000	200	16

Table A6.3. Minimum inhibitory concentration (MIC) of purified pediocin, AuNP-pediocin composite, SNP-pediocin composite and IONP-pediocin composite

Sample	**MIC Against Pathogenic Bacteria**		
	***L. monocytogenes* Scott A (AU/mL)**	***S. aureus* MTCC 96 (AU/mL)**	***E. faecalis* MTCC 439**
Purified pediocin	100	200	200
AuNP-pediocin composite	100	200	200
SNP-pediocin composite	100	200	200
IONP-pediocin composite	100	200	200

LIST OF PUBLICATIONS

List of Publications

Publications from Ph.D. Research Work:

(A) Journal Publications:

1. **Adhikari, M. D.**, Panda, B. R., Vudumula, U., Chattopadhyay, A. and Ramesh, A. (2012). A facile method for estimating viable bacterial cells in solution based on "subtractive-aggregation" of gold nanoparticles. *RSC Advances* **2**, 1782-1793.
2. **Adhikari, M. D.**, Das, G. and Ramesh, A. (2012). Retention of nisin activity at elevated pH in an organic acid complex and gold nanoparticle composite. *Chemical Communications* **48**, 8928-8930.
3. **Adhikari, M. D.**, Goswami, S., Panda, B. R., Chattopadhyay, A. and Ramesh, A. (2013). Membrane-directed high bactericidal activity of gold nanoparticle-polythiophene composite for niche applications against pathogenic bacteria. *Advanced Healthcare Materials* **2**, 599-606.
4. **Adhikari, M. D.**, Mukherjee, S., Saikia, J., Das, G. and Ramesh, A. (2014). Magnetic nanoparticles for selective capture and purification of an antimicrobial peptide secreted by food-grade lactic acid bacteria. *Journal of Materials Chemistry B*, **2**, 1432-1438.

(B) Conference Presentations:

1. **Adhikari, M.D.**, Panda, B.R., Singh, A.K., Chattopadhyay, A. and Ramesh, A. (2009). Antagonistic activity of a gold nanoparticle-polythiophene composite against pathogenic bacteria. Abstract PS 61. Presented in International Workshop on Nanotechnology and Advanced Functional Materials, National Chemical Laboratory, Pune, 9-11 July 2009.
2. **Adhikari, M.D.**, Panda, B.R., Vudumula, U., Chattopadhyay, A. and Ramesh, A. (2010). Facile estimation of bacterial cells based on poly-L-lysine mediated aggregation of gold nanoparticle. Presented in 51st Annual Conference of Association of Microbiologists of India (AMI), Ranchi, 14-17 December 2010.

Publications from Other Research Projects:

1. Ojha, B., Singh, A.K., **Adhikari, M.D.**, Ramesh, A. and Das. G. (2010). 2-Alkylmalonic acid: Amphiphilic chelator and a potent inhibitor of metalloenzyme. *Journal of Physical Chemistry B* **114**, 10835-10842.
2. Vudumula, U., **Adhikari, M. D.**, Ojha, B., Goswami, S., Das, G. and Ramesh, A. (2012). Tuning the bactericidal repertoire and potency of quinoline-based amphiphiles for enhanced killing of pathogenic bacteria. *RSC Advances* **2**, 3864-3871.
3. Singh, A.K., Mukherjee, S., **Adhikari, M. D.** and Ramesh, A. (2012). Fluorescence-based comparative evaluation of bactericidal potency and food application potential of anti-listerial bacteriocin produced by lactic acid bacteria isolated from indigenous samples. *Probiotics and Antimicrobial Proteins* **4**, 122-132.
4. Kar, C., **Adhikari, M. D.**, Ramesh, A. and Das, G. (2012). Selective sensing and effective separation of Hg^{2+} from aqueous medium with a pyrene based amphiphilic ligand. *RSC Advances* **2**, 9201-9206.
5. Kar, C., **Adhikari, M. D.**, Ramesh, A. and Das, G. (2013). NIR and FRET-based sensing of Cu^{2+} and S^{2-} in physiological conditions and in live cells. *Inorganic Chemistry* **52**, 743-752.
6. Mukherjee, S., Singh, A. K., **Adhikari, M.D.** and Ramesh, A. (2013). Quantitative appraisal of probiotic attributes and *in vitro* adhesion potential of anti-listerial bacteriocin-producing lactic acid bacteria. *Probiotics and Antimicrobial Proteins* **5**, 99-109.
7. Goswami, S., **Adhikari, M. D.**, Kar, C., Thiyagarajan, D., Das, G. and Ramesh, A. (2013). Synthetic amphiphiles as therapeutic antibacterials: Lessons on bactericidal efficacy and cytotoxicity and potential application as an adjuvant in antimicrobial chemotherapy. *Journal of Materials Chemistry B* **1**, 2612-2623.